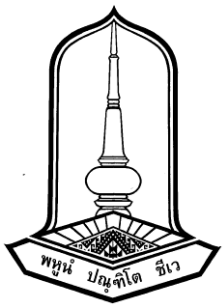

Synthesis and transfection efficiency of cholesterol and *β*-sitosterol-based cationic lipids

Chopaka Thongbamrer

A thesis submitted in partial fulfillment of the requirements for the degree of Master of Science Degree in Chemistry at Mahasarakham University

February 2018

Synthesis and transfection efficiency of cholesterol and *β*-sitosterol-based cationic lipids

Chopaka Thongbamrer

A thesis submitted in partial fulfillment of the requirements for the degree of Master of Science Degree in Chemistry at Mahasarakham University

February 2018

The examining committee has unanimously approved this thesis, submitted by Miss Chopaka Thongbamrer, as a partial fulfillment of the requirements for the Master of Science degree in Chemistry at Mahasarakham University.

Examining Committee

M. Nontakitticharoen	
(Mongkol Nontakitticharoen, Ph.D.)	Chairman (External expert)
W. Radchatawedchakoon	
(Asst. Prof. Widchaya Radchatawedchakoon, Ph.D.)	Committee (Advisor)
Boon-ek Yingyongnarongkul	
(Assoc. Prof. Boon-ek Yingyongnarongkul, Ph.D.)	Committee (Co-advisor)
Uthai Sakee	
(Assoc. Prof. Uthai Sakee, Ph.D.)	Committee (Co-advisor)
S. Saikrasun	
(Assoc. Prof. Sunan Saikrasun, Ph.D.)	Committee (Faculty graduate committee)
S. Pitchuanchom	
(Siripit Pitchuanchom, Ph.D.)	Committee (Faculty graduate committee)

Mahasarakham University has granted approval to accept this thesis as a partial fulfillment of the requirements for the Master of Science degree in Chemistry

Wichian Magtoon	
(Prof. Wichian Magtoon, Ph.D.)	
Dean of the Faculty of Science	
	(Prof. Pradit Terdtoon, Ph.D.)
	Dean of Graduate School
	February 28, 2018

ACKNOWLEDGEMENTS

This thesis was granted by Faculty of Science, Mahasarakham University and the Center of Excellence for Innovation in Chemistry (PERCH-CIC). I am very grateful to my scholarship, the Human Resource Development in Science Project (Science Achievement Scholarship of Thailand, SAST, since 2015) for the academic financial support since the first year of undergraduate.

The thesis would not be accomplished if without the help from several people. First of all, I would like to thank Dr. Mongkol Nontakitticharoen, Associate Professor Dr. Sunan Saikrasun and Dr. Siripit Pitchuanchom for generously offering their time to be the committee members for my defense examination and helpful suggestions in the thesis and research work.

I would like to express my sincere gratitude to my advisor, Assistant Professor Dr. Widchaya Radchatawedchakoon for teaching and giving me very useful advices and suggestions throughout this research. I would like to express my appreciation to Associate Professor Dr. Boon-ek Yingyongnarongkul and Associate Professor Dr. Uthai Sakee, my co-advisors for helpful comments and discussion on my work.

I would like to thank the staff and technicians in the Department of Chemistry, Faculty of Science, Mahasarakham University and Ramkhamhaeng University for the support on the analytical instruments and places to carry out this research. I would also like to thank my friends in the laboratory for their help, friendship and encouragement.

Finally, I am thankful to my parents. Their unconditional love and encouragement are always the driving force that help me a lot to achieve this degree.

Chopaka Thongbamrer

TITLE Synthesis and transfection efficiency of cholesterol and *β*-sitosterol-based cationic lipids

AUTHOR Miss Chopaka Thongbamrer

DEGREE Master of Science Degree

ADVISORS Assist. Prof. Dr. Widchaya Radchatawedchakoon

Assoc. Prof. Dr. Boon-ek Yingyongnarongkul

Assoc. Prof. Dr. Uthai Sakee

UNIVERSITY Mahasarakham University **YEAR** 2018

ABSTRACT

Cationic lipids containing cholesterol and β-sitosterol as core structures, carbamate moiety as a linker and ammonium, trimethyl ammonium, guanidinium and tetramethyl guanidinium as polar headgroups were synthesized. The transfection efficiency, cytotoxicity, gel retardation, particle size and zeta potential of the synthetic cationic lipids were evaluated. Cationic lipid **L4a** showed higher transfection efficiency to HEK293 cells in the presence of 10–40% serum than Lipofectamine2000. The cationic lipid **L4a** showed non-toxic to HEK293 cells. Gel electrophoresis assay revealed the strong retardation of DNA by lipoplex **L4a** (DNA/lipid 1:10 and 1:20 w/w). The particle size and zeta potential of lipoplex **L4a** were approximately 286–770 nm and 34–35 mV, respectively. Moreover, cationic lipids **L9**–**L12** containing spermine and 1,4-bis(3-aminopropoxy)butane as polar headgroups, carbamate as a linker and cholesterol as a hydrophobic tail were also prepared. From the result of transfection screening and gel retardation assay, cationic lipid **L10** with helper lipid (dioleoylphosphatidyl-ethanolamine; DOPE) weight ratios 1:1 showed 30% transfection in HEK293 cells compared to Lipofectamine2000 as the positive control (100%).

ชื่อเรื่อง การสังเคราะห์และประสิทธิภาพการนำพาดีเอ็นเอเข้าสู่เซลล์ของไขมันประจุบวกซึ่งมีคอเลสเตอรอลและเบต้าซิโทสเตอรอลเป็นส่วนหลัก

ผู้วิจัย นางสาวช่อผกา ทองบำเรอ

ปริญญา วิทยาศาสตรมหาบัณฑิต **สาขาวิชา** เคมี

กรรมการควบคุม ผู้ช่วยศาสตราจารย์ ดร. วิชญ รัชตเวชกุล
รองศาสตราจารย์ ดร. บุญเอก ยิ่งยงณรงค์กุล
รองศาสตราจารย์ ดร. อุทัย สาขี

มหาวิทยาลัย มหาวิทยาลัยมหาสารคาม **ปีที่พิมพ์** 2561

บทคัดย่อ

ได้สังเคราะห์ไขมันประจุบวกที่มีคอเลสเตอรอลและเบต้าซิโทสเตอรอลเป็นส่วนหลัก ส่วนเชื่อมต่อคาร์บาเมต และส่วนหัวเป็นหมู่แอมโมเนียม ไทรเมทิลแอมโมเนียม กัวนิดิเนียม และเททระเมทิลกัวนิดิเนียม การนำพาดีเอ็นเอเข้าสู่เซลล์ ความเป็นพิษต่อเซลล์ การจับกับดีเอ็นเอ ขนาดของอนุภาค และศักย์ไฟฟ้าของไขมันประจุบวก ผลการทดลองพบว่าไขมันประจุบวก **L4a** แสดงประสิทธิภาพในการนำพาดีเอ็นเอเข้าสู่เซลล์ HEK293 ในสภาวะที่มีซีรัม 10–40 เปอร์เซ็นต์ ได้ดีกว่า Lipofectamine2000 ไขมันประจุบวก **L4a** ไม่แสดงความเป็นพิษต่อเซลล์ HEK293 ในการทดลองเจลอิเล็กโทรฟอริซิสพบว่าไลโปเพล็กซ์ **L4a** (ดีเอ็นเอ/ไขมันประจุบวก) ที่อัตราส่วน 1:10 และ 1:20 โดยมวล สามารถหน่วงดีเอ็นเอได้ดีมาก ขนาดอนุภาคของไลโปเพล็กซ์ **L4a** ประมาณ 286–770 นาโนเมตร และศักย์ไฟฟ้าประมาณ 34–35 มิลลิโวลต์ นอกจากนั้นไขมันประจุบวก **L9**–**L12** ที่มีส่วนหัวเป็น สเปอร์มีนและ 1,4-บิส(3-แอมิโนโพรพอกซี)บิวเทน ส่วนเชื่อมต่อคาร์บาเมต และคอเลสเตอรอลเป็นส่วนหางยังได้มีการสังเคราะห์ขึ้นการทดลองเบื้องต้นของการนำพาดีเอ็นเอเข้าสู่เซลล์และการทดลองเจลอิเล็กโทรฟอริซิส ผลพบว่าไขมันประจุบวก **L10** ที่ผสมไขมันตัวช่วย (dioleoylphosphatidylethanolamine; DOPE) ที่อัตราส่วน 1:1 โดยมวล มีประสิทธิภาพในการนำพาดีเอ็นเอเข้าสู่เซลล์ประมาณ 30 เปอร์เซ็นต์ เมื่อเปรียบเทียบกับ Lipofectamine2000

CONTENTS

PAGE

CONTENTS (Continued)

PAGE

LIST OF FIGURES

PAGE

LIST OF FIGURES (Continued)

PAGE

LIST OF FIGURES (Continued)

PAGE

LIST OF FIGURES (Continued)

PAGE

LIST OF FIGURES (Continued)

PAGE

LIST OF FIGURES (Continued)

PAGE

LIST OF FIGURES (Continued)

PAGE

LIST OF FIGURES (Continued)

PAGE

LIST OF FIGURES (Continued)

PAGE

LIST OF FIGURES (Continued)

PAGE

LIST OF FIGURES (Continued)

PAGE

LIST OF FIGURES (Continued)

PAGE

LIST OF FIGURES (Continued)

PAGE

LIST OF FIGURES (Continued)

PAGE

LIST OF FIGURES (Continued)

PAGE

LIST OF FIGURES (Continued)

PAGE

LIST OF FIGURES (Continued)

PAGE

LIST OF SCHEMES

PAGE

LIST OF SCHEMES (Continued)

PAGE

CHAPTER 1

INTRODUCTION

1.1 Gene Therapy

Gene therapy technology is important for the treatment of genetic disorders. Gene therapy methods can treat many diseases such as atrial fibrillation (AF) [1], severe combined immunodeficiency (SCID) [2], chronic granulomatous disorder [3], Alzheimer [4] hemophilia [5], cancer [6], diabetes [7], cystic fibrosis [8], Parkinson's disease [9], cardiovascular [10] and lung cancer [11] etc. This technology is very helpful for human because several diseases caused from genetic disorder are unable to be cured by general medicines. Scientists have attempted to find out the most effective and safety process to transfer genes into cells. However, the process is still in the early stage and under evaluation.

Vectors are compounds having the ability to carry the specific gene into the target cells. There are two types of vectors: viral vectors and non-viral vectors [12]. The use of viral vectors were a popular method because of the effectiveness in gene transfer but the virus must be attenuated before using. The disadvantages of viral methods are toxicity to cells and effect to the immune system. The viral vectors such as retrovirus, lentivirus, adenovirus, adeno-associated virus, and herpes simplex virus have been extensively used as leaders for gene delivery [13]. The limitations of the viral method in clinical application are immunogenic response, toxicity, insertional mutagenesis and the limited amount of DNA transportable [14−17]. Non-viral vectors (synthetic vectors) were quite remarkable because they are safe and have no side effects. However, this vector also has a disadvantage in low transfection efficiency. There are two types of non-viral gene carriers including physical non-viral gene carriers (needle and jet injection, hydrodynamic gene transfer, electroporation, gene gun and sonoporation) and chemical-based non-viral vectors (lipid-based, polymeric, dendrimer-based, polypeptide and nanoparticles vectors). [18−21]. Cationic lipids are important non-viral vectors for gene delivery because of the capability to incorporate hydrophilic and hydrophobic drugs, low toxicity, no activation of immune system, and the ability to deliver bioactive

compounds to the targeted site of action [22]. The challenges of gene delivery are various, including toxicity, inhibition by serum in body system, uptake by the reticuloendothelial system (RES) and specificity to lead gene with respect to the cells of interest [23].

1.2 Cationic Lipids

A cationic lipid is a synthetic vector for non-viral gene delivery consisting of three parts as followed:

1.2.1 Polar headgroup has a positive charge which makes the compound to be dissolved in water. The typical polar headgroup is including amine, guanidine or natural amino acid as lysine and histidine. There are three types of the cationic lipids containing polar headgroups which are monovalent lipids such as DOEPC, DODAB (DDAB), DOTAP, DODAP [24], divalent lipids such as CTA14, DMKD, DMKE [24,25] and multivalent lipids such as DOSPA, DOGS,DOSPER, CCS, CDO14, MVL3, MVL5 [24-26] (Figure 1).

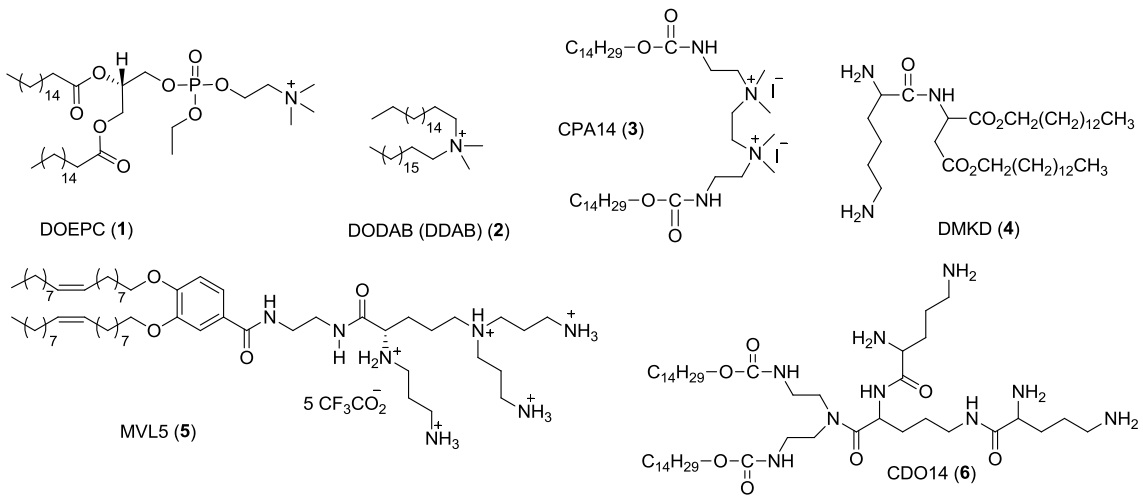

Figure 1 Structure of monovalent lipids (**1**–**2**), divalent lipids (**3**–**4**) and multivalent lipids (**5**–**6**).

In addition, the headgroup of cationic lipids are also divided into symmetric and asymmetric headgroup. For example, BGTC, RPR12058, GRcat, MM18, CHDTAEA, GR12, EDOPC, pcTG90, CDAND, DS(9-yne)PE, *N*-hexadeccyl(1,3,5-triaza-7-phophaadamantane hexafluorophosphate [27,28] are symmetric headgroups and CMVL2-5, lipids **9** and **10**, DPPES, GL67, BGSC [29,30] are asymmetric headgroups (Figure 2)

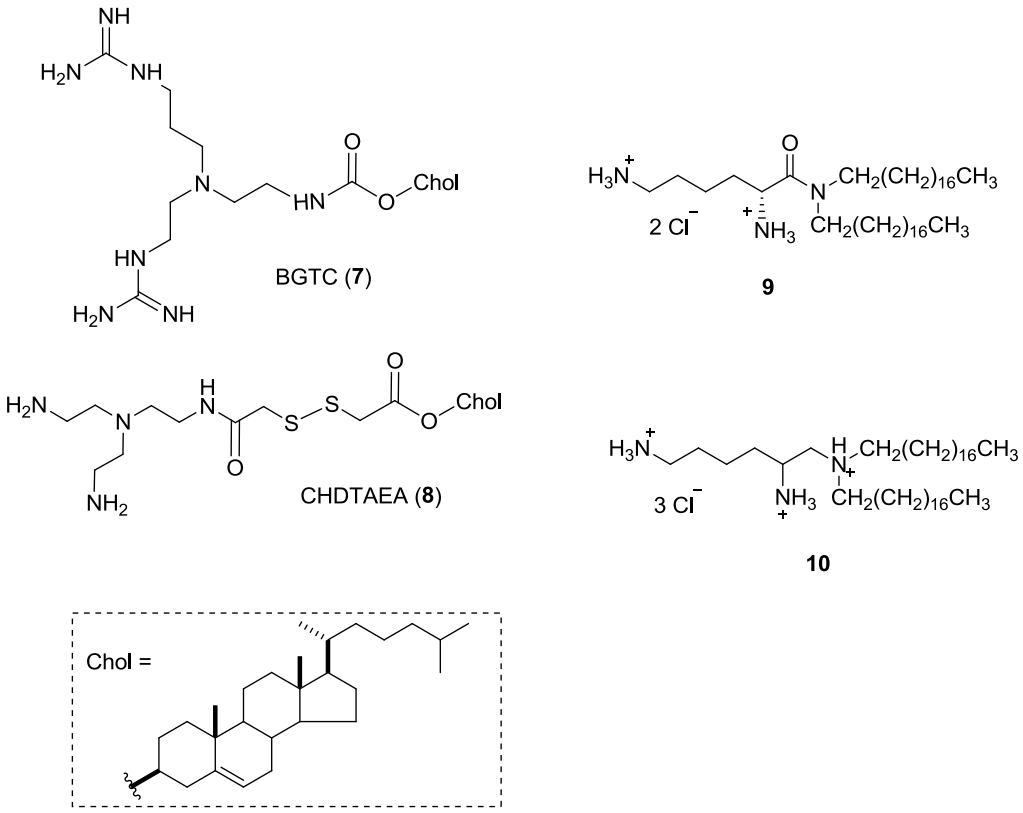

Figure 2 Symmetric headgroups (**7–8**) and asymmetric headgroups (**9–10**).

1.2.2 Linker is a chemical moiety that allows headgroup and tail joining together. Normally, this part is a chemical bond or functional group such as ether, ester, amide and carbamate [31−35] (Figure 3).

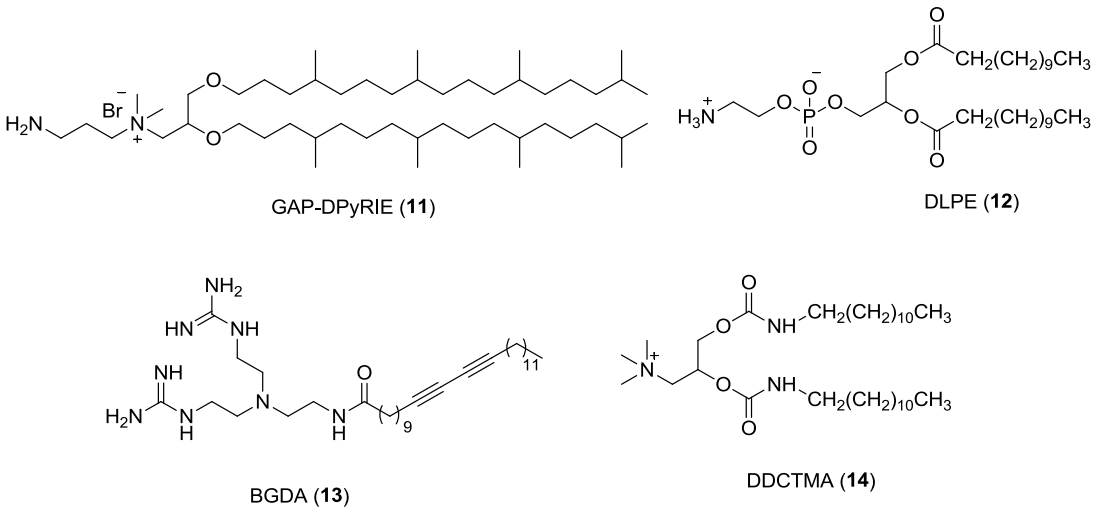

Figure 3 Cationic lipids with ether (**11**), ester (**12**), amide (**13**), and carbamate (**14**) linker.

1.2.3 Hydrophobic tail may be established from saturated or unsaturated long chain hydrocarbons or steroids [36].

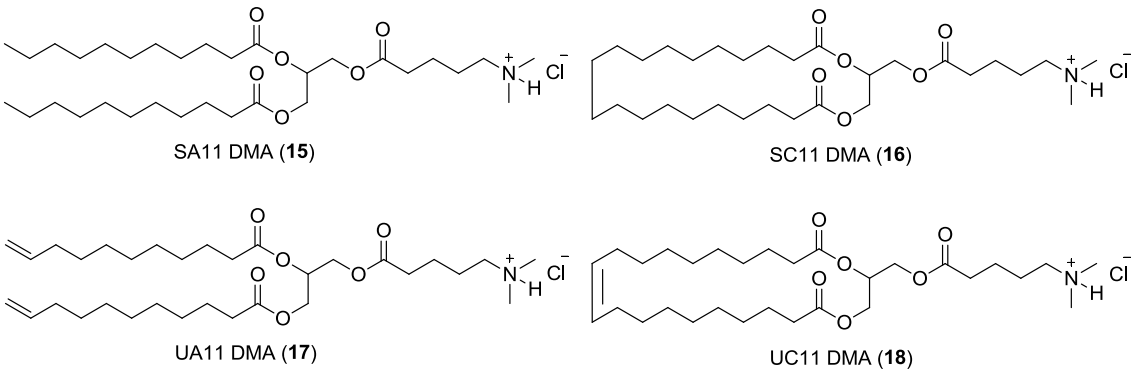

Figure 4 Saturated (**15**−**16**) and unsaturated (**17**−**18**) long chain hydrocarbons used as hydrophobic tails of cationic lipids.

1.3 Synthesis of Cationic Lipids

Cationic lipids can be synthesized by solution- and solid-phase synthesis. The solution-phase synthesis is a fundamental technique to synthesize many organic compounds. The specific reagents and reactants perform chemical reactions in the appropriate solvents and condition to provide the desired products.

In the year 2007, Tomé *et al*. [37] synthesized the neutral and cationic tripyridylporphyrin-D-galactose conjugates to test antiviral activity against herpes simplex virus type 1 (HSV-1) (Scheme 1).

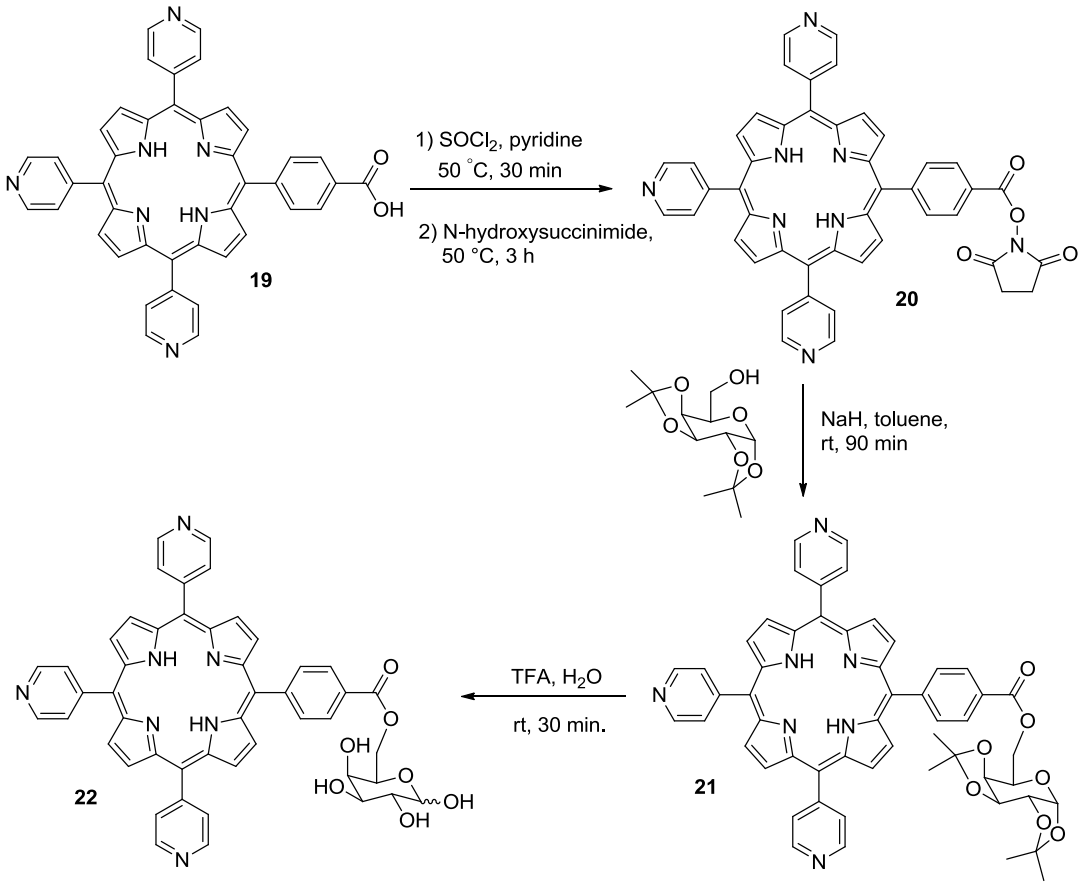

Scheme 1 The synthesis of cationic tripyridylporphyrin-D-galactose conjugates by solution-phase method.

Sakashita *et al*. [38] synthesized a galactose-modified lipid with aromatic ring using Click chemistry (Scheme 2). The lipoplex exhibited high gene expression to HepG2 cells, a human hepatocellular carcinoma cell line, but not to A549 cells.

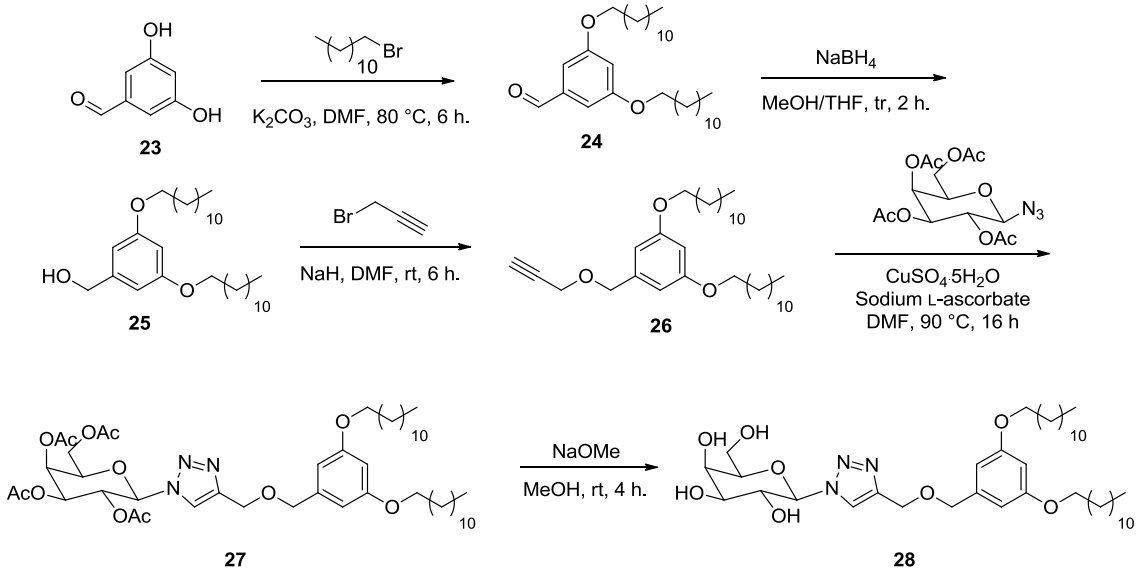

Scheme 2 The synthesis of the cationic galactose-modified lipid (**28**) with aromatic ring by solution-phase method.

Rathore *et al*. [39] synthesized hydrocortisone-conjugated cationic lipid derivatives (**34**) with long chain hydrocarbons containing between 8–6 carbon atoms to selectively induce the toxicity in cancer (e.g. melanoma, breast cancer and lung adenocarcinoma) cells with less toxicity in normal cells, through induction of apoptosis and cell cycle arrest at G2/M phase (Scheme 3).

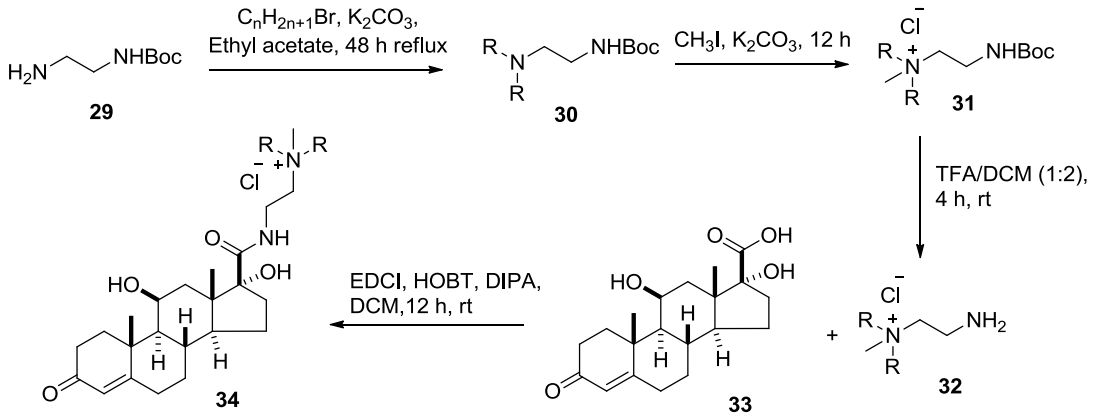

Scheme 3 The synthesis of hydrocortisone-conjugated cationic lipid derivatives (**34**) by solution-phase method.

In the solid-phase synthesis, polymeric solid-supports are employed for binding with the target molecule along the synthetic process. Since the solid-supports are not dissolvable and miscible in the solvent, this strategy allows the separation and purification steps more easier than those in the solution-phase synthesis. The most significant part of the solid-support is linker. The liker is a kind of functional groups coating on the polymer which could be matched to the synthetic compound. After completion of the synthesis, linker will be cleaved by using specific reagents to release the product from the solid support. The cleavage agents must be selective to the specific linker and no harm to any parts of the desired product.

Yingyongnarongkul *et al*. [40] synthesized aminoglycerol-diamine conjugate-based transfection agents containing urea linkage, diverse lengths of diamine headgroups and various lengths of hydrophobic tails by solid-phase synthesis (Scheme 4).

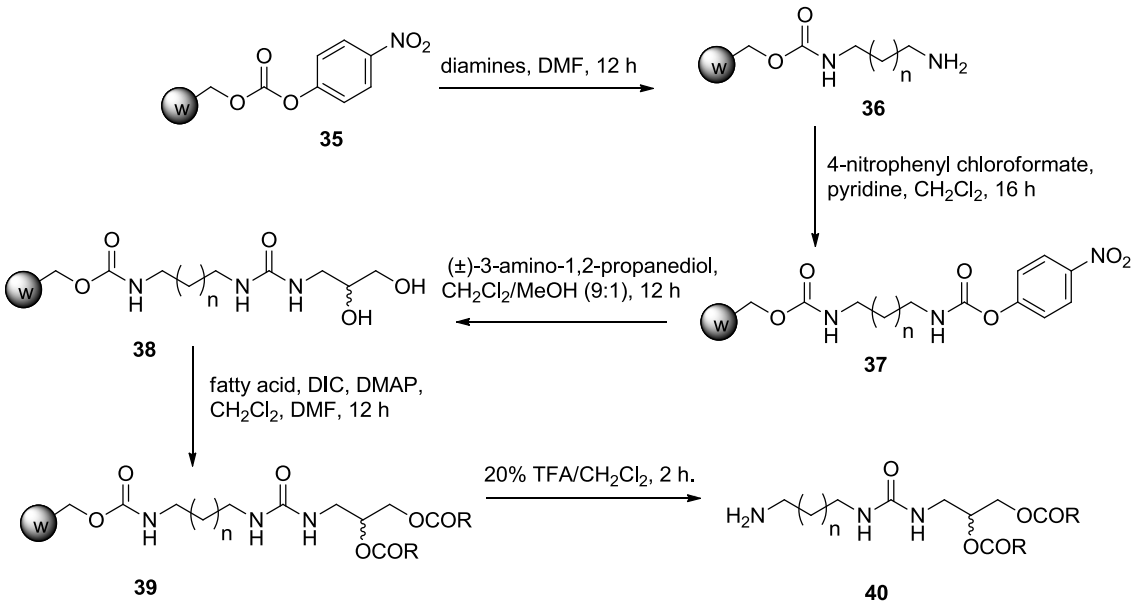

Scheme 4 The synthesis of aminoglycerol-diamine conjugate-based transfection agents by solid-phase method.

Radchatawedchakoon *et al*. [41] synthesized asymmetric divalent head group cholesterol-based cationic lipids by parallel solid-phase method (Scheme 5). The transfection efficiency of the cationic lipids was examined with various type cells. 3β-[*N*-(*N*′-Guanidinyl)-2′-aminoethyl)-*N*-(2-aminoethyl)carbamoyl] cholesterol showed highest transfection efficiency with minimal toxicity.

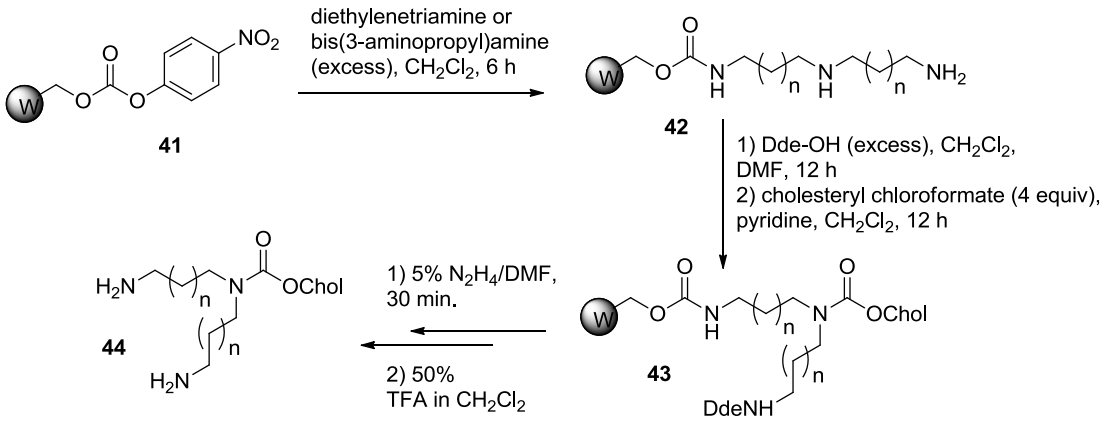

Scheme 5 The synthesis of asymmetric divalent head group cholesterol-based cationic lipids by parallel solid-phase method.

Niyomtham *et al*. [42] synthesized spermine-based cationic lipids by solid-phase method to test the gene delivery into cells (Scheme 6). The liposomes of the lipid containing 3-amino-1,2-dioxypropyl group as the central core structure showed highest transfection activity under serum-free condition and the lipid with 2-amino-1,3-dioxypropyl group as the core structure exhibited highest transfection under 10% serum condition.

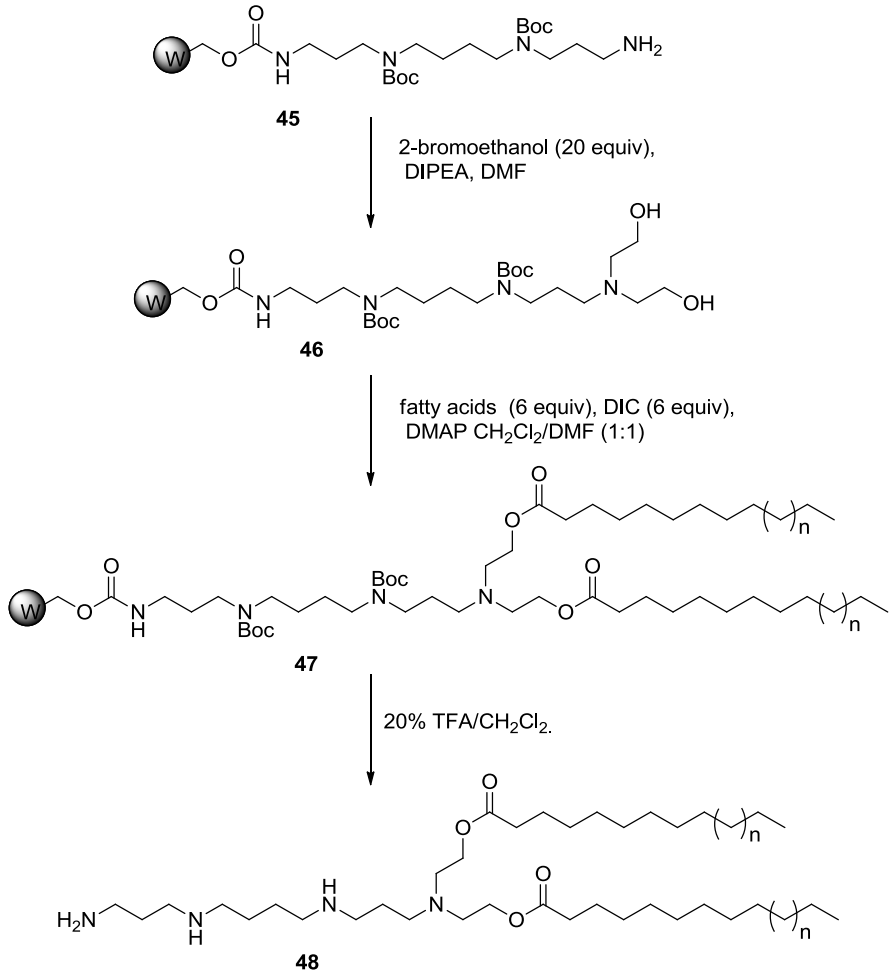

Scheme 6 The synthesis of spermine-based cationic lipid by solid-phase method.

1.4 Helper Lipids

The cationic liposomes have to be in an appropriate form and size in order to achieve the highest effectiveness in human gene therapy. The high transfection efficiency is mostly observed when a cationic lipid is mixed with helper lipids. The liposomes are constructed from helper lipids to improve the stability and transfection efficiency. Dioleoylphosphatidylethanolamine (DOPE) is one of the helper lipids that can promote endosomal to release the genetic material. It has the cone-shape geometry that favors the formation hexagonal II phase. Moreover, cylindrical-shaped lipid, for example phosphatidylcholine, can provide greater bilayer stability. Cholesterol is often used as a helper lipid to improve intercellular delivery as well as lipid nanoparticle (LNs) which is stable *in vivo*. Fatty acids and cholesteryl hemisuccinate (CHEMS) are pH-sensitive anionic helper lipids. They were subjected to trigger low-pH-induced changes in LNP surface charge and destabilization of endosome that can accommodate endosomal release of antisense oligonucleotides (ONs) [43].

ONs are emerging therapeutic modality with potential applications in many human diseases, such as metabolic diseases, infectious diseases, cancer and regenerative medicine. The structure of cationic lipids have been used in LNPs such as 1,2-dioctadecenoyl-3-trimethylammonium-propane (chloride salt) (DOTAP), 1,2-Dioleyl-oxy-3-dimethyamionopopane (DODMA), 1,2-Dillinoleyloxy-3-dimethylaminopropane (DLinDMA) and 2,2-Dilinoleyl-4-dimethylaminoethyl-(1,3)-dioxolane (DLin-KC2-DMA) (Figure 5) [43,44].

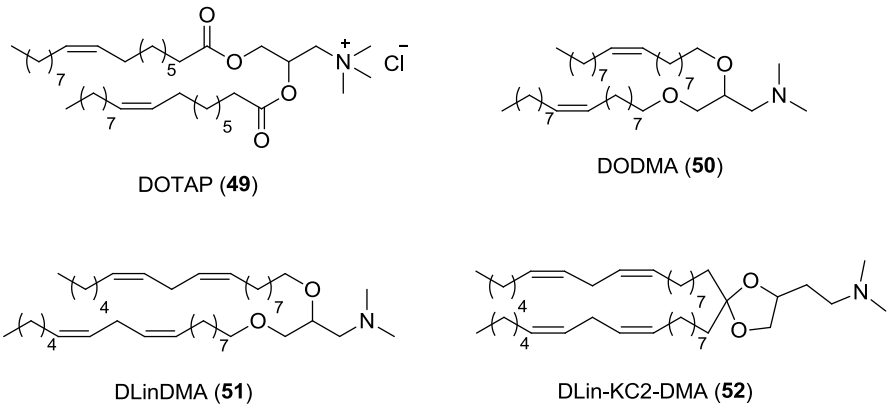

Figure 5 Structures of cationic lipids that have been used in LNPs.

Ojeda *et al*. [45] synthesized cationic amino lipid **53** and studied four different niosome formulations based on the same cationic lipid and non-ionic tensoactive (Figure 6). The pCMS-EGFP plasmids were mixed with niosome to prepare nioplex for gene delivery. The results suggested that the helper lipid composition is a crucial step to be considered in the design of niosome formulation for gene delivery applications since clearly modulates the cellular uptake, internalization mechanism and consequently, the final transfection efficiency.

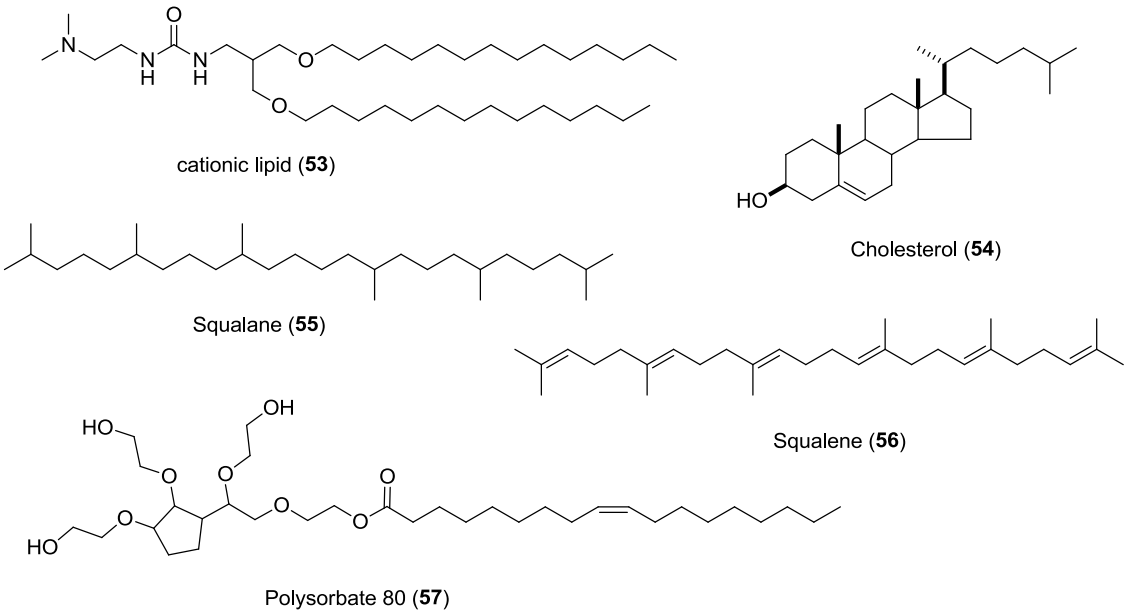

Figure 6 Chemical structures of niosome components.

In 2005, Hirsch-Lerner *et al*. [46] reported the effect of helper lipids on lipoplex electrostatics. They characterized lipoplex based on two commonly used monocationic lipids (DOTAP and DMRIE) and one polycationic lipids (DOSPA) with and without helper lipids (cholesterol or DOPE) (Figure 7). Electrical surface potential and surface pH were examined by several surface pH-sensitive fluorophores attached either to a one-chain lipid (4-heptadecyl hydroxycoumarin (C17HC)) or to the primary amino group of the two-chain lipids (1,2-dioleyl-*sn*-glycero-3-phosphoethanolamine-*N* carboxyfluorescein (CFPE) and 1,2-dioleyl-*sn*-glycero-3-phosphoethanolamine-*N*-7 hydroxycoumarin) (HC-DOPE). The one-chain C17HC comparing with the two-chain

HC-DOPE for monitoring lipoplex electrostatics reveals that both are suitable, as long as there is no serum present in the medium.

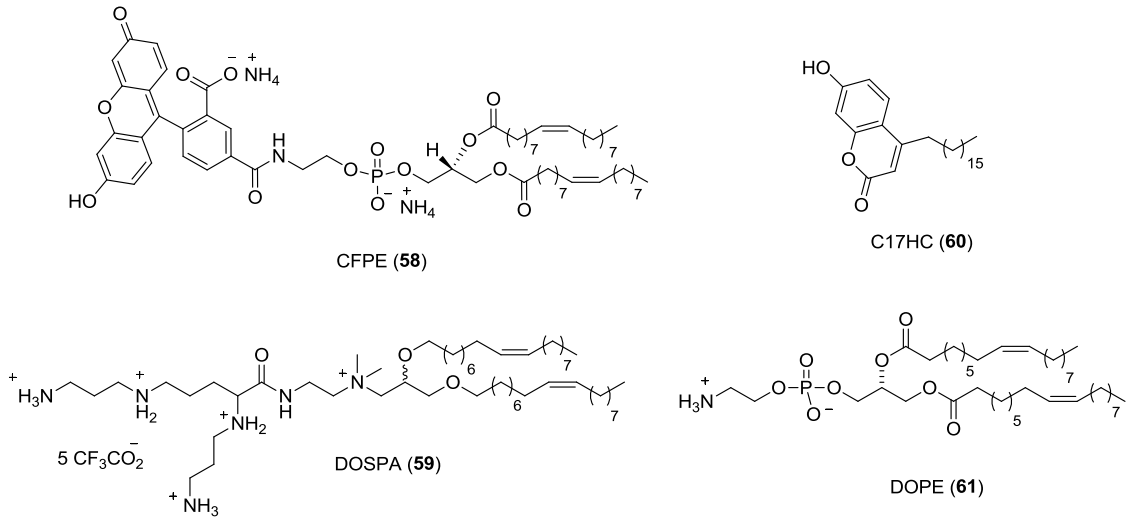

Figure 7 Structures of fluorophores CFPE (**58**) and C17HC (**60**), cationic lipid DOSPA (**59**) and helper lipid DOPE (**61**).

Zheng *et al*. [47] synthesized a novel series of cationic lipids containing *trans*-2-aminocyclohexanol (TACH)-based head groups and hydrocarbon tails moiety which are pH-sensitive conformational switches (“flipids”). The pH-sensitivity can improve the transfection efficiency. The lipoplexes were unified with 1,2-dioleoyl-3-trimethylammonio-propane (DOTAP) and plasmid DNA encoding a luciferase gene (Figure 8).

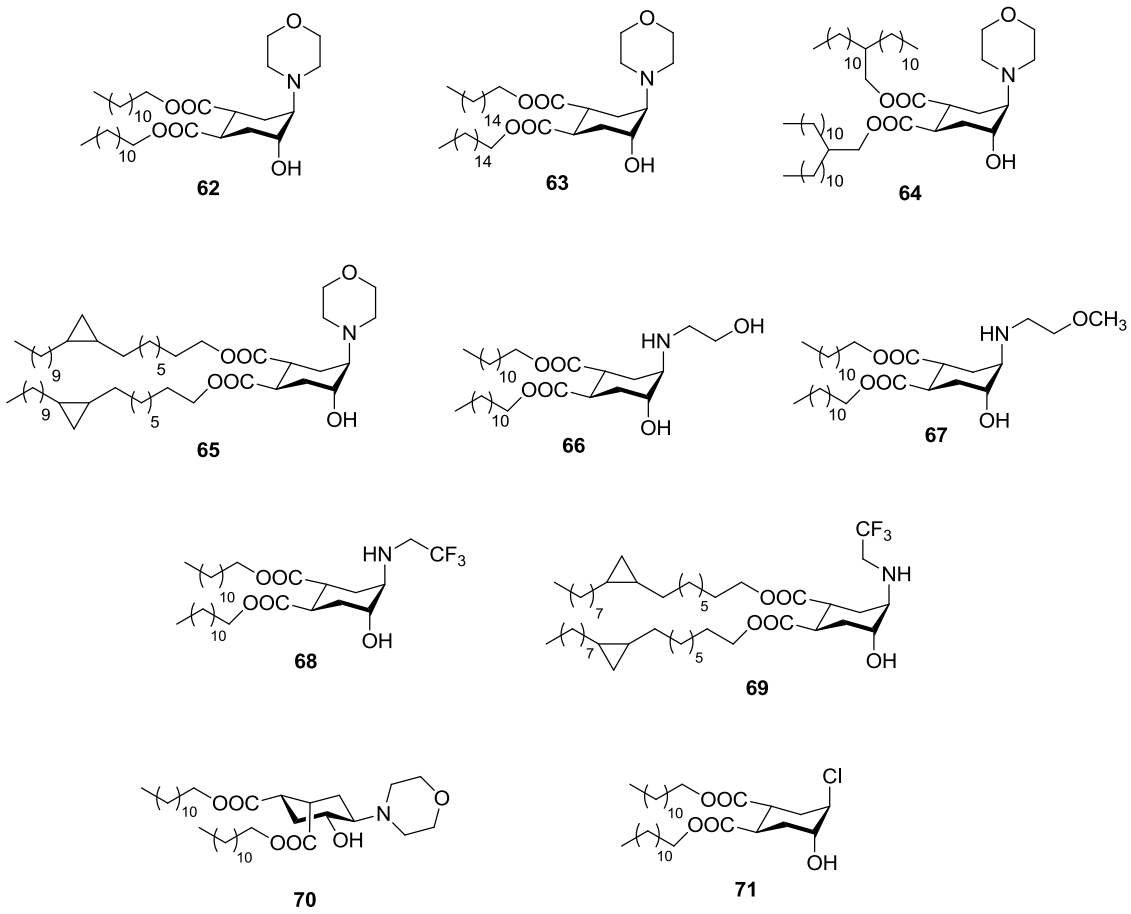

Figure 8 Structures of pH-sensitive helper lipids containing TACH-headgroup **62**–**69**. Non-switchable TACH analogs **70** and **71** were also prepared to be the controls.

Barbeau *et al*. [48] synthesized a novel archaeal tetraether-type lipid containing a diorthoester group as a helper lipid for gene delivery (Figure 9).

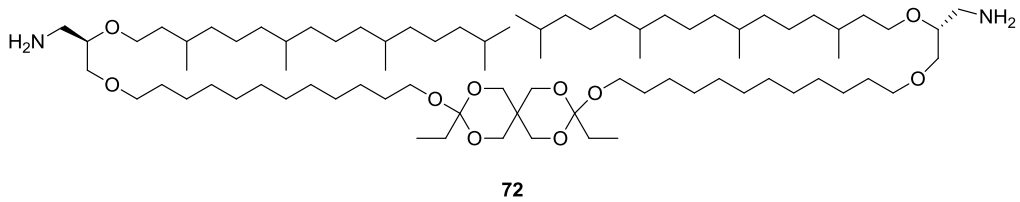

Figure 9 Structure of diorthoester-based tetraether (**72**).

Huang *et al*. [49] designed asymmetrical alkylacyl phosphatidylcholines (APC) as helper lipids for non-viral gene delivery. The fusogenicity of APC depends on the length and degree of saturation of the alkyl chain. The APC mediated high *in vitro* transfection efficiency, and had low cytotoxicity (Figure 10).

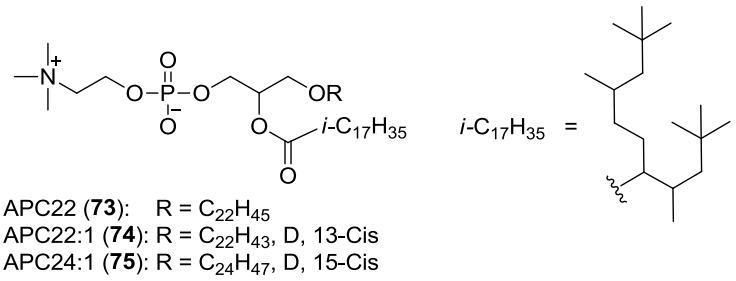

Figure 10 Structures of asymmetrical alkylacyl phosphatidylcholines (APC) derivatives.

CHAPTER 2

LITERATURE REVIEW

Aberle *et al*. [50] synthesized the tetraester-containing cationic lipids with dimyristoyl (**76**) and dioleoyl (**77**) hydrophobic tails from diesterification and amine quaternization (Figure 11). The synthesized lipids exhibited the transfection activity (luciferase) compared to the well-known lipids, DOTAP and DC-cholesterol, in NIH 3T3 and 16HBE14o– cells. The result from cell proliferation (MTS assay) revealed that the lipids showed no toxicity to NIH 3T3 cells and a slightly decrease of the toxicity in 16HBE14o– cells relative to DC-cholesterol. This result was also confirmed by using phase-contrast microscopy involved the expression of green fluorescent protein (GFP) in both cell lines.

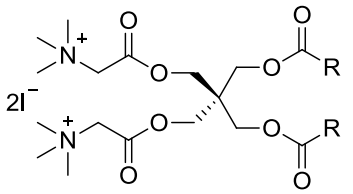

76: [DMTM(Gly)] R = $(CH_2)_{12}CH_3$
77: [DOTM(Gly)] R = (*Z*)-$(CH_2)_7C{=}C(CH_2)_7CH_3$

Figure 1 Structures of dimyristoyl and dioleoyl analogues.

Ren and Liu [51] reported that DOTMA, a diether-linked cationic lipid, possess a higher *in vivo* transfection activity than the lipid containing diester moiety. Moreover lipid **78a** also provided a better transfection activity than its diester derivatives with different hydrophobic domain and variable length of backbone. Thus, quaternary ammonium lipids **78b**–**d** containing butane and hexane backbone and diether linkages were synthesized in order to modified the length of linker between the headgroup and the hydrophobic (Figure 12).

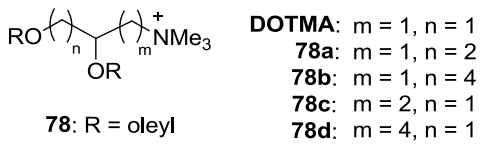

Figure 2 Structures of quaternary ammonium lipids.

Frederic *et al*. [52] modified lipopolyamines by introducing guanidine and cyclic guanidine moieties into the structures for study the gene delivery properties. The lipid-containing cyclic guanidine was used as a model compound specific to the active site of ribonuclease. Thus, lipopolyamine-guanidines (**79** and **81**) and lipopolyamine-cyclicguanidines (**80** and **82**) were synthesized. They also expanded the synthesis by vary the ring size of cyclic guanidine and the core structure of lipopolyamines by preparing lipids **83**–**85** (Figure 13).

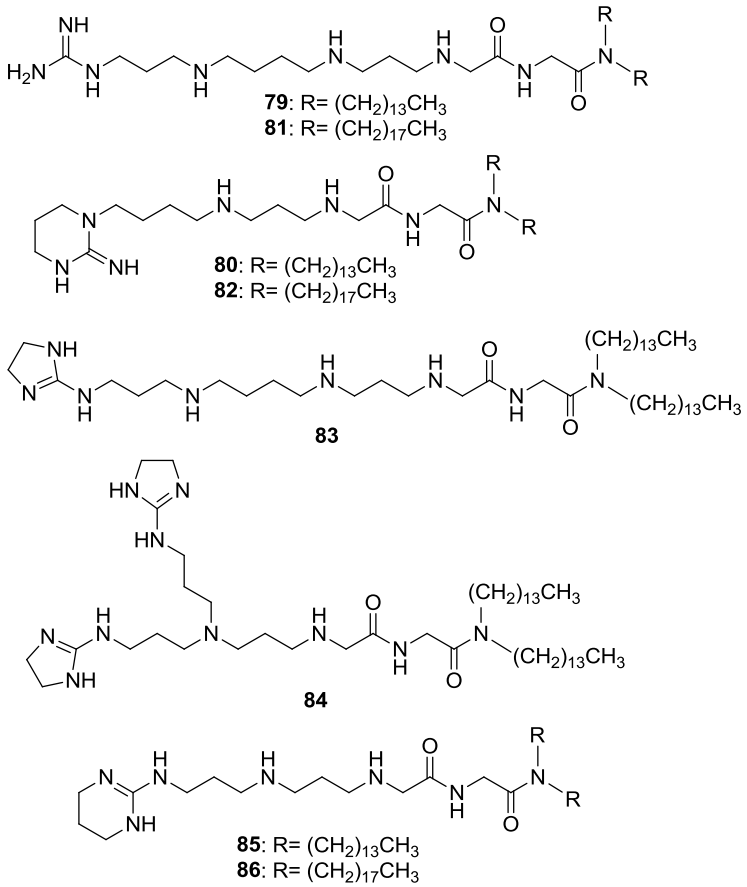

Figure 3 Structural modifications of lipopolyamines.

Bianco *et al*. [53] improved DC-chol (**87**) for preparation of liposome to be used in gene therapy (Figure 14). The literature described the synthetic DC-chol on the treatment of cholesterol with phosgene derivatives that they get the final product overall yield of 21%. Thus, they proposed Curtius reaction to improve synthesis of DC-Chol. The yield of improved method of DC-Chol cationic lipid was 92% and the total yield was about 74%.

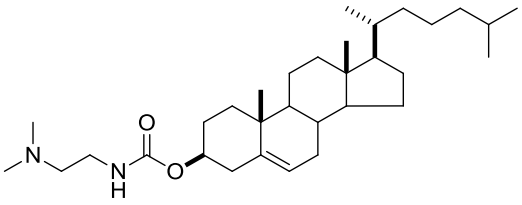

DC-Cholesterol (**87**)

Figure 4 Structure of DC-cholesterol cationic lipid.

Mukerherjee *et al*. [54] improved gene transfer properties to a novel series of cationic lipid **88a**-**e** by act in synergy of co-lipids DOPE, cholesterol and DOPC (Figure 15). They used a novel series of non-glycerol backbone based cationic lipid with 2-hydroxyethyl and 2-aminoethyl polar head-group. They found that DOPE, cholesterol and DOPC which were commonly used as co-lipids can act as synergies providing high gene delivery efficiency.

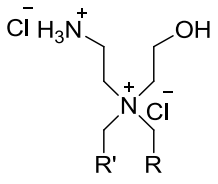

88

88a: R = R' = $C_{13}H_{27}$
88b: R = R' = $C_{15}H_{31}$
88c: R = R' = $C_{17}H_{35}$
88d: R = $C_{13}H_{27}$, R' = $C_{17}H_{33}$ (oleyl)
88e: R = R' = $C_{13}H_{33}$ (oleyl)

Figure 5 Structures of cationic lipids **88a**–**e**.

Ilies *et al*. [55] synthesized cationic lipids to compare the cellular toxicity and transfection efficiency between pyridinium polar head versus the tetramethylammonium in several tumor cell lines. The compound 1-(2,3-dioleoyloxypropyl)-2,4,6-trimethylpyridinium lipid **89Oc** was mixed with different helper lipids in various molar ratios to test with its ammonium congener DOTAP for the transfection. The formulated with cholesterol at 1:1 molar ratio, the pyridinium lipid **89Oc** was able to transfect several cancer cell lines with similar or better efficiency than its tetraalkylammonium congener DOTAP. *In vivo*, the lipid **89Oc** and DOTAP-based lipoplexes were tested with mice by injected intratumoral. Moreover, the red fluorescent protein reporter showed that the pyridinium cationic lipid provided higher efficiency in the transfecting the tissue on a higher area (Figure 16).

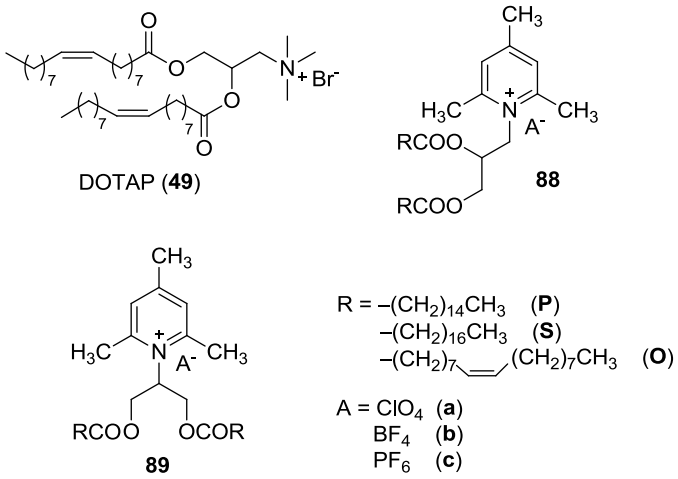

Figure 6 Structures of cationic lipids **89**–**90.**

Kim *et al.* [56] synthesized two different cationic lipids which consist of lysine polar head, two C-14 hydrocarbon chains, and either aspartatic acid or glutamic acid as core structures, **DMKD** (**91**) and **DMKE** (**92**) (Figure 17). Cationic liposomes were constructed with lipids DMKD and DMKE and DOPE and test for gene-transferring capabilities on various cell lines. They found that the order of *in vitro* gene transfection efficiency was **DMKE** (**92**) ≥ **DMKD** (**91**) > DOTAP. In addition, lipids **DMKE** (**92**) and **DMKD** (**91**) were assayed with *in vivo* by intravenously administered their exhibited different biodistribution characteristics. **DMKE** (**92**) lipoplexes were able to

induce more efficient transgene expression in tumor tissues than the DOTAP and **DMKD** (**91**) lipoplexes.

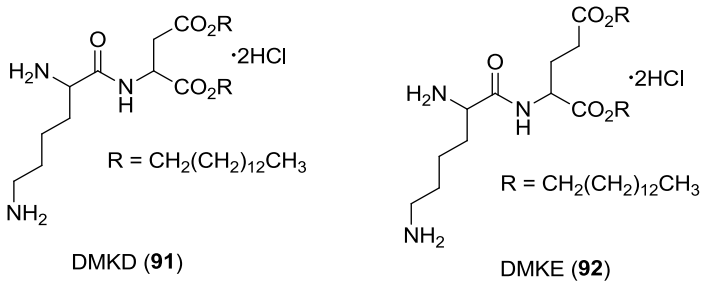

Figure 7 Structures of cationic lipids with lysine polar head.

Pual *et al*. [57] synthesized seven dimeric cationic lipids containing aromatic anchor between hydrocarbon chains and cationic headgroup. These lipids were examined the DNA binding properties and complexity by gel electrophoresis (Figure 18).

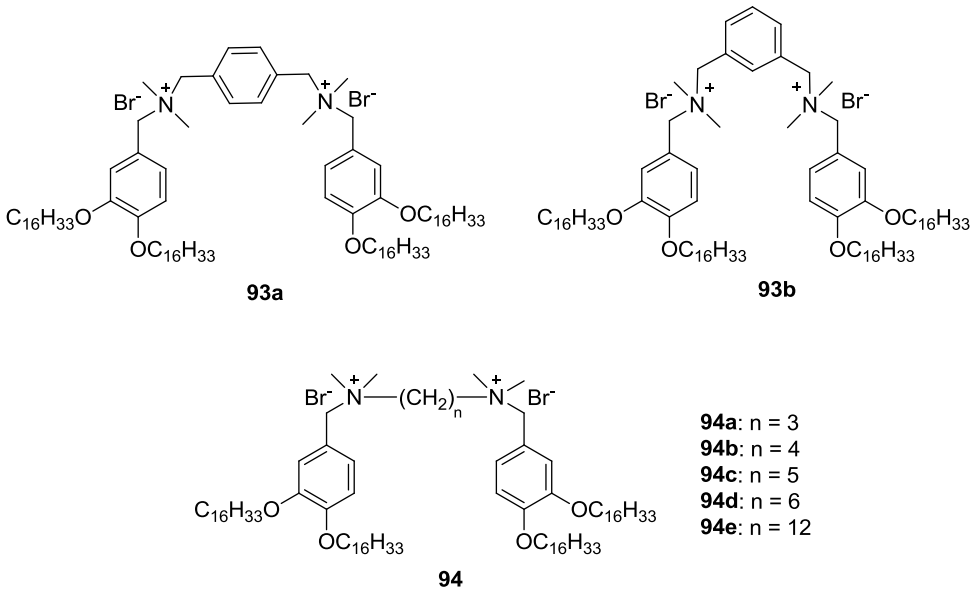

Figure 8 Structures of dimeric cationic lipids containing aromatic anchor between hydrocarbon chains and cationic headgroup.

Spolios *et al*. [58] investigated the transfection activity and physicochemical properties of the cationic lipids **95**–**97** having dimyristoyl tails (Figure 19). Two of the derivatives were established as isomers with the same headgroup and hydrophobic tails and the difference in linkages as diaminopropanol moieties. Another lipid was designed with a hydrophilic region containing only a single ionizable amine group. The physical studies such as pKa determination, Langmuir monolayer studies, fluorescence anisotropy, gel electrophoresis mobility shift assay, ethidium bromide displacement assay, particle size distribution, and zeta potential were tested. Physicochemical characterization that a symmetric bivalent was shown for high transfection activity.

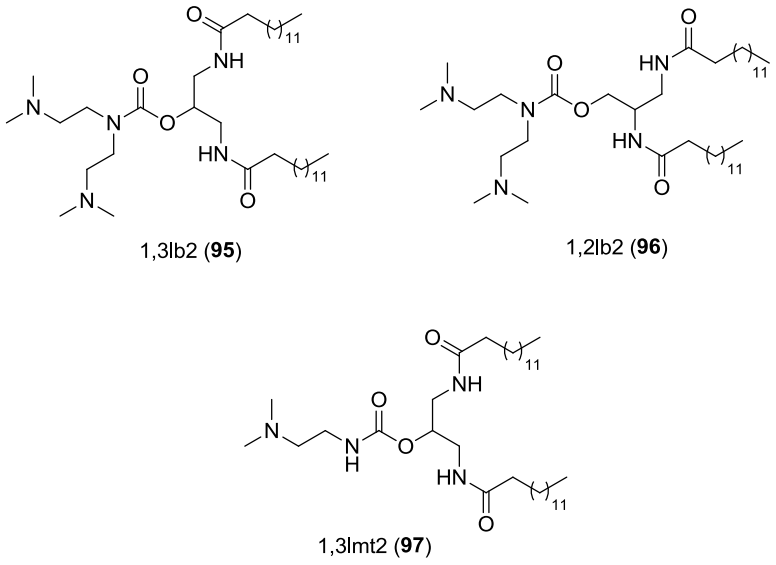

Figure 9 Structures of novel series of double-chained tertiary cationic lipids.

Cardiolipin mimicking gemini lipid analogues **98**–**101** were synthesized by Bajaj *et al.* [59] with variation of length and hydrophilicity of the spacer to study the structure-activity relationship. Gemini lipids **100**–**101** bearing an oxyethylene spacer provided the transfection efficiency greater than the lipids containing polymethylene spacer. Interestingly, the major characteristic of the gemini lipids is the compatibility in the serum system (Figure 20).

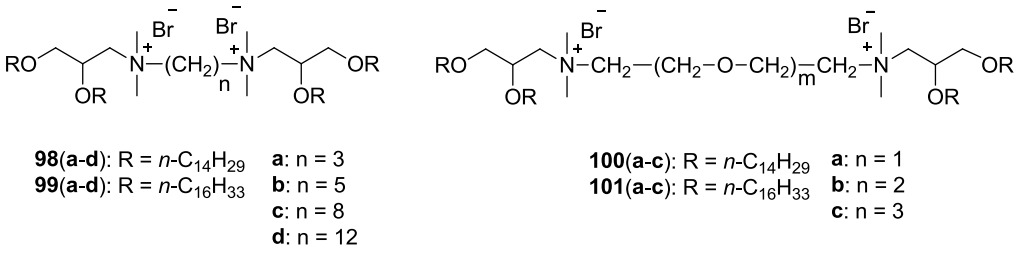

Figure 10 Structures of cardiolipin mimicking gemini lipid analogues.

Bajaj *et al*. [60] synthesized eight cholesterol based cationic lipids **102**–**109** with difference headgroups having ether linkage (Figure 21). The transfection efficiency were examined in the absence and presence of serum. They found that the transfection activity depend on the nature of the headgroup. The lipid **108** bearing 4-*N*,*N*′-dimethylaminopyridine (DMAP) as a headgroup showed the highest transfection efficiency in the presence of serum. The DNA binding abilities were revealed upon the headgroup of the cholesteryl lipid. The cytotoxicity showed that the positive charge decreased the cell viability of the cationic lipid formations.

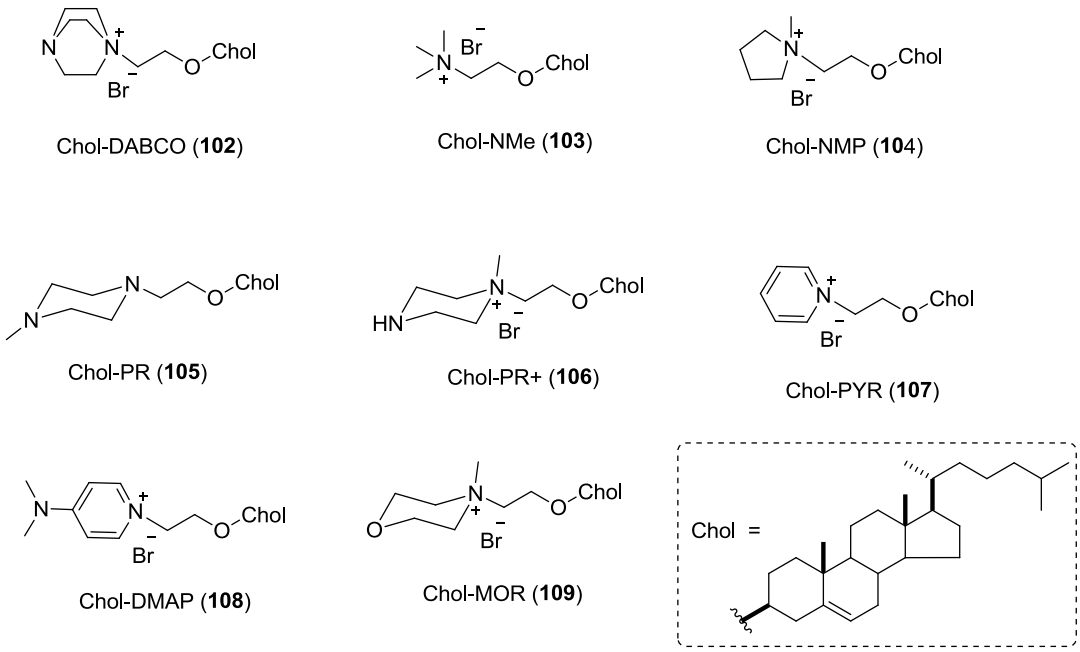

Figure 11 Structures of eight cholesterol based cationic lipids different in the headgroup.

Zhu *et al*. [61] synthesized a series of pyridine lipids containing a heterocyclic ring and a nitrogen atom and examined the structure-activity relationship for gene delivery (Figure 22). The liposomes were prepared by mixing a co-lipid such as L-α-dioleoylphosphatidylethanolamine (DOPE) and cholesterol (Chol). The lipoplexes were prepared by mixing between liposome and plasmid DNA encoding enhanced green fluorescent protein (pCMS-EGFP) or luciferase (pcDNA-3-Luc). Pyridinium lipids with amide linker exhibited significantly higher transfection efficiency compared to ester counterparts. The liposomes prepared from pyridinium lipids and co-lipids at 1:1 molar ratio were used to generated the lipoplexes (liposomes/plasmid DNA = 3:1). The resulting lipoplexes exhibited high transfection activity. The pyridinium liposomes based on a hydrophobic anchor chain length of 16 showed high transfection efficiency and low cytotoxicity. The structural trans-configuration of double bond in the fatty acid revealed higher transfection efficiency than its counterpart with cis-configuration at the same fatty acid chain length. The lipid **C16:0** and Lipofectamine significantly decreased transfection activity under 30% serum condition while C16:1 *trans*-isomer still had high transfection efficiency under this condition.

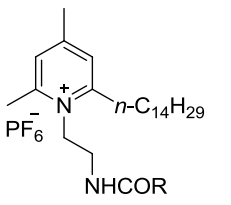

110(**a**-**j**)

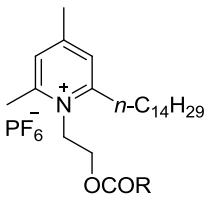

111(**k**-**o**)

a, **k**; R= —$CH_2(CH_2)_{11}CH_3$ (14:0)

b, **m**; R= —$CH_2(CH_2)_{13}CH_3$ (16:0)

c; R= —$CH_2(CH_2)_6CH{=}CH(CH)_5CH_3$ (16:1 *cis*-9)

d; R= —$CH_2(CH_2)_6CH{=}CH(CH)_5CH_3$ (16:1 *trans*-9)

e, **n**; R= —$CH_2(CH_2)_{15}CH_3$ (18:0)

f, **o**; R= —$CH_2(CH_2)_6CH{=}CH(CH)_7CH_3$ (18:1 *cis*-9)

g; R= —$CH_2(CH_2)_6CH{=}CH(CH)_7CH_3$ (18:1 *trans*-9)

h; R= —$CH_2(CH_2)_8CH{=}CH(CH)_7CH_3$ (20:1 *cis*-11)

i; R= —$CH_2(CH_2)_8CH{=}CH(CH)_7CH_3$ (20:1 *trans*-11)

l; R= —$CH_2(CH_2)_{12}CH_3$ (15:0)

j; R= —$HC(CH_2(CH_2)_5CH_3)(CH_2(CH_2)_7CH_3)$ (18 branch)

Figure 12 Structures of a series of pyridine lipids.

Rajesh *et al*. [62] have designed and synthesized two structurally isomeric amphiphiles **112** and **113** (Figure 23). The only structural difference between lipid **112** and **113** is the orientation of their linker ester functionality. Lipid **112** showed high transfection in multiple cultured animal cells, lipid **113** did not show transfection efficiency. Findings have indicated that a structural variation as linker orientation reversal in cationic amphiphiles can profoundly influence DNA-binding characteristics, membrane rigidity, membrane fusibility, cellular uptake, and consequently gene delivery efficacies of cationic liposomes.

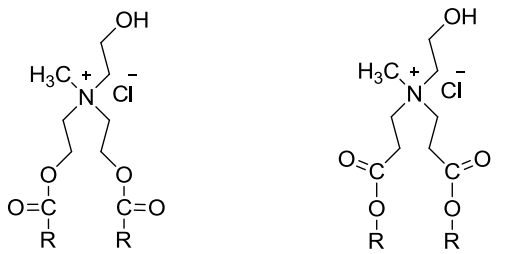

Figure 13 Structures of isomeric remarkable similar amphiles.

Randazzo *et al*. [63] synthesized cholic acid cationic lipids analogs. Four monosubstituted spermines (**114**–**117**) and a bis-substituted spermine (**118**) were tested as gene transfer agents, bacteriostatic agents, and bactericidal agents (Figure 24). The double bond in the sterol moiety increased transfection efficiency significantly. These compounds showed no effect of increasing bactericidal activity with increasing sterol hydrophobicity. The bis- substituted compound **118** showed minimum inhibitor concentrations (MIC) (4 μM against *Bacillus subtilis* and 16 μM against *Escherichia coli*) and therapeutic indexes (minimum hemolytic concentration/minimum inhibitory concentration) of 61 and 15, respectively.

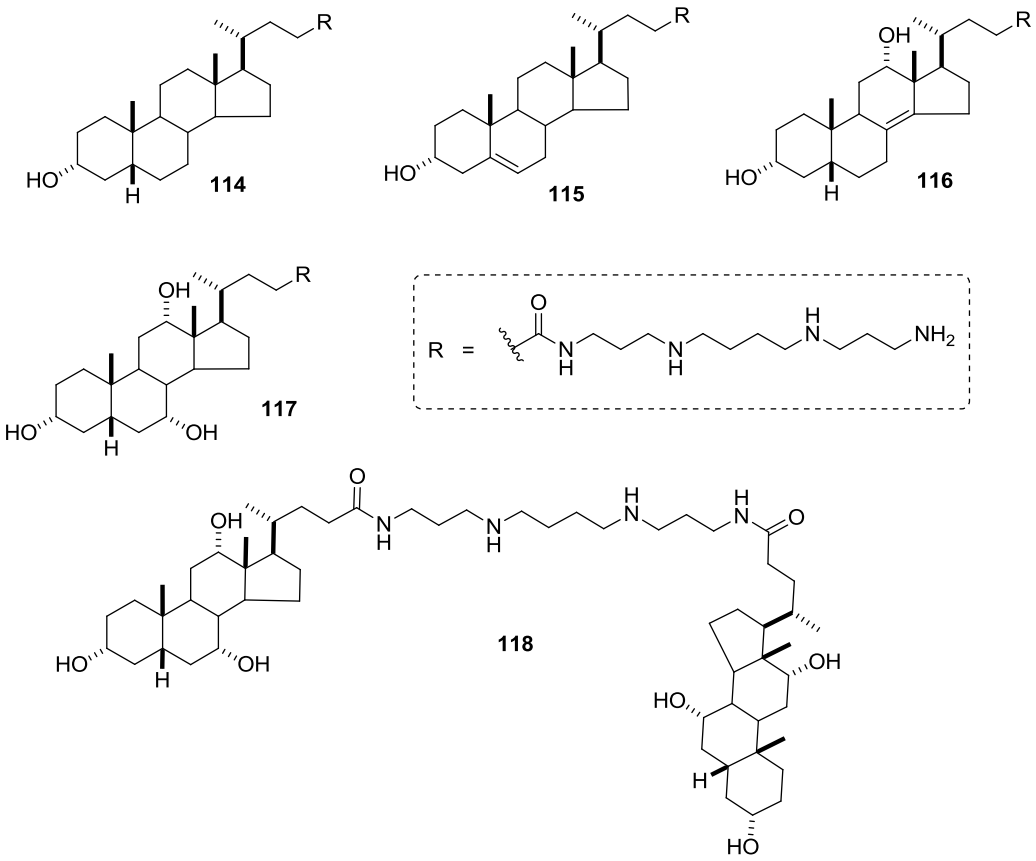

Figure 14 Structures of cholic acid analogs cationic lipids.

Obeta *et al*. [64] synthesized the cationic amino acid-based lipids **119**–**121** to examine the influence of the spacer on liposome gene delivery (Figure 25). A hydrophobic spacer with a hydrocarbon chain composed of 0, 3, 5, 7, or 11 carbons, and a hydrophilic spacer with an oxyethylene chain (10 carbon and 3 oxygen molecules) were considered. The zeta potentials and cellular uptake efficiency of the cationic liposome were almost equivalent.

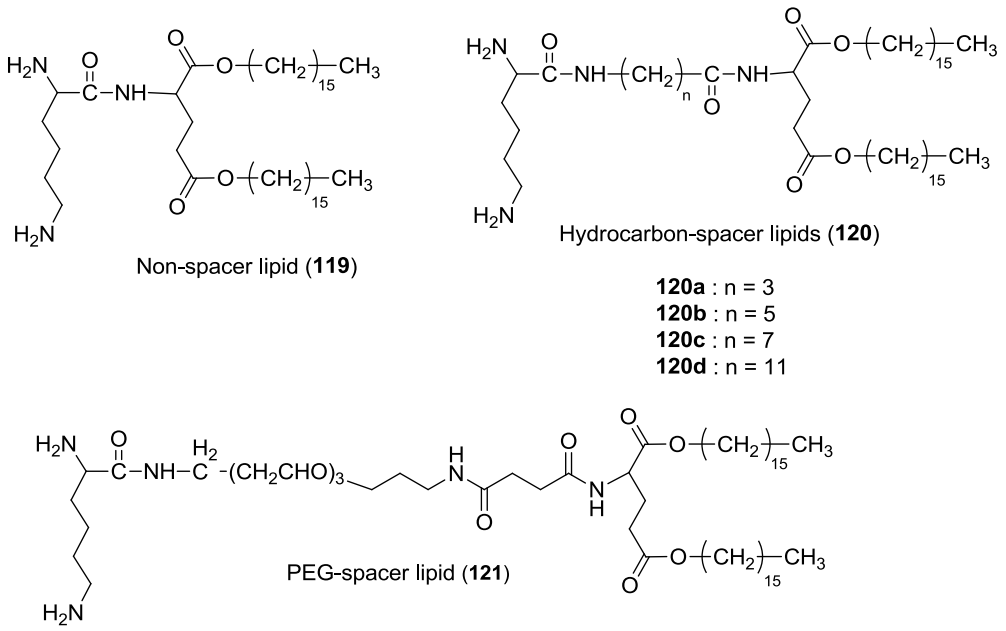

Figure 15 Structures of a series of cationic amino acid-based lipids.

Mével *et al*. [65] synthesized the novel cationic lipids **122**–**125** including cholesteryl moieties linked to guanidinium group and also cationic lipids comprising a dialkylglycylamide moiety conjugated with a polyamine or a guanidinium group (Figure 26). The liposomes were prepared with the neutral co-lipid dioleoyl-L-α-phosphatidylethanolamine (DOPE) or with neutral lipophosphoramidate derivative of histamine (MM27). The cationic lipid *N*′,*N*′-dioctadecyl-*N*-4,8-diaza-10-aminodecanoylglycine amide (DODAG) formulated with DOPE showed the highest transfection *in vitro* in all three different cell lines studied (OVCAR-3, IGROV-1 and HeLa) both in the presence or absence of serum. DODAG form lipoplex with small interfering RNA (siRNA) which is able to mediate the delivery of anti-hepatitis B virus (HBV) with low liver toxicity and immune stimulation.

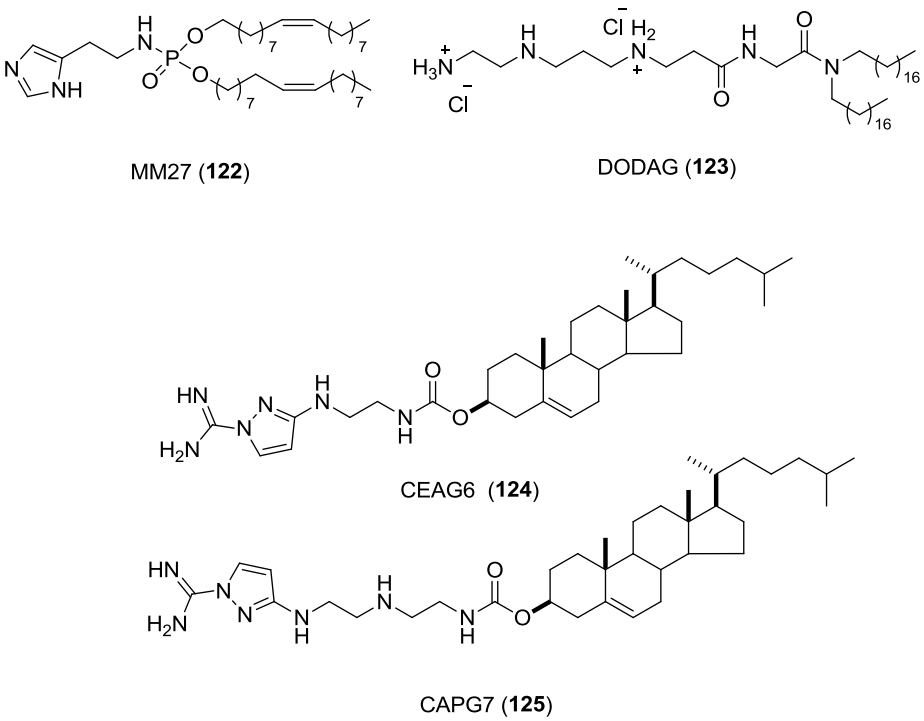

Figure 16 Structures of novel cationic lipids including of cholesteryl-moieties linked to guanidinium group and a dialkylglycylamide moiety conjugated with a polyamine or a guanidinium group.

Gall *et al*. [66] synthesized and studied a novel lipophosphoramidate derivative with an arsonium headgroup, a phosphoramidate linker and two diunsaturated linoleic chains. The specific fluidity and fusogenicity properties of the liposomes were examined for the physicochemical studies. The complexes showed a remarkably efficiency to transfect mouse lung. The diunsaturated showed higher transfection level than a monosaturated analogue. This diunsaturated cationic lipophosphoramidate established an efficient and versatile non-viral vector for gene transfection (Figure 27).

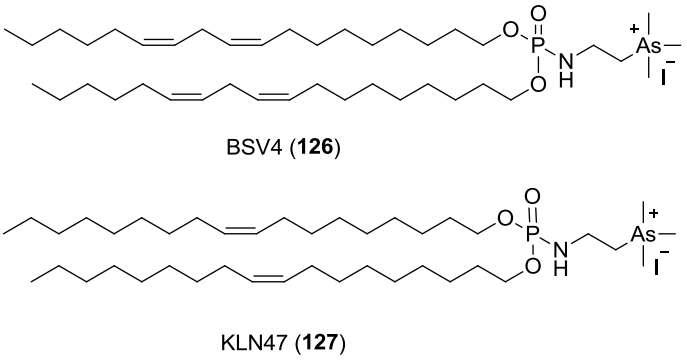

Figure 17 Structures of a novel lipophosphoramidate derivative.

Maslov *et al*. [67] synthesized the cationic lipid **128**–**131** containing pyridinium, *N*-methylimidazolium, *N*-methylmorpholinium, and *N*-methylpiper-idinium headgroup linked via β-glucosyl spacer and cholesterol hydrophobic tails (Figure 28). The cytotoxicity of the synthesized lipids was examined and has IC_{50} value in the range of 20–35 μM. Moreover, the liposomal formulations with DOPE (1:1) were found to be significantly less toxic and provided the accumulation of FITC-labeled nucleotide in cells. The cationic liposomes can transfer siRNA into the cells and the lipid **130d** formulated with DOPE provided the most EGFP expression both in the presence and absence of serum.

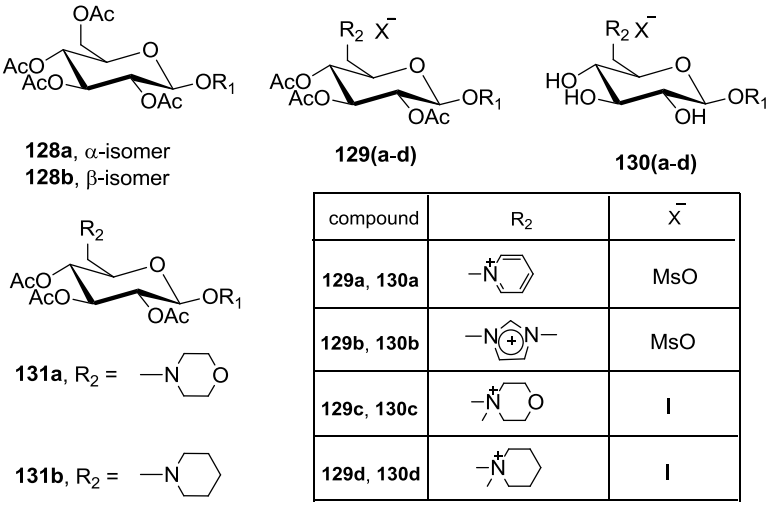

compound	R_2	X^-
129a, **130a**		MsO
129b, **130b**		MsO
129c, **130c**		I
129d, **130d**		I

Figure 18 Structures of the cationic lipids containing headgroup (pyridinium, *N*-methylimidazolium, *N*-methylmorpholinium, and *N*-methylpiperidinium).

Li *et al*. [68] synthesized linear cyclen (**133a**–**c**) and cross-linked cyclen (**136a**–**d**) polymers containing 1,4,7,10-tetraazacyclododecane and ester or disulfide bonds via ring-opening polymerization from various diol glycidyl ethers (Figure 29). The molecular weights of the synthesized polymers, retardation assays and the degradation of the polymers were examined. The polymers can be formed polyplexes with DNA which provided appropriate sizes around 400 nm and zeta-potential values in the ranged of 15–40 mV. MTT assay revealed that polymers **136** has the cytotoxicity lower than that of polyethyleneimine (PEI, 25 kDa), a non-viral cationic gene carrier. **136c**/DNA polyplex (weight ratio of 4) exhibited the transfection efficiency to A549 and 293 cells close to that of 25 kDa PEI. Moreover, it has been found that the transfection efficiency of **136** in the presence of serum could be improved by adding chloroquine or Ca^{2+} to the pretreated cells.

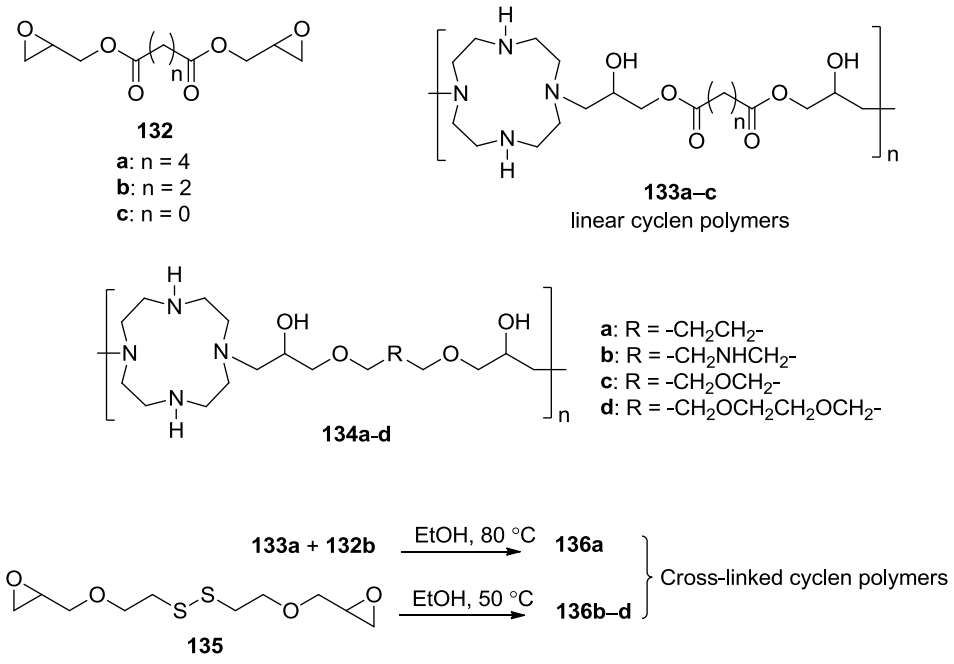

Figure 19 Structures of 1,4,7,10-tetraazacyclododecane (cyclen)-based linear (**133a**–**c**) and cross-linked (**136a**–**d**).

Huang *et al*. [69] synthesized two novel protonated cyclen and imidazolium salt-containing cationic lipids **137**–**139** that are different in only the hydrophobic region (cholesterol or deasgenin) for gene delivery (Figure 30). The liposomes were easily prepared from each of lipid and the mixture of the lipid with dioleoylphosphatidyl ethanolamine (DOPE). The amphiphilic molecule demonstrated to bind and compact DNA to form nanometer particles that could be used as non-viral gene delivery. *In vitro* transfection showed two cationic lipids with DOPE can induce effective gene transfection in HEK293 cells. In addition, two cationic lipids were sensibly increased in the presence of calcium ion (Ca^{2+}). The cytotoxic had different for two cationic lipids and this study demonstrated that the little cationic lipids have potential to be efficient non-viral gene vector.

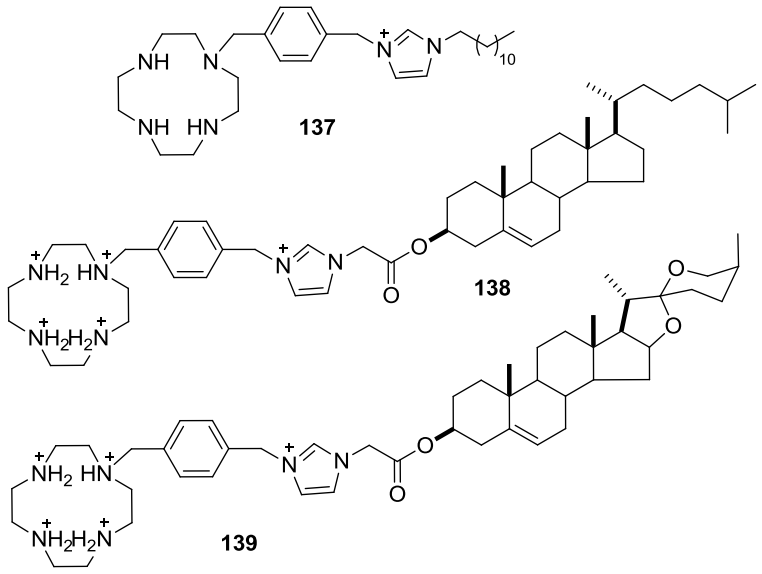

Figure 20 Structures of novel protonated cyclen and inidazolium salt-containing cationic lipids.

Lui *et al*. [70] have designed and synthesized cationic lipids **140**–**142** that bearing protonated cyclen and different hydrophobic group (cholesterol, dodecanol or diosgenin) as non-viral vecters (Figure 31). Their liposomes were easily prepared by mixing the synthesized lipids with dioleoylphosphatidyl ethanolamine (DOPE) under suitable mole ratios. The liposome could retard pDNA at N/P ratio of 3 and formed lipoplexes with sizes around 200–300 nm and zeta-potential values of +20–50 mV at N/P ratio from 4 to 10. *In vitro* transfection toward HEK 293T and A549 cell lines showed that DOPE/DNA lipoplex at an N/P ratio of 6 and lipid/DOPE mole ratio of 1:2 provided the transfection efficiency slightly higher than that of Lipofectamine 2000.

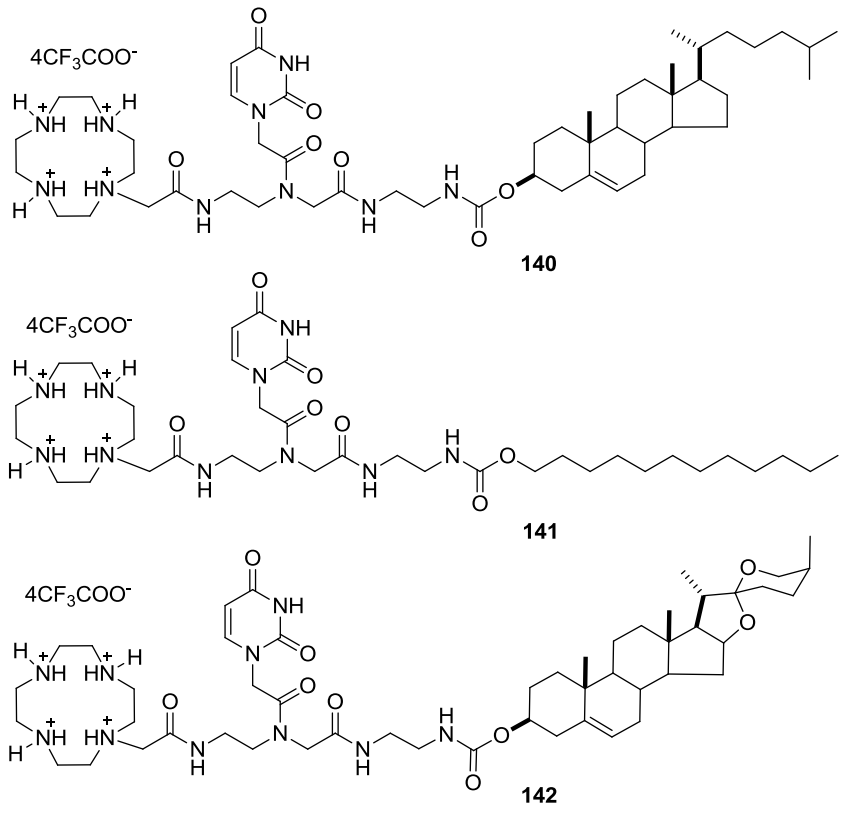

Figure 21 Structures of cationic lipids that bearing protonated cyclen and different hydrophobic group.

Øpstad *et al*. [71] synthesized a new class of cationic phospholipids with a highly unsaturated conjugated fatty acid (**143**) as shown in Figure 32. The lipoplexes were prepared by employing 1,2-dioleoyl-*sn*-glycero-3-phosphoethanolamine (DOPE) as helper lipid with and without the polycationic peptide protamine, together with a plasmid DNA (pDNA). The novel unsaturated lipid exhibited pDNA binding and protection from DNase I degradation. The transfection efficiency of the new lipid showed comparable gene transfer with a commercial reference, 1,2-dimyristoyl-sn-glycero-3-ethylphophocholine (EPC), and also performed equally to the Lipofectamine2000.

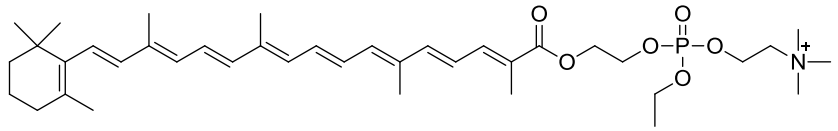

C30-2 (**143**)

Figure 22 Structure of a highly unsaturated conjugated fatty acid.

Sheng *et al*. [72] have prepared a series of new sterol-based cationic lipids (**144**–**147**) through an efficient 'Click' chemistry approach (Figure 33). The pDNA binding ability of these lipids was examined by gel electrophoresis. The average particle sizes and surface charges of cationic lipid/pDNA lipoplexes were determined by dynamic laser light scattering instrument (DLS), the morphologies of the lipoplexes were analyzed by atomic force microscopy (AFM). MTT and LDH assay were verified the toxic of the cationic lipid and the transfection efficiency which was investigated by luciferase gene expression in various cells. The structural factors including sterol-skeletons and headgroup have effected to the pDNA loading capacity, lipoplex particle size, zeta potential and morphology of the sterol lipids/pDNA lipoplexes. Interestingly, they found that the cholesterol-bearing lipids **144** and **145** showed higher transfection capability than lithocholate-bearing lipids **146** and **147** in A549 and HeLa cell lines. They have developed the low cytotoxic and high efficient lipid by selecting appropriate sterol hydrophobic and cationic headgroup.

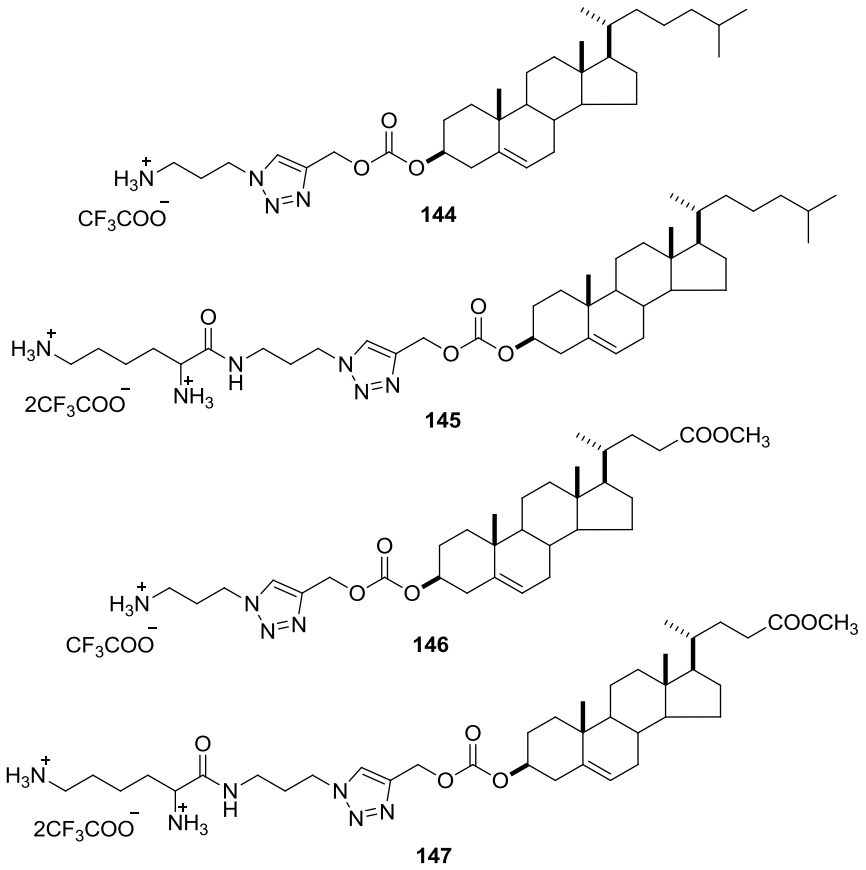

Figure 23 Structures of a series of new sterol-based cationic lipid.

Kedika *et al*. [73] synthesized benzothiazol-based lipids (**148a–j**) containing different derivatives of benzothiazole headgroup to determine the structure-activity relationship for gene delivery (Figure 34). The lipoplexes were prepared by mixing between cationic lipid and plasmid DNA encoding green fluorescent protein (a5GFP) or β-galactosidase (pCMV-SPORT-b-gal) and transfected into B16F10 (Human melanoma cancer cells), CHO (Chinese hamster ovary), A-549 (Human lung carcinoma cells) and MCF-7 (Human breast carcinoma cells) cell lines. The results showed that lipids **148i** and **148j** exhibited comparable gene delivery to that of Lipofectamine2000. The benzothiazole headgroup has the potential to be used transfection reagents for *in vitro* and *in vivo* applications.

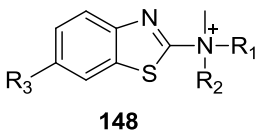

a: $R_1,R_2 = C_{16}H_{33}$; $R_3 = H$
b: $R_1,R_2 = C_{18}H_{37}$; $R_3 = H$
c: $R_1,R_2 = C_{16}H_{33}$; $R_3 = OCH_3$
d: $R_1,R_2 = C_{18}H_{37}$; $R_3 = OCH_3$
e: $R_1,R_2 = C_{16}H_{33}$; $R_3 = OH$
f: $R_1,R_2 = C_{18}H_{37}$; $R_3 = OH$
g: $R_1,R_2 = C_{16}H_{33}$; $R_3 = NO_2$
h: $R_1,R_2 = C_{18}H_{37}$; $R_3 = NO_2$
i: $R_1,R_2 = C_{16}H_{33}$; $R_3 = NH_2$
j: $R_1,R_2 = C_{18}H_{37}$; $R_3 = NH_2$

Figure 24 Structures of benzothiazole-based lipids.

Shang *et al*. [74] have prepared a series of cholesterol-based cationic (Cho-cat) lipid containing cholesterol as a tail, natural amino acid headgroup (lysine/histidine) and carbonate ester and ether linkgages. The lipids carrying L-lysine headgroup (**149** and **151**) were demonstrated higher pDNA binding affinity and higher surface charge lipoplexes than of L-histidine headgroup bearing lipids (**150** and **152**). The structure-activity relationship of cholesterol based cationic lipid was enhanced by the simple modification of suitable headgroups on lipid gene carriers (Figure 35).

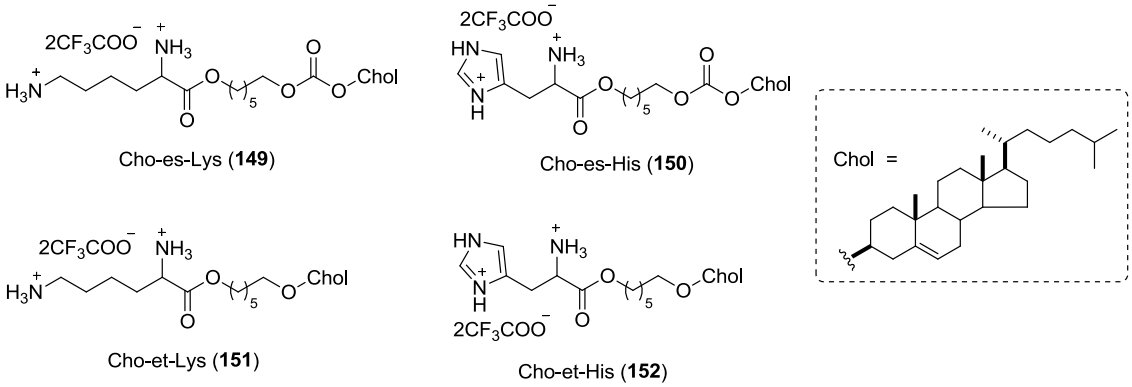

Figure 25 Structures of a series of cholesterol-based cationic (Cho-cat).

Parvizi *et al*. [75] synthesized cationic pyridinium lipids **153**–**155** which were mixed with 1,2-dimyristoyl-*sn*-glycero-3-ethylphosphocholine (EPC, 1:1 w/w) to form liposome with the neutral lipids 1,2-dioleoyl-*sn*-glycero-3-phosphatidylethanolamine (DOPE) or cholesterol (3:2 w/w) (Figure 36). Gel electrophoresis of all lipoplexes formulations revealed that plasmid DNA was protected from DNase I degradation. The

small-angle X-ray scattering experiments were examined to determine the shape parameter values that correctly correlated with observed hexagonal lipid phase behavior of lipoplexes. The factor of partition coefficient, shape parameter, lipoplex packing produced a direct correlation with transfection efficiency.

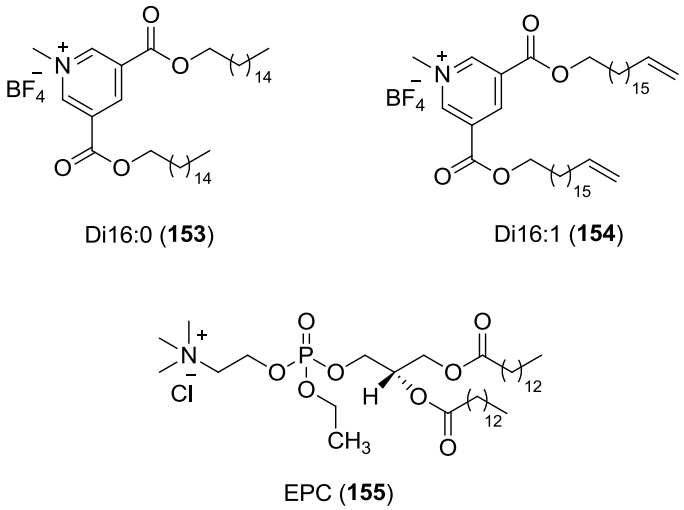

Figure 26 Structures of cationic pyridinium lipids.

Zhang *et al*. [11] have studied the influence of the structure of lipid to gene transfection efficiency. Thus, the novel 1,4,7,10-tetraazacyclododecane (cyclen)-based cationic lipids **L1**–**L6** (**156**–**161**) containing double oleyl as hydrophobic tails were designed and synthesized (Figure 37). The liposomes were prepared from the mixture of lipid and DOPE. The result showed good DNA binding affinity, and full DNA condensation to succeed at N/P 4 to form lipoplexes with appropriate size and zeta-potentials for gene delivery. The *in vitro* gene delivery was investigated by the structure-activity relationship and found that the lipid **L4** (**159**) containing amide linking bond gave the best transfection efficiency. In addition, they found that these lipids showed low cytotoxicity and good biocompatibility.

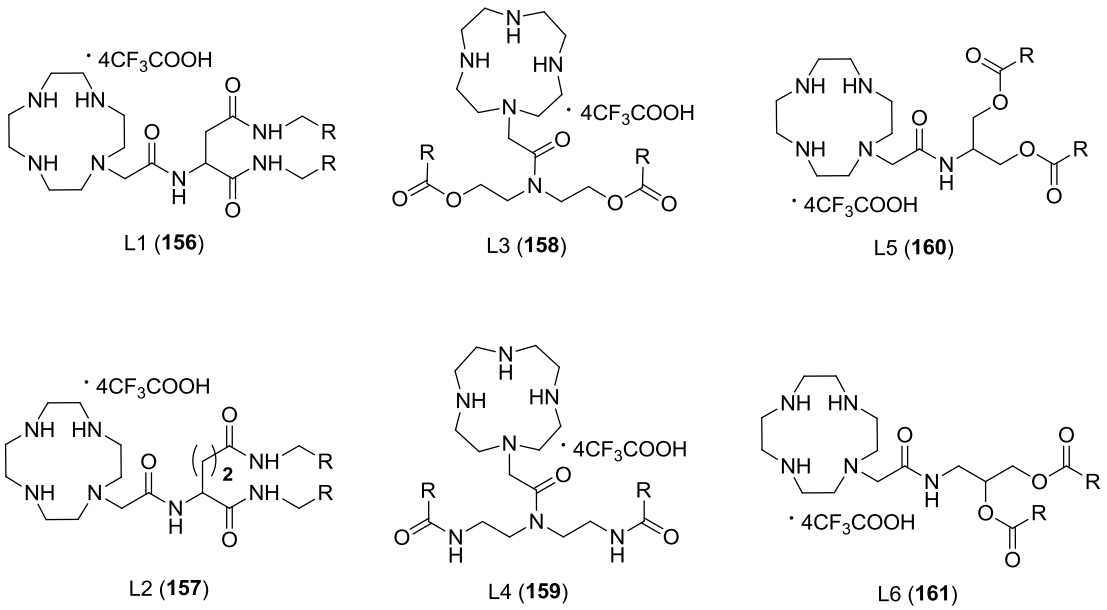

Figure 27 Structures of the novel 1,4,7,10-tetraazacyclododecane (cyclen)-based cationic lipids.

Ju *et al*. [76] have designed cholesterol derivatives **M1**−**M6** (**162**−**167**) and evaluated the cationic liposome as a non-viral vector (Figure 38). The lipoplexes were prepared by the cationic lipid mixing with pEGFP-N to transfect into 293T cells and evaluated GFP expression. All lipids exhibited good transfection activity. Lipids **M2** (**163**) and **M4** (**165**) provided the transfection efficiency at the same level with DC-Chol derived from the same backbone while lipids **M1** (**162**) and **M6** (**167**) are superior. The lipid **M6** (**167**) showed comparable transfection efficiency to Lipofectamine2000. The optimal ratio for the formulation of **M1** and **M6** were at a mole ratio of 1:0.5 for the cationic lipid/DOPE, and at N/P charge mole ratio of 3:1 for liposome/DNA. At the optimal condition, lipids **M1** (**162**) and **M6** (**167**) were better than that of the commercial liposome DC-chol and Lipofectamine2000 even in the presence of serum. The lipids **M1** (**162**) and **M6** (**167**) exhibited low cytotoxicity, good serum compatibility and efficient transfection, having the potential of being excellent non-viral vectors for gene delivery.

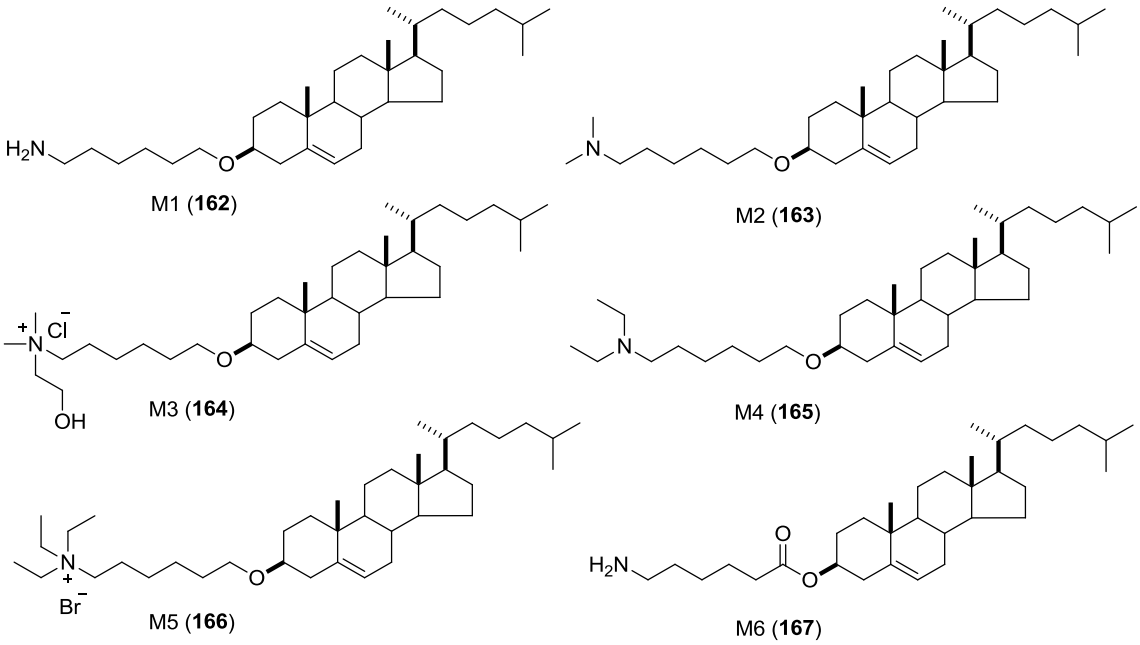

Figure 28 Structures of cationic lipids having cholesterol hydrophobic tail.

CHAPTER 3

RESEARCH METHODOLOGY

3.1 General Technique

3.1.1 Solvents

All solvents (methanol, ethyl acetate, dichloromethane, hexane) were distilled before use.

3.1.2 Reagents

Reagents were purchased from commercial suppliers. Starting materials including cholesteryl chloroformate, 4-nitrophenyl chloroformate, *N*,*N*'-diisopropylethylamine and 1,3-bis(*tert*-butoxycarbonyl)-2-methyl-2-thiopseudourea were purchased from Acros Organics. Methyl iodide and *O*-(benzotriazol-1-yl)-*N*,*N*,*N*′,*N*′-tetramethyluro-niumhexafluorophosphate (HBTU) were purchased from Sigma-Aldrich.

3.1.3 The Analytical Instrument for Structural Elucidation

IR spectra were recorded on a Perkin-Elmer Spectrum GX60237 spectrophotometer. NMR spectra were recorded on a Bruker AVANCE 400 spectrometer operating at 400 MHz for ^{1}H and 100 MHz for ^{13}C. All coupling constants (*J* values) were measured in Hertz. MS spectra were recorded with a Finnigan LCQ mass spectrometer and HRMS spectra were obtained from a Bruker microOTOF-II mass spectrometer.

3.1.4 Thin Layer Chromatography (TLC)

Adsorbent: MERCK precoated TLC plates (silica gel 60 F-254). The TLC plates were visualized as follows:

3.1.4.1 Ultraviolet (UV) light at 254 nm. This technique was used to monitor and evaluate the reactions. Organic compounds which are able to absorb the UV light will appear as dark blue spots. Compounds containing aromatic rings, α,β-unsaturated carbonyl groups and π-conjugated systems can also adsorb the UV light.

3.1.4.2 Stains for developing TLC plates. There are two techniques for this experiment. Ninhydrin reagent was used to detect the compound containing amino groups. *p*-Anisaldehyde reagent was employed to visualize phenols, terpenes, sugars, and steroids which shows the colors as violet, blue, red, grey or green.

3.1.5 Column Chromatography

The column chromatography was carried out to purify the crude products from the reactions using SiliaFlash® irregular silica gels, F60, 40–63 μm (230–400 mesh) as the adsorbent. An individual solvent (hexane, dichloromethane and methanol) or the mixture in an appropriate ratio was used as the eluent.

3.1.6 Cell Lines

Human embryonic kidney cells 293 (HEK293), human cervical adenocarcinoma (HeLa), human colon adenocarcinoma (HT29) and human breast adenocarcinoma (MCF7) were used all cells to evaluate transfection efficiency and HEK293 for cytotoxicity assay.

3.2 Overviews of Synthesis

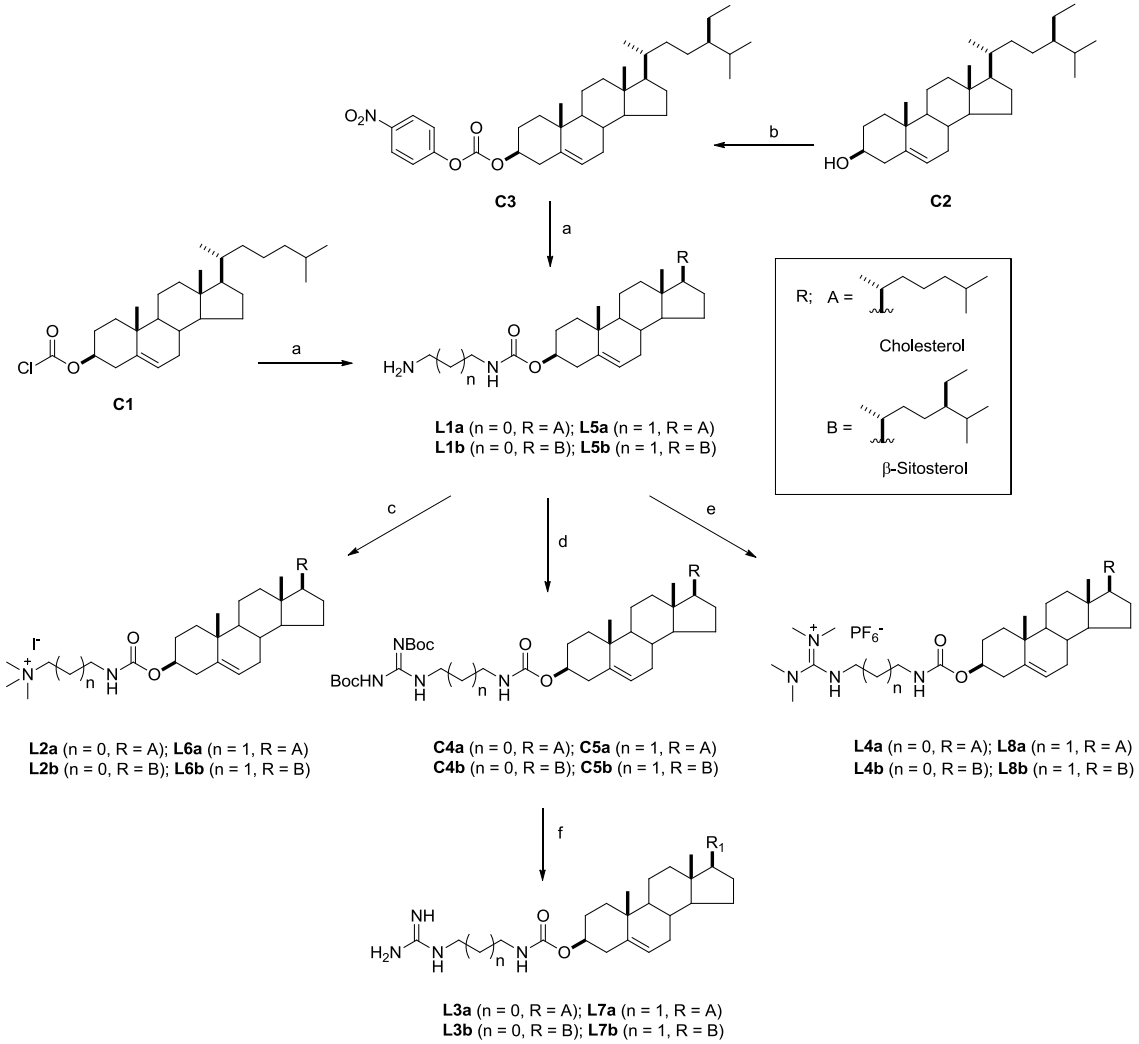

Scheme 1 Synthesis of lipids **L1a**–**L8a** and **L1b**–**L8b**. Reagents and conditions: (a) 1,2-diaminoethane (ethylenediamine) or 1,3-diaminopropane (1 equiv), CH_2Cl_2, 24 h; (b) 4-nitrophenyl chloroformate (1.2 equiv), CH_2Cl_2, Et_3N, 1 h; (c) CH_3I (4 equiv), DIEA, DMF, 12 h; (d) 1,3-bis(*tert*-butoxycarbonyl)-2-methyl-2-thiopseudourea (1.2 equiv), DIEA, DMF, 12 h; (e) *O*-(benzotriazol-1-yl)-*N*,*N*,*N*′,*N*′-tetramethyluronium hexafluorophosphate (1.2 equiv), DIEA, DMF, 12 h; (f) 20% TFA in CH_2Cl_2, 2 h.

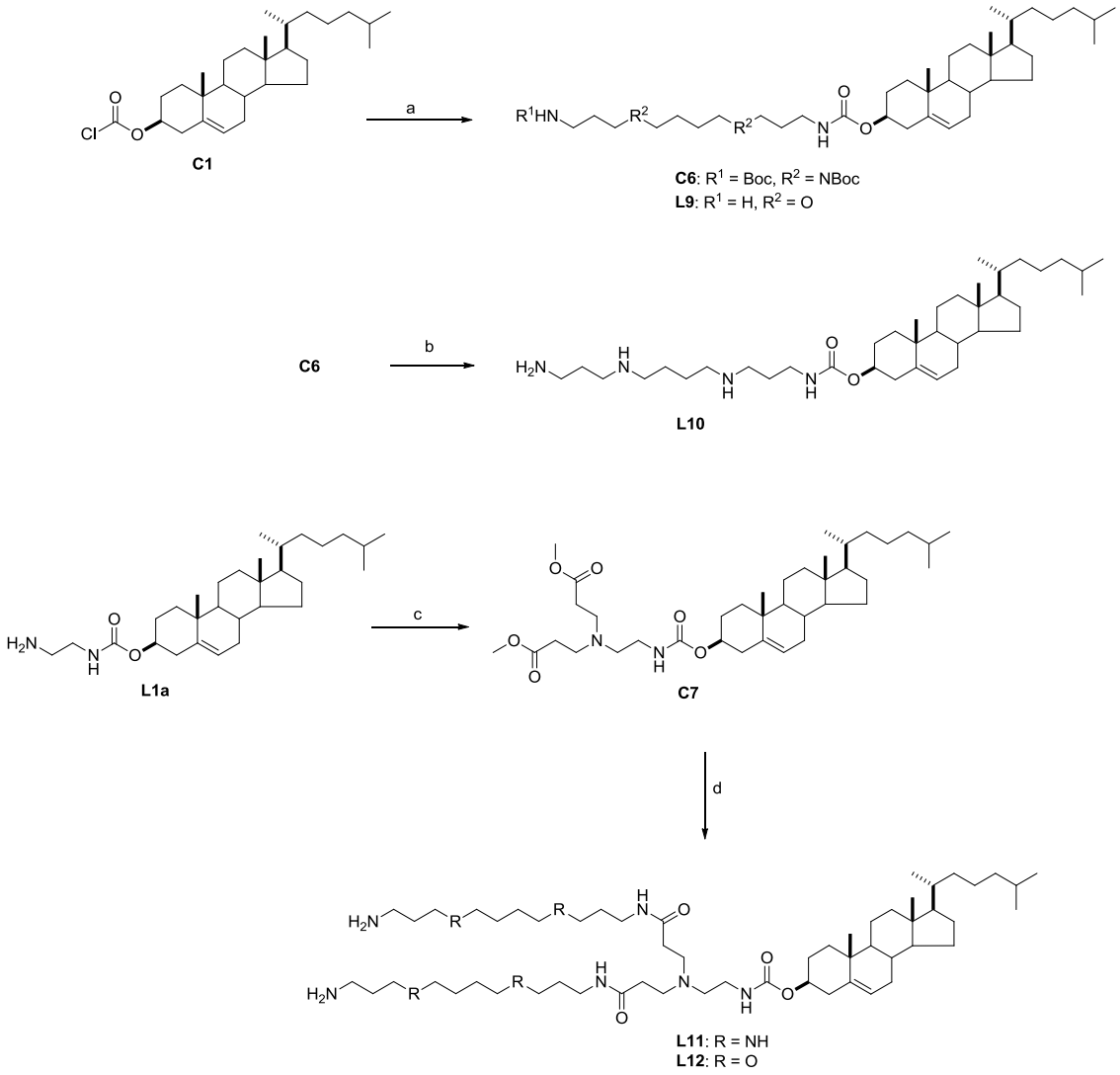

Scheme 2 Synthesis of cationic lipids **L9**–**L12**. Reagents and conditions: (a) spermine-Boc or 1,4-bis(3-aminopropoxy)butane (1.0 equiv), CH_2Cl_2, 24 h; (b) 20% TFA in CH_2Cl_2, 2 h; (c) methyl acrylate, MeOH, 5 days; (d) spermine or 1,4-bis(3-aminopropoxy)butane (2 equiv), MeOH, 5 days.

3.3 Synthesis

3.3.1 Synthesis of Lipids L1a and L5a

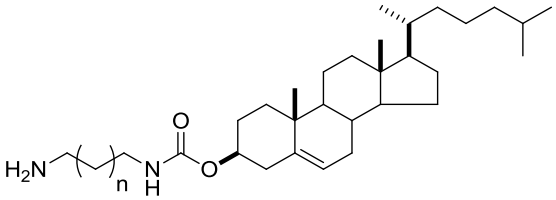

L1a; n = 0
L5a; n = 1

To a solution of ethylenediamine or 1,3-diaminopropane (0.74 mL, 11.12 mmol and 0.99 mL, 10.75 mmol, respectively) in CH_2Cl_2 was added dropwise the solution of cholesteryl chloroformate (1.0 g, 2.22 mmol or 0.96 g, 2.15 mmol) in CH_2Cl_2 (200 mL) at room temperature. The reaction mixture was stirred for 24 h and then washed with water (3×200 mL). The organic layer was combined, dried over Na_2SO_4, filtered, and concentrated to afford a white amorphous solid, which was purified by silica gel column chromatography (CH_2Cl_2 to 15% MeOH/CH_2Cl_2).

3β-[*N*-(2-Aminoethyl)carbamoyl]cholesterol (L1a). 800 mg (76%); IR: ν_{max} 3336, 2939, 2892, 2867, 2851, 1695, 1550, 1468, 1375, 1275, 1248, 1138, 1016 cm^{-1}; ^1H NMR (400 MHz, $CDCl_3$): δ 0.65 (s, 3H, CH_3-18), 0.83 (d, J = 5.8 Hz, 6H, CH_3-26 and CH_3-27), 0.88 (d, J = 6.3 Hz, 3H, CH_3-21), 0.98 (s, 3H, CH_3-19), 1.05−2.34 (m, protons in cholesteryl skeleton), 2.82 (t, J = 5.5 Hz, 2H, $NH_2C\underline{H}_2CH_2NHCO_2$-Chol), 3.22 (m, 2H, $NH_2CH_2C\underline{H}_2NHCO_2$-Chol), 4.46 (m, 1H, H-3-Chol), 5.07 (s, 1H, $-N\underline{H}CO_2$-Chol), 5.34 (br s, 1H, H-6-Chol); ^{13}C NMR (100 MHz, $CDCl_3$): 11.8, 18.7, 19.3, 21.0, 22.5, 22.8, 23.8, 24.3, 27.9, 28.1, 28.2, 31.9, 31.9, 35.8, 36.2, 36.5, 37.0, 39.5, 39.7, 41.6, 42.3, 50.0, 56.1, 56.7, 74.4, 122.5, 139.8 (carbons in cholesteryl skeleton), 38.6 ($NH_2\underline{C}H_2CH_2NHCO_2$-Chol), 43.2 ($NH_2CH_2\underline{C}H_2NHCO_2$-Chol), 156.5 (C=O carbamoyl); MS (ESI^+): *m/z* 473.6 ($[M + H]^+$, 100%); HRMS (ESI-TOF) *m/z*: $[M + H]^+$ calcd for $C_{30}H_{53}N_2O_2$: 473.4102; found 473.4115.

3β-[*N*-(3-Aminopropyl)carbamoyl]cholesterol (L5a). 780 mg (75%); IR: ν_{max} 3355, 2936, 2867, 2898, 1691, 1521, 1466, 1437, 1379, 1256, 1135, 1035, 1014 cm^{-1}; ^1H NMR (400 MHz, $CDCl_3$): δ 0.64 (s, 3H, CH_3-18), 0.82 (d, *J* = 5.8 Hz, 6H, CH_3-26 and CH_3-27), 0.87 (d, *J* = 6.3 Hz, 3H, CH_3-21), 0.97 (s, 3H, CH_3-19), 1.02−2.33 (m, $NH_2CH_2C\underline{H}_2CH_2NHCO_2$-Chol and protons in cholesteryl skeleton), 2.74 (br s, 2H, $NH_2C\underline{H}_2CH_2CH_2NHCO_2$-Chol), 3.22 (br t, 2H, *J* = 5.5 Hz, $NH_2CH_2CH_2C\underline{H}_2NHCO_2$-Chol), 3.43 (s, 1H, $-N\underline{H}CO_2$-Chol), 4.44 (m, 1H, H-3-Chol), 5.10 (m, 2H, $N\underline{H}_2CH_2CH_2CH_2NHCO_2$-Chol), 5.34 (m, 1H, H-6-Chol); ^{13}C NMR (100 MHz, $CDCl_3$): 11.8, 18.7, 19.3, 21.0, 22.5, 22.8, 23.8, 24.3, 28.0, 28.2, 31.9, 31.9, 32.8, 35.8, 36.2, 36.5, 37.0, 38.8, 39.5, 39.5, 42.3, 50.0, 56.1, 56.7, 74.2, 122.4, 139.8 (carbons in cholesteryl skeleton), 31.9 ($NH_2CH_2\underline{C}H_2CH_2NHCO_2$-Chol), 38.6 ($NH_2\underline{C}H_2CH_2CH_2NHCO_2$-Chol), 39.7 ($NH_2CH_2CH_2\underline{C}H_2NHCO_2$-Chol), 156.4 (C=O carbamoyl); MS (ESI^+): *m/z* 488.0 ($[M + H]^+$, 100%); HRMS (ESI-TOF) *m/z*: $[M + H]^+$ calcd for $C_{31}H_{55}N_2O_2$: 487.4258; found 487.4256.

3.3.2 Synthesis of Lipids L2a and L6a

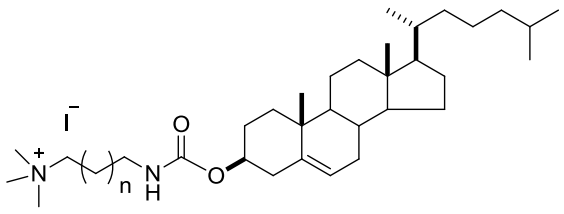

L2a; n = 0
L6a; n = 1

To a solution of lipid **L1a** (120 mg, 0.26 mmol) or **L5a** (150 mg, 0.31 mmol) in DMF (10 mL) was added methyl iodide (66 µL, 1.07 mmol and 76 µL, 1.23 mmol) and DIEA (3 drops). The reaction mixture was stirred at room temperature for 12 h and then washed with water (3×100 mL). The organic layer was combined, dried over Na_2SO_4, filtered, and concentrated to afford a white amorphous solid. The crude product was purified by silica gel column chromatography eluted by MeOH.

3β-[*N*-(2-(*N′*,*N′*,*N′*-Trimethyl)aminoethyl)carbamoyl]cholesterol (L2a). 35 mg (21%); IR: ν_{max} 3415, 2946, 2930, 2868, 2852, 1708, 1449, 1406, 1250, 1197, 1139, 1072, 1025 cm^{-1}; ^1H NMR (400 MHz, $CDCl_3$): δ 0.65 (s, 3H, CH_3-18), 0.84 (d, *J* = 6.3 Hz, 6H, CH_3-26 and CH_3-27), 0.89 (d, *J* = 6.3 Hz, 3H, CH_3-21), 0.98 (s, 3H, CH_3-19), 1.02−2.34 (m, protons in cholesteryl skeleton), 3.40 (s, 9H, $N^+(CH_3)_3$), 3.76 (br s, 2H, $N^+(CH_3)_3CH_2C\underline{H}_2NHCO_2$-Chol), 3.80 (d, *J* = 3.80, 2H, $N^+(CH_3)_3C\underline{H}_2CH_2NHCO_2$-Chol), 4.44 (m, 1H, H-3-Chol), 5.35 (br s, 1H, H-6-Chol), 6.51 (s, 1H, NH); ^{13}C NMR (100 MHz, $CDCl_3$): 10.6, 18.6, 19.2, 20.9, 22.5, 22.7, 23.7, 24.2, 27.9, 28.0, 28.1, 31.7, 31.8, 35.7, 36.0, 36.4, 36.8, 38.4, 39.4, 39.6, 42.2, 49.9, 56.0, 56.6, 74.9, 122.4, 139.6 (carbons in cholesteryl skeleton), 42.3 ($(CH_3)_3N^+CH_2\underline{C}H_2NHCO_2$-Chol), 53.2 ($N^+(CH_3)_3$), 65.5 ($(CH_3)_3N^+\underline{C}H_2CH_2NHCO_2$-Chol), 156.5 (C=O carbamoyl); MS (ESI^+): *m/z* 516.0 ($[M]^+$, 100%); HRMS (ESI-TOF) *m/z*: $[M]^+$ calcd for $C_{33}H_{59}N_2O_2$: 515.4571; found 515.4610.

3β-[*N*-(3-(*N′*,*N′*,*N′*-Trimethyl)aminopropyl)carbamoyl]cholesterol (L6a). 51 mg (25%); IR: ν_{max} 3295, 2940, 2867, 2850, 1624, 1543, 1481, 1468, 1380, 1330, 1287, 1251, 1133, 1033 cm^{-1}; ^1H NMR (400 MHz, $CDCl_3$): δ 0.65 (s, 3H, CH_3-18), 0.83 (d, *J* = 6.5 Hz, 6H, CH_3-26 and CH_3-27), 0.88 (d, *J* = 6.0 Hz, 3H, CH_3-21), 0.97 (s, 3H, CH_3-19), 1.07−2.26 (m, $N^+(CH_3)_3CH_2C\underline{H}_2CH_2NHCO_2$-Chol and protons in cholesteryl skeleton), 3.22 (s, 9H, $N^+(CH_3)_3$), 3.51 (m, 4H, $N^+(CH_3)_3C\underline{H}_2CH_2C\underline{H}_2NHCO_2$-Chol), 4.37 (m, 1H, H-3-Chol), 5.31 (br s, 1H, H-6-Chol), 6.69 (s, 1H, $N\underline{H}CO_2$-Chol); ^{13}C NMR (100 MHz, $CDCl_3$): 11.8, 18.6, 19.2, 20.9, 22.5, 22.8, 23.8, 24.2, 27.9, 28.0, 28.1, 31.7, 31.8, 35.7, 36.1, 36.5, 36.9, 39.4, 39.6, 42.2, 42.2, 49.9, 56.0, 56.6, 74.4, 122.3, 139.8 (carbons in cholesteryl skeleton), 27.9 ($(CH_3)_3N^+CH_2\underline{C}H_2CH_2NHCO_2$-Chol), 38.4 ($(CH_3)_3N^+CH_2CH_2\underline{C}H_2NHCO_2$-Chol), 53.4 ($N^+(CH_3)_3$), 63.0 ($(CH_3)_3N^+\underline{C}H_2CH_2CH_2NHCO_2$-Chol), 156.9 (C=O carbamoyl); MS (ESI^+): *m/z* 530.1 ($[M]^+$, 100%); HRMS (ESI-TOF) *m/z*: $[M]^+$ calcd for $C_{34}H_{61}N_2O_2$: 529.4728; found 529.4730.

3.3.3 Synthesis of Compounds C4a and C5a

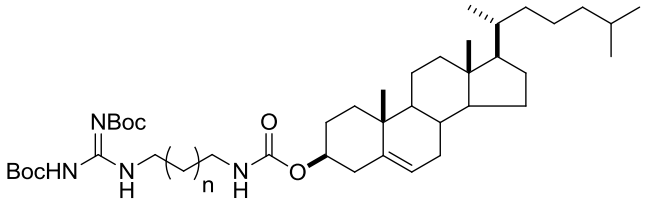

C4a; n = 0
C5a; n = 1

To a solution of lipid **L1a** (100 mg, 0.21 mmol) or **L5a** (150 mg, 0.31 mmol) in DMF (10 mL) was added 1,3-bis(*tert*-butoxycarbonyl)-2-methyl-2-thiopseudourea (73.15 mg, 0.25 mmol and 107.57 mg, 0.37 mmol, respectively) and DIEA (3 drops). The reaction mixture was stirred at room temperature for 12 h and then washed with water (3×100 mL). The organic layer was combined, dried over Na_2SO_4, filtered, and concentrated to afford a white amorphous solid, which was purified by silica gel column chromatography (1:1 hexane/CH_2Cl_2 to CH_2Cl_2).

3β-[(2-((*N′*,*N″*-Di(*tert*-butoxycarbonyl)guanidinyl)ethyl)carbamoly] cholesterol (C4a). 64 mg (43%); IR: ν_{max} 3377, 3323, 3292, 2936, 2867, 1724, 1647, 1618, 1522, 1440, 1361, 1337, 1282, 1237, 1144, 1056, 1017 cm^{-1}; ^1H NMR (400 MHz, $CDCl_3$): δ 0.65 (s, 3H, CH_3-18), 0.83 (d, *J* = 6.5 Hz, 6H, CH_3-26 and CH_3-27), 0.89 (d, *J* = 6.4 Hz, 3H, CH_3-21), 0.98 (s, 3H, CH_3-19), 1.01−1.41 and 1.54−2.35 (m, protons in cholesteryl skeleton), 1.47 (s, 9H, $C(CH_3)_3$), 1.48 (s, 9H, $C(CH_3)_3$), 3.34 (d, *J* = 4.8 Hz, 2H, −$NHCH_2C\underline{H}_2NHCO_2$-Chol), 3.52 (d, *J* = 5.2, 2H, −$NHC\underline{H}_2CH_2NHCO_2$-Chol), 4.46 (m, 1H, H-3-Chol), 5.34 (br s, 1H, H-6-Chol), 5.53 (br s, 1H, −$N\underline{H}CH_2CH_2NHCO_2$-Chol), 8.50 (s, 1H, −$N\underline{H}CO_2$-Chol), 11.42 (s, 1H, $N\underline{H}CO_2C(CH_3)_3$); ^{13}C NMR (100 MHz, $CDCl_3$): 11.8, 18.7, 19.3, 21.1, 22.5, 22.8, 23.8, 24.3, 28.1, 28.2, 28.3, 31.9, 31.9, 35.8, 36.2, 36.6, 37.0, 39.5, 39.8, 40.7, 41.3, 50.1, 56.2, 56.7, 74.3, 122.4, 139.9 (carbons in cholesteryl skeleton), 28.1 and 28.2 (($CH_3)_3$), 38.5 (−$NH\underline{C}H_2CH_2NHCO_2$-Chol), 42.3 (−$NHCH_2\underline{C}H_2NHCO_2$-Chol), 79.3 and 83.2 ($\underline{C}(CH_3)_3$), 153.1 and 163.3 (C=O of Boc group), 156.3 (C=O carbamoyl), 156.9 (C=NH); MS (ESI^+): *m/z* 715.8 ($[M + H]^+$, 100%); HRMS (ESI-TOF) *m/z*: $[M + H]^+$ calcd for $C_{41}H_{71}N_4O_6$: 715.5368; found 715.5375.

3β-[(3-((*N′*,*N″*-Di(*tert*-butoxycarbonyl))guanidinyl)propyl)carbamoyl] cholesterol (C5a). 126 mg (56%); IR: ν_{max} 3332, 2939, 2907, 2867, 2852, 1715, 1643, 1619, 1571, 1506, 1415, 1368, 1349, 1331, 1286, 1228, 1156, 1125, 1070, 1026 cm^{-1}; ^1H NMR (400 MHz, $CDCl_3$): δ 0.65 (s, 3H, CH_3-18), 0.83 (d, *J* = 5.8 Hz, 6H, CH_3-26 and CH 3-27), 0.88 (d, *J* = 6.3 Hz, 3H, CH_3-21), 0.97 (s, 3H, CH_3-19), 1.01−1.40 and 1.54−2.43 (m, $NHCH_2C\underline{H}_2CH_2NHCO_2$-Chol and protons in cholesteryl skeleton), 1.47 (s, 9H, $C(CH_3)_3$), 1.48 (s, 9H, $C(CH_3)_3$), 3.16 (d, *J* = 5.5 Hz, 2H, $-NHCH_2CH_2C\underline{H}_2NHCO_2$-Chol), 3.46 (m, 2H, $-NHC\underline{H}_2CH_2CH_2NHCO_2$-Chol), 4.47 (m, 1H, H-3-Chol), 5.34 (br s, 1H, H-6-Chol), 6.01 (s, 1H, $N\underline{H}CO_2$-Chol), 8.34 (s, 1H, $NHC(=N)N\underline{H}(CH_2)_3$), 11.35 (s, 1H, $(CH_3)_3COCON\underline{H}$); ^{13}C NMR (100 MHz, $CDCl_3$): 11.8, 18.7, 19.3, 21.0, 22.5, 22.8, 23.8, 24.3, 28.0, 28.1, 28.2, 30.3, 31.9, 35.8, 36.2, 36.6, 37.0, 37.4, 39.5, 39.8, 42.3, 50.0, 56.2, 56.7, 74.0, 122.3, 140.1 (carbons in cholesteryl skeleton), 28.1 and 28.3 ($(CH_3)_3$), 32.0 ($-NHCH_2\underline{C}H_2CH_2NHCO_2$-Chol), 38.6 ($-NH\underline{C}H_2CH_2CH_2NHCO_2$-Chol), 39.5 ($-NHCH_2CH_2\underline{C}H_2NHCO_2$-Chol), 79.3 and 83.3 ($\underline{C}(CH_3)_3$), 153.2 and 163.2 (C=O of Boc group), 156.5 (C=O carbamoyl), 156.8 (C=NH); MS (ESI^+): *m/z* 729.7 ($[M + H]^+$, 100%); HRMS (ESI-TOF) *m/z*: $[M + H]^+$ calcd for $C_{42}H_{73}N_4O_6$: 729.5525; found 729.5536.

3.3.4 Synthesis of Lipids L3a and L7a

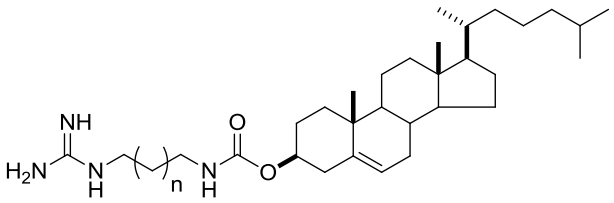

L3a; n = 0
L7a; n = 1

To a solution of **C4a** (45.3 mg, 0.095 mmol) or **C5a** (115 mg, 0.24 mmol) in CH_2Cl_2 (2 mL) was added TFA (0.5 mL). The reaction mixture was stirred at room temperature for 2 h. The solvent was removed by flowing nitrogen gas. The residue was purified by silica gel column chromatography (1:1 hexane/CH_2Cl_2 to 95:5 CH_2Cl_2/MeOH).

3β-[(2-(Guanidinyl)ethyl)carbamoyl]cholesterol (L3a). 35 mg (72%); IR: ν_{max} 3324, 3194, 2941, 2869, 1672, 1520, 1461, 1252, 1200, 1144, 1014 cm^{-1}; ^{1}H NMR (400 MHz, $CDCl_3$): δ 0.63 (s, 3H, CH_3-18), 0.81 (d, *J* = 6.3 Hz, 6H, CH_3-26 and CH_3-27), 1.01 (d, *J* = 6.3 Hz, 3H, CH_3-21), 1.15 (s, 3H, CH_3-19), 1.07−2.92 (m, protons in cholesteryl skeleton), 3.21 (m, 4H, $-NH(C\underline{H}_2)_2NHCO_2$-Chol), 4.50 (m, 1H, H-3-Chol), 5.63 (br s, 1H, H-6-Chol); ^{13}C NMR (100 MHz, $CDCl_3$): 11.8, 18.7, 19.3, 21.0, 22.5, 22.8, 23.8, 24.2, 27.8, 28.0, 29.7, 31.8, 31.8, 35.8, 36.1, 36.5, 36.8, 39.2, 39.4, 42.3, 42.6, 49.9, 56.1, 56.6, 75.9, 122.9, 139.3 (carbons in cholesteryl skeleton), 38.3 ($-NH\underline{C}H_2CH_2NHCO_2$-Chol), 39.6 ($-NHCH_2\underline{C}H_2NHCO_2$-Chol), 155.2 (C=O carbamoyl), 159.7 (C=NH); MS (ESI^+): *m/z* 516.4 ($[M + H]^+$, 100%); HRMS (ESI-TOF) *m/z*: $[M + H]^+$ calcd for $C_{31}H_{55}N_4O_2$: 515.4319; found 515.4330.

3β-[(3-(Guanidinyl)propyl)carbamoyl]cholesterol (L7a). 95 mg (75%); IR: ν_{max} 3350, 3196, 2943, 2904, 2868, 2852, 1672, 1533, 1438, 1271, 1197, 1135, 1025 cm^{-1}; ^{1}H NMR (400 MHz, $CDCl_3$ + 10 drops of CD_3OD): δ 0.58 (s, 3H, CH_3-18), 0.76 (d, *J* = 5.8 Hz, 6H, CH_3-26 and CH_3-27), 0.81 (d, *J* = 6.3 Hz, 3H, CH_3-21), 0.90 (s, 3H, CH_3-19), 0.93−2.44 (m, $-NHCH_2C\underline{H}_2CH_2NHCO_2$-Chol and protons in cholesteryl skeleton), 3.05 (m, 2H, $-NHC\underline{H}_2CH_2CH_2NHCO_2$-Chol), 3.05 (m, 2H, $-NHC\underline{H}_2CH_2$ CH_2NHCO_2-Chol), 4.33 (m, 1H, H-3-Chol), 5.26 (br s, 1H, H-6-Chol); ^{13}C NMR (100 MHz, $CDCl_3$ + 10 drops of CD_3OD): 11.7, 18.5, 19.1, 20.9, 22.4, 22.7, 23.7, 24.1, 27.9, 28.1, 28.9, 31.7, 31.7, 35.7, 36.0, 36.4, 36.8, 39.4, 39.6, 42.1, 42.1, 49.8, 56.0, 56.5, 74.6, 122.4, 139.6 (carbons in cholesteryl skeleton), 27.9 ($-NHCH_2\underline{C}H_2CH_2NHCO_2$-Chol), 38.3 ($-NH\underline{C}H_2CH_2CH_2NHCO_2$-Chol), 38.6 ($-NHCH_2CH_2\underline{C}H_2NHCO_2$-Chol), 157.1 (C=O carbamoyl), 157.2 (C=NH); MS (ESI^+): *m/z* 530.1 ($[M + H]^+$, 100%); HRMS (ESI-TOF) *m/z*: $[M + H]^+$ calcd for $C_{32}H_{57}N_4O_2$: 529.4476; found 529.4505.

3.3.5 Synthesis of Lipids L4a and L8a

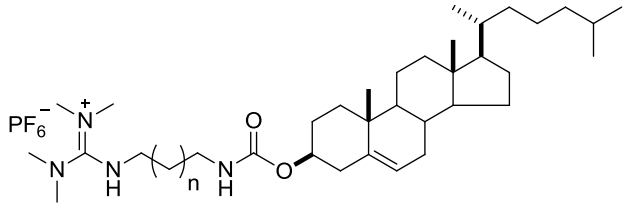

L4a; n = 0
L8a; n = 1

To a solution of lipid **L1a** (150 mg, 0.21 mmol) or **L5a** (150 mg, 0.31 mmol) DMF (10 mL) was added *O*-(Benzotriazol-1-yl)-*N*,*N*,*N*′,*N*′-tetramethyluronium hexafluorophosphate (144.37 mg, 0.25 mmol and 140.23 mg, 0.37 mmol, respectively) and DIEA (3 drops). The reaction mixture was stirred at room temperature for 12 h and then washed with water (3×100 mL). The organic layer was combined, dried over Na_2SO_4, filtered, and concentrated to afford a white amorphous solid, which was purified by silica gel column chromatography (CH_2Cl_2 to 90:10 CH_2Cl_2/MeOH).

3β-[(2-((*N*′,*N*′,*N*′′,*N*′′-Tetramethyl)guanidinyl)ethyl)carbamoyl]cholesterol (L4a). 99 mg (66%); IR: ν_{max} 3403, 3360, 2939, 2867, 2848, 1693, 1620, 1582, 1522, 1404, 1237, 1225, 1011, 832, 776 cm^{-1}; ^1H NMR (400 MHz, $CDCl_3$ + 10 drops of CD_3OD): δ 0.57 (s, 3H, CH_3-18), 0.76 (d, *J* = 6.0 Hz, 6H, CH_3-26 and CH_3-27), 0.82 (d, *J* = 6.4 Hz, 3H, CH_3-21), 0.90 (s, 3H, CH_3-19), 0.88−2.20 (m, protons in cholesteryl skeleton), 2.88 (s, 10H, (−NHC$\underline{H}_2$C$\underline{H}_2$NHC(N(C$\underline{H}_3$)$_2$)), 3.35 (s, 6H, −NHCH$_2$CH$_2$NHC(N$^+$(C$\underline{H}_3$)$_2$)), 4.32 (m, 1H, H-3-Chol), 5.26 (br s, 1H, H-6-Chol), 6.82 (s, 1H, N=CN$\underline{H}$CH$_2$CH$_2$NHCO$_2$-Chol), 7.87 (s, 1H, N$\underline{H}$CO$_2$-Chol); ^{13}C NMR (100 MHz, $CDCl_3$ + 10 drops of CD_3OD): 11.8, 18.6, 19.2, 20.9, 22.5, 22.7, 23.7, 24.2, 27.9, 28.0, 28.1, 31.7, 31.8, 35.7, 36.1, 36.5, 36.9, 39.6, 40.0, 42.2, 42.6, 49.9, 56.0, 56.6, 74.5, 122.4, 139.7 (carbons in cholesteryl skeleton), 38.5 (C=N$^+$(C$\underline{H}_3$)$_2$), 39.7 (N(CH$_3$)$_2$), 39.4 (−NHC$\underline{H}_2$CH$_2$NHCO$_2$-Chol), 40.0 (−NHCH$_2$C$\underline{H}_2$NHCO$_2$-Chol), 157.2 (C=O carbamoyl), 161.9 (C=NH); MS (ESI$^+$): *m/z* 572.4 ([M]$^+$, 100%); HRMS (ESI-TOF) *m/z*: [M]$^+$ calcd for $C_{35}H_{63}N_4O_2$: 571.4945; found 571.4916.

3β-[(3-((*N′*,*N′*,*N″*,*N″*-Tetramethyl)guanidinyl)propyl)carbamoyl]cholesterol (L8a). 201 mg (89%); IR: ν_{max} 3447, 3287, 2952, 2937, 2908, 2869, 2850, 1697, 1624, 1598, 1459, 1410, 1332, 1042, 843, 834 cm^{-1}; ^1H NMR (400 MHz, $CDCl_3$): δ 0.65 (s, 3H, CH_3-18), 0.84 (d, *J* = 5.9 Hz, 6H, CH_3-26 and CH_3-27), 0.88 (d, *J* = 6.4 Hz, 3H, CH_3-21), 0.98 (s, 3H, CH_3-19), 1.02−2.77 (m, −$NHCH_2C\underline{H}_2CH_2NHCO_2$-Chol and protons in cholesteryl skeleton), 2.97 (s, 12H, ($NHC(=N^+(C\underline{H}_3)_2)(N(C\underline{H}_3)_2)$), 3.22 (s, 2H, −$NHCH_2CH_2C\underline{H}_2NHCO_2$-Chol), 4.23 (s, 2H, −$NHC\underline{H}_2CH_2CH_2NHCO_2$-Chol), 4.39 (m, 1H, H-3-Chol), 5.05 (s, 1H, −$N\underline{H}(CH_3)_2NHCO_2$-Chol), 5.32 (br s, 1H, H-6-Chol), 6.29 (s, 1H, $N\underline{H}CO_2$-Chol); ^{13}C NMR (100 MHz, $CDCl_3$): 11.9, 18.7, 19.3, 21.1, 22.5, 22.8, 23.8, 24.3, 28.0, 28.1, 28.2, 31.1, 31.9, 35.8, 36.2, 36.6, 37.0, 37.4, 39.8, 39.9, 42.3 , 50.1, 56.2, 56.8, 74.8, 122.5, 139.8 (carbons in cholesteryl skeleton), 28.1 (−$NH\,CH_2\underline{C}H_2CH_2NHCO_2$-Chol), 38.5 ($C=N^+(\underline{C}H_3)_2$), 39.5 ($N(CH_3)_2$), 39.5 (−$NH\underline{C}H_2CH_2\,CH_2NHCO_2$-Chol), 39.9 (−$NHCH_2CH_2\underline{C}H_2NHCO_2$-Chol), 157.3 (C=O carbamoyl), 161.8 (C=NH); MS (ESI^+): *m/z* 586.4 ($[M]^+$, 100%); HRMS (ESI-TOF) *m/z*: $[M]^+$ calcd for $C_{36}H_{65}N_4O_2$: 585.5102; found 585.5099.

3.3.6 Synthesis of Lipids L1b and L5b

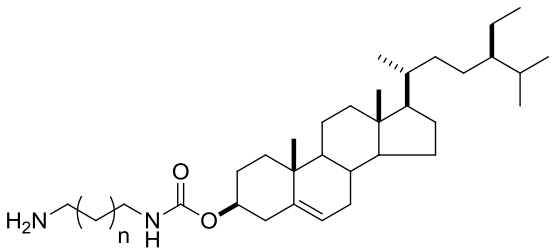

L1b; n = 0
L5b; n = 1

To a solution of β-sitosterol (1.5 g, 3.62 mmol) and triethylamine (2 mL) in CH_2Cl_2 (200 mL) was added dropwise 4-nitrophenyl chloroformate (0.942 g, 4.67 mmol). The reaction mixture was stirred at room temperature for 1 h and then added to the solution of ethylenediamine (1.20 mL, 18.09 mmol) or 1,3-diaminopropane (1.68 mL, 18.15 mmol) in CH_2Cl_2 (250 mL). The resulting mixture was stirred at room temperature for 24 h and then washed with water (3×200 mL). The organic layer was combined, dried over Na_2SO_4, filtered, and concentrated to afford a white amorphous

solid, which was purified by silica gel column chromatography (CH_2Cl_2 to 85:15 CH_2Cl_2/MeOH).

3β-[*N*-(2-Aminoethyl)carbamoyl]β-sitosterol (L1b). 1.27 g (70%); IR: ν_{max} 3338, 2937, 2891, 2866, 2852, 1696, 1550, 1464, 1364, 1276, 1247, 1142, 1123, 1928, 1016, 958 cm^{-1}; ^1H NMR (400 MHz, $CDCl_3$): δ 0.65 (s, 3H, CH_3-18), 0.81 (m, 9H, CH_3-26, CH_3-27 and CH_3-29), 0.90 (d, *J* = 6.4 Hz, 3H, CH_3-21), 0.98 (s, 3H, CH_3-19), 1.02−2.29 (m, CH_2-28 and protons in β-sitosteryl skeleton), 3.14 (t, *J* = 5.5 Hz, 2H, $NH_2CH_2C\underline{H}_2NHCO_2$-Chol), 3.46 (m, 2H, $NH_2C\underline{H}_2CH_2NHCO_2$-Chol), 4.44 (m, 1H, H-3-Chol), 5.04 (br s, 1H, $-N\underline{H}CO_2$-Chol), 5.34 (br s, 1H, H-6-Chol); ^{13}C NMR (100 MHz, $CDCl_3$): 11.8, 12.0, 18.8, 19.0, 19.3, 19.8, 21.0, 23.1, 24.3, 26.2, 28.2, 28.2, 29.1, 31.9, 31.9, 34.0, 36.2, 36.2, 36.6, 38.6, 39.7, 42.3, 45.9, 50.0, 56.1, 56.7, 74.4, 122.5, 139.8 (carbons in β-sitosteryl skeleton), 41.6 ($NH_2\underline{C}H_2CH_2NHCO_2$-Chol), 43.2 ($NH_2CH_2\underline{C}H_2NHCO_2$-Chol), 156.5 (C=O carbamoyl); MS (ESI^+): *m/z* 501.6 ($[M + H]^+$, 100%); HRMS (ESI-TOF) *m/z*: $[M + H]^+$ calcd for $C_{32}H_{57}N_2O_2$: 501.4415; found 501.4417.

3β-[*N*-(3-Aminopropyl)carbamoyl]β-sitosterol (L5b). 1.19 g (64%); IR: ν_{max} 3337, 2954, 2936, 2867, 2851, 1690, 1530, 1464, 1439, 1378, 1366, 1331, 1315, 1249, 1135, 1019, 959 cm^{-1}; ^1H NMR (400 MHz, $CDCl_3$): δ 0.65 (s, 3H, CH_3-18), 0.81 (m, 9H, CH_3-26, CH_3-27 and CH_3-29), 0.89 (d, *J* = 6.2 Hz, 3H, CH_3-21), 0.98 (s, 3H, CH3-19), 1.03−2.30 (m, CH_2-28, $NH_2CH_2C\underline{H}_2CH_2NHCO_2$-Chol and protons in β-sitosteryl skeleton), 2.80 (br t, *J* = 6.0 Hz, 2H, $NH_2C\underline{H}_2CH_2CH_2NHCO_2$-Chol), 3.22 (br t, *J* = 5.5 Hz, 2H, $NH_2CH_2CH_2C\underline{H}_2NHCO_2$-Chol), 4.44 (m, 1H, H-3-Chol), 5.27 (br s, 1H, $NH_2CH_2CH_2CH_2N\underline{H}CO_2$-Chol), 5.34 (br s, 1H, H-6-Chol); ^{13}C NMR (100 MHz, $CDCl_3$): 11.9, 12.0, 18.8, 19.0, 19.3, 19.8, 21.0, 23.1, 24.3, 26.2, 28.2, 28.2, 29.2, 31.9, 32.2, 34.0, 36.2, 36.6, 37.0, 38.6, 39.2, 42.3, 44.7, 45.9, 50.0, 56.1, 56.7, 74.3, 122.5, 139.8 (carbons in β-sitosteryl skeleton), 31.9 ($NH_2CH_2\underline{C}H_2CH_2NHCO_2$-Chol), 38.6 ($H_2N\underline{C}H_2CH_2CH_2NHCO_2$-Chol), 39.7 ($H_2NCH_2CH_2\underline{C}H_2NHCO_2$-Chol), 156.5 (C=O carbamoyl); MS (ESI^+): *m/z* 515.7 ($[M + H]^+$, 100%); HRMS (ESI-TOF) *m/z*: $[M + H]^+$ calcd for $C_{33}H_{59}N_2O_2$: 515.4571; found 515.4568.

3.3.7 Synthesis of Lipids L2b and L6b

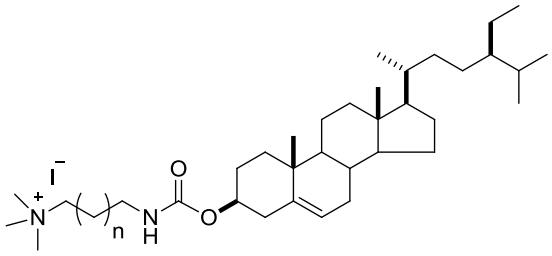

L2b; n = 0
L6b; n = 1

To a solution of lipid **L1b** (150 mg, 0.30 mmol) or **L5b** (150 mg, 0.29 mmol) in DMF (10 mL) was added MeI (74 µL, 1.20 mmol and 72 µL, 1.16 mmol) and DIEA (3–4 drops). The reaction mixture was stirred at room temperature for 12 h and then washed with water (3×100 mL). The organic layer was combined, dried over Na_2SO_4, filtered, and concentrated to afford a white amorphous solid, which was purified by silica gel column chromatography eluted by MeOH.

3β-[N-(2-(*N′*,*N′*,*N′*-Trimethyl)aminoethyl)carbamoyl]β-sitosterol (L2b). 100 mg (50%); IR: ν_{max} 3283, 3038, 2945, 2866, 2852, 1539, 1467, 1377, 1331, 1258, 1072, 958, 925 cm^{-1}; ^1H NMR (400 MHz, $CDCl_3$): δ 0.65 (s, 3H, CH_3-18), 0.81 (m, 9H, CH_3-26, CH_3-27 and CH_3-29), 0.89 (d, *J* = 5.4 Hz, 3H, CH_3-21), 0.97 (s, 3H, CH_3-19), 1.08−2.12 (m, CH_2-28 and protons in β-sitosteryl skeleton), 3.35 (s, 9H, $N^+(C\underline{H}_3)_3$), 3.72 (br s, 2H, $N^+(CH_3)_3CH_2C\underline{H}_2NHCO_2$-Chol), 3.72 (m, 2H,$N^+(CH_3)_3C\underline{H}_2CH_2NHCO_2$-Chol), 4.41 (m, 1H, H-3-Chol), 5.33 (br s, 1H, H-6-Chol), 6.70 (s, 1H, NH); ^{13}C NMR (100 MHz, $CDCl_3$): 11.8, 11.9, 18.7, 18.9, 19.2, 19.7, 21.0, 23.0, 24.2, 26.0, 28.0, 28.2, 29.0, 31.8, 31.8, 33.8, 36.1, 36.5, 36.9, 38.4, 39.7, 42.2 , 45.7, 50.4, 56.0, 56.6, 74.9, 122.5, 139.6 (carbons in β-sitosteryl skeleton), 42.2 ($(CH_3)_3N^+CH_2\underline{C}H_2NHCO_2$-Chol), 53.7 ($N^+(CH_3)_3$), 64.9 ($(CH_3)_3N^+\underline{C}H_2CH_2NHCO_2$-Chol), 156.9 (C=O carbamoyl); MS (ESI^+): *m/z* 543.9 ($[M]^+$, 100%); HRMS (ESI-TOF) *m/z*: $[M]^+$ calcd for $C_{35}H_{63}N_2O_2$: 543.4884; found 543.4863.

3β-[*N*-(3-(*N′*,*N′*,*N′*-Trimethyl)aminopropyl)carbamoyl]β-sitosterol (L6b). 91 mg (46%); IR: ν_{max} 3455, 2956, 2939, 2868, 2852, 1698, 1443, 1270, 1115, 965 cm^{-1}; ^1H NMR (400 MHz, $CDCl_3$): δ 0.65 (s, 3H, CH_3-18), 0.81 (m, 9H, CH_3-26, CH_3-27 and CH_3-29), 0.89 (d, *J* = 5.6 Hz, 3H, CH_3-21), 0.99 (s, 3H, CH_3-19), 1.06-2.30 (m, CH_2-28, $-NHCH_2C\underline{H}_2CH_2NHCO_2$-Chol and protons in β-sitosteryl skeleton), 3.29 (s, 9H, $N^+(C\underline{H}_3)_3$), 3.29 (s, 2H, $N^+(CH_3)_3CH_2CH_2C\underline{H}_2NHCO_2$-Chol), 3.77 (m, 2H, $N^+(CH_3)_3C\underline{H}_2CH_2CH_2NHCO_2$-Chol), 4.43 (m, 1H, H-3-Chol), 5.33 (br s, 1H, H-6-Chol), 6.19 (s, 1H, $N\underline{H}CO_2$-Chol); ^{13}C NMR (100 MHz, $CDCl_3$): 11.7, 11.8, 18.6, 18.9, 19.2, 19.7, 21.3, 23.4, 24.2, 25.9, 28.1, 29.0, 29.6, 31.7, 31.8, 33.8, 36.0, 36.4, 36.8, 38.4, 39.6, 42.2, 45.7 , 50.1, 55.9, 56.6, 74.6, 122.4, 139.7 (carbons in β-sitosteryl skeleton), 28.0 ($(CH_3)_3N^+CH_2\underline{C}H_2CH_2NHCO_2$-Chol), 39.8 ($(CH_3)_3N^+CH_2CH_2\underline{C}H_2$ $NHCO_2$-Chol), 53.3 ($N^+(CH_3)_3$), 64.7 ($(CH_3)_3N^+\underline{C}H_2CH_2CH_2NHCO_2$-Chol), 157.1 (C=O carbamoyl); MS (ESI^+): *m/z* 558.0 ($[M]^+$, 100%); HRMS (ESI-TOF) *m/z*: $[M]^+$ calcd for $C_{36}H_{65}N_2O_2$: 557.5041; found 557.5020.

3.3.8 Synthesis of Compounds C4b and C5b

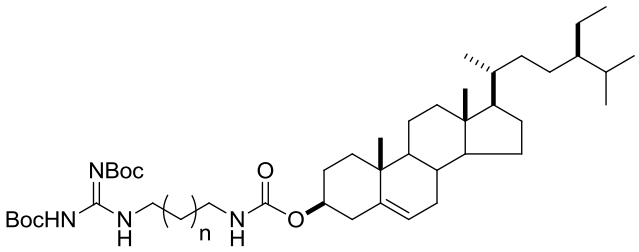

C4b; n = 0
C5b; n = 1

To a solution of lipid **L1b** (100 mg, 0.20 mmol) or **L5b** (100 mg, 0.19 mmol) in DMF (10 mL) was added 1,3-bis(*tert*-butoxycarbonyl)-2-methyl-2-thiopseudourea (69.62 mg, 0.24 mmol and 67.74 mg, 0.23 mmol, respectively) and DIEA (3 drops). The reaction mixture was stirred at room temperature for 12 h and then washed with water (3×100 mL). The organic layer was combined, dried over Na_2SO_4, filtered, and concentrated to afford a white amorphous solid, which was purified by silica gel column chromatography (1:1 hexane/CH_2Cl_2 to CH_2Cl_2).

3β-[(2-((*N′*,*N″*-Di(*tert*-butoxycarbonyl)guanidinyl)ethyl)carbamoly]β-sitosterol (C4b). 114 mg (77%); IR: ν_{max} 3385, 3327, 2945, 2869, 1648, 1616, 1524, 1451, 1412, 1366, 1335, 1276, 1259, 1141, 1054, 1016 cm^{-1}; ^1H NMR (400 MHz, $CDCl_3$): δ 0.65 (s, 3H, CH_3-18), 0.81 (m, 9H, CH_3-26, CH_3-27 and CH_3-29), 0.89 (d, *J* = 6.4 Hz, 3H, CH_3-21), 0.98 (s, 3H, CH_3-19), 1.07−1.37 and 1.63−2.55 (m, CH_2-28 and protons in β-sitosteryl skeleton), 1.46 (s, 9H, $C(CH_3)_3$), 1.47 (s, 9H, $C(CH_3)_3$), 3.34 (d, *J* = 5.0 Hz, 2H, −$NHCH_2C\underline{H}_2NHCO_2$-Chol), 3.51 (d, *J* = 5.7, 2H, −$NHC\underline{H}_2CH_2NHCO_2$-Chol), 4.46 (m, 1H, H-3-Chol), 5.34 (d, *J* = 4.6 Hz, 1H, H-6-Chol), 5.53 (br s, 1H, −$N\underline{H}CH_2CH_2NHCO_2$-Chol), 8.48 (s, 1H, −$N\underline{H}CO_2$-Chol), 11.41 (s, 1H, −$N\underline{H}CO_2C(CH_3)_3$)); ^{13}C NMR (100 MHz, $CDCl_3$): 11.8, 12.0, 18.8, 19.0, 19.3, 19.8, 21.0, 23.1, 24.3, 26.1, 27.9, 28.0, 29.2, 31.9, 32.0, 33.9, 36.1, 36.5, 37.0, 38.5, 39.7, 42.3, 45.8, 50.0, 56.0, 56.7, 74.3, 122.4, 139.9 (carbons in β-sitosteryl skeleton), 28.3 and 28.1 ($(CH_3)_3$), 40.7 (−$NH\underline{C}H_2CH_2NHCO_2$-Chol), 41.2 (−$NHCH_2\underline{C}H_2NHCO_2$-Chol), 79.3 and 83.3 ($\underline{C}(CH_3)_3$), 153.1 and 163.3 (C=O of Boc group), 156.3 (C=O carbamoyl), 156.9 (C=NH); MS (ESI^+): *m/z* 743.6 ($[M + H]^+$, 100%). HRMS (ESI-TOF) *m/z*: $[M + H]^+$ calcd for $C_{43}H_{75}N_4O_6$: 743.5681; found 743.5684.

3β-[(3-((*N′*,*N″*-Di(*tert*-butoxycarbonyl))guanidinyl)propyl)carbamoyl]β-sitosterol (C5b). 113 mg (79%); IR: ν_{max} 3332, 2959, 2937, 2869, 1692, 1644, 1620, 1572, 1514, 1415, 1367, 1329, 1275, 1258, 1231, 1155, 1133, 1072, 1052, 1027 cm^{-1}; ^1H NMR (400 MHz, $CDCl_3$): δ 0.65 (s, 3H, CH_3-18), 0.81 (m, 9H, CH_3-26, CH_3-27 and CH_3-29), 0.89 (d, *J* = 6.4 Hz, 3H, CH_3-21), 0.97 (s, 3H, CH_3-19), 1.03−1.40 and 1.66−2.35 (m, CH_2-28, −$NHCH_2C\underline{H}_2CH_2NHCO_2$-Chol and protons in β-sitosteryl skeleton), 1.47 (s, 9H, $C(CH_3)_3$), 1.48 (s, 9H, $C(CH_3)_3$), 3.16 (d, *J* = 5.0 Hz, 2H, −$NHCH_2CH_2C\underline{H}_2NHCO_2$-Chol), 3.48 (d, *J* = 5.7, 2H, −$NHC\underline{H}_2CH_2CH_2NHCO_2$-Chol), 4.47 (m, 1H, H-3-Chol), 5.35 (br s, 1H, H-6-Chol), 6.02 (s, 1H, −$N\underline{H}CO_2$-Chol), 8.38 (s, 1H, −$NHC(=N)N\underline{H}(CH_2)_3$), 11.36 (s, 1H, $(CH_3)_3COCON\underline{H}$); ^{13}C NMR (100 MHz, $CDCl_3$): 11.8, 11.9, 18.7, 19.0, 19.3, 19.8, 21.0, 23.1, 24.3, 26.1, 28.1, 28.3, 29.2, 31.2, 31.9, 34.0, 36.1, 36.6, 38.3, 38.7, 39.7, 42.3, 45.9, 50.0, 56.1, 56.4, 73.9, 122.1, 139.4 (carbons in β-sitosteryl skeleton), 28.1 and 28.3 ($(CH_3)_3$), 30.3 (−$NHCH_2\underline{C}H_2CH_2NHCO_2$-Chol), 37.4 (−$NH\underline{C}H_2CH_2CH_2NHCO_2$-Chol), 39.0 (−$NHCH_2CH_2\underline{C}H_2NHCO_2$-Chol), 79.3 and 83.3 ($\underline{C}(CH_3)_3$), 153.2 and 163.1 (C=O of Boc group), 156.6 (C=O

carbamoyl), 157.6 (C=NH); MS (ESI^+): *m/z* 757.7 ($[M + H]^+$, 100%); HRMS (ESI-TOF) *m/z*: $[M + H]^+$ calcd for $C_{44}H_{77}N_4O_6$: 757.5838; found 757.5821.

3.3.9 Synthesis of Lipids L3b and L7b

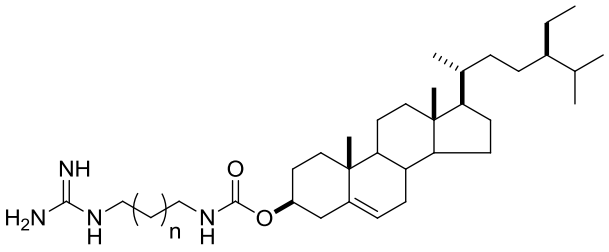

L3b; n = 0
L7b; n = 1

To a solution of **C4b** or **C5b** (80.0 mg, 0.11 mmol) in CH_2Cl_2 (2 mL) was added TFA (0.5 mL). The reaction mixture was stirred at room temperature for 2 h. The solvent was removed by flowing nitrogen gas. The residue was purified by silica gel column chromatography (1:1 hexane/CH_2Cl_2 to 95:5 CH_2Cl_2/MeOH).

3β-[(2-(Guanidinyl)ethyl)carbamoyl]β-sitosterol (L3b). 50 mg (84%); IR: ν_{max} 3364, 3213, 2956, 2868, 1664, 1536, 1445, 1380, 1278, 1192, 1134, 1016 cm^{-1}; ^1H NMR (400 MHz, $CDCl_3$): δ 0.61 (s, 3H, CH_3-18), 0.75 (m, 9H, CH_3-26, CH_3-27 and CH_3-29), 0.85 (d, *J* = 6.3 Hz, 3H, CH_3-21), 0.93 (s, 3H, CH_3-19), 0.97−2.24 (m, CH_2-28 and protons in β-sitosteryl skeleton), 3.16 (m, 4H, −NH($C\underline{H}_2$)$_2$NHCO$_2$-Chol), 4.36 (m, 1H, H-3-Chol), 5.29 (br s, 1H, H-6-Chol), 6.20 (−N$\underline{H}$(CH_2)$_2$NHCO$_2$-Chol), 6.99 (−NH C(C=N$\underline{H}$)NH_2), 7.95 (−NHC(C=NH)N$\underline{H}_2$); ^{13}C NMR (100 MHz, $CDCl_3$): 11.7, 11.8, 18.7, 18.9, 19.2, 19.7, 20.9, 23.0, 24.2, 26.0, 27.9, 28.1, 29.0, 31.8, 31.8, 33.8, 36.0, 36.5, 36.8, 38.3, 39.6, 42.2, 45.7, 50.0, 56.0, 56.6, 75.1, 122.5, 139.6 (carbons in β-sitosteryl skeleton), 39.4 (−NH$\underline{C}H_2CH_2$NHCO$_2$-Chol), 40.8 (−NHCH$_2\underline{C}H_2$NHCO$_2$-Chol), 157.5 (C=O carbamoyl), 157.7 (C=NH); MS (ESI^+): *m/z* 543.9 ($[M + H]^+$, 38%); HRMS (ESI-TOF) *m/z*: $[M + H]^+$ calcd for $C_{33}H_{59}N_4O_2$: 543.4633; found 543.4614.

3β-[(3-(Guanidinyl)propyl)carbamoyl]β-sitosterol (L7b). 48 mg (78%); IR: ν_{max} 3402, 1672, 1440, 1189, 1129 cm^{-1}; ^{1}H NMR (400 MHz, $CDCl_3$): δ 0.54 (s, 3H, CH_3-18), 0.69 (m, 9H, CH_3-26, CH_3-27 and CH_3-29), 0.78 (d, *J* = 6.0 Hz, 3H, CH_3-21), 0.87 (s, 3H, CH_3-19), 0.99−2.17 (m, CH_2-28, −$NHCH_2C\underline{H}_2CH_2NHCO_2$-Chol and protons in β-sitosteryl skeleton), 3.02 (d, *J* = 5.0 Hz, 2H, −$NHCH_2CH_2C\underline{H}_2NHCO_2$-Chol), 3.24 (m, 2H, −$NHC\underline{H}_2CH_2CH_2NHCO_2$-Chol), 4.29 (m, 1H, H-3-Chol), 5.22 (br s, 1H, H-6-Chol); ^{13}C NMR (100 MHz, $CDCl_3$): 11.9, 12.0, 18.2, 18.7, 18.9, 19.0, 19.8, 23.0, 26.1, 26.2, 28.2, 28.5, 29.1, 31.9, 32.4, 33.9, 35.4, 35.9, 36.1, 36.1, 38.8, 42.5, 45.7, 50.6, 56.2, 56.4, 74.5, 121.7, 139.6 (carbons in β-sitosteryl skeleton), 29.1 (−NH $CH_2\underline{C}H_2CH_2NHCO_2$-Chol), 38.4 (−$NH\underline{C}H_2CH_2CH_2NHCO_2$-Chol), 40.1 (−$NHCH_2CH_2$ $\underline{C}H_2NHCO_2$-Chol), 157.2 (C=O carbamoyl), 165.4 (C=NH); MS (ESI^+): *m/z* 557.8 ($[M + H]^+$, 100%); HRMS (ESI-TOF) *m/z*: $[M + H]^+$ calcd for $C_{34}H_{61}N_4O_2$: 557.4789; found 557.4773.

3.3.10 Synthesis of Lipids L4b and L8b

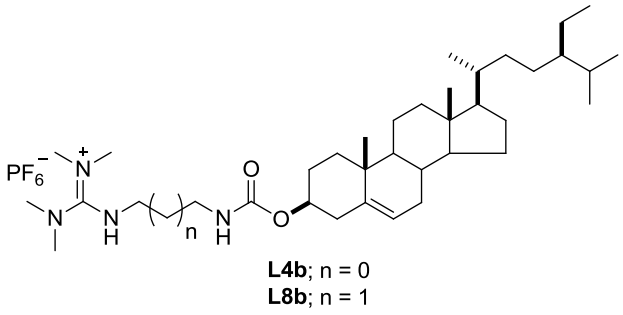

L4b; n = 0
L8b; n = 1

To a solution of lipid **L1b** (100 mg, 0.20 mmol) or **L5b** (100 mg, 0.19 mmol) in DMF (10 mL) was added *O*-(benzotriazol-1-yl)-*N*,*N*,*N*′,*N*′-tetramethyluronium hexafluorophosphate (90 mg, 0.24 mmol and 88.46 mg, 0.23 mmol, respectively) and DIEA (3 drops). The reaction mixture was stirred at room temperature for 12 h and then washed with water (3×100 mL). The organic layer was combined, dried over Na_2SO_4, filtered, and concentrated to afford a white amorphous solid, which was purified by silica gel column chromatography (CH_2Cl_2 to 90:10 CH_2Cl_2/MeOH).

3β-[(2-((*N′*,*N′*,*N″*,*N″*-Tetramethyl)guanidinyl)ethyl)carbamoyl]β-sitosterol (L4b). 149 mg (quant.); IR: ν_{max} 3418, 3298, 2957, 2933, 2868, 2851, 1689, 1590, 1463, 1421, 1405, 1378, 1332, 1224, 1173, 1097, 1007 cm^{-1}; ^{1}H NMR (400 MHz, $CDCl_3$ + 10 drops of CD_3OD): δ 0.65 (s, 3H, CH_3-18), 0.83 (m, 9H, CH_3-26, CH_3-27 and CH_3-29), 0.89 (d, *J* = 6.4 Hz, 3H, CH_3-21), 0.98 (s, 3H, CH_3-19), 1.02−2.28 (m, CH_2-28 and protons in β-sitosteryl skeleton), 2.98 (s, 10H, (−NHC$\underline{H}_2$C$\underline{H}_2$NHC(N(C$\underline{H}_3$)$_2$)), 3.40 (s, 6H, −NHCH$_2$CH$_2$NHC(N$^+$(C$\underline{H}_3$)$_2$)), 4.42 (m, 1H, H-3-Chol), 5.33 (br s, 1H, H-6-Chol), 6.72 (s, 1H, N=CN$\underline{H}$CH$_2$CH$_2$NHCO$_2$-Chol); ^{13}C NMR (100 MHz, $CDCl_3$ + 10 drops of CD_3OD): 11.8, 12.0, 18.8, 19.0, 19.3, 19.8, 21.0, 23.3, 24.3, 26.1, 28.0, 28.2, 29.1, 31.8, 31.9, 33.9, 36.1, 36.6, 36.9, 38.5, 40.0, 42.3 , 45.8, 50.1, 56.1, 56.7, 75.1, 122.6, 139.7 (carbons in β-sitosteryl skeleton), 39.4 (C=N$^+$(C$\underline{H}_3$)$_2$), 40.0 (−NH$\underline{C}$H$_2$CH$_2$NHCO$_2$-Chol), 40.3 (N(CH$_3$)$_2$), 40.0 (−NHCH$_2$$\underline{C}H_2$NHCO$_2$-Chol), 157.8 (C=O carbamoyl), 161.9 (C=NH); MS (ESI$^+$): *m/z* 600.0 ([M]$^+$, 100%); HRMS (ESI-TOF) *m/z*: [M]$^+$ calcd for $C_{37}H_{67}N_4O_2$: 599.5259; found 599.5256.

3β-[(3-((*N′*,*N′*,*N″*,*N″*-Tetramethyl)guanidinyl)propyl)carbamoyl]β-sitosterol (L8b). 144 mg (quant.); IR: ν_{max} 3451, 3291, 2944, 2908, 2870, 1697, 1665, 1623, 1598, 1459, 1409,1379, 1333,1308, 1208, 1171, 1101, 1042, 835 cm^{-1}; ^{1}H NMR (400 MHz, $CDCl_3$): δ 0.64 (s, 3H, CH_3-18), 0.82 (m, 9H, CH_3-26, CH_3-27 and CH_3-29), 0.88 (d, *J* = 6.4 Hz, 3H, CH_3-21), 0.98 (s, 3H, CH_3-19), 1.02−2.27 (m, CH_2-28, −NHCH$_2$C$\underline{H}_2$CH$_2$NHCO$_2$-Chol and protons in β-sitosteryl skeleton), 2.97 (s, 12H, (−NHC (=N$^+$(C$\underline{H}_3$)$_2$)(N(C$\underline{H}_3$)$_2$)), 3.24 (s, 2H, −NHCH$_2$CH$_2$C$\underline{H}_2$NHCO$_2$-Chol), 3.24 (s, 2H, −NHC$\underline{H}_2$CH$_2$CH$_2$NHCO$_2$-Chol), 4.39 (m, 1H, H-3-Chol), 5.03 (m, 1H, −N$\underline{H}$(CH$_3$)$_2$NHCO$_2$-Chol), 5.32 (br s, 1H, H-6-Chol), 6.43 (s, 1H, −N$\underline{H}$CO$_2$-Chol), 7.99 (s, 1H, −N$\underline{H}$CO$_2$-Chol); ^{13}C NMR (100 MHz, $CDCl_3$): 11.8, 12.0, 18.8, 19.0, 19.3, 19.8, 21.0, 23.1, 24.3, 26.1, 28.1, 28.2, 29.1, 31.8, 31.9, 33.9, 36.1, 36.6, 37.0, 38.5, 39.7, 42.3, 45.8, 50.0, 56.1, 56.7, 74.7, 122.5, 139.8 (carbons in β-sitosteryl skeleton), 30.1 (−NHCH$_2$$\underline{C}H_2CH_2$NHCO$_2$-Chol), 37.4 (−NH$\underline{C}H_2CH_2CH_2$NHCO$_2$-Chol), 39.9 (C=N$^+$(C$\underline{H}_3$)$_2$), 39.9 (N(CH$_3$)$_2$), 39.9 (−NHCH$_2CH_2$$\underline{C}H_2$NHCO$_2$-Chol), 157.3 (C=O carbamoyl), 161.8 (C=NH); MS (ESI$^+$): *m/z* 614.2 ([M]$^+$, 100%); HRMS (ESI-TOF) *m/z*: [M]$^+$ calcd for $C_{38}H_{69}N_4O_2$: 613.5415; found 613.5410.

3.3.11 Synthesis of Lipid L9

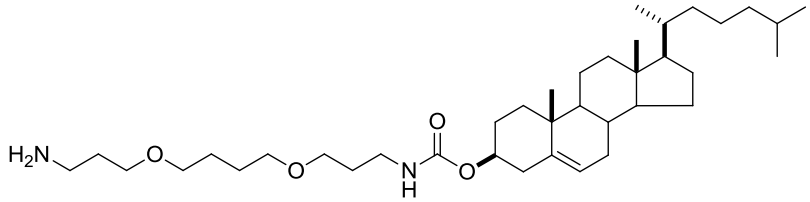

L9

To a solution of cholesteryl chloroformate (500 mg, 1.1 mmol) in CH_2Cl_2 (10 mL) was added 1,4-bis(3-aminopropoxy)butane (224.4 mg, 1.1 mmol). The reaction mixture was stirred at room temperature for 24 h and then washed with water (3×100 mL). The organic layer was combined, dried over Na_2SO_4, filtered, and concentrated to afford a yellow oil, which was purified by silica gel column chromatography (1:1 hexane/CH_2Cl_2 to 80:20 CH_2Cl_2/MeOH) to give lipid **L9** (536 mg, 79%). IR: ν_{max} 3356, 3346, 2936, 2866, 1695, 1523, 1466, 1376, 1366, 1249, 1105, 1031, 1011 cm^{-1}; ^1H NMR (400 MHz, $CDCl_3$ + CD_3OD): δ 0.58 (s, 3H, CH_3-18), 0.76 (d, *J* = 6.4 Hz, 6H, CH_3-26 and CH_3-27), 0.83 (d, *J* = 6.2 Hz, 3H, CH_3-21), 0.90 (s, 3H, CH_3-19), 0.91-1.40 and 0.94−2.23 (m, protons in cholesteryl skeleton), 1.53 (m, 6H, –$OCH_2C\underline{H}_2C\underline{H}_2CH_2O$–, $NH_2CH_2C\underline{H}_2CH_2O$–), 1.93 (m 2H, –$OCH_2C\underline{H}_2CH_2NHCO_2$-Chol), 2.99 (br s, 2H, –$OC\underline{H}_2CH_2CH_2CH_2O$–), 3.12 (m, 2H, –$OCH_2CH_2C\underline{H}_2NHCO_2$-Chol), 3.34 (m, 6H $NH_2C\underline{H}_2CH_2C\underline{H}_2O$–, –$OCH_2CH_2$-$CH_2C\underline{H}_2O$–), 3.48 (br s, 2H (–$OC\underline{H}_2CH_2CH_2NHCO_2$-Chol)), 4.35 (m, 1H, H-3-Chol), 5.27 (br s, 1H, H-6-Chol); ^{13}C NMR (100 MHz, $CDCl_3$ + CD_3OD): 11.7, 18.5, 19.1, 20.9, 22.3, 22.6, 23.6, 24.1, 27.8, 28.0, 28.1, 31.6, 31.7, 35.6, 36.0, 36.4, 36.8, 38.4, 39.3, 39.5, 42.1, 49.8, 55.9, 56.5, 74.3, 122.4, 139.6 (carbons in cholesteryl skeleton), 26.0, 27.8, 29.5, 31.7, 38.5, 38.6, 68.6, 68.8, 70.5, 71.1 (carbons in 1,4-bis(3-aminopropoxy)butane), 156.5 (CO carbamoyl); HRMS (ESI-TOF) *m/z*: $[M + H]^+$ calcd for $C_{38}H_{69}N_2O_4$: 617.5252; found 617.5221.

3.3.12 Synthesis of Compound C6

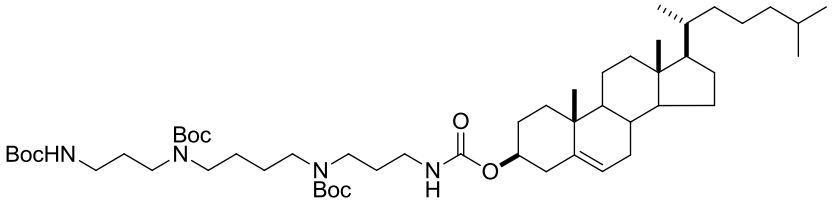

C6

To a solution of cholesteryl chloroformate (500 mg, 1.1 mmol) in CH_2Cl_2 (10 mL) was added spermine-Boc (442 mg, 1.1 mmol). The reaction mixture was stirred at room temperature for 24 h and then washed with water (3×100 mL). The organic layer was combined, dried over Na_2SO_4, filtered, and concentrated to afford a white amorphous solid, which was purified by silica gel column chromatography (CH_2Cl_2) to afford **C6** (705 mg, 70%) as a white solid. IR: ν_{max} 3348, 3006, 2968, 2941, 2868, 1688, 1514, 1470, 1417, 1364, 1273, 1258, 1160, 1082, 1032 cm^{-1}; ^1H NMR (400 MHz, $CDCl_3$ + CD_3OD + D_2O): δ 0.65 (s, 3H, CH_3-18), 0.83 (d, *J* = 6.4 Hz, 6H, CH_3-26 and CH_3-27), 0.88 (d, *J* = 6.2 Hz, 3H, CH_3-21), 0.98 (s, 3H, CH_3-19), 1.43 (s, 27H, 3×Boc groups), 1.05−1.31 and 2.00−2.33 (m, protons in cholesteryl skeleton), 1.62 (m, 4H, ($BocNCH_2C\underline{H}_2C\underline{H}_2CH_2NBoc$)), 1.83 (m, 4H, ($BocNHCH_2C\underline{H}_2CH_2NBoc$), ($BocNCH_2C\underline{H}_2CH_2NHCO_2$-Chol)), 3.11-3.21 (m, 12H, ($BocNHC\underline{H}_2CH_2C\underline{H}_2NBoc$), ($BocNC\underline{H}_2CH_2CH_2C\underline{H}_2NBoc$), ($BocNC\underline{H}_2CH_2C\underline{H}_2NHCO_2$-Chol)), 4.45 (m, 1H, H-3-Chol), 5.27 (br s, 1H, $N\underline{H}CO_2$-Chol), 5.34 (br s, 1H, H-6-Chol); ^{13}C NMR (100 MHz, $CDCl_3$ + CD_3CD + D_2O): 11.8, 18.7, 19.3, 21.0, 22.5, 22.8, 23.8, 24.3, 28.0, 28.2, 28.4, 29.1, 31.9, 35.7, 36.2, 36.6, 37.0, 38.6, 39.5, 39.7, 42.3, 50.0, 55.1, 56.7, 74.2, 122.3, 140.0 (carbons in cholesteryl skeleton), 25.5, 25.9, 28.9, 28.0, 37.5, 37.6, 43.9, 46.3, 46.4, 46.7 (carbons in spermine), 28.4 (3 × $(CH_3)_3$ of Boc groups), 79.6 (3 × $CO_2\underline{C}(CH_3)_3$ of Boc groups), 156.2 (CO carbamoyl), 156.0, 155.4, 155.6 (CO of Boc groups); MS (ES^+): m/z 938.3 ($[M + Na]^+$, 100%); HRMS (ESI-TOF) *m/z*: $[M + Na]^+$ calcd for $C_{53}H_{94}N_4NaO_8$: 937.6964; found 937.6966.

3.3.13 Synthesis of Lipid L10

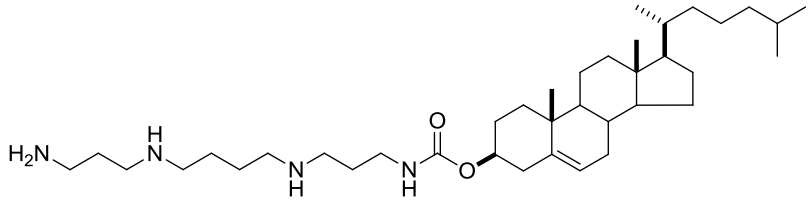

L10

To a solution of **C6** (200 mg, 0.21 mmol) CH_2Cl_2 (2 mL) was added TFA (0.5 mL). The reaction mixture was stirred at room temperature for 2 h. The solvent was removed by flowing nitrogen gas. The residue was purified by silica gel column chromatography (1:1 hexane/CH_2Cl_2 to 80:20 CH_2Cl_2/MeOH) to afford **L10** (119 mg, 92%). IR: ν_{max} 3402, 3027, 2944, 2868, 1666, 1604, 1527, 1485, 1430, 1258, 1197, 1176, 1128, 1043 cm^{-1}; ^1H NMR (400 MHz, $CDCl_3$ + CD_3OD): δ 0.51 (s, 3H, CH_3-18), 0.69 (d, *J* = 6.4 Hz, 6H, CH_3-26 and CH_3-27), 0.75 (d, *J* = 6.2 Hz, 3H, CH_3-21), 0.84 (s, 3H, CH_3-19), 0.91−1.40 and 1.68−2.13 (m, protons in cholesteryl skeleton), 1.57 (m, 4H, −NHCH$_2$C<u>H$_2$</u>C<u>H$_2$</u>CH$_2$NH−), 1.67 (m, 4H, NH$_2$CH$_2$C<u>H$_2$</u>CH$_2$-NH−, −NHCH$_2$C<u>H$_2$</u>CH$_2$NHCO$_2$-Chol), 2.81−2.92 (m, 8H, NH$_2$C<u>H$_2$</u>CH$_2$C<u>H$_2$</u>NH−, −NHC<u>H$_2$</u>CH$_2$CH$_2$C<u>H$_2$</u>NH−), 3.01 (m, 2H −NHC<u>H$_2$</u>CH$_2$CH$_2$NHCO$_2$-Chol), 3.17 (m, 2H −NHCH$_2$CH$_2$C<u>H$_2$</u>NHCO$_2$-Chol), 4.24 (m, 1H, H-3-Chol), 5.19 (br s, 1H, H-6-Chol); ^{13}C NMR (100 MHz, $CDCl_3$ + CD_3OD): 11.5, 18.3, 18.9, 20.7, 22.1, 22.4, 23.5, 23.9, 27.7, 27.9, 29.8, 31.6, 32.0, 35.5, 35.9, 36.2, 36.7, 38.1, 39.2, 39.4, 42.0, 49.8, 55.9, 56.4, 74.6, 122.3, 139.5 (carbons in cholesteryl skeleton), 26.1, 26.2, 27.7, 29.4, 37.1, 39.2, 44.2, 45.1, 46.7, 46.7 (carbons in spermine), 157.2 (CO carbamoyl); MS (ES^+): m/z 615.0 ($[M + H]^+$, 100%); HRMS (ESI-TOF) *m/z*: $[M+H]^+$ calcd for $C_{38}H_{70}N_4NaO_2$: 637.5391; found 637.5435.

3.3.14 Synthesis of Compound C7

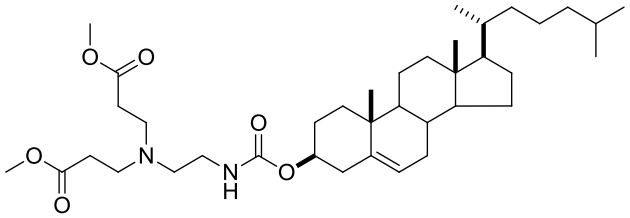

C7

To a solution of lipid **L1a** (502 mg, 1.06 mmol) in MeOH (10 mL) was added methyl acrylate (10.0 mL, 0.12 mol). The reaction mixture was stirred at room temperature for 5 days. The solvent was removed under reduced pressure to afford a yellow oil, which was purified by silica gel column chromatography (CH_2Cl_2) to afford **C7** (560 mg, 82%) as a yellow oil. IR: ν_{max} 3390, 2955, 2934, 2867, 2851, 1724, 1515, 1463, 1438, 1377, 1258, 1197, 1047, 1029, 1009, 959 cm^{-1}; ^1H NMR (400 MHz, $CDCl_3$): δ 0.65 (s, 3H, CH_3-18), 0.84 (d, J = 6.5 Hz, 6H, CH_3-26 and CH_3-27), 0.89 (d, J = 6.4 Hz, 3H, CH_3-21), 0.98 (s, 3H, CH_3-19), 0.93−2.0 (m, protons in cholesteryl skeleton), 2.26−2.52 (m, 6H, 2×COC$\underline{H}_2$$CH_2$N−, −NC$\underline{H}_2$$CH_2NHCO_2$-Chol), 2.74 (br s, 4H, (2×CH_2C$\underline{H}_2$N−), 3.22 (br s, 2H, −NCH_2C$\underline{H}_2$NHCO_2-Chol), 3.67 (s, 6H, 2×OCH_3), 4.47 (m, 1H, H-3-Chol), 5.20 (br s, 1H, N$\underline{H}$CO_2-Chol), 5.35 (br s, 1H, H-6-Chol); ^{13}C NMR (100 MHz, $CDCl_3$): 11.8, 18.7, 19.3, 21.0, 22.5, 22.8, 23.8, 24.3, 28.0, 28.2, 28.2, 31.9, 31.9, 35.8, 36.2, 36.6, 37.0, 38.6, 39.5, 39.7, 42.3, 50.0, 55.2, 56.7, 74.2, 122.4, 139.9 (carbons in cholesteryl skeleton), 32.6, 32.6, 49.3, 51.7, 51.7, 51.8 (2×CO$\underline{C}$$H_2$$\underline{C}$$H_2$N−, −N$\underline{C}$$H_2$$\underline{C}$$H_2CO_2$-Chol), 53.2 (2×$OCH_3$), 156.3 (CO carbamoyl), 172.9 (CO(OCH_3)$_2$); MS (ES^+): m/z 646.6 ($[M + H]^+$, 100%); HRMS (ESI-TOF) *m/z*: $[M + H]^+$ calcd for $C_{38}H_{65}N_2O_6$: 645.4837; found 645.4832.

3.3.15 Synthesis of Lipid L11

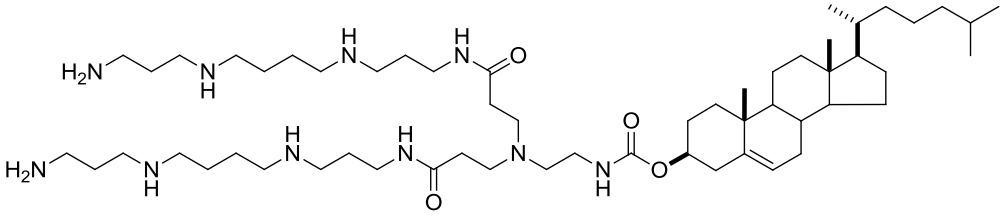

L11

To a solution of lipid **C7** (200 mg, 0.31 mmol) in MeOH (10 mL) was added spermine (125 mg, 0.62 mol). The reaction mixture was stirred at room temperature for 5 days. The solvent was removed under reduced pressure to afford a yellow oil, which was purified by sephadex column chromatography (MeOH) to give **L11** (272 mg, 89%). IR: ν_{max} 3248, 3115, 2927, 2867, 1704, 1621, 1582, 1476, 1396, 1370, 1274, 1262, 1127 cm^{-1}; ^{1}H NMR (400 MHz, $CDCl_3$ + CD_3OD): δ 0.58 (s, 3H, CH_3-18), 0.77 (d, *J* = 6.6 Hz, 6H, CH_3-26 and CH_3-27), 0.82 (d, *J* = 6.5 Hz, 3H, CH_3-21), 0.91 (s, 3H, CH_3-19), 0.98−1.44 and 1.75−2.35 (m, protons in cholesteryl skeleton), 1.47 (m, 8H, 2×NHCH$_2$C<u>H$_2$</u>C<u>H$_2$</u>CH$_2$NH), 1.61 (m, 8H, 2×NH$_2$CH$_2$C<u>H$_2$</u>CH$_2$NH−, 2× −NHCH$_2$C<u>H$_2$</u>CH$_2$NHCO), 2.38 (m, 2H, NC<u>H$_2$</u>CH$_2$NHCO$_2$-Chol), 2.45, 3.28 (m, 4H, 2×COC<u>H$_2$</u>CH$_2$N), 2.35, 3.59 (m, 4H, 2×COCH$_2$C<u>H$_2$</u>N−), 2.55−2.69 (m, 20H 2×NH$_2$C<u>H$_2$</u>CH$_2$C<u>H$_2$</u>NH−, 2× −NHC<u>H$_2$</u>CH$_2$CH$_2$C<u>H$_2$</u>NH−, 2× −NHC<u>H$_2$</u>CH$_2$CH$_2$NHCO), 3.09−3.17 (m, 6H 2×NHCH$_2$CH$_2$C<u>H$_2$</u>NHCO, −NCH$_2$C<u>H$_2$</u>NHCO$_2$-Chol), 4.36 (m, 1H, H-3-Chol), 5.27 (br s, 1H, H-6-Chol); ^{13}C NMR (100 MHz, $CDCl_3$ + CD_3OD): 11.7, 18.5, 19.1, 20.9, 22.4, 22.6, 23.6, 24.1, 26.8, 28.0, 28.1, 31.7, 31.7, 35.6, 36.0, 36.4, 36.8, 38.4, 39.3, 39.6, 42.1, 51.6, 55.9, 56.5, 74.3, 122.4, 139.6 (carbons in cholesteryl skeleton), 23.6, 24.1, 27.8, 31.3, 36.4, 39.3, 39.6, 42.1, 47.1, 47.1 (carbons in spermine), 33.6, 44.4, 52.6, 53.3 (2×CO<u>C</u>H$_2$<u>C</u>H$_2$N−, −N<u>C</u>H$_2$<u>C</u>H$_2$CO$_2$-Chol), 156.5 (CO carbamoyl), 173.0, 173.6 (CO amide); HRMS (ESI-TOF) *m/z*: $[M + H]^+$ calcd for $C_{60}H_{113}N_4O_6$: 985.8654; found 985.8644.

3.3.16 Synthesis of Lipids L12

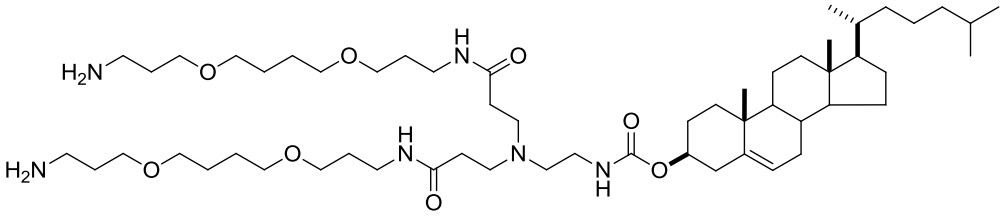

L12

To a solution of lipid **C7** (200 mg, 0.31 mmol) in MeOH (10 mL) was added 1,4-bis(3-aminopropoxy)butane (126 mg, 0.62 mol). The reaction mixture was stirred at room temperature for 5 days. The solvent was removed under reduced pressure to afford a yellow oil, which was purified by sephadex column chromatography (MeOH) to give **L12** (285 mg, 93%). IR: ν_{max} 3359, 3305, 2936, 2863, 1642, 1553, 1467, 1372, 1275, 1260, 1103, 1032 cm^{-1}; ^{1}H NMR (400 MHz, $CDCl_3$ + CD_3OD): δ 0.51 (s, 3H, CH_3-18), 0.69 (d, *J* = 6.6 Hz, 6H, CH_3-26 and CH_3-27), 0.74 (d, *J* = 6.5 Hz, 3H, CH_3-21), 0.84 (s, 3H, CH_3-19), 0.86−1.86 (m, protons in cholesteryl skeleton), 1.44 (m, 12H, 2× $–OCH_2C\underline{H}_2C\underline{H}_2CH_2O–$, 2× $NH_2CH_2C\underline{H}_2CH_2O–$), 1.60 (m, 4H, 2× $–OCH_2C\underline{H}_2CH_2$-NHCO), 2.14 (t, *J* = 6.2 Hz, 6H, $–NCH_2C\underline{H}_2NHCO_2$-Chol, 2× $COCH_2C\underline{H}_2N–$), 2.34 (t, *J* = 6.1 Hz, 2H, $–NC\underline{H}_2CH_2NHCO_2$-Chol), 2.54 (t, *J* = 6.6 Hz, 4H, 2×$NH_2C\underline{H}_2CH_2CH_2O–$), 2.65 (t, *J* = 6.8 Hz, 4H, (2×$COC\underline{H}_2CH_2N–$)), 3.09 (t, *J* = 7.0 Hz, 4H, 2× $NH_2CH_2CH_2C\underline{H}_2O–$), 3.19−3.36 (m, 16H, 2× $–OC\underline{H}_2CH_2C\underline{H}_2$NHCO, 2× $–OC\underline{H}_2CH_2CH_2C\underline{H}_2O–$), 4.25 (m, 1H, H-3-Chol), 5.20 (br s, 1H, H-6-Chol); ^{13}C NMR (100 MHz, $CDCl_3$ + CD_3OD): 11.7, 18.5, 19.2, 20.9, 22.4, 22.6, 23.7, 24.1, 27.9, 28.0, 29.1, 31.8, 31.8, 36.1, 36.4, 36.8, 36.9, 38.3, 38.5, 39.6, 42.2, 49.7, 56.0, 56.6, 74.4, 122.5, 139.7 (carbons in cholesteryl skeleton), 26.2, 26.2, 28.1, 33.7, 39.0, 39.4, 68.4, 68.9, 70.6, 70.8 (2×carbons in 1,4-bis(3-aminopropoxy)butane), 35.7, 44.9, 49.9, 52.5 (2×$CO\underline{C}H_2\underline{C}H_2N–$, $–N\underline{C}H_2\underline{C}H_2CO_2$-Chol), 156.9 (CO carbamoyl), 173.2 (CO amide); HRMS (ESI-TOF) *m/z*: $[M + H]^+$ calcd for $C_{56}H_{105}N_6O_8$: 989.7988; found 989.8028.

3.4 Liposome Preparation

A thin film was prepared from the stock solution of cationic lipid and DOPE (1μg/μL in CH_2Cl_2 or EtOH). DOPE (250 μL) and cationic lipid (250 μL) were mixed together in an eppendrof and the solvent was evaporated to dryness under a stream of nitrogen. The trace of solvent was completely removed under high vacuum for 4–8 h. The thin film was dissolved with PBS buffer, vortex for 30 seconds and sonicated for 20 minutes at room temperature.

3.5 DNA Binding Affinities

Gel electrophoresis was used to evaluate the formulated between DNA and cationic lipids. The complexes were prepared by adding liposome into DNA (0.1 μg). The DNA/lipid ratios of 1:5, 1:10 and 1:20 were examined for the ability to retard DNA migration through 1.0% agarose gel electrophoresis. Ethidium bromide was contained in agarose plate. Loading dry reagent was then added to the lipoplexes. The solutions (10 μL) were loaded into gel and run at 100 V for 30 minutes.

3.6 Transfection Procedure

Human embryonic kidney cells 293 (HEK293), human cervical adenocarcinoma (HeLa), human colon adenocarcinoma (HT29) and human breast adenocarcinoma (MCF7) were grown in DMEM medium supplemented with 10% fetal bovine serum, penicillin (100% units/mL), streptomycin (100 mg/mL) and L-glutamine (4 mM) at 37 °C under 5% CO_2. The cells were seeded up to 1×10^4 cells/well in a 96-well plate to give 50–70% confluence and used on the next day. The old medium was removed and washed with PBS and replaced with 100 μL of fresh serum-free DMEM medium. Lipoplexes were prepared by added liposome (1 μg/μL) into DNA (0.1 μg/μL) and diluted with PBS buffer to total volume about 10 μL. The lipoplexes were added into the cells and incubated at 37 °C under 5% CO_2 for 48 h. The procedure for Lipofectamine2000 transfection was followed the manufacturer's instruction. After 48 h, the old medium was removed and the Z buffer (100 μL) and SDS agent (50 μL) were

added into the cells, after 15 minutes, ONPG solution (10 mg/mL; 100 µL) was added and then the cells were incubated for 4 h before measuring the absorbance at 405 nm. In order to evaluate the transfection efficiency, the pEGFP-C2 plasmid DNA, encoding green fluorescent protein (GFP) was employed. After incubating at 37 °C under 5% CO_2, the cell was measured by fluorescent microscopy.

3.7 Transfection Toxicity

HEK293 cells were seeded on a 96-well plate. The cells were incubated for 24 h at 37 °C under 5% CO_2. The procedure was the same as transfection experiment. After the incubation, MTT (3-(4,5-Dimethylthiazol-2-yl)-2,5-diphenyltetrazolium bromide) (Invitrogen dissolved in PBS) was added to each well to reach the final concentration of 3 mg/mL. The cells were incubated again for 2 h at 37 °C under 5% CO_2. The absorbance was measured at 520 nm on micro plate reader.

3.8 Serum Stability of ODN

Serum stability assay was examined according to previously reported procedures [42]. The serum stability was compared between liposomal ODN with free ODN in the presence and absence of serum. The lipoplexes were incubated with fetal bovine serum at 37 °C for 1, 2, 4, 6, 12 and 24 h. Serum enzyme was inactivated by heating the final mixture at 70 °C for 15 minutes. Gel electrophoresis was performed on 1% agarose gel, containing ethidium bromide for visualization. 10 µL of lipoplexes (the mixture of 0.1 µg of DNA, 2 µg of liposome in PBS and loading dye) were loaded into gel plate and run at 100 V for 30 minutes.

3.9 Size and Zeta Potential Measurements

Photon correlation spectroscopy using a Zeta sizer Nano ZS (Malvern Instrument Ltd. Malvern, UK) was used to analyze particle size and surface charge of DNA/liposome complexes. The prepared complexes was diluted with distilled water and then filtered through a 0.22 μm membrane before performing the measurements in five replicates at room temperature.

CHAPTER 4

RESULTS AND DISCUSSION

4.1 Synthesis

The synthesis of cationic lipids **L1a**–**b** and **L5a**–**b** containing cholesterol and β-sitosterol as the hydrophobic tails, primary amine as the polar head group and carbamate linker started by using cholesteryl chloroformate (**C1**) and β-sitosterol (**C2**) as the staring materials (Scheme 9). Using ethylenediamine and 1,3-diaminopropane to react with **C1** in CH_2Cl_2 provided cholesterol-containing lipids **L1a** and **L5a**, respectively, in one step with different length of the spacers. To synthesize the β-sitosterol-containing lipids, the hydroxyl group of **C2** was activated by treating with *p*-nitrophenyl chloroformate to give carbonate **C3** which was then converted to lipids **L1b** and **L5b** by the reaction with the diamine compounds.

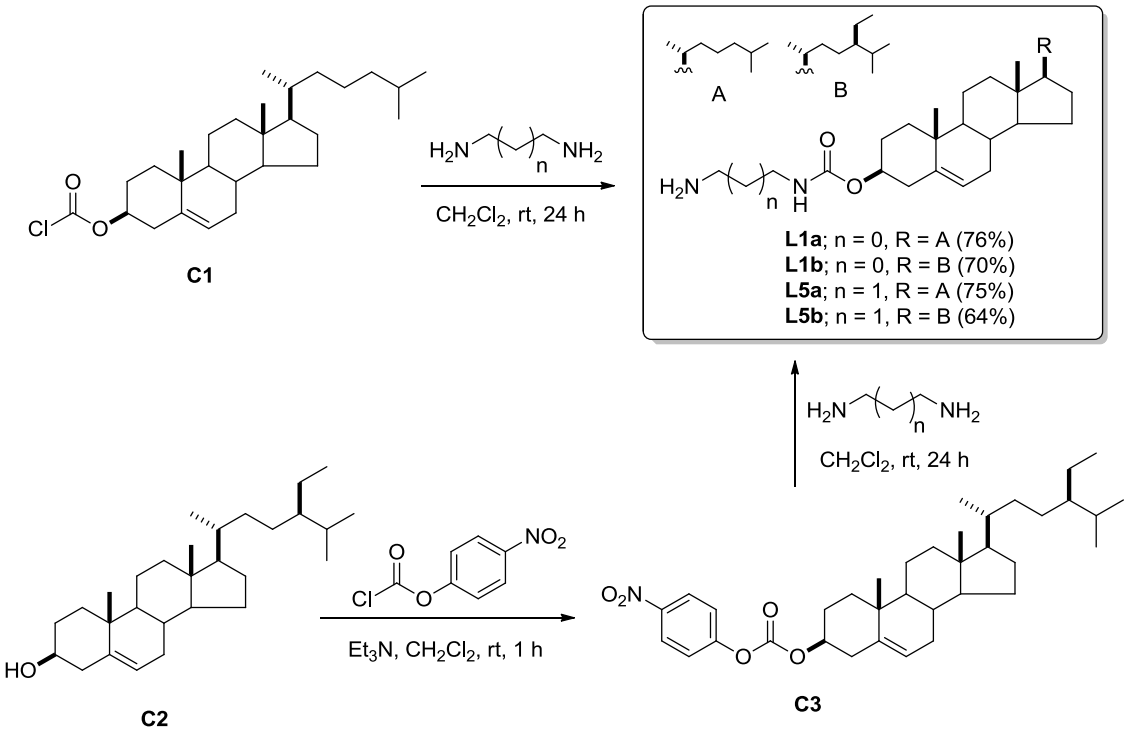

Scheme 1 Synthetic approach to cationic lipids **L1a**–**b** and **L5a**–**b**.

The structural modification of the cationic lipid was considered by converting the free amino group of **L1a**–**b** and **L5a**–**b** to various polar headgroups. Lipids **L2a**–**b** and **L6a**–**b** containing trimethyl ammonium headgroup were prepared from the reaction with methyl iodide and DIEA as shown in Scheme 10. The yields were quite low because these compounds are very high polar and were lost in the separation and purification step due to the existence of the ionic region in the structure.

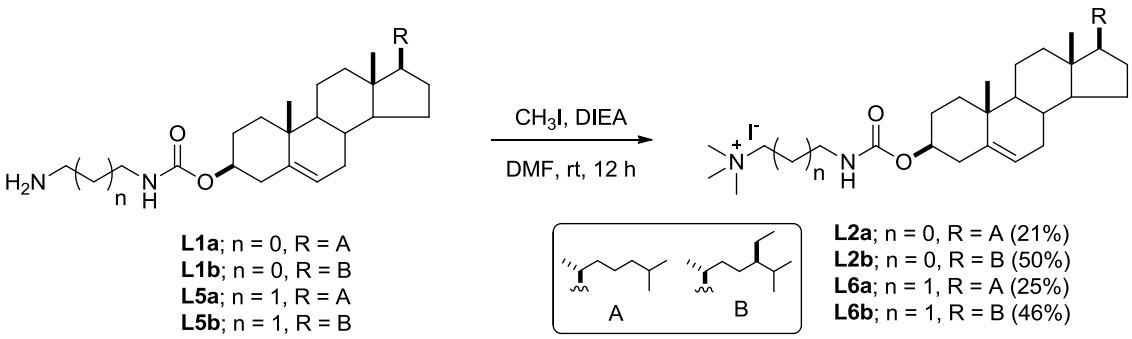

Scheme 2 Synthesis of cationic lipids **L2a**–**b** and **L6a**–**b** containing trimethyl ammonium headgroup.

Guanidine group was also employed to be a polar head group. The reaction with1,3-bis(*tert*-butoxycarbonyl)-2-methyl-2-thiopseudourea provided **C4a**–**b** and **C5a**–**b** (Scheme 13). Removing Boc groups by 20% TFA in CH_2Cl_2 afforded lipids **L3a–b** and **L7a–b** in moderate yield. Moreover, lipids **L4a**–**b** and **L8a**–**b** with tetramethylguanidinium headgroups were synthesized by reaction with HBTU/DIEA as shown in Scheme 12. These compounds were obtained in modest yields after purification because the delocalized positive charge at tetramethylguanidinium group and PF_6^- which is a bulky counterion can generate a weak ionic attraction force in the structure.

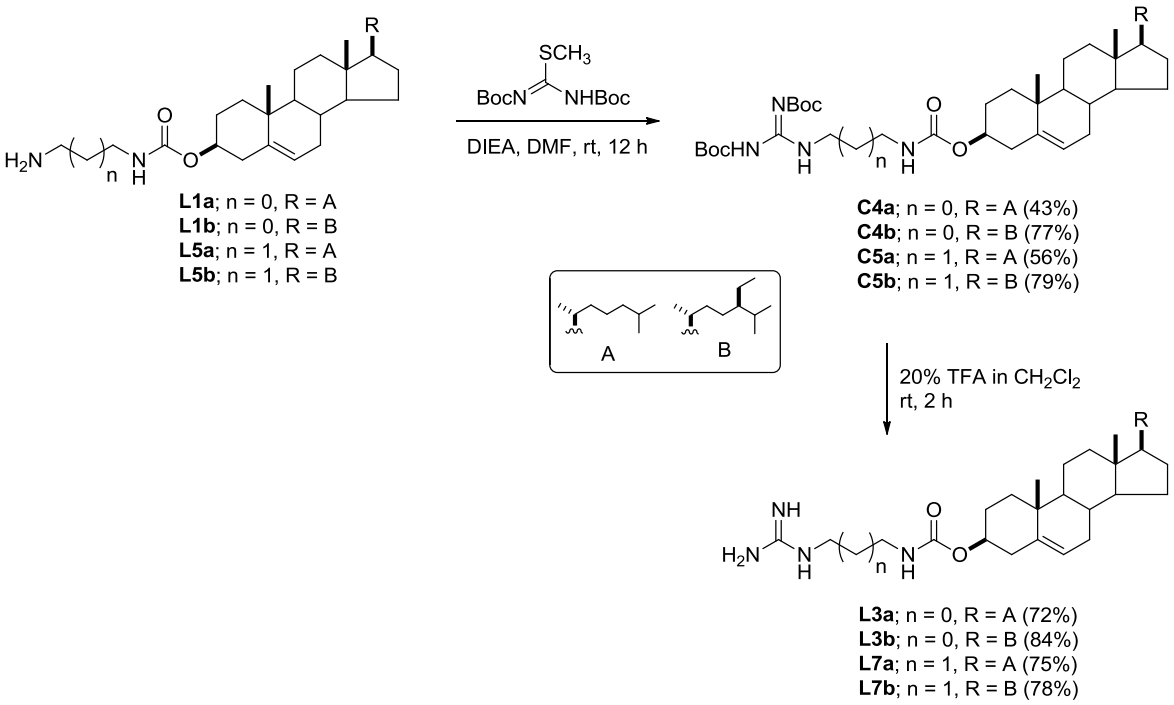

L1a; n = 0, R = A
L1b; n = 0, R = B
L5a; n = 1, R = A
L5b; n = 1, R = B

C4a; n = 0, R = A (43%)
C4b; n = 0, R = B (77%)
C5a; n = 1, R = A (56%)
C5b; n = 1, R = B (79%)

L3a; n = 0, R = A (72%)
L3b; n = 0, R = B (84%)
L7a; n = 1, R = A (75%)
L7b; n = 1, R = B (78%)

Scheme 3 Synthesis of cationic lipids **L3a**–**b** and **L7a**–**b** containing guanidinyl headgroup.

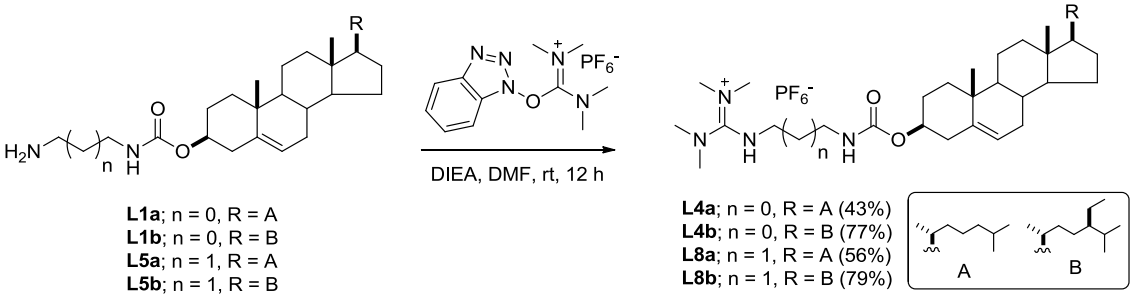

L1a; n = 0, R = A
L1b; n = 0, R = B
L5a; n = 1, R = A
L5b; n = 1, R = B

L4a; n = 0, R = A (43%)
L4b; n = 0, R = B (77%)
L8a; n = 1, R = A (56%)
L8b; n = 1, R = B (79%)

Scheme 4 Synthesis of cationic lipids **L4a**–**b** and **L8a**–**b** containing tetramethyl guanidinium headgroup.

Cholesteryl chloroformate (**C1**) was also utilized to synthesized lipid **L9** containing two oxy groups in the spacer and primary amine as the polar headgroup in one step (Scheme 13). The possible side reaction leading to generate bis-cholesteryl product could be avoided by adding one mole equivalent of 1,4-bis(3-aminopropoxy)butane to react with **C1** under highly diluted condition. **C1** was also reacted with Boc-protected spermine, a polyamine compound, to provide **C6** in moderate yield. Deprotection of Boc groups by 20% TFA in CH_2Cl_2 gave lipid **L10** in excellent yield.

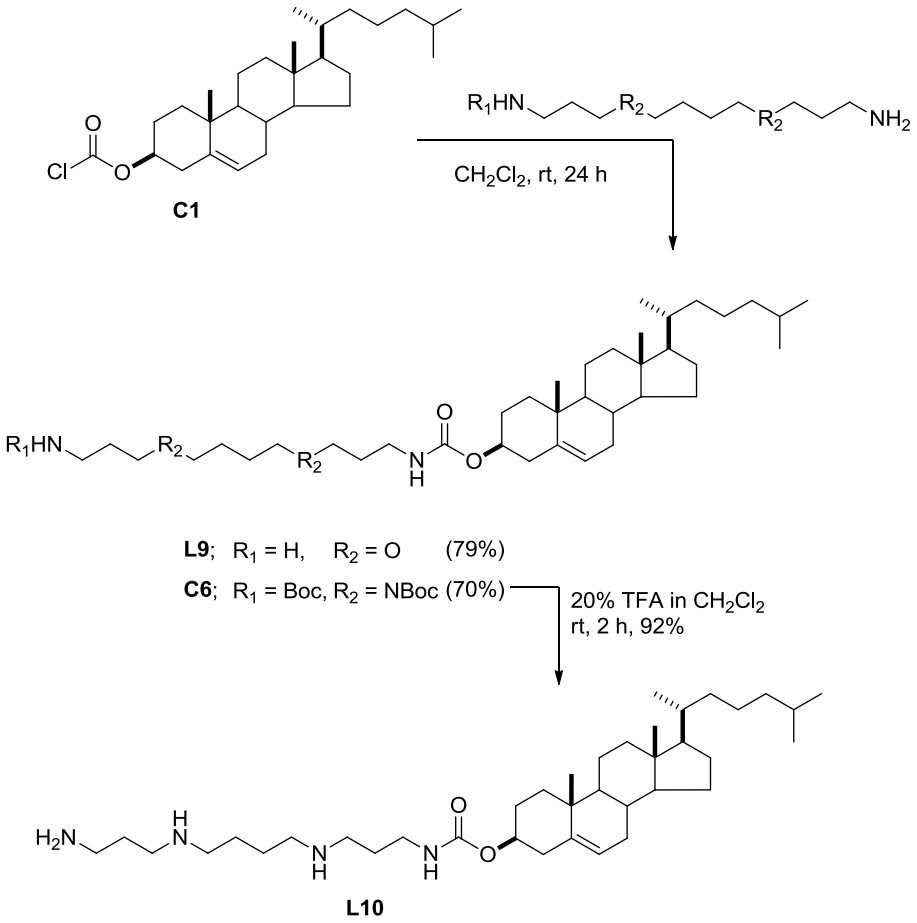

Scheme 5 Synthesis of cationic lipids **L9** and **L10**.

The structural modification was expanded by the synthesis of two-headgroup cationic lipids. Lipid **L1a** was reacted with methyl acrylate in order to introduced two methyl ester groups to provide diester **C7** in good yield. Due to low reactivity of the methyl ester compared to the chloroformate, **C7** can be directly reacted with 2 equiv. of spermine and 1,4-bis(3-aminopropoxy)butane to provide lipids **L11** and **L12** in good yields, respectively (Scheme 14).

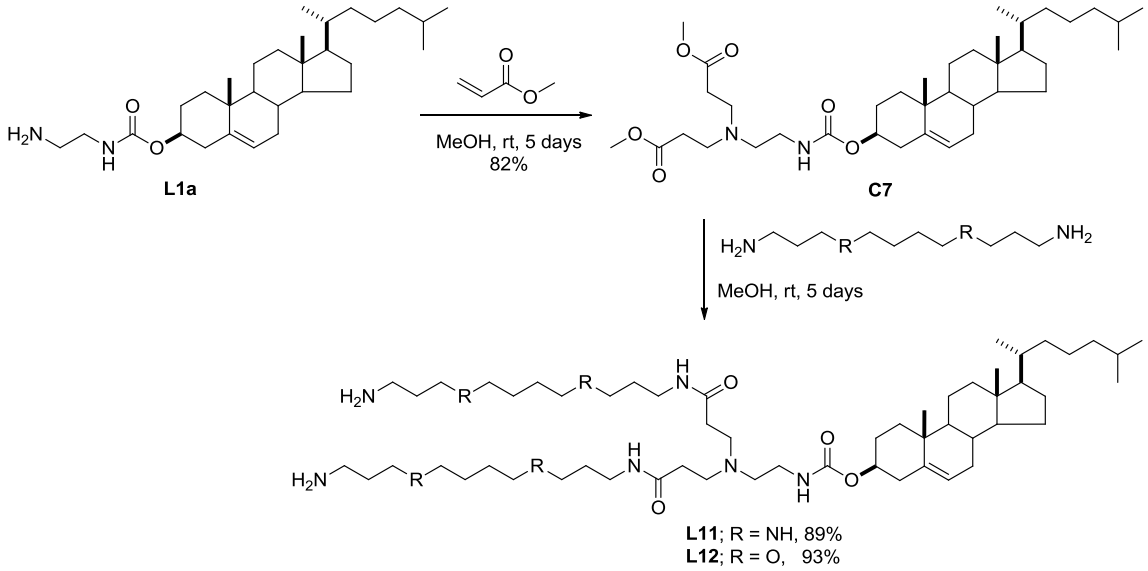

Scheme 6 Synthesis of two-head cationic lipids **L11** and **L12**.

4.2 DNA Binding Affinities

Gel retardation assay was used to measure the DNA binding affinity of the synthesized cationic lipids. The DNA binding ability of the cationic lipids was examined with and without DOPE. The liposomes with DOPE were prepared from individual lipids **L1a**–**L8a** and **L1b**–**L8b** and DOPE at 1:1 weight ratio. The lipoplexes were formulated with plasmid DNA at ratios of 1:5, 1:10 and 1:20 (DNA/lipid, w/w). The gel electrophoresis experiment revealed that lipids **L6a**, **L8a** and **L8b** (DNA:lipid = 1:20, 1:10 and 1:20, respectively) without DOPE showed the strong retardation of DNA movement (Figure 39a and 39c) while lipids **L4a**, **L6a**, **L8a**, **L2b**, **L4b** and **L8b** (DNA:lipid = 1:10 and 1:20) with DOPE showed high DNA binding activity (Figure 41b and 41d). These cationic lipids containing tetramethylguanidinuim and trimethyl guanidinuim as polar head have remarkable ability to form the corresponding liposomes and lipoplexes which is important for transfection process. As shown in Figure 41a and 41c, lipoplexes **L1a**–**L8a** and **L1b**–**L8b** without DOPE could not retard the DNA migration.

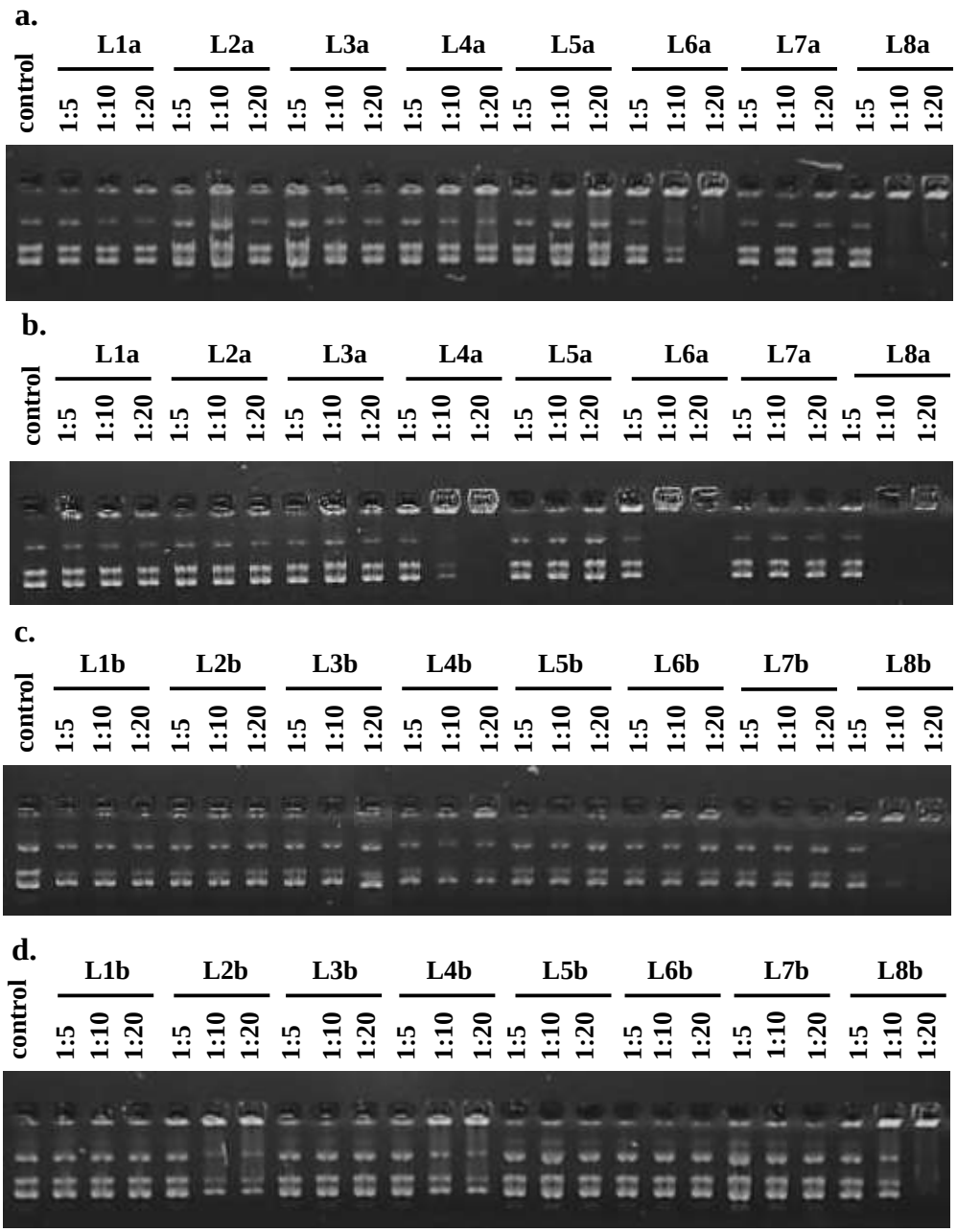

Figure 1 Electrophoretic gel retardation assays of lipoplexes at weight ratios of 1:5, 1:10 and 1:20. (a) Lipoplexes **L1a**–**L8a** without DOPE (b) Lipoplexes **L1a**–**L8a** with DOPE (c) Lipoplexes **L1b**–**L8b** without DOPE (d) Lipoplexes **L1b**–**L8b** with DOPE. The samples were electrophoresed on 1% agarose gel in TBE buffer at 100 V for 30 minutes.

The lipoplexes prepared from the corresponding liposomes **L9**–**L12** both with and without DOPE were also studied for DNA binding affinity. As seen on Figure 40, all formulation completely bound to DNA.

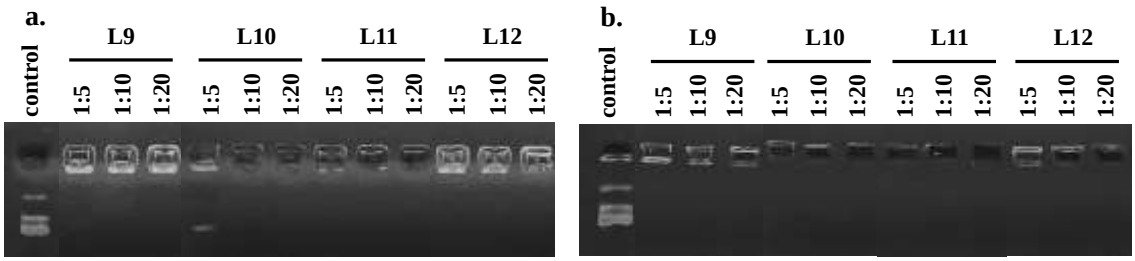

Figure 2 Electrophoretic gel retardation assays of lipoplexes at weight ratios of 1:5, 1:10 and 1:20. (a) Lipoplexes **L9**–**L12** with DOPE (b) Lipoplexes **L9**–**L12** without DOPE. The samples were electrophoresed on 1% agarose gel in TBE buffer at 100 V for 30 minutes.

4.3 Particle Size and Zeta-Potential Measurements

Particle size and zeta potential of lipoplexes were analyzed by dynamic light scattering assay (DLS). The result indicated that the largest particle size was obtained when decrease the DNA/liposome ratio to 1:10 (Figure 41a). Lipoplex **L4a** has the particle size approximately 286–770 nm which has been proved that this range of average particle size are suitable for gene delivery [68,77]. The zeta potential of lipoplex is an indirect measurement for the surface charge. It can be used to evaluate the degree of interaction between the liposomal cationic surface charges and the anionic charges of DNA [78]. In Figure 41b, when increase the amount of liposome, the zeta potential tended to be increased from negative (around -12 and -7 mV at ratio of 1:2 and 1:5, respectively) to positive values (around +0.12, +35 and +34 mV at ratio of 1:10, 1:20 and 1:30). The highest zeta potential was observed at the weight ratio 1:20 which indicate the fully DNA condensation form a lipoplex.

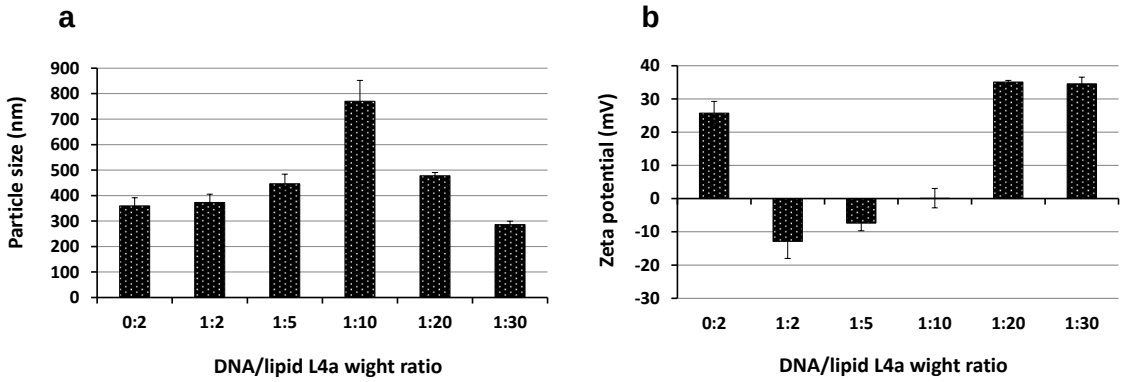

Figure 3 (a) The mean of particle size and (b) zeta potential of the lipoplexes **L4a** under various liposomes/DNA weight ratios. Each value represents the mean ± standard deviation of five measurements.

4.4 Transfection Activity

4.4.1 Transfection Screening

The transfection activity of synthesized cationic lipids was evaluated against HEK293 cells (human embryonic kidney cell lines). ONPG (*O*-nitrophenyl-β-D-galactopyranoside) was used as a substrate to determine the gene expression of β-galactosidase [79,80]. The 0.1 μg of DNA/well and 1:20 DNA/lipids with and without DOPE were selected as the condition for transfection screening. The ratio of liposome and DOPE was used at 1:1 w/w. The relative transfection efficiency screening was shown in Figure 42. Lipids **L4a** and **L6a**, bearing cholesterol as hydrophobic tail, with DOPE showed higher transfection efficiency than other lipids compared with Lipofectamine2000, transfection = 100%, while the lipids with β-sitosterol as hydrophobic tail did not exhibit the transfection activity. Lipids **L4a**, **L4b**, **L6a** and **L6b** were subjected to optimize the transfection efficiency by varying the lipid/DOPE ratios, the DNA/lipid ratios, and the amounts of DNA per well.

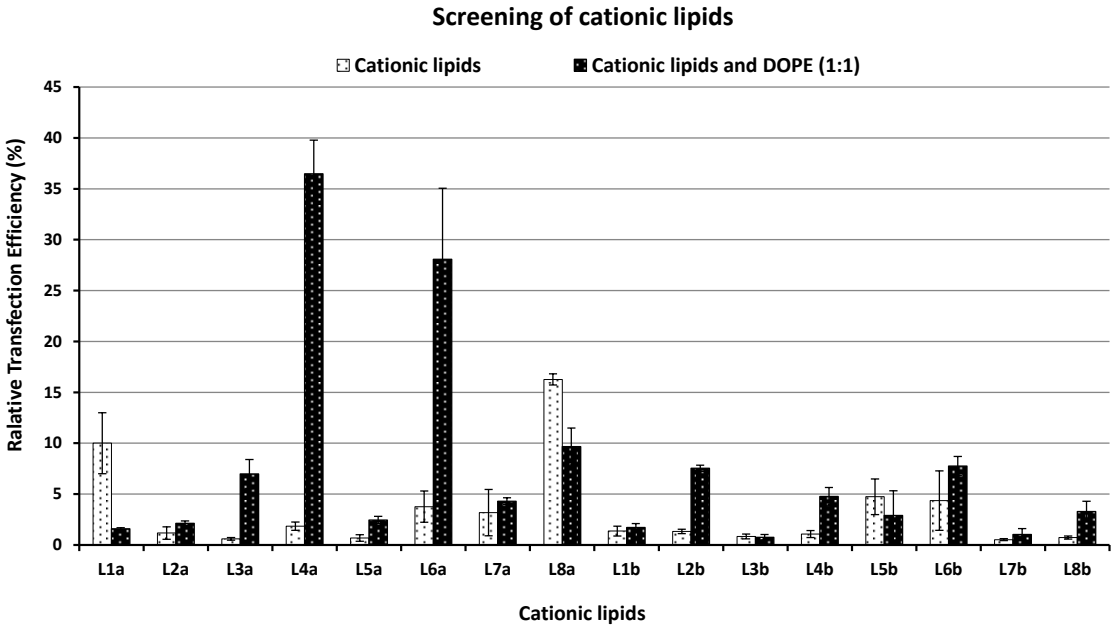

Figure 4 Relative transfection efficiency screening of cationic lipids with DOPE ratio of 1:1 and without DOPE. The corresponding lipoplexes were prepared from pCH110-encoding β-galactosidase (0.1 μg/well) and the lipids in the ratio of 1:20 by weight.

The lipids **L9**−**L12** bearing cholesterol as hydrophobic tail were also examined in the HEK293 cells. The ratio of liposome and DOPE was mixed 1:1 weight ratio. DNA 0.1 μg and 1:20 DNA/lipids were added in well plate. As shown in Figure 43 the lipid **L10** with DOPE showed higher transfection efficiency than other lipids (~30 % transfection efficiency) compared to Lipofectamine2000, transfection = 100%. Other lipids **L9**, **L11** and **L12** with and without DOPE were showed the transfection efficiency less than 20% transfection efficiency. Lipid **L10** was subjected to optimize the transfection efficiency by varying the lipid/DOPE ratios, the DNA/lipid ratios, and the amounts of DNA per well.

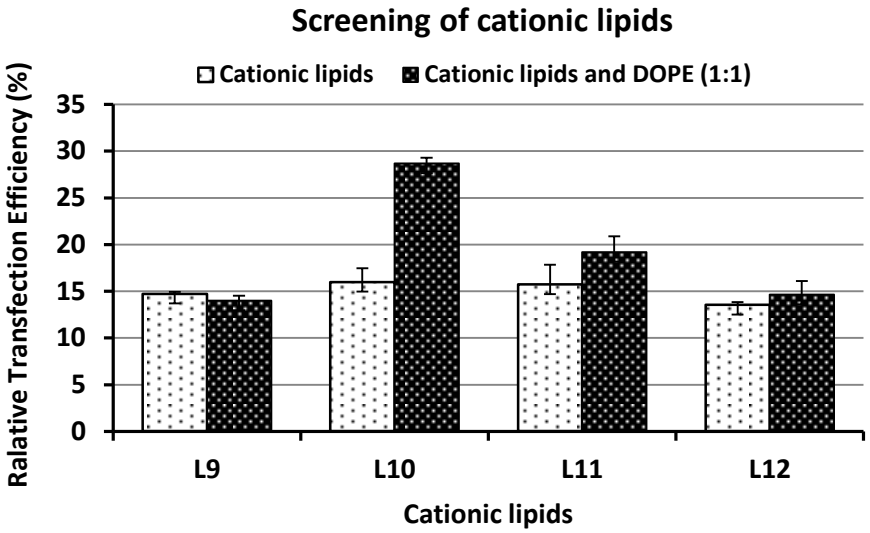

Figure 5 Relative transfection efficiency screening of cationic lipids with DOPE ratio of 1:1 and without DOPE. The lipoplexes were prepared from DNA 0.1 μg/well and the lipids in the ratio of 1:20 by weight.

4.4.2 Optimization of Cationic Lipid/DOPE Ratios

A neutral lipid dioleylphosphatidylethanolamine (DOPE) is a well-known helper lipid [81]. DOPE is a fusogenic lipid to destabilize bilayer in liposome inducing the DNA to be released from lipoplex [82]. In this experiment, the cationic liposomes are constructed from the synthesized lipids and helper-lipid (DOPE) at lipid/DOPE ratios of 3:1, 2:1, 1:1, 1:2 and 1:3. The lipoplexes were prepared by mixing the DNA and liposomes at the DNA concentration about 0.1 μg/well (DNA/lipid ratio 1:20). The appropriate lipid/DOPE ratios for **L4a** were 2:1 and 1:1 and for **L6a** was 1:1 (Figure 44). The result showed that lipids **L4a** and **L6a**, bearing the cholesterol domain, displayed the significant values of the relative transfection efficiency. In contrast, lipids **L4b** and **L6b**, containing β-sitosterol, showed low transfection activity. In addition, the low transfection efficiency was also found at the ratios of 1:2 and 1:3 for all cationic lipids. Therefore, the amount of DOPE has the considerable influence on gene delivery. The optimal ratios for lipid **L4a** and **L6a** will be subjected to the next experiment to vary the amount of DNA.

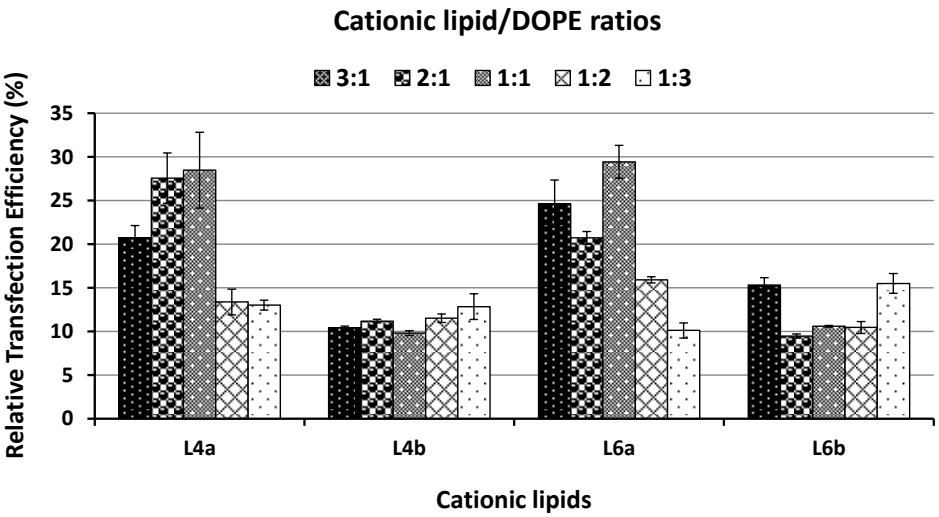

Figure 6 Relative transfection efficiency of cationic lipid **L4a**, **L4b**, **L6a** and **L6b** with the different ratios of lipid:DOPE at 1:1, 1:2, 1:3, 3:1 and 2:1, and 0.1 μg of DNA/well in HEK293 cells. Commercially available Lipofectamine2000 was used as the reference (100%) for the transfection (data not shown).

4.4.3 Optimization of DNA:Cationic Lipids Ratios

The optimal condition to prepare the liposomes from **L4a** and **L6a** at 1:1 lipid:DOPE ratio was used for varying the amount of cationic liposome. The ratios of DNA: cationic liposome at 1:5, 1:10, 1:20, 1:30, 1:40 and 1:50 (w/w) were assayed the transfection activity (0.1 μg of DNA/well). We found that lipid **L4a** and **L6a** at ratios 1:20 and 1:10, respectively showed the highest transfection efficiency (Figure 45). The result indicated that the low transfection efficiency was observed when increasing the amount of cationic lipids.

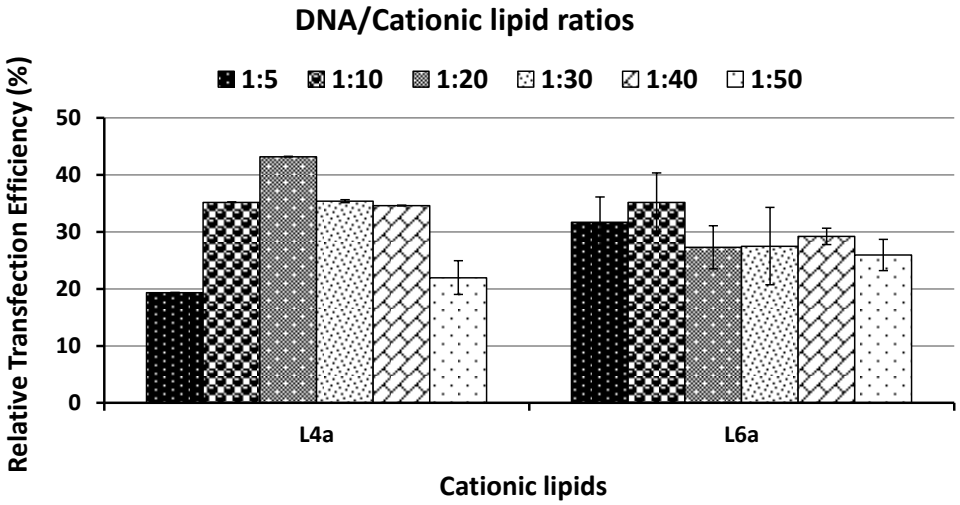

Figure 7 Relative transfection efficiency of cationic lipid **L4a** and **L6a** containing the appropriate amount of DOPE from Figure 44 with the ratios of DNA:cationic lipid at 1:5, 1:10, 1:20, 1:30, 1:40 and 1:50, and 0.1 μg of DNA/well in HEK293 cells. Commercially available Lipofectamine2000 was used as the reference for the transfection (data not shown).

4.4.4 Optimization of the Amount of DNA

In the previous experiment, we had received the optimal ratio of the cationic lipid/DOPE (Figure 44) and the amount of cationic lipids (Figure 45). The transfection efficiency was increased along with the amount of DNA. In addition, we also varied the amount of DNA at various ratios (Figure 46). Here in, the amount of DNA was used at 0.1, 0.2 and 0.4 μg/well. It has been found that lipid **L4a** exhibited the highest transfection activity at 0.2 μg of DNA.

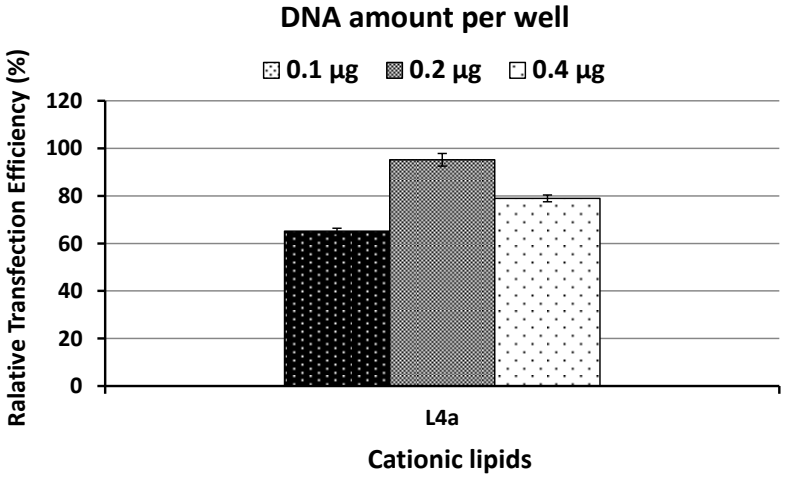

Figure 8 Relative transfection efficiency of DNA amount for gene transfer. The optimal amount of DOPE (Figure 44) and DNA/cationic lipids ratios (Figure 45) were selected to use with different amount of DNA as 0.1, 0.2 and 0.4 µg, and 0.1 µg of DNA/well. Commercially available Lipofectamine2000 was used as the reference (100%) for the transfection (data not shown).

4.4.5 The Effect of Serum

The environment in body system contains serum nuclease which affects the transportation of gene [83]. A number of reports revealed that cationic liposomes with high transfection activity in the absence of serum will lose their efficiency when serum is present [41,79,84,85]. Therefore, the transfection activity of lipid **L4a** was examined in the presence of 0, 10, 20, and 40% serum by using the optimal conditions from the previous experiments. As shown in Figure 47a, the transfection efficiency of lipid **L4a** was tested by using ONPG as the substrate for gene expression. Each percentage of serum was compared with transfection agent (Lipofectamine2000) as the external reference (100%).

The transfected cells were counted and reported as the number of the cells per square centimeter as shown in Figure 47b. Lipofectamine2000 showed the transfection efficiency higher than lipid **L4a** in serum-free condition (8140 ± 98 cells/cm^2 for Lipofectamine2000 and 6280 ± 26 cells/cm^2 for lipid **L4a**) but in the 10–40% serum, the lipid **L4a** showed the higher efficiency than that of the control.

However, the transfection efficiency was significantly decreased when increase the amount of serum. In addition, we also employed pEGFP-C2 to confirm the results by measuring fluorescent emission of GFP protein (Figure 47c). At 10 and 20% serum, lipid **L4a** still provided the efficient transfection activity as same as the serum-free condition.

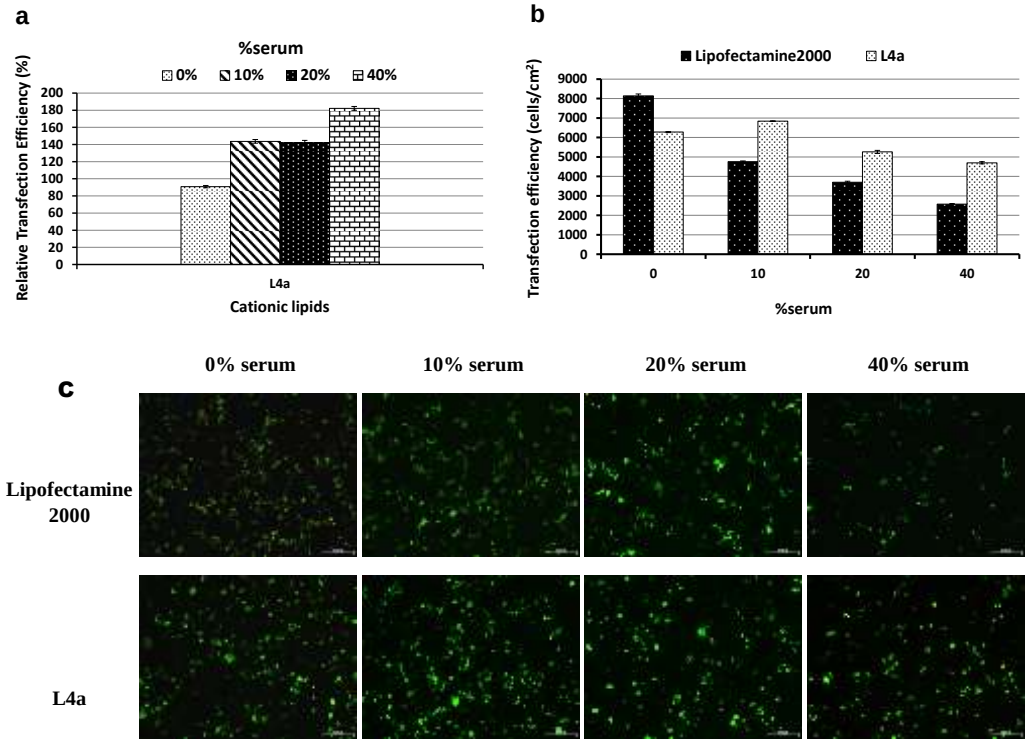

Figure 9 (a) Transfection efficiency of lipid **L4a** in the presence of different percentages of serum. (b) Comparison of the transfection efficiency of lipid **L4a** and the control reported as number of the transfected cells per square centimeter (cells/cm^2). (c) Expression of gene encoding for GFP transferred by **L4a**/DOPE = 1/1 at ratio of 1:20 (DNA/lipid) and Lipofectamine2000. All experiments were tested in HEK293 cells and evaluated under 0%, 10%, 20% and 40% serum.

4.4.6 Transfection Efficiency toward Different Cell Lines

Transfection efficiency of the lipid **L4a** was also carried out in the different mammalian cell lines including HeLa, MCF7, and HT29. These experiments were performed under serum-free condition. The optimal ratios from the previous conditions were subjected to evaluate the gene delivery. The results indicated that lipid **L4a** can transfect the DNA into HeLa and MCF7 cells compared to Lipofectamine2000 as positive control.

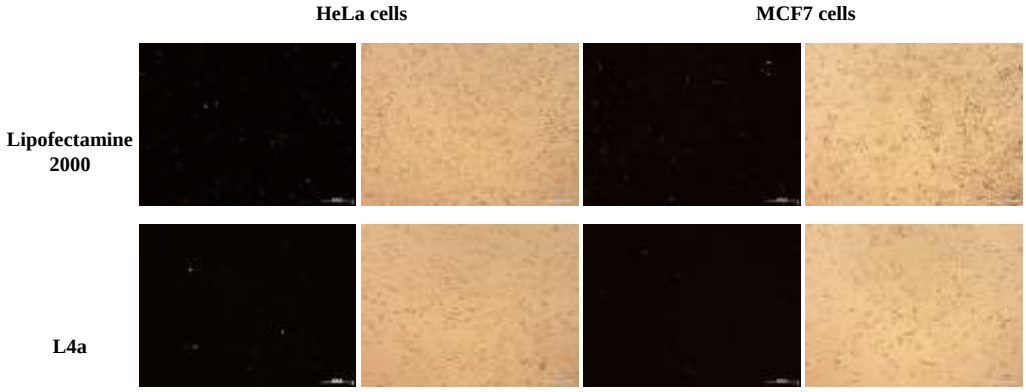

Figure 10 GFP gene expressions in HeLa and MCF7 cells observed after 48 h of transfection under fluorescence microscopy and normal light as the control.

4.5 Cytotoxicity

The cytotoxicity of lipid **L4a** was investigated by MTT assay on HEK293 cells. The optimal ratios from the previous experiment of lipid **L4a** were tested. DNA/cationic lipid ratios of 1:2, 1:5, 1:10, 1:20, 1:30, 1:40 and 1:50 were examined by using the DNA concentration at 0.2 µg DNA/well. The result was shown in Figure 49 that this liposome is not toxic to the tested cells.

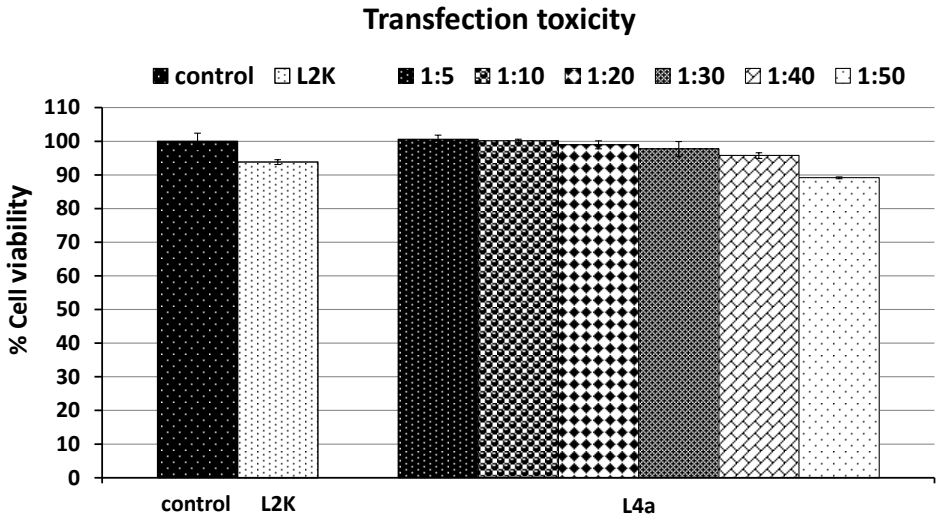

Figure 11 The cytotoxic essay in HEK293 cells indicated by the percentage of cells viability. The ratios of DNA/lipid are at 1:2, 1:5, 1:10, 1:20, 1:30, 1:40 and 1:50. Cell metabolic activity was determined by MTT assay.

4.6 Serum Stability of ODN

The exonucleolytic degradation of deoxyoligonucleotide (ODN) by serum was tested based on the previous report [42,84,86,87]. Free or encapsulated ODN was incubated at 30 °C in several times. ODN encapsulation showed that the DNA in 10% serum was completely degraded. When the lipoplex **L4a** was treated in the presence of 0.5% SDS, it could not bind DNA. In contrast, the lipoplex **L4a** in the absence of 0.5% SDS could retard the migration of DNA. The result indicated that the lipoplex can be encapsulated ODN in 10% serum. Using Lipofectamine^{TM} 2000 as the positive control provided the same result (See Figure 50). Moreover, the 40% serum also showed the approximate ODN encapsulation efficiency (See Figure 51).

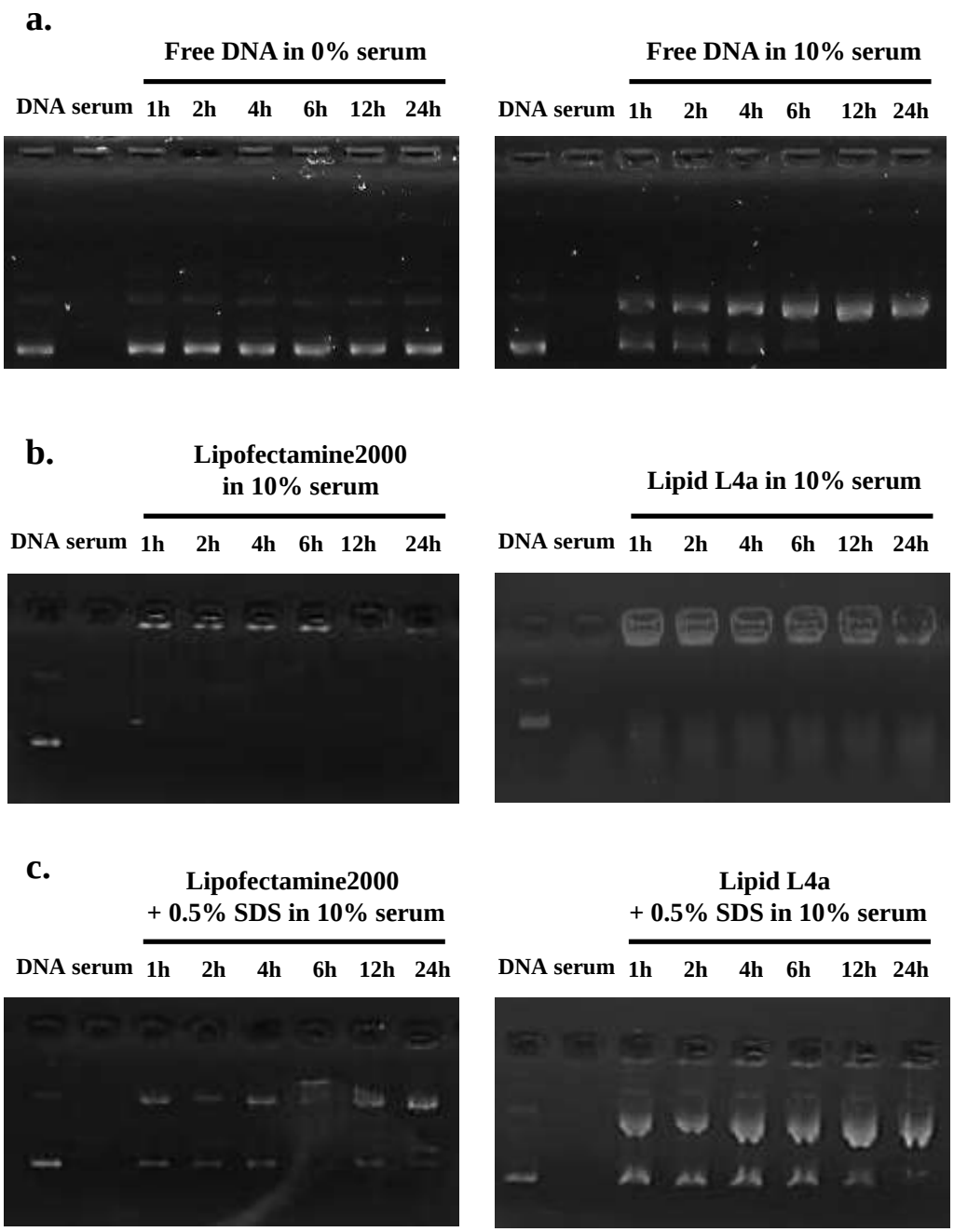

Figure 12 At 10% serum, serum stability of pDNA in different time. (a) Both DNA in serum and pure DNA, (b) Lipofectamine2000 and lipid **L4a** in 10% serum and (c) Lipofectamine2000 and lipid **L4a** in 10% serum that contained 0.5% SDS.

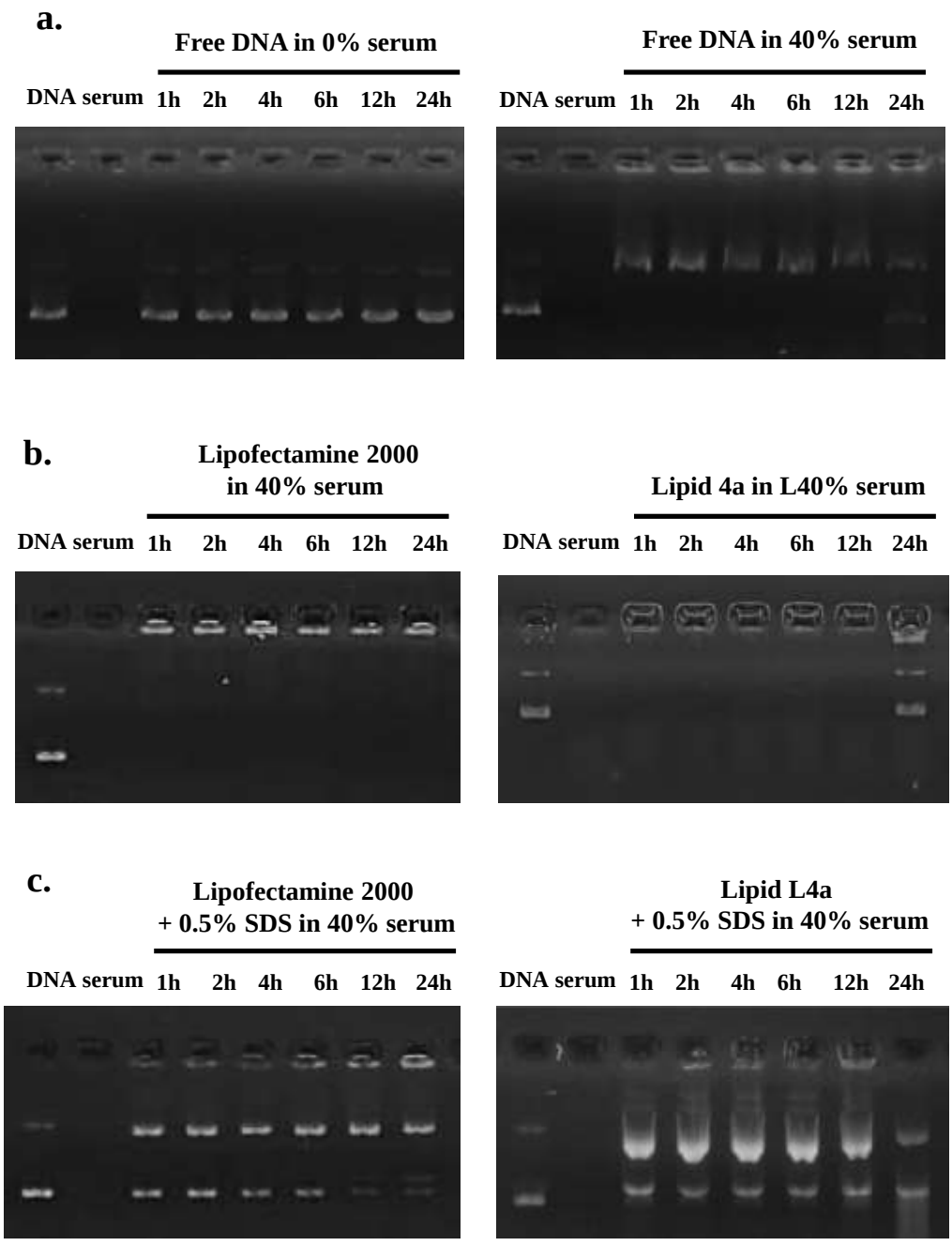

Figure 13 At 40% serum, serum stability of pDNA in different time. (a) Both DNA in serum and pure DNA, (b) Lipofectamine2000 and lipid **L4a** in 40% serum and (c) Lipofectamine2000 and lipid **L4a** in 40% serum that contained 0.5% SDS.

CHAPTER 5

CONCLUSION

The cationic lipids containing cholesterol and β-sitosterol as hydrophobic tails were successfully synthesized under mild conditions. Polar headgroups including ammonium, trimethyl ammonium, guanidinium and tetramethyl guanidinium and carbamate linker were employed. Novel lipid **L4a** with tetramethyl guanidinium headgroup showed the highest transfection efficiency in the presence of a helper lipid, DOPE. However, the cationic lipids with trimethyl ammonium headgroup and cholesterol tail also showed sufficient transfection efficiency. Some cationic lipids with β-sitosterol tail could provide transfection efficiency especially the lipids containing trimethyl ammonium headgroup. The optimal conditions of the lipid **L4a** providing the highest transfection efficiency into HEK293 cells consists of lipid/DOPE at weight ratio of 1:1, DNA/liposome ratio of 1:20 and the amount of DNA 0.2 μg/well. The gel electrophoresis experiment indicated that liposomes fully formulated with DNA could retard the migration of DNA. In addition, we also found that the transfection activity was related to the DNA binding affinities. Lipoplex **L4a** has the particle size approximately in the range of 286–770 nm and the zeta potential of 34–35 mV at ratio of 1:20 (DNA/lipid).

Cationic lipids **L9**–**L12** containing spermine and 1,4-bis(3-aminopropoxy)butane as the polar headgroups, carbamate linker and cholesterol as the hydrophobic tail were synthesized. These lipids showed strong retardation in gel electrophoresis assay. The screening transfection showed that the relative transfection efficiency of lipid **L10** was around 30% compared to Lipofectamine2000 as the positive control.

Lipid **L4a** also exhibited the transfection efficiency higher than Lipofectamine2000 in the presence of 10%, 20% and 40% serum and this liposome was not toxic to the tested cells. This condition could be applied as a non-viral transfection vector for further *in vivo* study based on the presence of serum.

REFERENCES

REFERENCES

[1] Farraha M, Chong JJH, Kizana E. Therapeutic Prospects of Gene Therapy for Atrial Fibrillation. Heart Lung Circ. 2016;25(8):808–13.

[2] van Til NP, Sarwari R, Visser TP, et al. Recombination-activating gene 1 (Rag1)-deficient mice with severe combined immunodeficiency treated with lentiviral gene therapy demonstrate autoimmune Omenn-like syndrome. J Allergy Clin Immunol. 2014;133(4):1116–23.

[3] Bianchi M, Niemiec MJ, Siler U, Urban CF, Reichenbach J. Restoration of anti-Aspergillus defense by neutrophil extracellular traps in human chronic granulomatous disease after gene therapy is calprotectin-dependent. J Allergy Clin Immunol. 2011;127(5):1243–52.e7.

[4] Tuszynski MH, Thal L, Pay M, et al. A phase 1 clinical trial of nerve growth factor gene therapy for Alzheimer disease. Nat Med. 2005;11(5):551–5.

[5] Lheriteau E, Davidoff AM, Nathwani AC. Haemophilia gene therapy: Progress and challenges. Blood Rev. 2015;29(5):321–8.

[6] Yin PT, Shah S, Pasquale NJ, Garbuzenko OB, Minko T, Lee K-B. Stem cell-based gene therapy activated using magnetic hyperthermia to enhance the treatment of cancer. Biomaterials. 2016;81:46–57.

[7] Tian C, Bagley J, Cretin N, Seth N, Wucherpfennig KW, Iacomini J. Prevention of type 1 diabetes by gene therapy. J Clin Invest. 2004;114(7):969–78.

[8] Chen Q, Osada K, Ishii T, et al. Homo-catiomer integration into PEGylated polyplex micelle from block-catiomer for systemic anti-angiogenic gene therapy for fibrotic pancreatic tumors. Biomaterials. 2012;33(18):4722–30.

[9] Kaplitt MG, Feigin A, Tang C, et al. Safety and tolerability of gene therapy with an adeno-associated virus (AAV) borne GAD gene for Parkinson's disease: an open label, phase I trial. Lancet. 2007;369(9579):2097–105.

[10] Rosengart TK, Lee LY, Patel SR, et al. Six-month assessment of a phase I trial of angiogenic gene therapy for the treatment of coronary artery disease using direct intramyocardial administration of an adenovirus vector expressing the VEGF121 cDNA. Ann Surg. 1999;230(4):466–70.

[11] Zhang YM, Chang DC, Zhang J, Liu YH, Yu XQ. Cyclen-based double-tailed lipids for DNA delivery: Synthesis and the effect of linking group structures. Bioorg Med Chem. 2015;23(17):5756–63.

[12] Trapani I, Puppo A, Auricchio A. Vector platforms for gene therapy of inherited retinopathies. Prog Retin Eye Res. 2014;43:108–28.

[13] Merten O-W, Gaillet B. Viral vectors for gene therapy and gene modification approaches. Biochem Eng J. 2016;108:98–115.

[14] Khan MA, Wu VM, Ghosh S, Uskokovic V. Gene delivery using calcium phosphate nanoparticles: Optimization of the transfection process and the effects of citrate and poly(L-lysine) as additives. J Colloid Interface Sci. 2016;471:48–58.

[15] Mun JY, Shin KK, Kwon O, Lim YT, Oh DB. Minicircle microporation-based non-viral gene delivery improved the targeting of mesenchymal stem cells to an injury site. Biomaterials. 2016;101:310–20.

[16] Nayerossadat N, Maedeh T, Ali PA. Viral and nonviral delivery systems for gene delivery. Adv Biomed Res. 2012;1:1–11.

[17] Pierrat P, Kereselidze D, Lux M, Lebeau L, Pons F. Enhanced gene delivery to the lung using biodegradable polyunsaturated cationic phosphatidylcholine-detergent conjugates. Int J Pharm. 2016;511(1):205–18.

[18] Al-Dosari MS, Gao X. Nonviral Gene Delivery: Principle, Limitations, and Recent Progress. AAPS J. 2009;11(4):671–81.

[19] Conwell CC, Huang L. Recent advances in non-viral gene delivery. Adv Genet. 2005;53:3–18.

[20] Mintzer MA, Simanek EE. Nonviral vectors for gene delivery. Chem Rev. 2009;109(2):259–302.

[21] Rezaee M, Oskuee RK, Nassirli H, Malaekeh-Nikouei B. Progress in the development of lipopolyplexes as efficient non-viral gene delivery systems. J Control Release. 2016;236:1–14.

[22] Schmidt-Wolf GD, Schmidt-Wolf IG. Non-viral and hybrid vectors in human gene therapy: an update. Trends Mol Med. 2003;9(2):67–72.

[23] Zhang Y, Satterlee A, Huang L. *In vivo* gene delivery by nonviral vectors: overcoming hurdles? Mol Ther. 2012;20(7):1298–304.

[24] Lonez C, Vandenbranden M, Ruysschaert JM. Cationic liposomal lipids: from gene carriers to cell signaling. Prog Lipid Res. 2008;47(5):340–7.

[25] Zhao Y, Zhu J, Zhou H, et al. Sucrose ester based cationic liposomes as effective non-viral gene vectors for gene delivery. Colloids Surf B Biointerfaces. 2016;145:454–61.

[26] Farago O, Ewert K, Ahmad A, Evans HM, Grønbech-Jensen N, Safinya CR. Transitions between Distinct Compaction Regimes in Complexes of Multivalent Cationic Lipids and DNA. Biophys J. 2008;95(2):836–46.

[27] Cortesi R, Damiani C, Ravani L, et al. Lipid-based nanoparticles containing cationic derivatives of PTA (1,3,5-triaza-7-phosphaadamantane) as innovative vehicle for Pt complexes: Production, characterization and *in vitro* studies. Int J Pharm. 2015;492(1–2):291–300.

[28] Labas R, Beilvert F, Barteau B, David S, Chèvre R, Pitard B. Nature as a source of inspiration for cationic lipid synthesis. Genetica. 2009;138(2):153–68.

[29] Eastman SJ, Siegel C, Tousignant J, Smith AE, Cheng SH, Scheule RK. Biophysical characterization of cationic lipid: DNA complexes. Biochim Biophys Acta. 1997;1325(1):41–62.

[30] Shirazi RS, Ewert KK, Leal C, Majzoub RN, Bouxsein NF, Safinya CR. Synthesis and characterization of degradable multivalent cationic lipids with disulfide-bond spacers for gene delivery. Biochim Biophys Acta. 2011;1808(9):2156–66.

[31] Felgner JH, Kumar R, Sridhar CN, et al. Enhanced gene delivery and mechanism studies with a novel series of cationic lipid formulations. J Biol Chem. 1994;269(4):2550–61.

[32] Ferrari ME, Rusalov D, Enas J, Wheeler CJ. Synergy between cationic lipid and co-lipid determines the macroscopic structure and transfection activity of lipoplexes. Nucleic Acids Res. 2002;30(8):1808–16.

[33] Patel M, Vivien E, Hauchecorne M, et al. Efficient gene transfection by bisguanylated diacetylene lipid formulations. Biochem Biophys Res Commun. 2001;281(2):536–43.

[34] Zhi D, Zhang S, Qureshi F, et al. Synthesis and biological activity of carbamate-linked cationic lipids for gene delivery *in vitro*. Bioorg Med Chem Lett. 2012;22(11):3837–41.

[35] Zhi D, Zhang S, Wang B, Zhao Y, Yang B, Yu S. Transfection efficiency of cationic lipids with different hydrophobic domains in gene delivery. Bioconjug Chem. 2010;21(4):563–77.

[36] Jubeli E, Maginty AB, Abdul Khalique N, et al. Next generation macrocyclic and acyclic cationic lipids for gene transfer: Synthesis and *in vitro* evaluation. Bioorg Med Chem. 2015;23(19):6364–78.

[37] Tome JP, Silva EM, Pereira AM, et al. Synthesis of neutral and cationic tripyridylporphyrin-D-galactose conjugates and the photoinactivation of HSV-1. Bioorg Med Chem. 2007;15(14):4705–13.

[38] Sakashita M, Mochizuki S, Sakurai K. Hepatocyte-targeting gene delivery using a lipoplex composed of galactose-modified aromatic lipid synthesized with click chemistry. Bioorg Med Chem. 2014;22(19):5212–9.

[39] Rathore B, Chandra Sekhar Jaggarapu MM, Ganguly A, Reddy Rachamalla HK, Banerjee R. Cationic lipid-conjugated hydrocortisone as selective antitumor agent. Eur J Med Chem. 2016;108:309–21.

[40] Yingyongnarongkul BE, Radchatawedchakoon W, Krajarng A, Watanapokasin R, Suksamrarn A. High transfection efficiency and low toxicity cationic lipids with aminoglycerol-diamine conjugate. Bioorg Med Chem. 2009;17(1):176–88.

[41] Radchatawedchakoon W, Watanapokasin R, Krajarng A, Yingyongnarongkul BE. Solid phase synthesis of novel asymmetric hydrophilic head cholesterol-based cationic lipids with potential DNA delivery. Bioorg Med Chem. 2010;18(1):330–42.

[42] Niyomtham N, Apiratikul N, Suksen K, Opanasopit P, Yingyongnarongkul BE. Synthesis and *in vitro* transfection efficiency of spermine-based cationic lipids with different central core structures and lipophilic tails. Bioorg Med Chem Lett. 2015;25(3):496–503.

[43] Cheng X, Lee RJ. The role of helper lipids in lipid nanoparticles (LNPs) designed for oligonucleotide delivery. Adv Drug Deliv Rev. 2016;99(Pt A):129–37.

[44] Kurosaki T, Kitahara T, Teshima M, et al. Exploitation of De Novo helper-lipids for effective gene delivery. J Pharm Pharm Sci. 2008;11(4):56–67.

[45] Ojeda E, Puras G, Agirre M, et al. The role of helper lipids in the intracellular disposition and transfection efficiency of niosome formulations for gene delivery to retinal pigment epithelial cells. Int J Pharm. 2016;503(1–2):115–26.

[46] Hirsch-Lerner D, Zhang M, Eliyahu H, Ferrari ME, Wheeler CJ, Barenholz Y. Effect of "helper lipid" on lipoplex electrostatics. Biochim Biophys Acta. 2005;1714(2):71–84.

[47] Zheng Y, Liu X, Samoshina NM, Samoshin VV, Franz AH, Guo X. *trans*-2-Aminocyclohexanol-based amphiphiles as highly efficient helper lipids for gene delivery by lipoplexes. Biochim Biophys Acta. 2015;1848(12):3113–25.

[48] Barbeau J, Belmadi N, Montier T, et al. Synthesis of a novel archaeal tetraether-type lipid containing a diorthoester group as a helper lipid for gene delivery. Tetrahedron Lett. 2016;57(27–28):2976-80.

[49] Huang Z, Li W, Szoka FC, Jr. Asymmetric 1-alkyl-2-acyl phosphatidylcholine: a helper lipid for enhanced non-viral gene delivery. Int J Pharm. 2012;427(1):64–70.

[50] Aberle AM, Tablin F, Zhu J, Walker NJ, Gruenert DC, Nantz MH. A novel tetraester construct that reduces cationic lipid-associated cytotoxicity. Implications for the onset of cytotoxicity. Biochemistry. 1998;37(18):6533–40.

[51] Ren T, Liu D. Synthesis of diether-linked cationic lipids for gene delivery. Bioorg Med Chem Lett. 1999;9(9):1247–50.

[52] Frederic M, Scherman D, Byk G. Introduction of cyclic guanidines into cationic lipids for non-viral gene delivery. Tetrahedron Lett. 2000;41(5):675–9.

[53] Bianco A, Bonadies F, Napolitano R, Ortaggi G. Improved synthesis of DC-Chol, a cationic lipid for gene therapy. Comptes Rendus Chimie. 2003;6(5–6):613–5.

[54] Mukherjee K, Sen J, Chaudhuri A. Common co-lipids, in synergy, impart high gene transfer properties to transfection-incompetent cationic lipids. FEBS Lett. 2005;579(5):1291–300.

[55] Ilies MA, Johnson BH, Makori F, et al. Pyridinium cationic lipids in gene delivery: an *in vitro* and *in vivo* comparison of transfection efficiency versus a tetraalkylammonium congener. Arch Biochem Biophys. 2005;435(1):217–26.

[56] Kim HS, Song IH, Kim JC, Kim EJ, Jang DO, Park YS. *In vitro* and *in vivo* gene-transferring characteristics of novel cationic lipids, DMKD (*O*,*O*'-dimyristyl-*N*-lysyl aspartate) and DMKE (*O*,*O*'-dimyristyl-*N*-lysyl glutamate). J Control Release. 2006;115(2):234–41.

[57] Paul B, Bajaj A, Indi SS, Bhattacharya S. Synthesis of novel dimeric cationic lipids based on an aromatic backbone between the hydrocarbon chains and headgroup. Tetrahedron Lett. 2006;47(47):8401–5.

[58] Spelios M, Nedd S, Matsunaga N, Savva M. Effect of spacer attachment sites and pH-sensitive headgroup expansion on cationic lipid-mediated gene delivery of three novel myristoyl derivatives. Biophys Chem. 2007;129(2–3):137–47.

[59] Bajaj A, Paul B, Kondaiah P, Bhattacharya S. Structure-activity investigation on the gene transfection properties of cardiolipin mimicking gemini lipid analogues. Bioconjug Chem. 2008;19(6):1283–300.

[60] Bajaj A, Mishra SK, Kondaiah P, Bhattacharya S. Effect of the headgroup variation on the gene transfer properties of cholesterol based cationic lipids possessing ether linkage. BBA-Biomembranes. 2008;1778(5):1222–36.

[61] Zhu L, Lu Y, Miller DD, Mahato RI. Structural and formulation factors influencing pyridinium lipid-based gene transfer. Bioconjug Chem. 2008;19(12):2499–512.

[62] Rajesh M, Sen J, Srujan M, Mukherjee K, Sreedhar B, Chaudhuri A. Dramatic influence of the orientation of linker between hydrophilic and hydrophobic lipid moiety in liposomal gene delivery. J Am Chem Soc. 2007;129(37):11408–20.

[63] Randazzo RA, Bucki R, Janmey PA, Diamond SL. A series of cationic sterol lipids with gene transfer and bactericidal activity. Bioorg Med Chem. 2009;17(9):3257–65.

[64] Obata Y, Saito S, Takeda N, Takeoka S. Plasmid DNA-encapsulating liposomes: effect of a spacer between the cationic head group and hydrophobic moieties of the lipids on gene expression efficiency. Biochim Biophys Acta. 2009;1788(5):1148–58.

[65] Mevel M, Kamaly N, Carmona S, et al. DODAG; a versatile new cationic lipid that mediates efficient delivery of pDNA and siRNA. J Control Release. 2010;143(2):222–32.

[66] Le Gall T, Loizeau D, Picquet E, et al. A novel cationic lipophosphoramide with diunsaturated lipid chains: synthesis, physicochemical properties, and transfection activities. J Med Chem. 2010;53(4):1496–508.

[67] Maslov MA, Morozova NG, Chizhik EI, et al. Synthesis and delivery activity of new cationic cholesteryl glucosides. Carbohyd Res. 2010;345(17):2438–49.

[68] Li S, Wang Y, Wang S, et al. Biodegradable cyclen-based linear and cross-linked polymers as non-viral gene vectors. Bioorg Med Chem. 2012;20(4):1380–7.

[69] Huang Q-D, Ou W-J, Chen H, et al. Novel cationic lipids possessing protonated cyclen and imidazolium salt for gene delivery. Eur J Pharm Biopharm. 2011;78(3):326–35.

[70] Liu JL, Ma QP, Huang QD, et al. Cationic lipids containing protonated cyclen and different hydrophobic groups linked by uracil-PNA monomer: synthesis and application for gene delivery. Eur J Med Chem. 2011;46(9):4133–41.

[71] Øpstad CL, Sliwka H-R, Partali V, et al. Synthesis, self-assembling and gene delivery potential of a novel highly unsaturated, conjugated cationic phospholipid. Chem Phys Lipids. 2013;170–171:65–73.

[72] Sheng R, Luo T, Li H, Sun J, Wang Z, Cao A. 'Click' synthesized sterol-based cationic lipids as gene carriers, and the effect of skeletons and headgroups on gene delivery. Bioorg Med Chem. 2013;21(21):6366–77.

[73] Kedika B, Patri SV. Benzothiazole head group based cationic lipids: Synthesis and application for gene delivery. Eur J Med Chem. 2014;74:703–16.

[74] Sheng R, Luo T, Li H, Sun J, Wang Z, Cao A. Cholesterol-based cationic lipids for gene delivery: contribution of molecular structure factors to physico-chemical and biological properties. Colloids Surf B Biointerfaces. 2014;116:32–40.

[75] Parvizi P, Jubeli E, Raju L, et al. Aspects of nonviral gene therapy: Correlation of molecular parameters with lipoplex structure and transfection efficacy in pyridinium-based cationic lipids. Int J Pharm. 2014;461(1–2):145–56.

[76] Ju J, Huan ML, Wan N, et al. Cholesterol derived cationic lipids as potential non-viral gene delivery vectors and their serum compatibility. Bioorg Med Chem Lett. 2016;26(10):2401–7.

[77] Paecharoenchai O, Niyomtham N, Apirakaramwong A, et al. Structure relationship of cationic lipids on gene transfection mediated by cationic liposomes. AAPS PharmSciTech. 2012;13(4):1302–8.

[78] Yan Z, Wang F, Wen Z, et al. LyP-1-conjugated PEGylated liposomes: a carrier system for targeted therapy of lymphatic metastatic tumor. J Control Release. 2012;157(1):118–25.

[79] Karmali PP, Majeti BK, Sreedhar B, Chaudhuri A. *In vitro* gene transfer efficacies and serum compatibility profiles of novel mono-, di-, and tri-histidinylated cationic transfection lipids: a structure-activity investigation. Bioconjug Chem. 2006;17(1):159–71.

[80] Radchatawedchakoon W, Krajarng A, Niyomtham N, Watanapokasin R, Yingyongnarongkul BE. High transfection efficiency of cationic lipids with asymmetric acyl-cholesteryl hydrophobic tails. Chemistry. 2011;17(11):3287–95.

[81] Mochizuki S, Kanegae N, Nishina K, et al. The role of the helper lipid dioleoylphosphatidylethanolamine (DOPE) for DNA transfection cooperating with a cationic lipid bearing ethylenediamine. Biochim Biophys Acta. 2013;1828(2):412–8.

[82] Hattori Y, Suzuki S, Kawakami S, Yamashita F, Hashida M. The role of dioleoylphosphatidylethanolamine (DOPE) in targeted gene delivery with mannosylated cationic liposomes via intravenous route. J Control Release. 2005;108(2–3):484–95.

[83] Zhang C, Tang N, Liu X, Liang W, Xu W, Torchilin VP. siRNA-containing liposomes modified with polyarginine effectively silence the targeted gene. J Control Release. 2006;112(2):229–39.

[84] Gebrekidan S, Woo BH, DeLuca PP. Formulation and in vitro transfection efficiency of poly (D, L-lactideco-glycolide) microspheres containing plasmid DNA for gene delivery. AAPS PharmSciTech. 2000;1(4):17–25.

[85] Ghosh YK, Visweswariah SS, Bhattacharya S. Nature of linkage between the cationic headgroup and cholesteryl skeleton controls gene transfection efficiency. FEBS Lett. 2000;473(3):341–4.

[86] Semple SC, Klimuk SK, Harasym TO, et al. Efficient encapsulation of antisense oligonucleotides in lipid vesicles using ionizable aminolipids: formation of novel small multilamellar vesicle structures. Biochim Biophys Acta. 2001;1510(1–2):152–66.

[87] Saffari M, F HS, Oghabian MA, Moghimi HR. Preparation and in-vitro Evaluation of an Antisense-containing Cationic Liposome against Non-small Cell Lung Cancer: a Comparative Preparation Study. Iran J Pharm Res. 2013;12:3–10.

APPENDIX

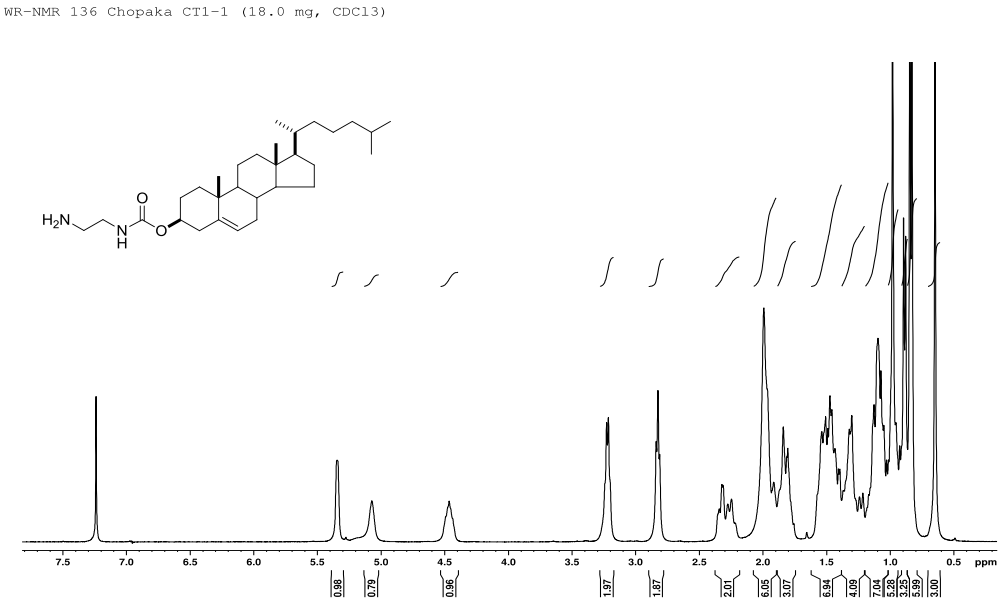

Appendix Figure 1 ^{1}H NMR Spectrum (400 MHz, $CDCl_3$) of Lipid 3β-[*N*-(2-Aminoethyl)carbamoyl]cholesterol (**L1a**)

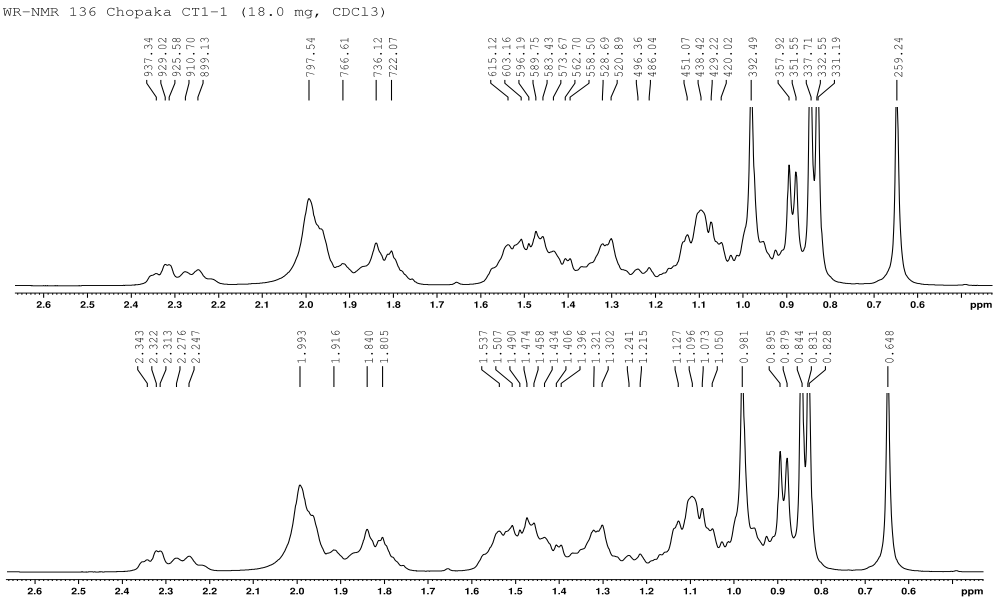

Appendix Figure 2 Expansion of ^{1}H NMR Spectrum (400 MHz, $CDCl_3$) of Lipid 3β-[*N*-(2-Aminoethyl)carbamoyl]cholesterol (**L1a**)

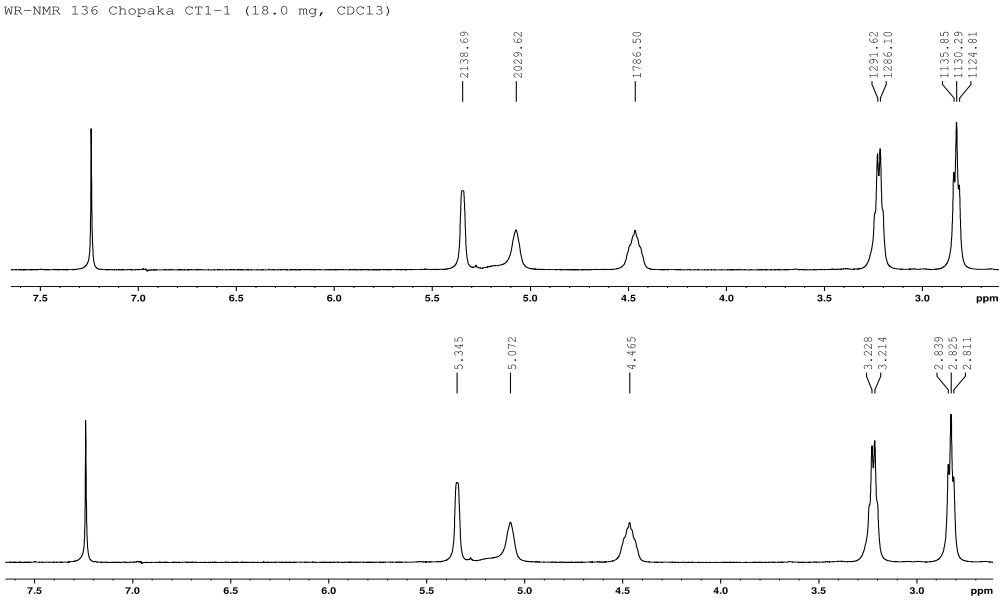

Appendix Figure 3 Expansion (cont.) of ^{1}H NMR Spectrum (400 MHz, $CDCl_3$) of Lipid 3β-[*N*-(2-Aminoethyl)carbamoyl]cholesterol (**L1a**)

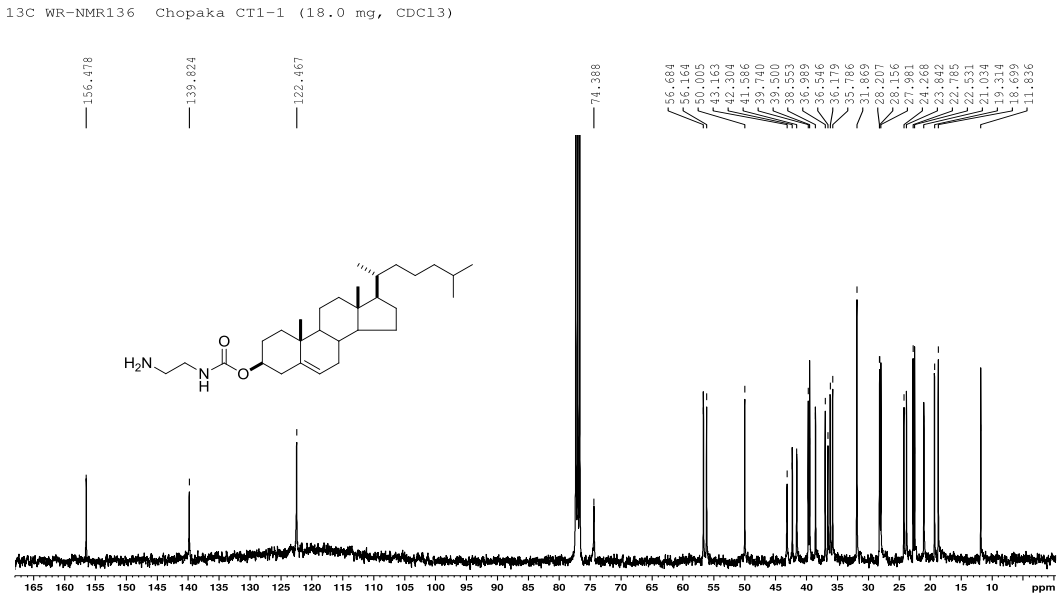

Appendix Figure 4 ^{13}C NMR Spectrum (100 MHz, $CDCl_3$) of Lipid 3β-[*N*-(2-Aminoethyl)carbamoyl]cholesterol (**L1a**)

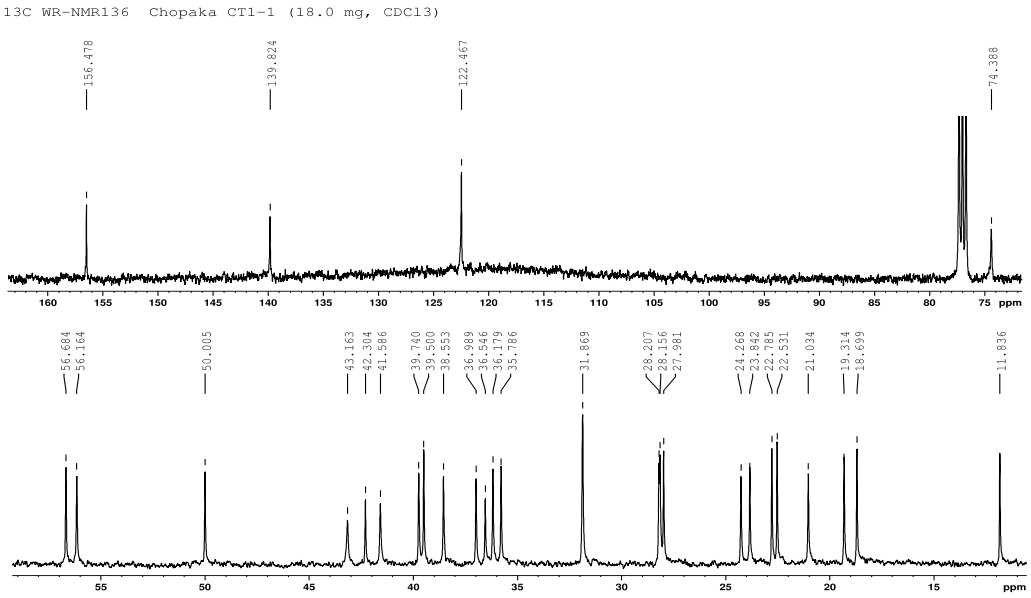

Appendix Figure 5 Expansion of ^{13}C NMR Spectrum (100 MHz, $CDCl_3$) of Lipid 3β-[*N*-(2-Aminoethyl)carbamoyl]cholesterol (**L1a**)

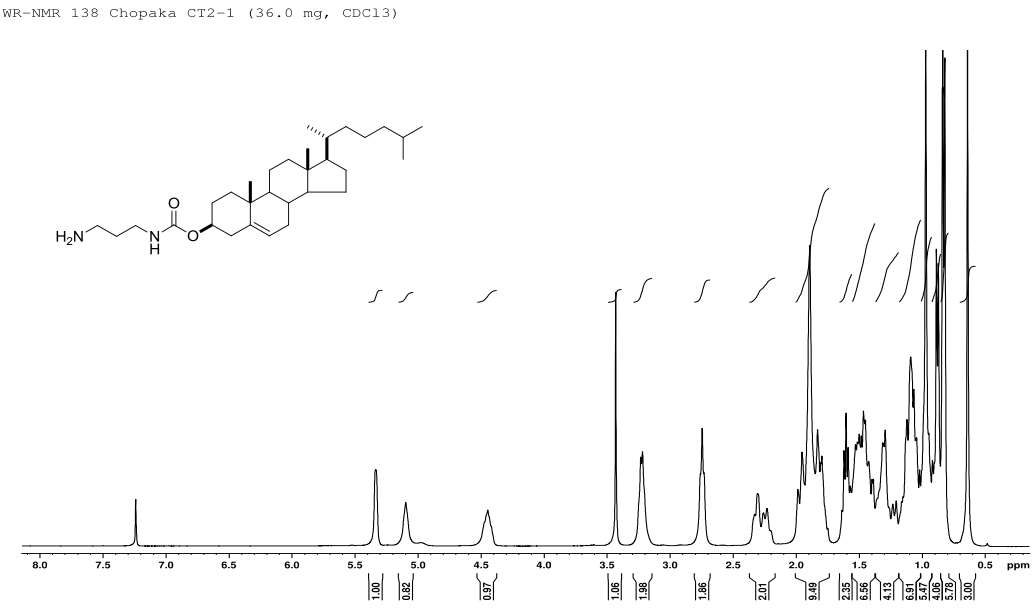

Appendix Figure 6 ^{1}H NMR Spectrum (400 MHz, $CDCl_3$) of Lipid 3β-[*N*-(3-Aminopropyl)carbamoyl]cholesterol (**L5a**)

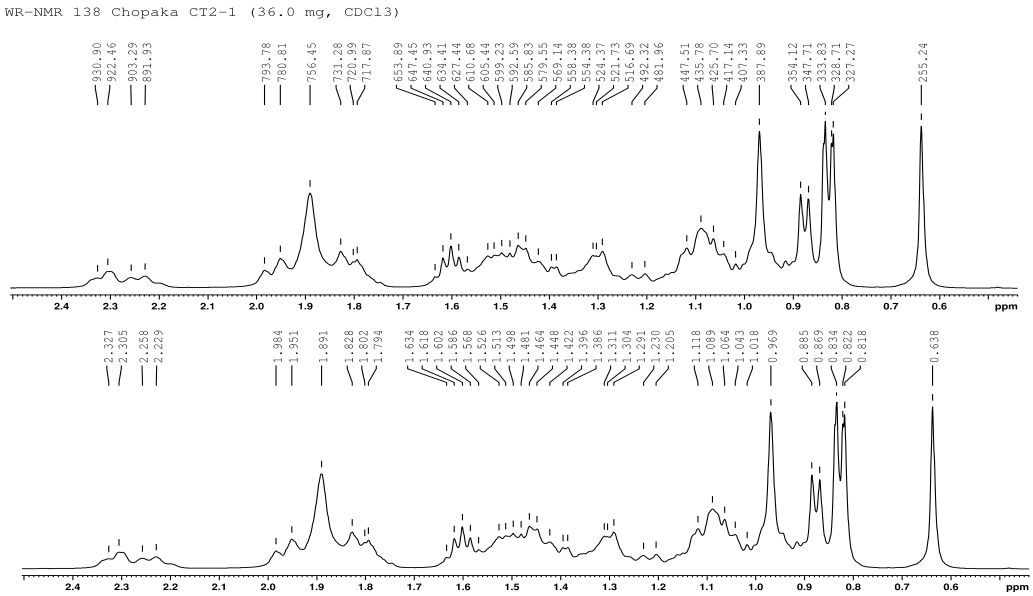

Appendix Figure 7 Expansion of ^{1}H NMR Spectrum (400 MHz, $CDCl_3$) of Lipid 3β-[*N*-(3-Aminopropyl)carbamoyl]cholesterol (**L5a**)

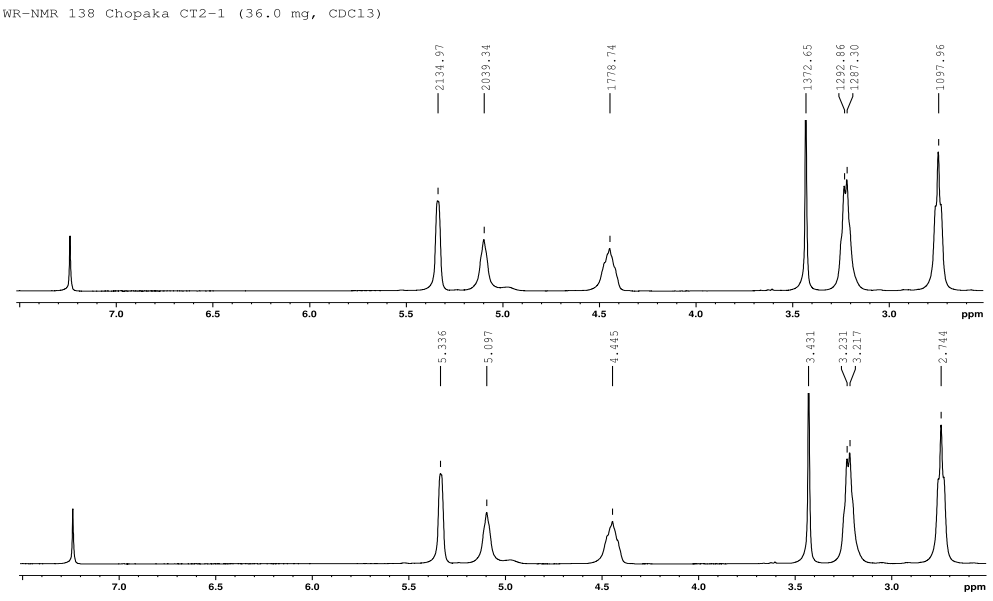

Appendix Figure 8 Expansion (cont.) of ^{1}H NMR Spectrum (400 MHz, $CDCl_3$) of Lipid 3β-[*N*-(3-Aminopropyl)carbamoyl]cholesterol (**L5a**)

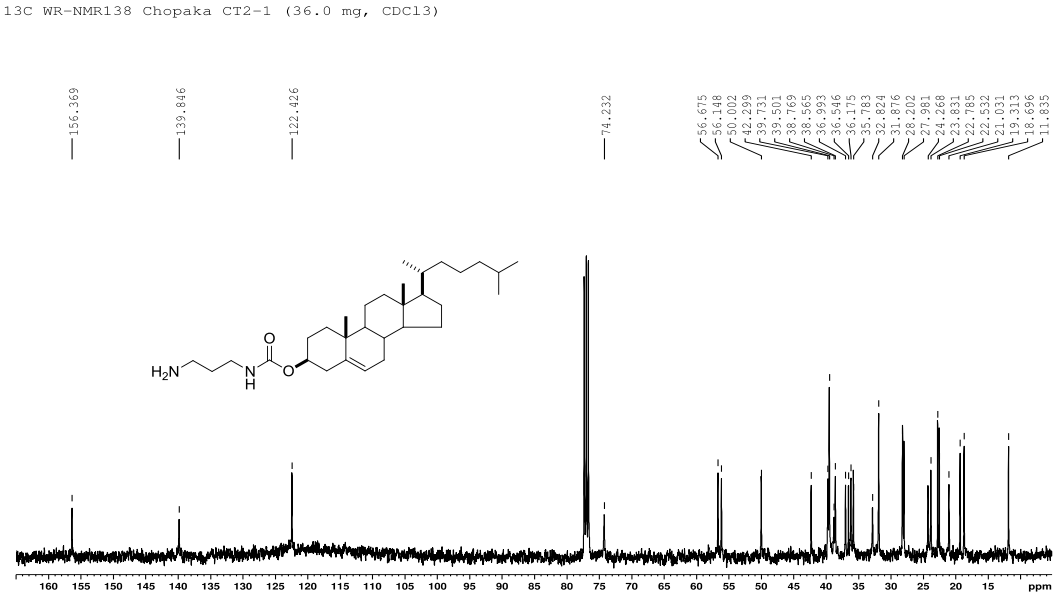

Appendix Figure 9 ^{13}C NMR Spectrum (100 MHz, $CDCl_3$) of Lipid 3β-[*N*-(3-Aminopropyl)carbamoyl]cholesterol (**L5a**)

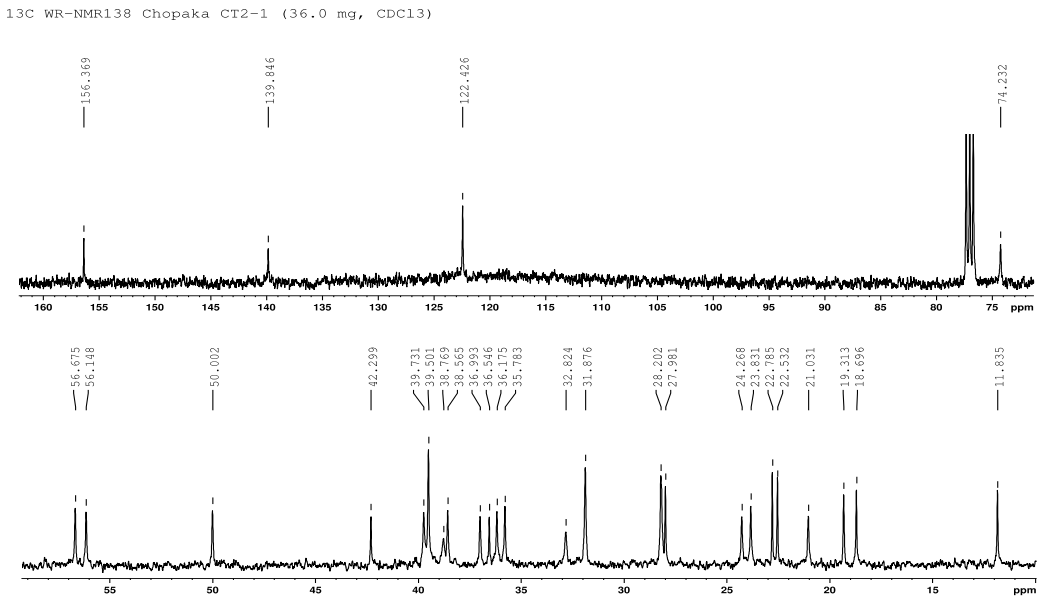

Appendix Figure 10 Expansion of ^{13}C NMR Spectrum (100 MHz, $CDCl_3$) of Lipid 3β-[*N*-(3-Aminopropyl)carbamoyl]cholesterol (**L5a**)

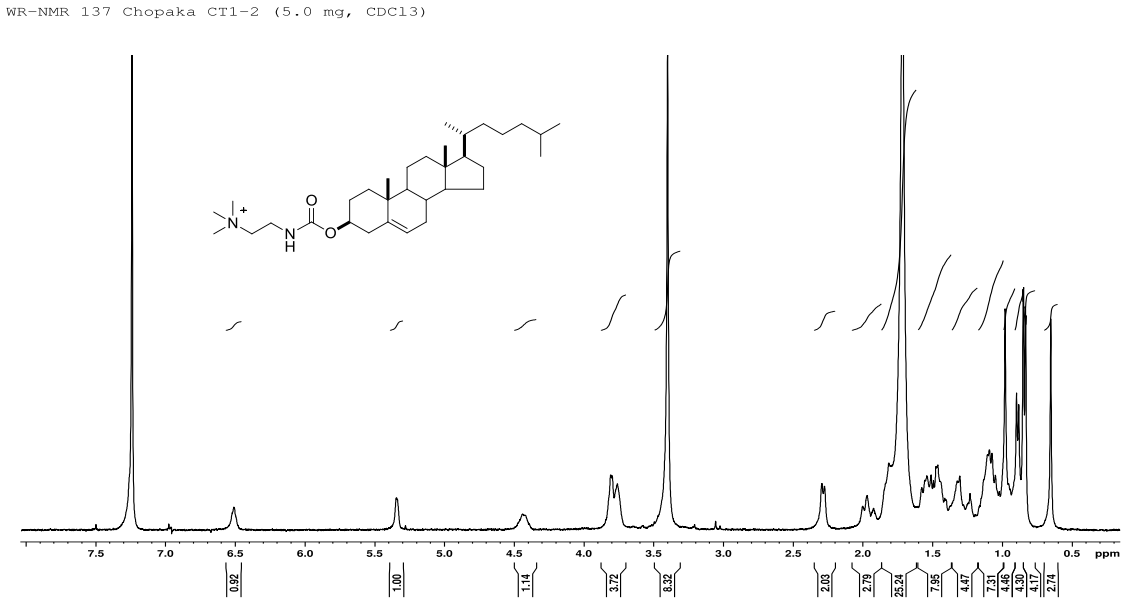

Appendix Figure 11 ^{1}H NMR Spectrum (400 MHz, $CDCl_3$) of Lipid 3β-[*N*-(2-(*N*′, *N*′,*N*′-Trimethyl)aminoethyl)carbamoyl]cholesterol (**L2a**)

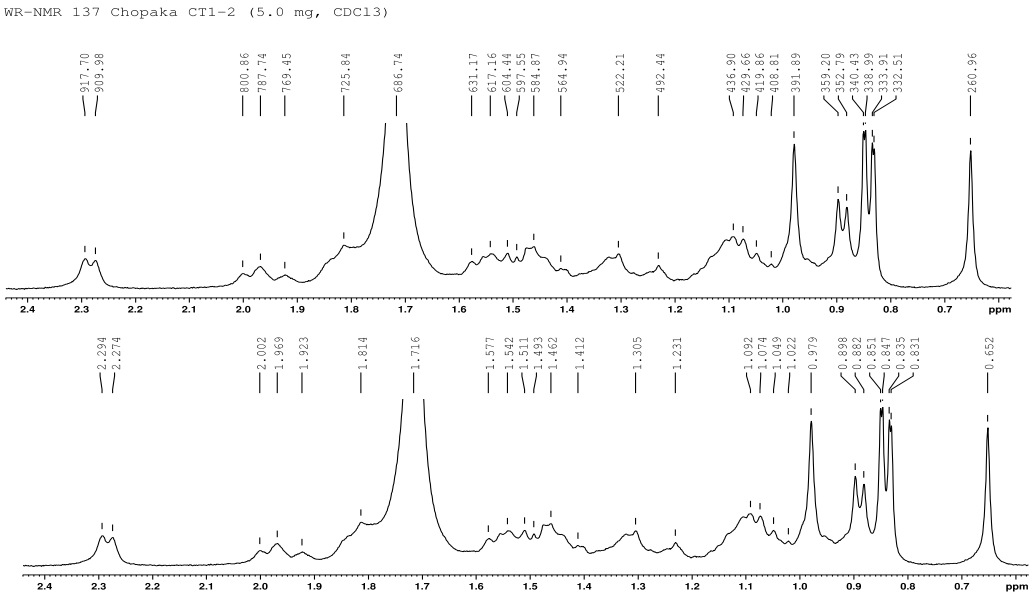

Appendix Figure 12 Expansion of ^{1}H NMR Spectrum (400 MHz, $CDCl_3$) of Lipid 3β-[*N*-(2-(*N*′,*N*′,*N*′-Trimethyl)aminoethyl)carbamoyl]cholesterol (**L2a**)

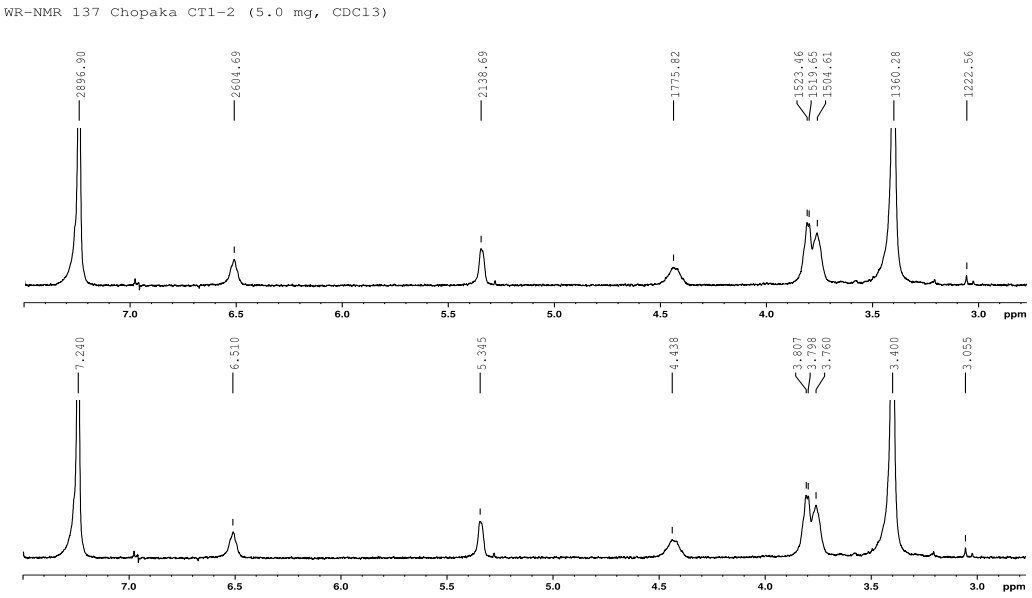

Appendix Figure 13 Expansion (cont.) of ^{1}H NMR Spectrum (400 MHz, $CDCl_3$) of Lipid 3β-[*N*-(2-(*N*′,*N*′,*N*′-Trimethyl)aminoethyl)carbamoyl] cholesterol (**L2a**)

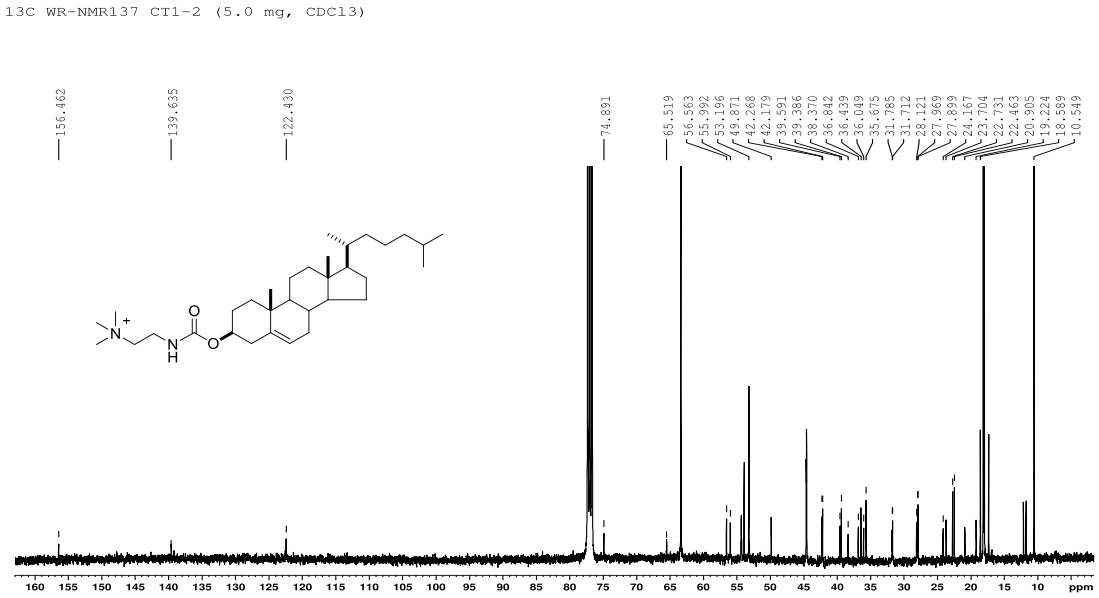

Appendix Figure 14 ^{13}C NMR Spectrum (100 MHz, $CDCl_3$) of Lipid 3β-[*N*-(2-(*N*′,*N*′,*N*′-Trimethyl)aminoethyl)carbamoyl]cholesterol (**L2a**)

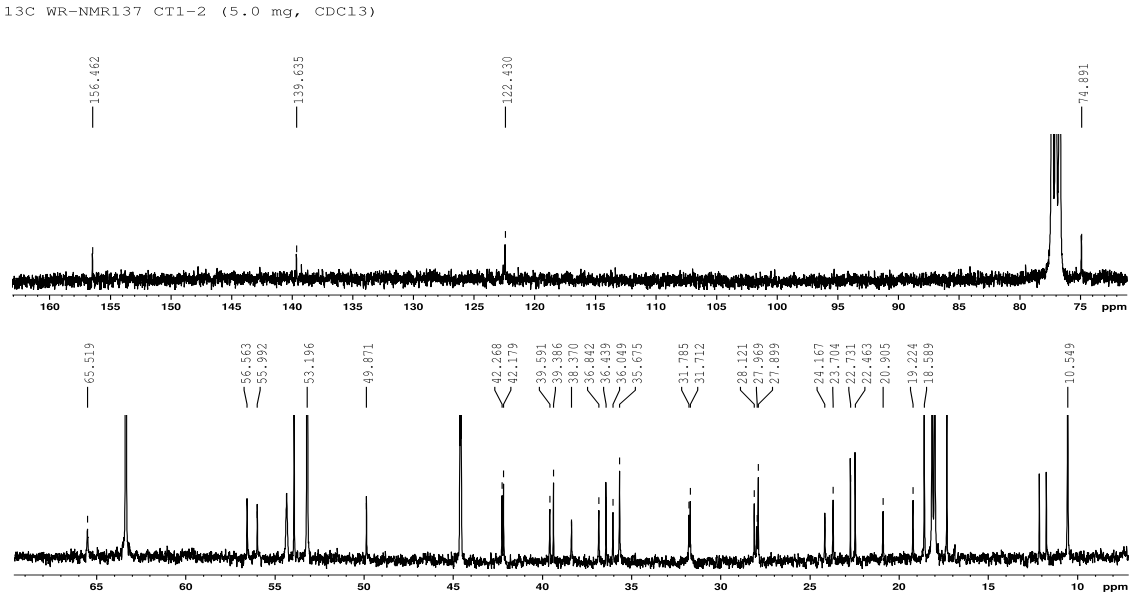

Appendix Figure 15 Expansion of ^{13}C NMR Spectrum (100 MHz, $CDCl_3$) of Lipid 3β-[*N*-(2-(*N*′,*N*′,*N*′-Trimethyl)aminoethyl)carbamoyl]cholesterol (**L2a**)

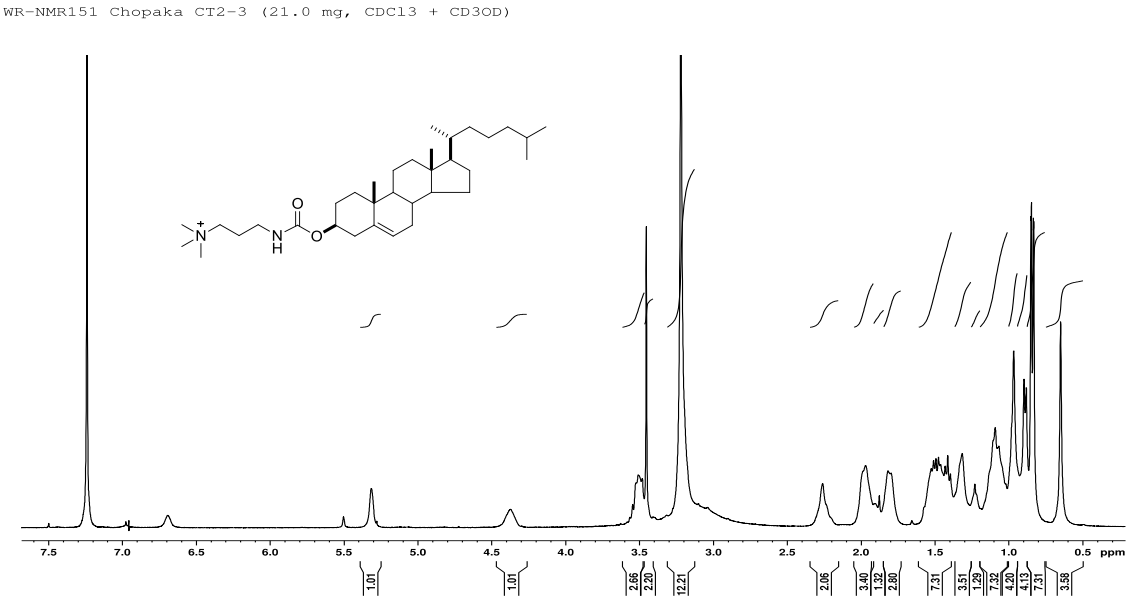

Appendix Figure 16 ^{1}H NMR Spectrum (400 MHz, $CDCl_3$ + CD_3OD) of Lipid 3β-[*N*-(3-(*N*′,*N*′,*N*′-Trimethyl)aminopropyl)carbamoyl]cholesterol (**L6a**)

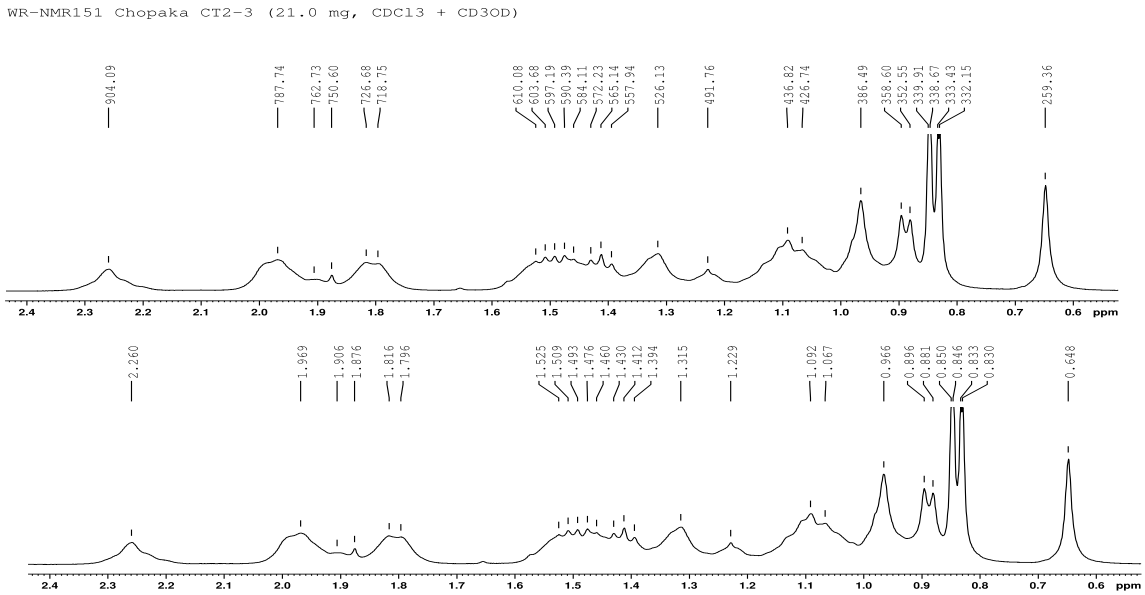

Appendix Figure 17 Expansion of ^{1}H NMR Spectrum (400 MHz, $CDCl_3$ + CD_3OD) of Lipid 3β-[*N*-(3-(*N*′,*N*′,*N*′-Trimethyl)aminopropyl)carbamoyl] cholesterol (**L6a**)

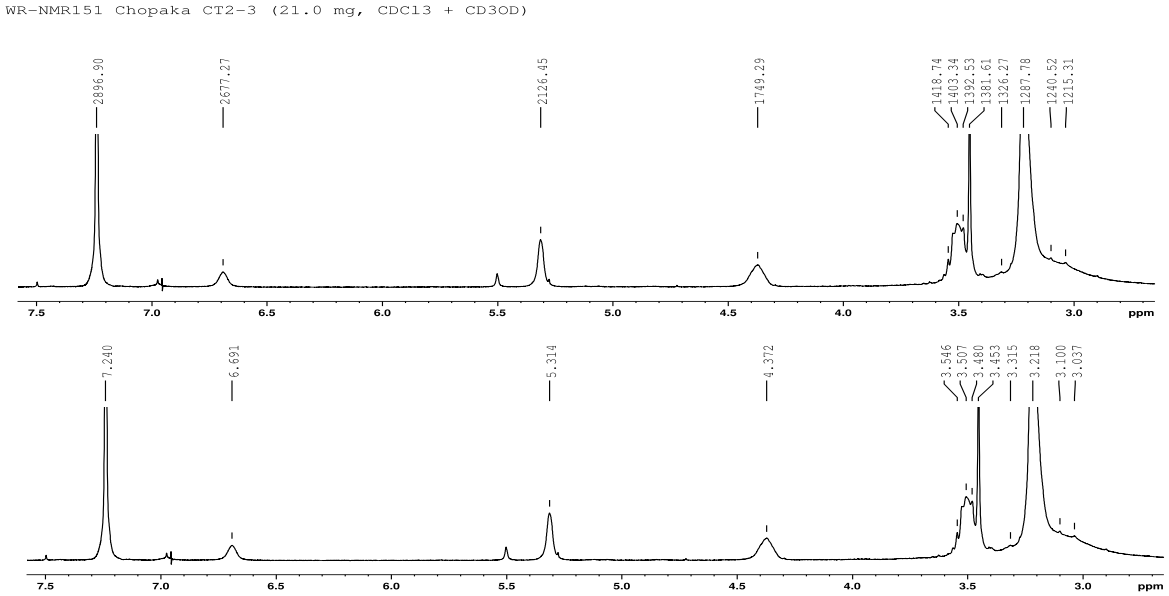

Appendix Figure 18 Expansion (cont.) of ^{1}H NMR Spectrum (400 MHz, $CDCl_3$ + CD_3OD) of Lipid 3β-[*N*-(3-(*N*′,*N*′,*N*′-Trimethyl)aminopropyl) carbamoyl]cholesterol (**L6a**)

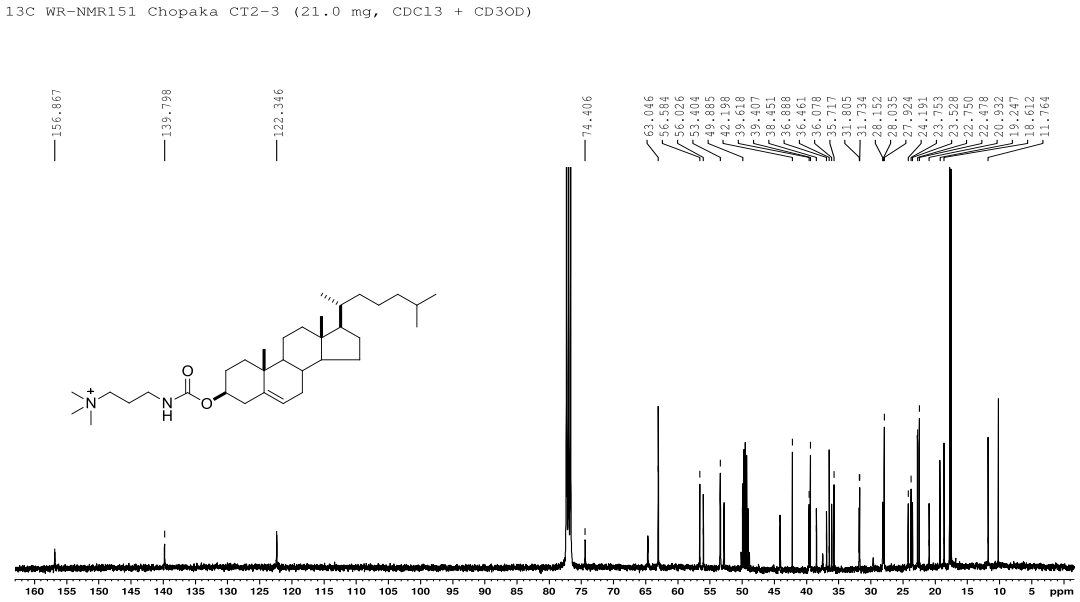

Appendix Figure 19 ^{13}C NMR Spectrum (100 MHz, $CDCl_3$ + CD_3OD) of Lipid 3β-[*N*-(3-(*N*′,*N*′,*N*′-Trimethyl)aminopropyl)carbamoyl]cholesterol (**L6a**)

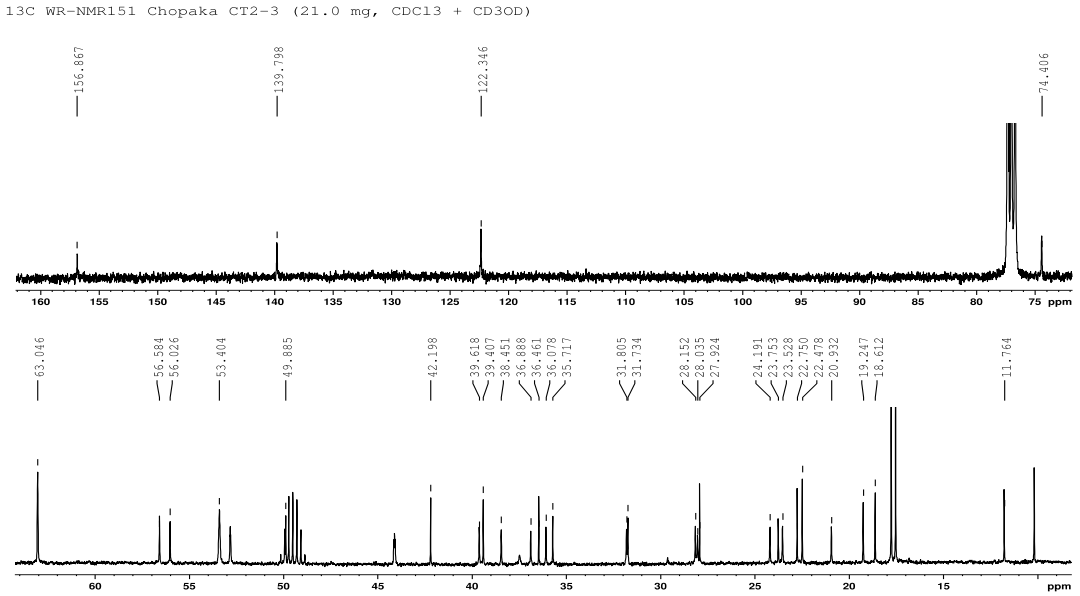

Appendix Figure 20 Expansion of ^{13}C NMR Spectrum (100 MHz, $CDCl_3$ + CD_3OD) of Lipid 3β-[*N*-(3-(*N*′,*N*′,*N*′-Trimethyl)aminopropyl) carbamoyl]cholesterol (**L6a**)

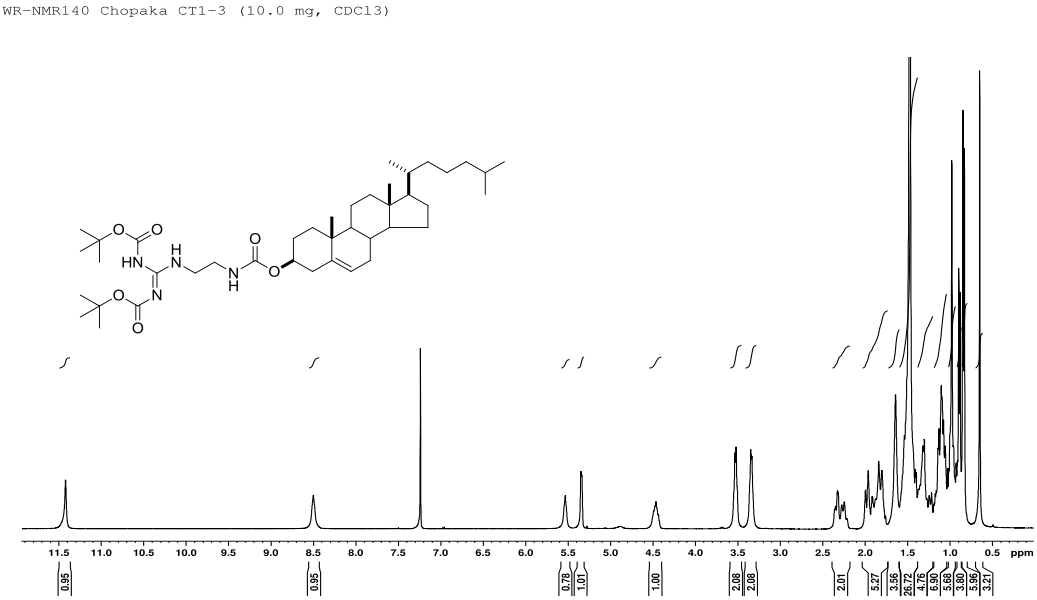

Appendix Figure 21 ^{1}H NMR Spectrum (400 MHz, $CDCl_3$) of 3β-[(2-((*N*′,*N*″-Di(*tert*-butoxycarbonyl)guanidinyl)ethyl)carbamoly] cholesterol (**C4a**)

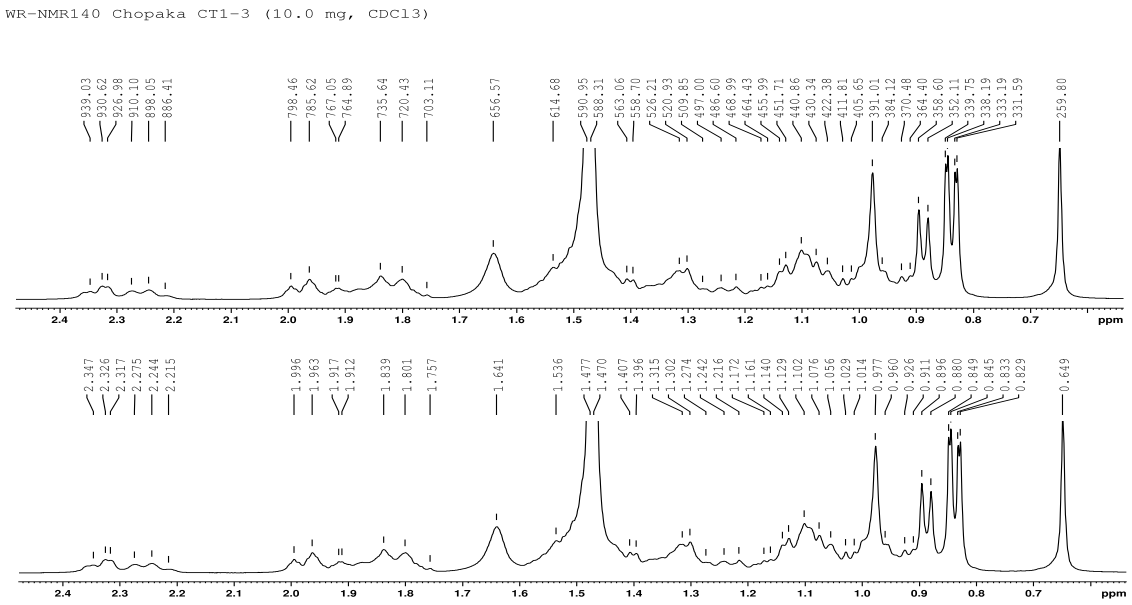

Appendix Figure 22 Expansion of ^{1}H NMR Spectrum (400 MHz, $CDCl_3$) of 3β-[(2-((*N*′,*N*″-Di(*tert*-butoxycarbonyl)guanidinylethyl)carbamoly] cholesterol (**C4a**)

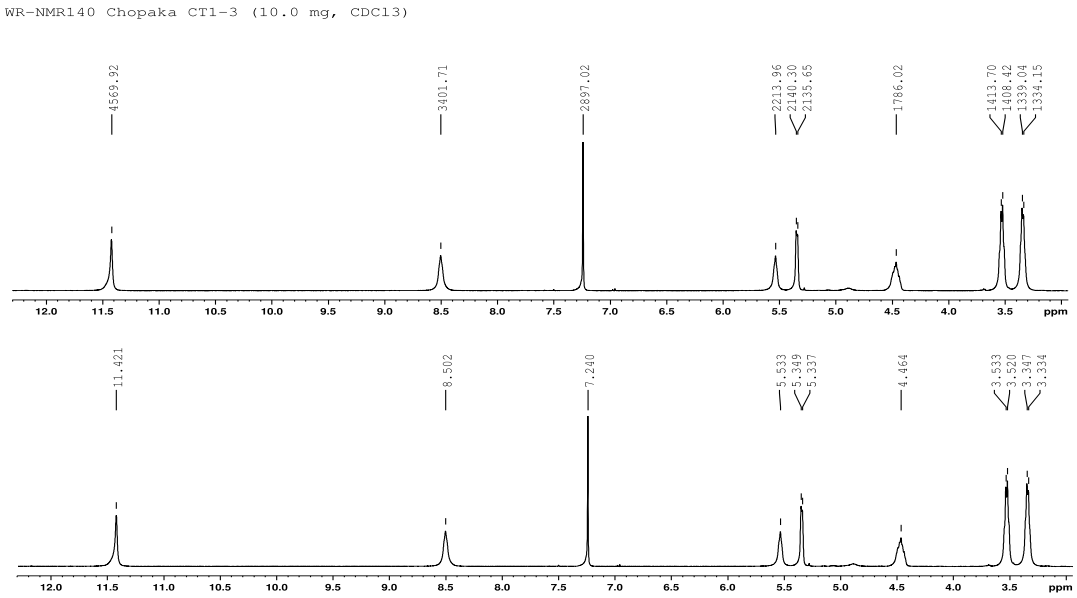

Appendix Figure 23 Expansion (cont.) of ^{1}H NMR Spectrum (400 MHz, $CDCl_3$) of 3β-[(2-((*N*′,*N*″-Di(*tert*-butoxycarbonyl)guanidinyl)ethyl) carbamoly]cholesterol (**C4a**)

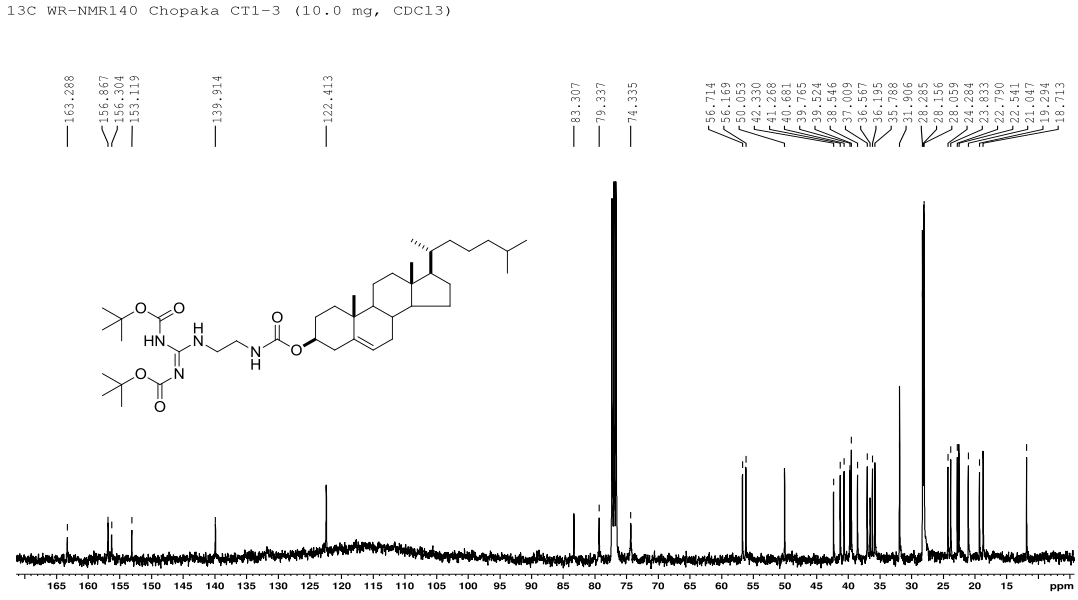

Appendix Figure 24 ^{13}C NMR Spectrum (100 MHz, $CDCl_3$) of 3β-[(2-((*N*′,*N*″-Di(*tert*-butoxycarbonyl)guanidinyl)ethyl)carbamoly] cholesterol (**C4a**)

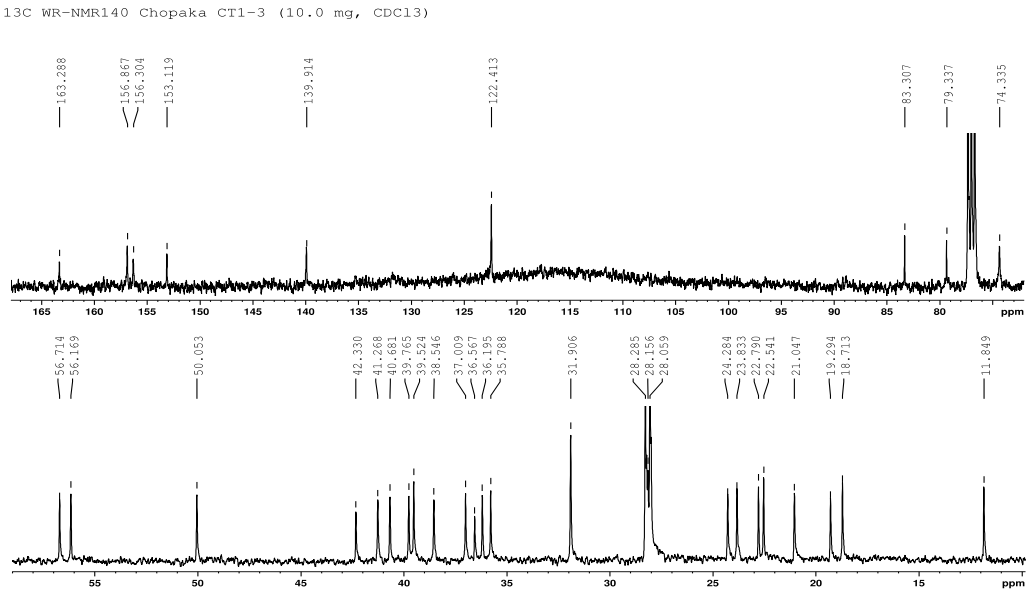

Appendix Figure 25 Expansion of ^{13}C NMR Spectrum (100 MHz, $CDCl_3$) of 3β-[(2-((*N*′,*N*″-Di(*tert*-butoxycarbonyl)guanidinyl)ethyl) carbamoly]cholesterol (**C4a**)

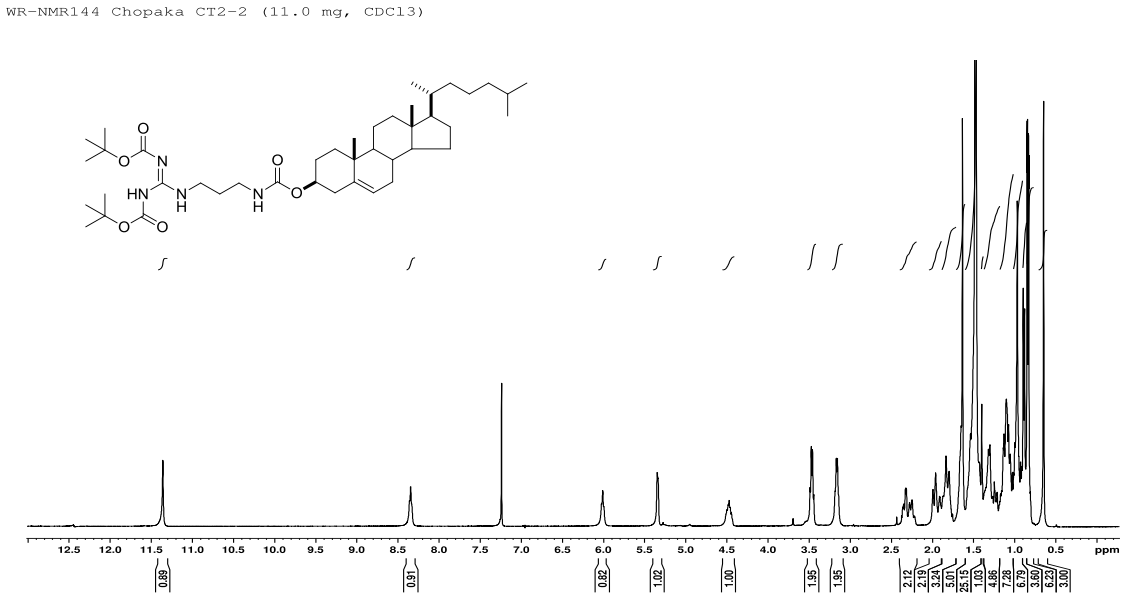

Appendix Figure 26 ^{1}H NMR Spectrum (400 MHz, $CDCl_3$) of 3β-[(3-((*N*′,*N*″-Di(*tert*-butoxycarbonyl))guanidinyl)propyl)carbamoyl] cholesterol (**C5a**)

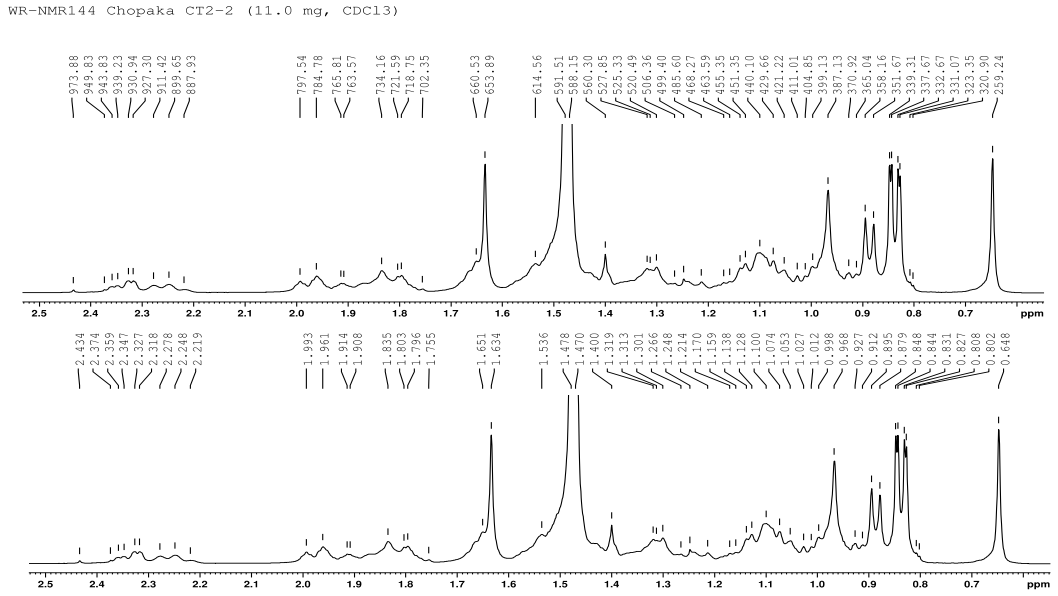

Appendix Figure 27 Expansion of ^{1}H NMR Spectrum (400 MHz, $CDCl_3$) of 3β-[(3-((*N′*,*N″*-Di(*tert*-butoxycarbonyl))guanidinyl)propyl)carbamoyl] cholesterol (**C5a**)

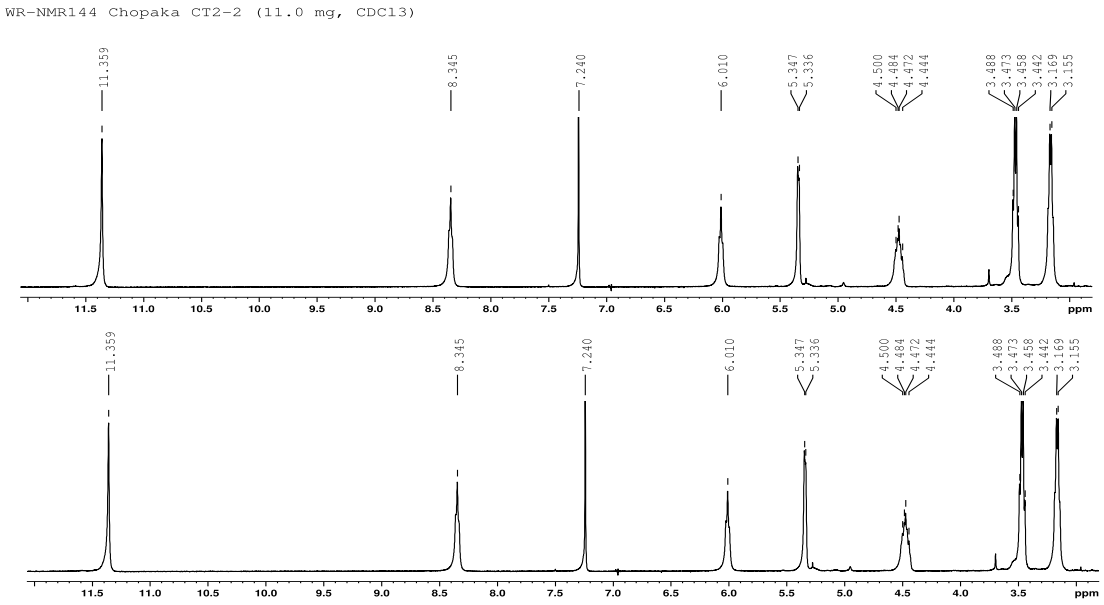

Appendix Figure 28 Expansion (cont.) of ^{1}H NMR Spectrum (400 MHz, $CDCl_3$) of 3β-[(3-((*N′*,*N″*-Di(*tert*-butoxycarbonyl))guanidinyl)propyl) carbamoyl]cholesterol (**C5a**)

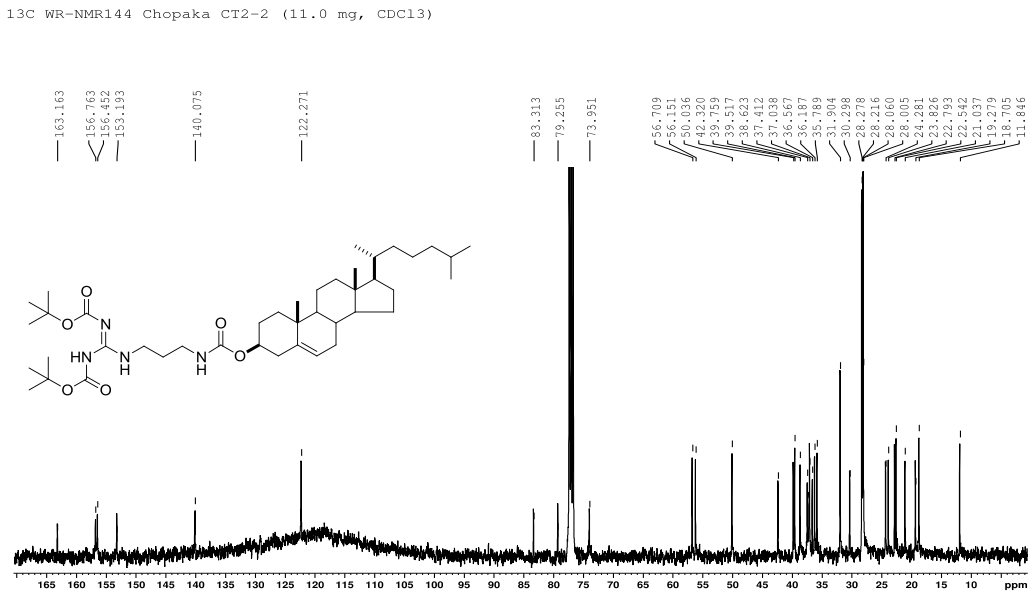

Appendix Figure 29 ^{13}C NMR Spectrum (100 MHz, $CDCl_3$) of 3β-[(3-((*N*′,*N*″-Di(*tert*-butoxycarbonyl))guanidinyl)propyl)carbamoyl] cholesterol (**C5a**)

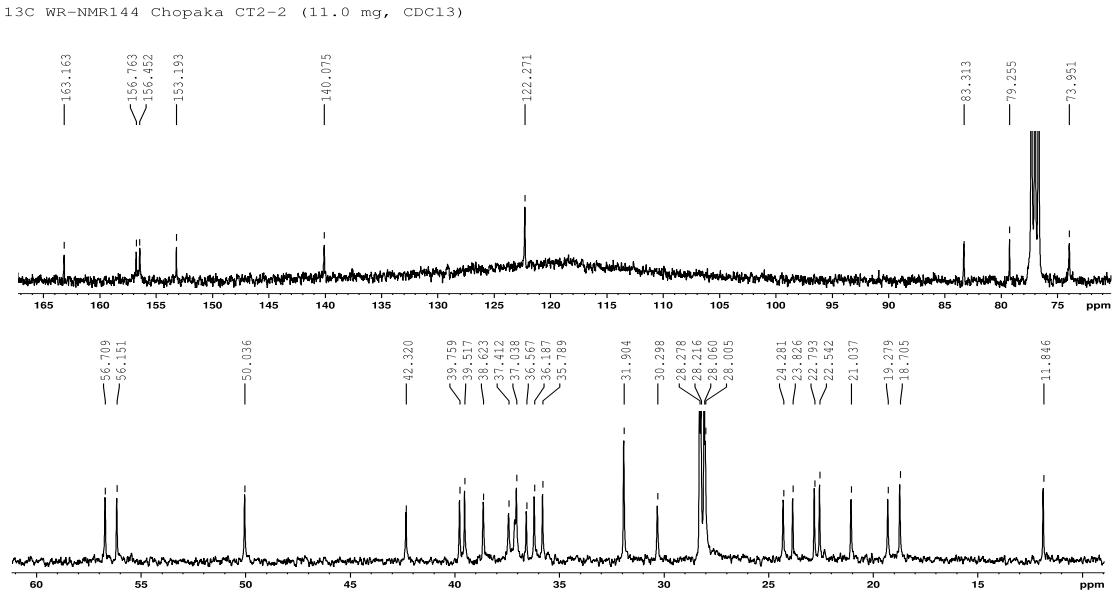

Appendix Figure 30 Expansion of ^{13}C NMR Spectrum (100 MHz, $CDCl_3$) of 3β-[(3-((*N*′,*N*″-Di(*tert*-butoxycarbonyl))guanidinyl)propyl)carbamoyl] cholesterol (**C5a**)

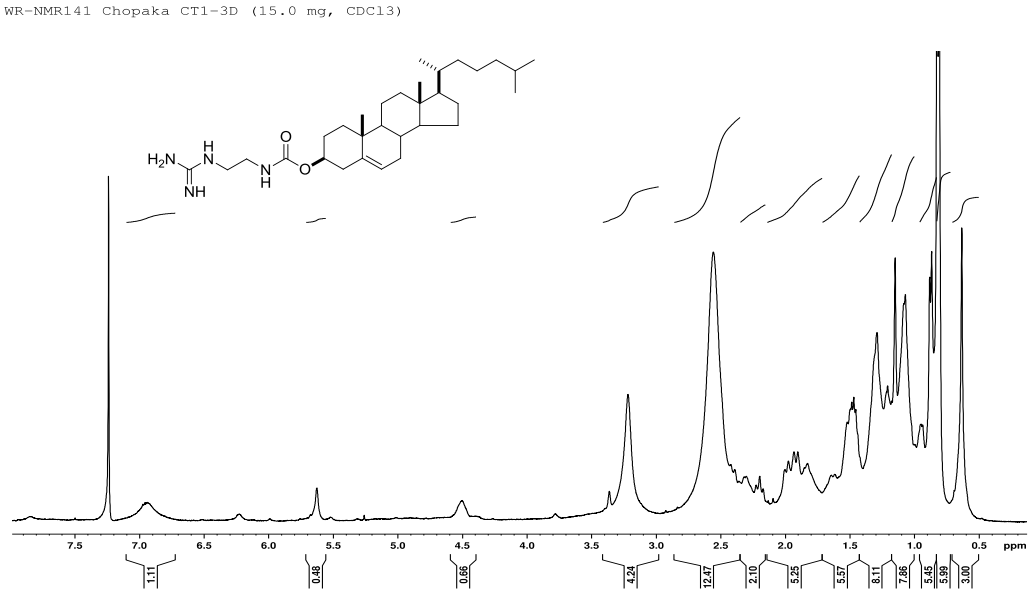

Appendix Figure 31 ^{1}H NMR Spectrum (400 MHz, $CDCl_3$) of Lipid 3β-[(2-(Guanidinyl)ethyl)carbamoyl]cholesterol (**L3a**)

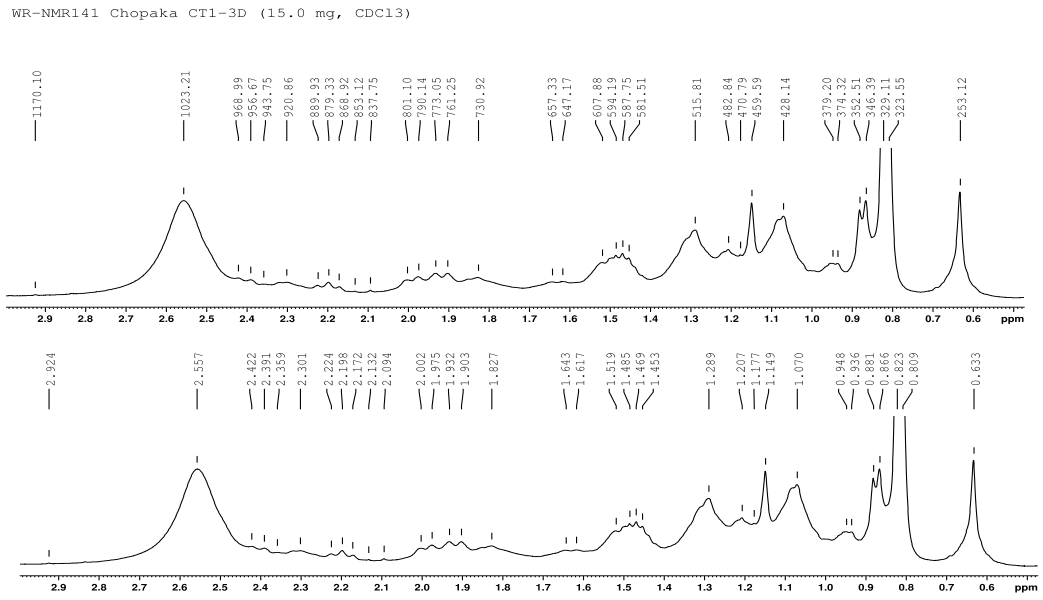

Appendix Figure 32 Expansion of ^{1}H NMR Spectrum (400 MHz, $CDCl_3$) of Lipid 3β-[(2-(Guanidinyl)ethyl)carbamoyl]cholesterol (**L3a**)

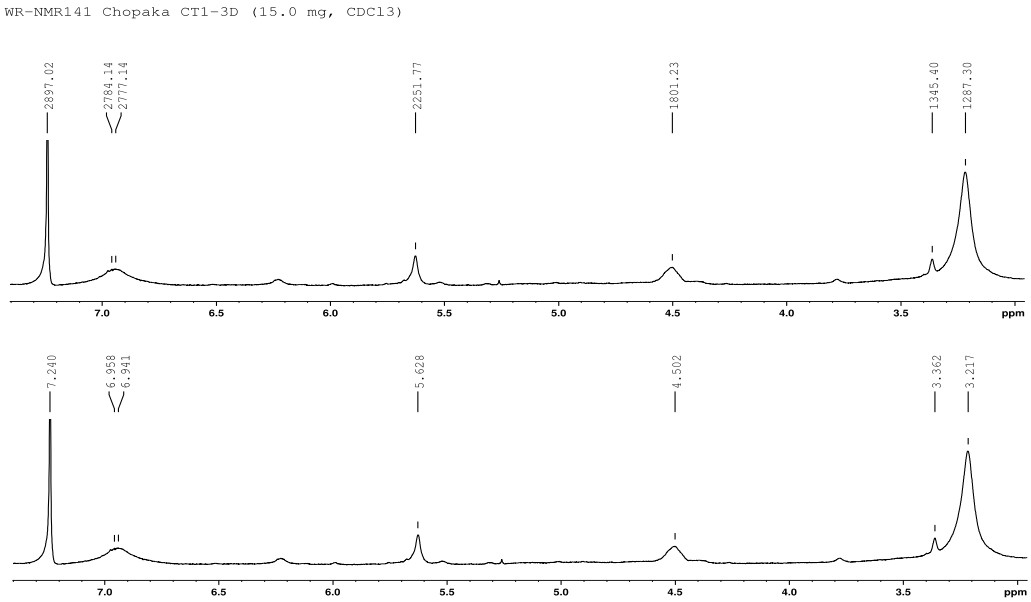

Appendix Figure 33 Expansion (cont.) of ^{1}H NMR Spectrum (400 MHz, $CDCl_3$) of Lipid 3β-[(2-(Guanidinyl)ethyl)carbamoyl]cholesterol (**L3a**)

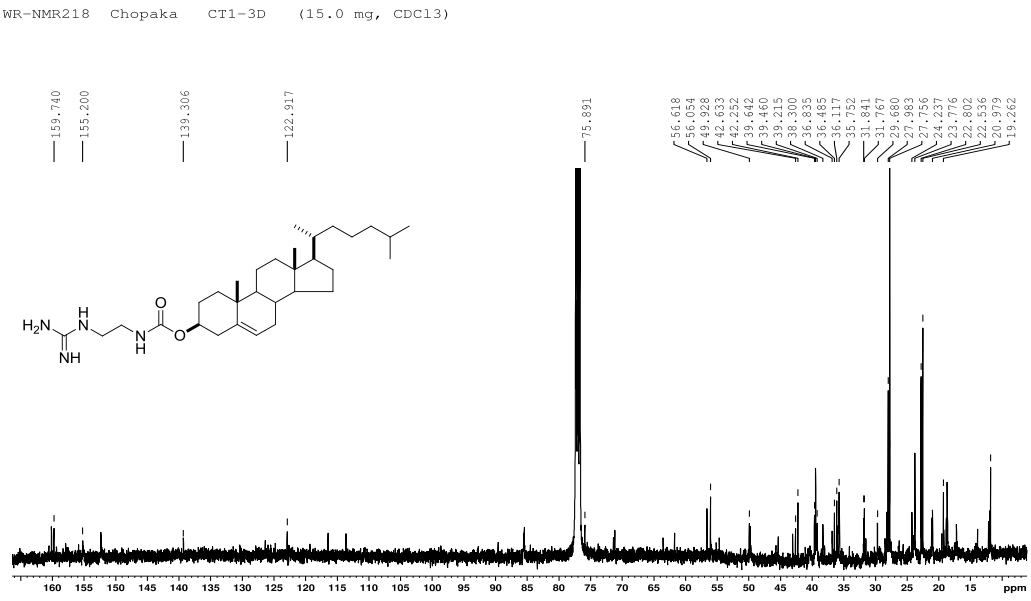

Appendix Figure 34 ^{13}C NMR Spectrum (100 MHz, $CDCl_3$) of Lipid 3β-[(2-(Guanidinyl)ethyl)carbamoyl]cholesterol (**L3a**)

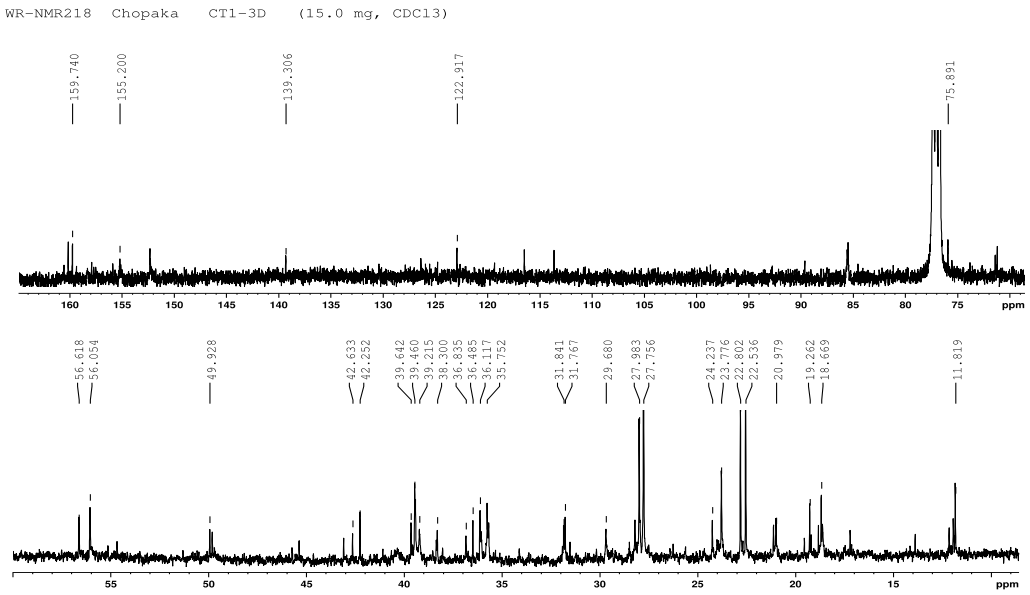

Appendix Figure 35 Expansion of ^{13}C NMR Spectrum (100 MHz, $CDCl_3$) of Lipid 3β-[(2-(Guanidinyl)ethyl)carbamoyl]cholesterol (**L3a**)

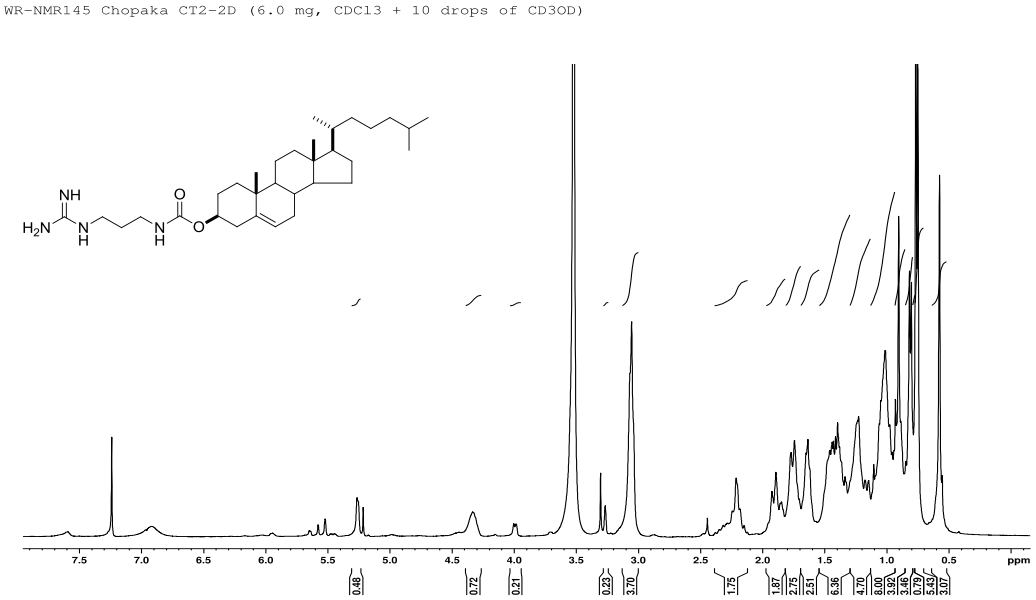

Appendix Figure 36 ^1H NMR Spectrum (400 MHz, $CDCl_3$ + CD_3OD) of Lipid 3β-[(3-(Guanidinyl)propyl)carbamoyl]cholesterol (**L7a**)

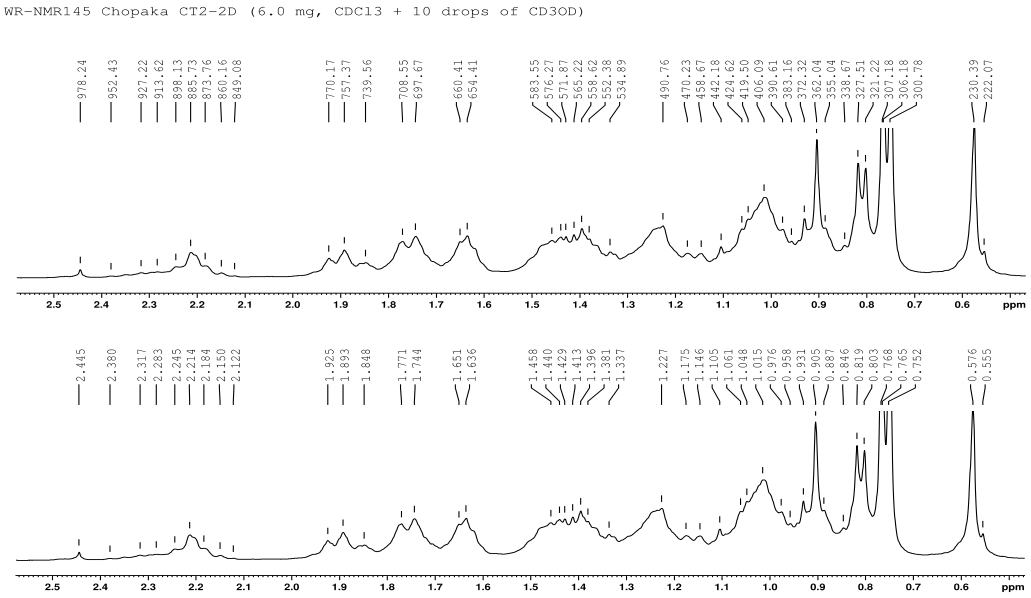

Appendix Figure 37 Expansion of ^{1}H NMR Spectrum (400 MHz, $CDCl_3$ + CD_3OD) of Lipid 3β-[(3-(Guanidinyl)propyl)carbamoyl]cholesterol (**L7a**)

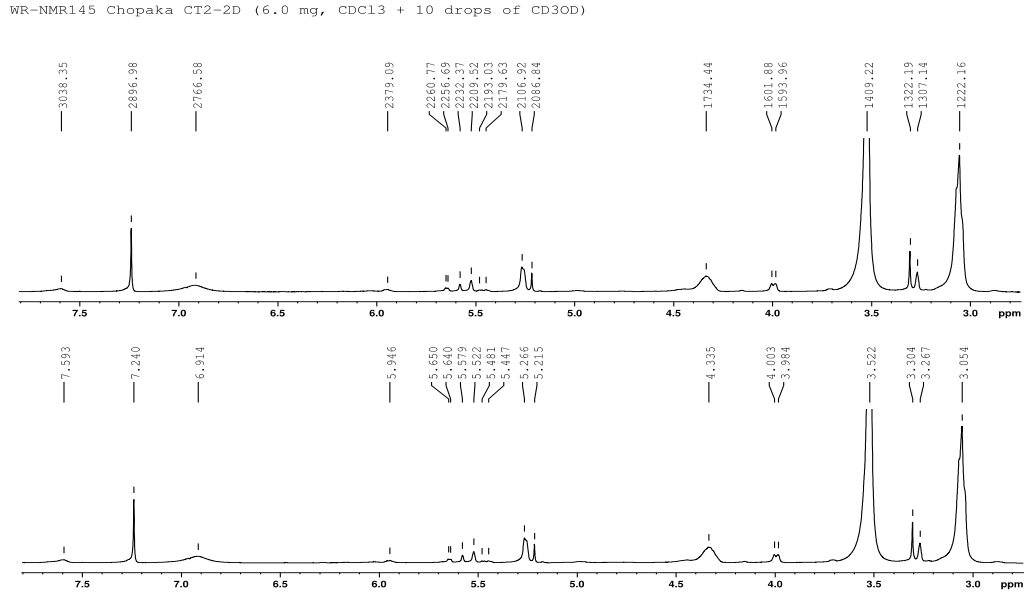

Appendix Figure 38 Expansion (cont.) of ^{1}H NMR Spectrum (400 MHz, $CDCl_3$ + CD_3OD) of Lipid 3β-[(3(Guanidinyl)propyl) carbamoyl]cholesterol (**L7a**)

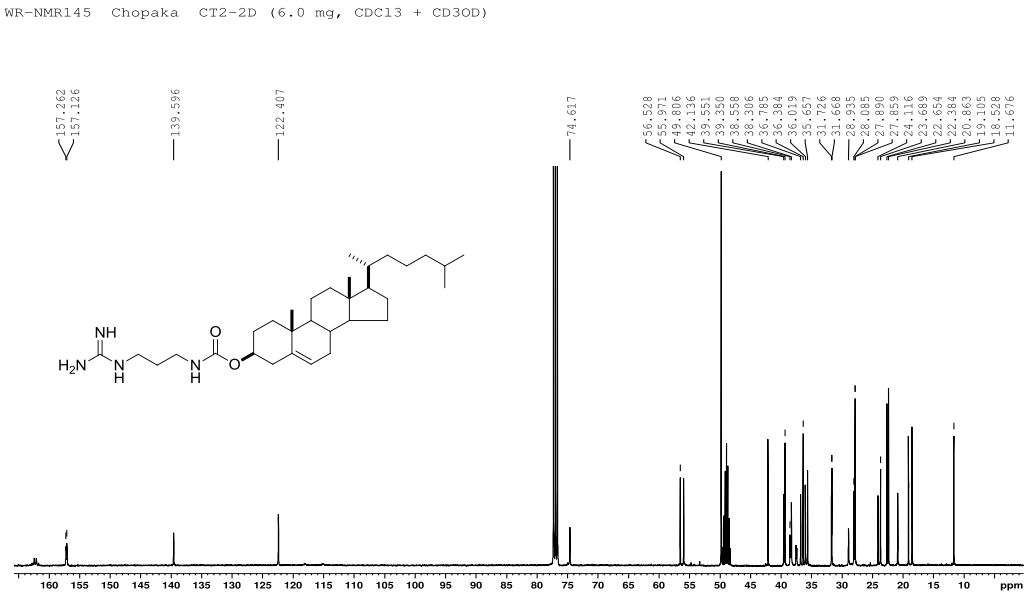

Appendix Figure 39 ^{13}C NMR Spectrum (100 MHz, $CDCl_3$ + CD_3OD) of Lipid 3β-[(3-(Guanidinyl)propyl)carbamoyl]cholesterol (**L7a**)

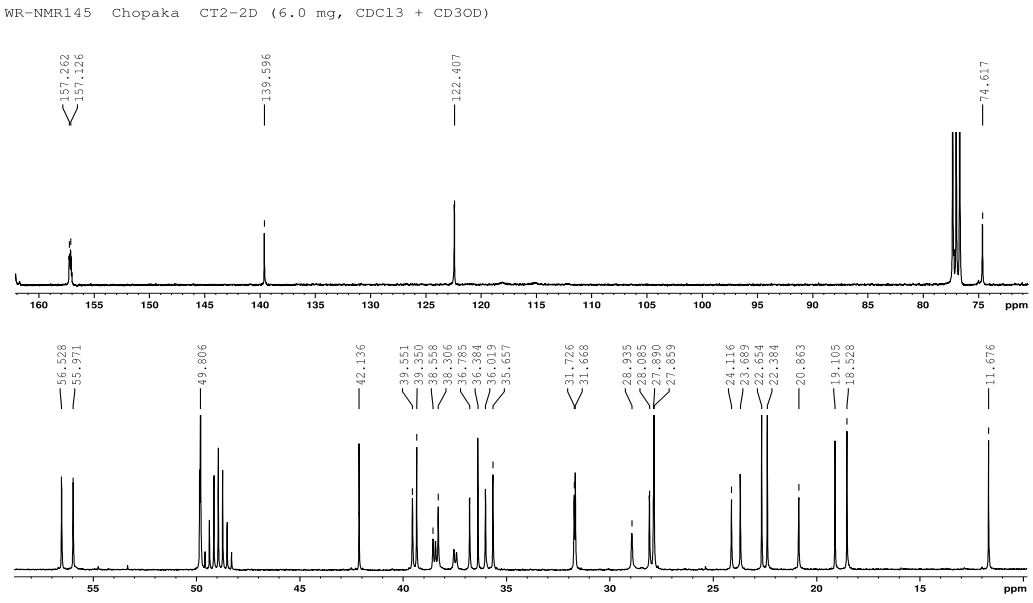

Appendix Figure 40 Expansion of ^{13}C NMR Spectrum (100 MHz, $CDCl_3$ + CD_3OD) of Lipid 3β-[(3-(Guanidinyl)propyl)carbamoyl]cholesterol (**L7a**)

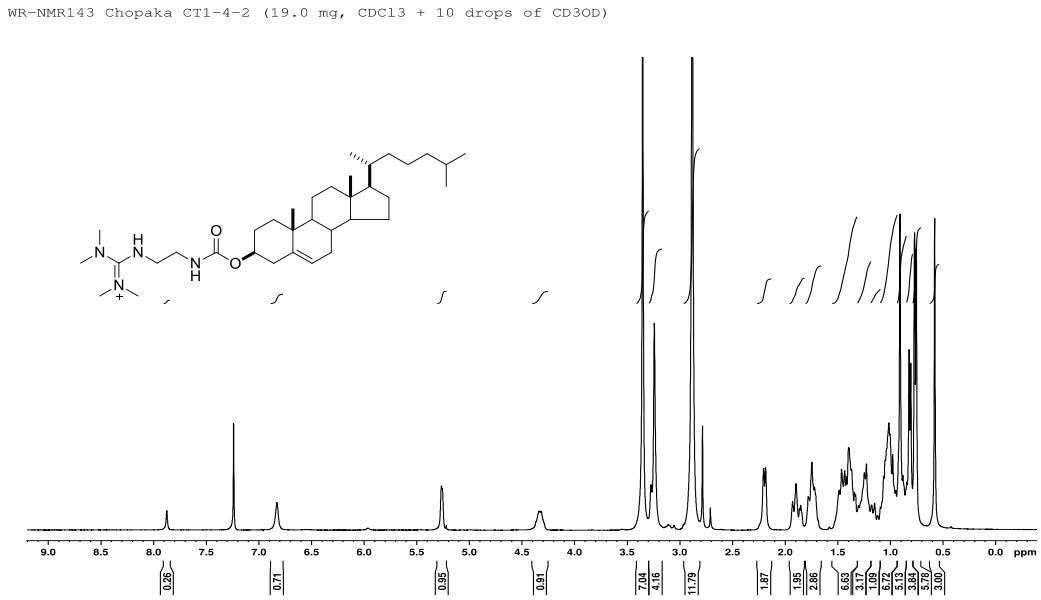

Appendix Figure 41 ^{1}H NMR Spectrum (400 MHz, $CDCl_3$ + CD_3OD) of Lipid 3β-[(2-((*N*′,*N*′,*N*″,*N*″-Tetramethyl)guanidinyl)ethyl)carbamoyl] cholesterol (**L4a**)

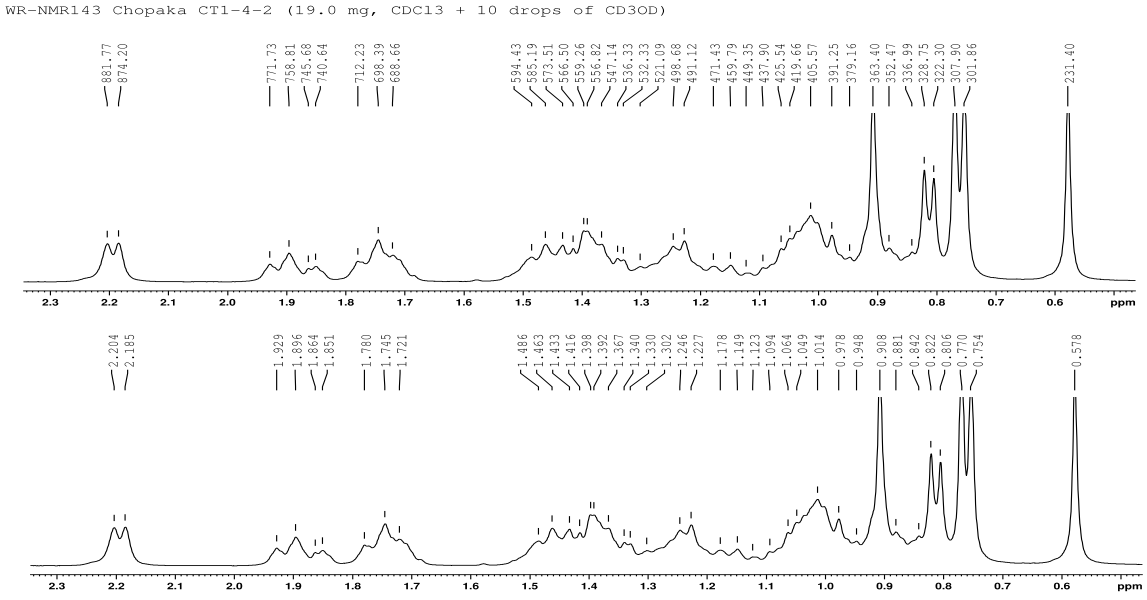

Appendix Figure 42 Expansion of ^{1}H NMR Spectrum (400 MHz, $CDCl_3$ + CD_3OD) of Lipid 3β-[(2-((*N*′,*N*′,*N*″,*N*″-Tetramethyl)guanidinyl)ethyl) carbamoyl]cholesterol (**L4a**)

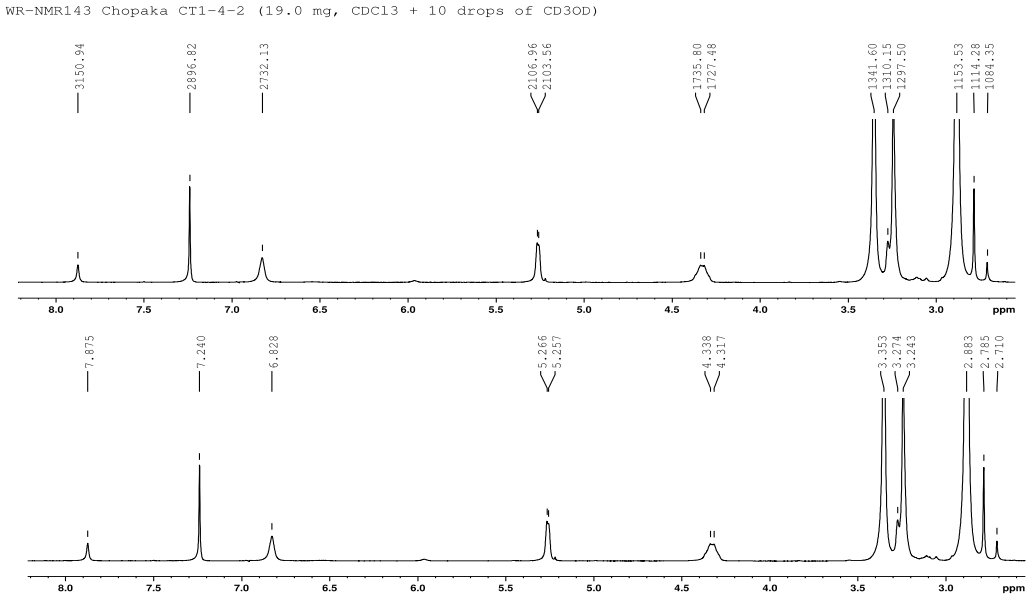

Appendix Figure 43 Expansion (cont.) of ^{1}H NMR Spectrum (400 MHz, $CDCl_3$ + CD_3OD) of Lipid 3β-[(2-((*N*′,*N*′,*N*″,*N*″-Tetramethyl) guanidinyl)ethyl)carbamoyl]cholesterol (**L4a**)

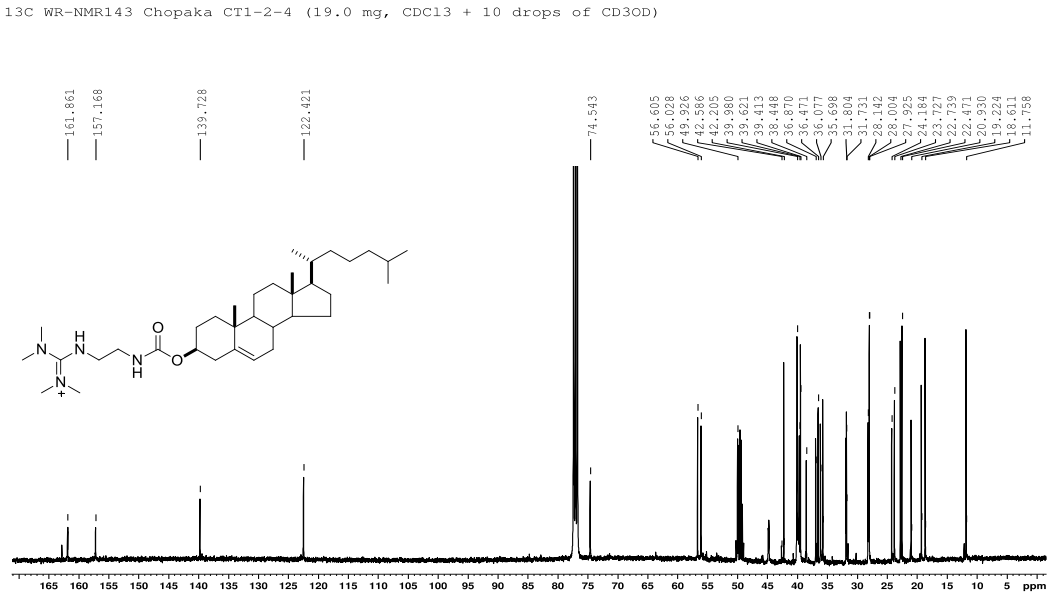

Appendix Figure 44 ^{13}C NMR Spectrum (100 MHz, $CDCl_3$ + CD_3OD) of Lipid 3β-[(2-((*N*′,*N*′,*N*″,*N*″-Tetramethyl)guanidinyl)ethyl)carbamoyl] cholesterol (**L4a**)

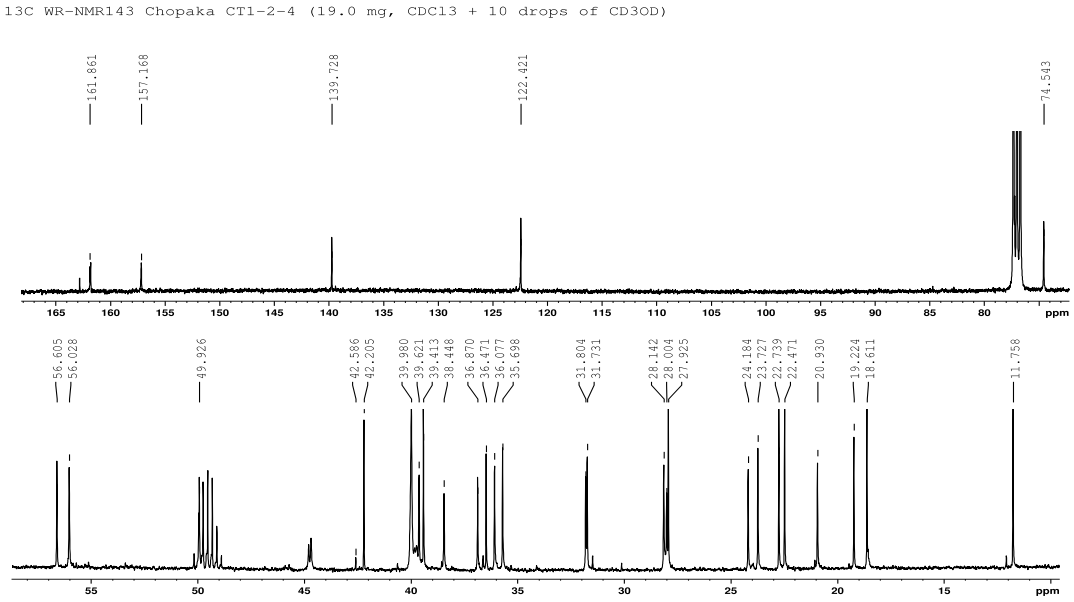

Appendix Figure 45 Expansion of ^{13}C NMR Spectrum (100 MHz, $CDCl_3$ + CD_3OD) of Lipid 3β-[(2-((*N*′,*N*′,*N*″,*N*″-Tetramethyl)guanidinyl)ethyl) carbamoyl]cholesterol (**L4a**)

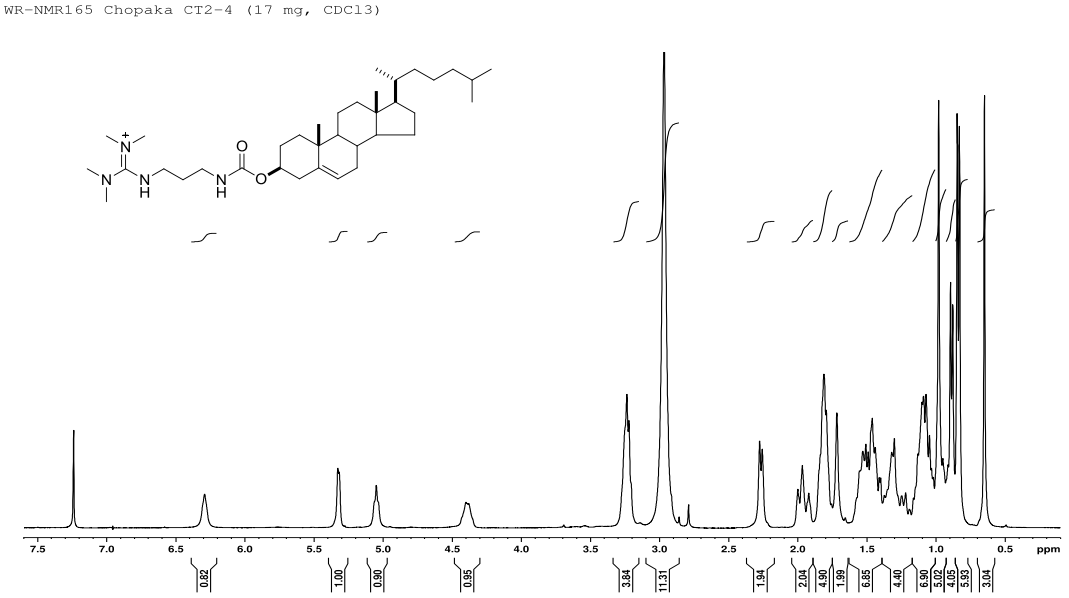

Appendix Figure 46 ^1H NMR Spectrum (400 MHz, $CDCl_3$) of Lipid 3β-[(3-((*N*′, *N*′,*N*″,*N*″-Tetramethyl)guanidinyl)propyl)carbamoyl]cholesterol (**L8a**)

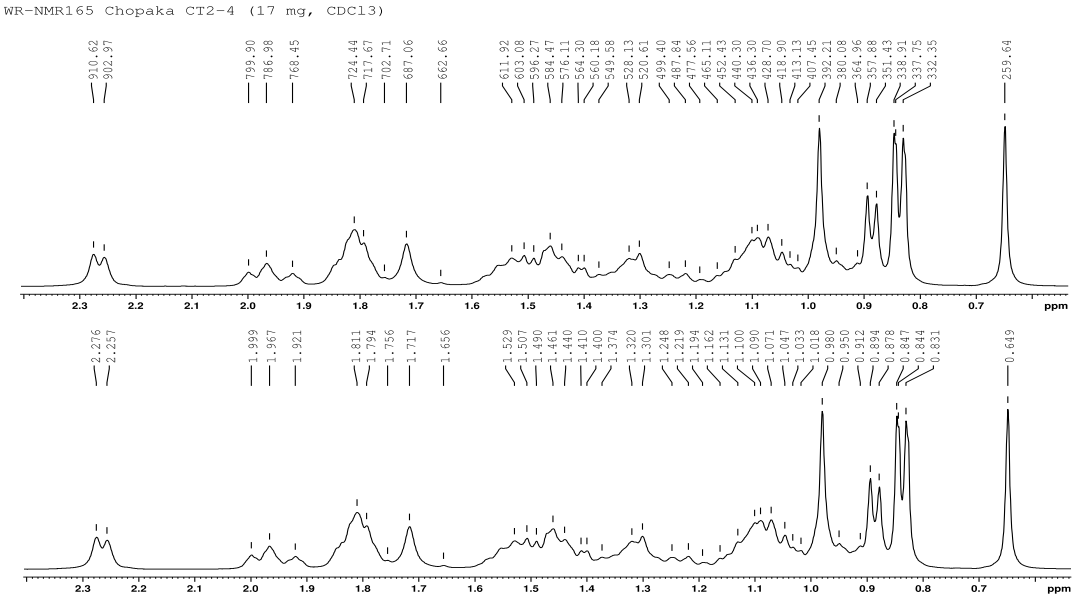

Appendix Figure 47 Expansion of ^{1}H NMR Spectrum (400 MHz, $CDCl_3$) of Lipid 3β-[(3-((*N*′,*N*′,*N*″,*N*″-Tetramethyl)guanidinyl)propyl) carbamoyl]cholesterol (**L8a**)

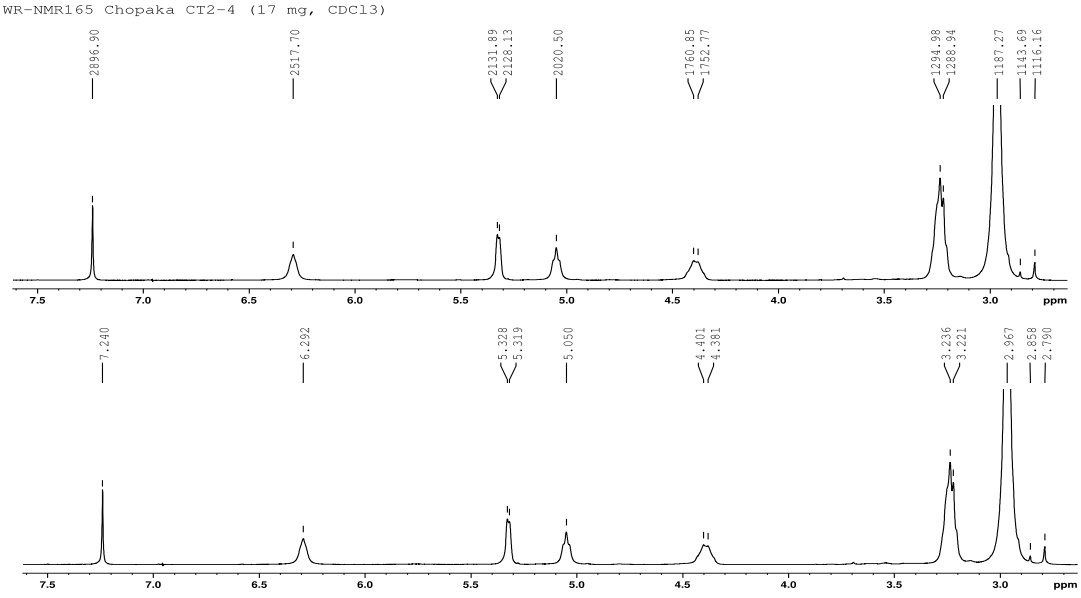

Appendix Figure 48 Expansion (cont.) of ^{1}H NMR Spectrum (400 MHz, $CDCl_3$) of Lipid 3β-[(3-((*N*′,*N*′,*N*″,*N*″-Tetramethyl)guanidinyl)propyl) carbamoyl]cholesterol (**L8a**)

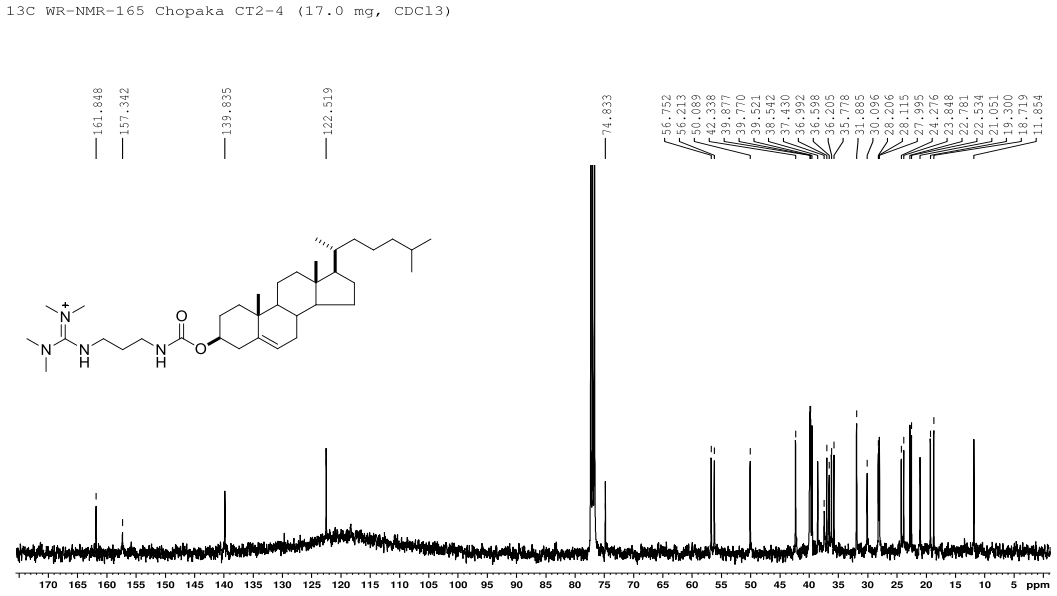

Appendix Figure 49 ^{13}C NMR Spectrum (100 MHz, $CDCl_3$) of Lipid 3β-[(3-((*N*′,*N*′,*N*′′,*N*′′-Tetramethyl)guanidinyl)propyl)carbamoyl]cholesterol (**L8a**)

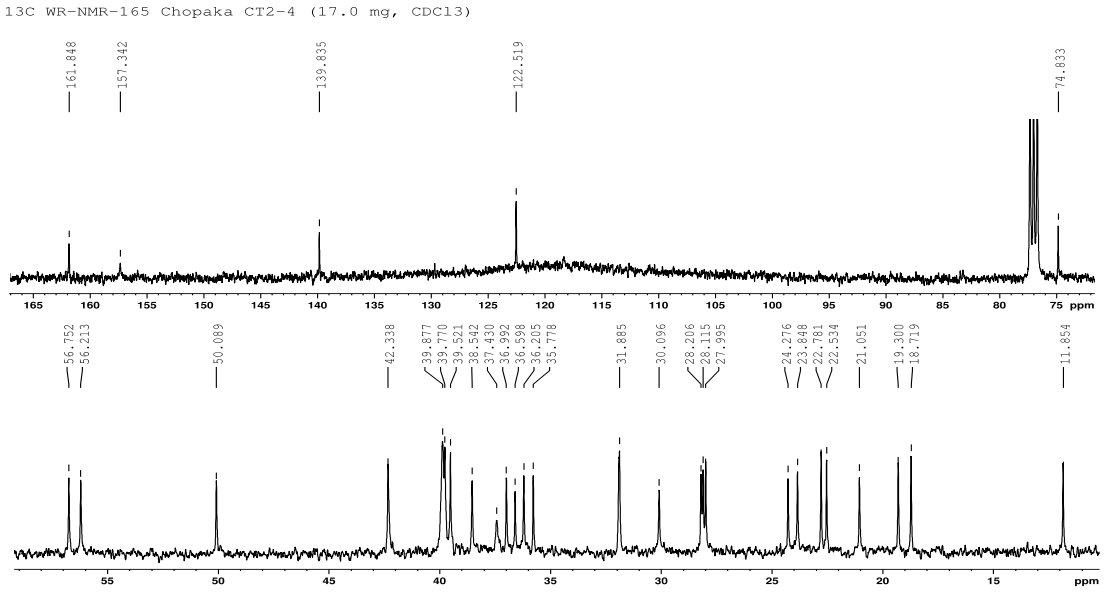

Appendix Figure 50 Expansion of ^{13}C NMR Spectrum (100 MHz, $CDCl_3$) of Lipid 3β-[(3-((*N*′,*N*′,*N*′′,*N*′′-Tetramethyl)guanidinyl)propyl) carbamoyl]cholesterol (**L8a**)

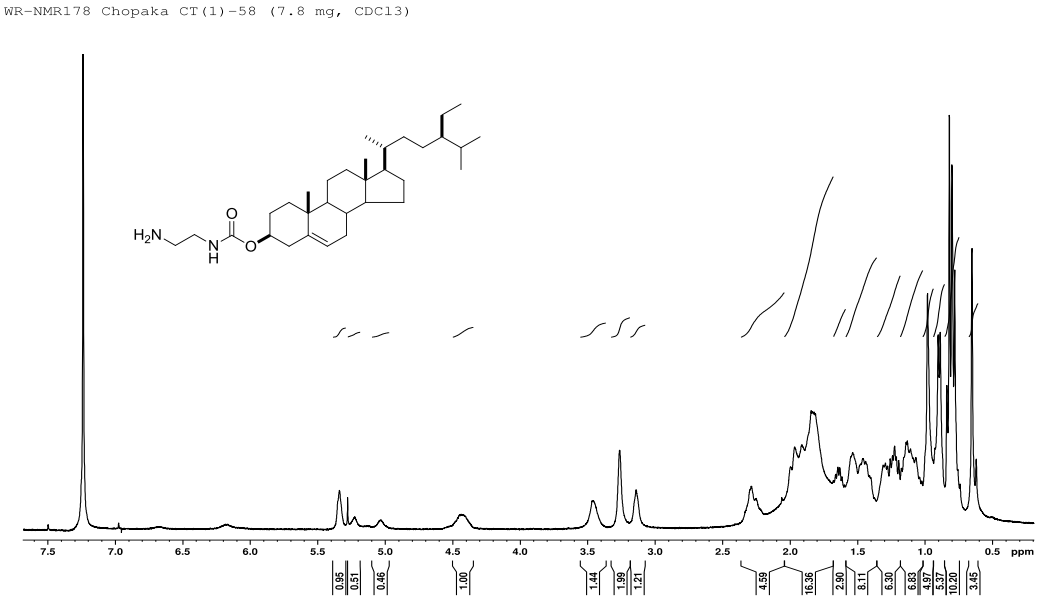

Appendix Figure 51 ^{1}H NMR Spectrum (400 MHz, $CDCl_3$) of Lipid 3β-[*N*-(2-Aminoethyl)carbamoyl]β-sitosterol (**L1b**)

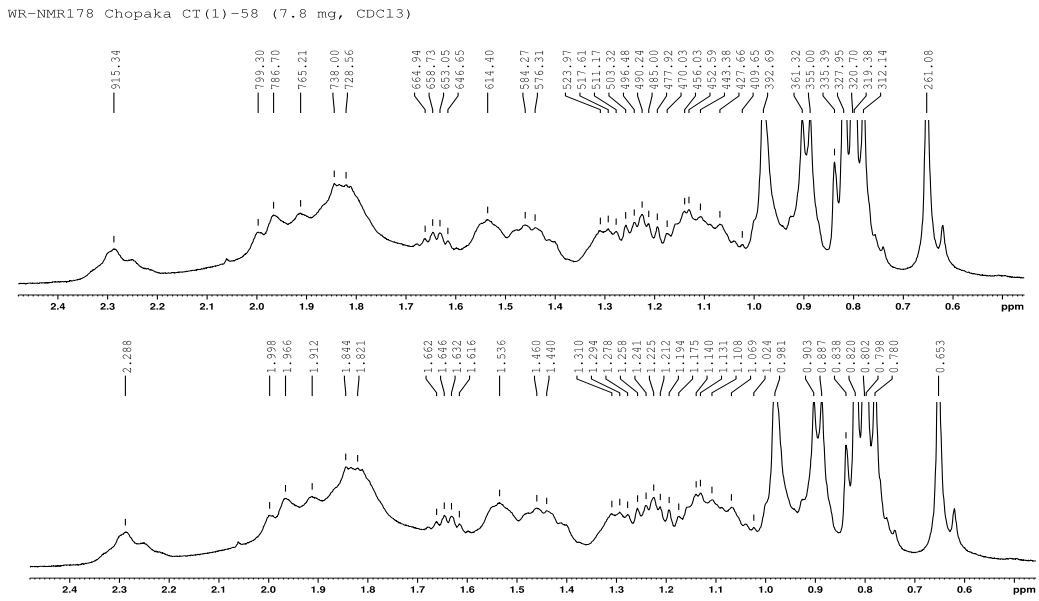

Appendix Figure 52 Expansion of ^{1}H NMR Spectrum (400 MHz, $CDCl_3$) of Lipid 3β-[*N*-(2-Aminoethyl)carbamoyl]β-sitosterol (**L1b**)

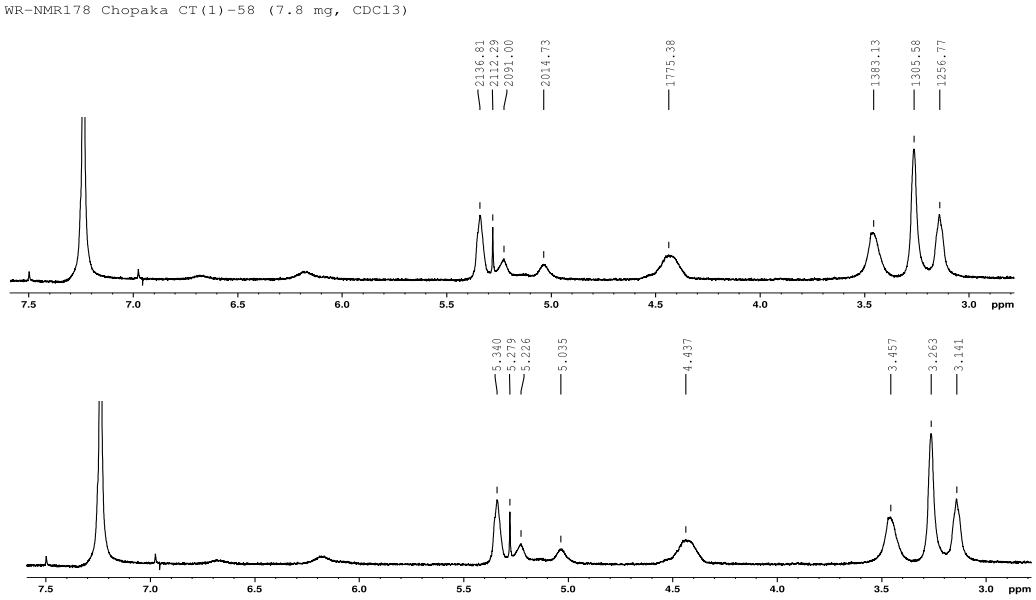

Appendix Figure 53 Expansion (cont.) of ^{1}H NMR Spectrum (400 MHz, $CDCl_3$) of Lipid 3β-[*N*-(2-Aminoethyl)carbamoyl]β-sitosterol (**L1b**)

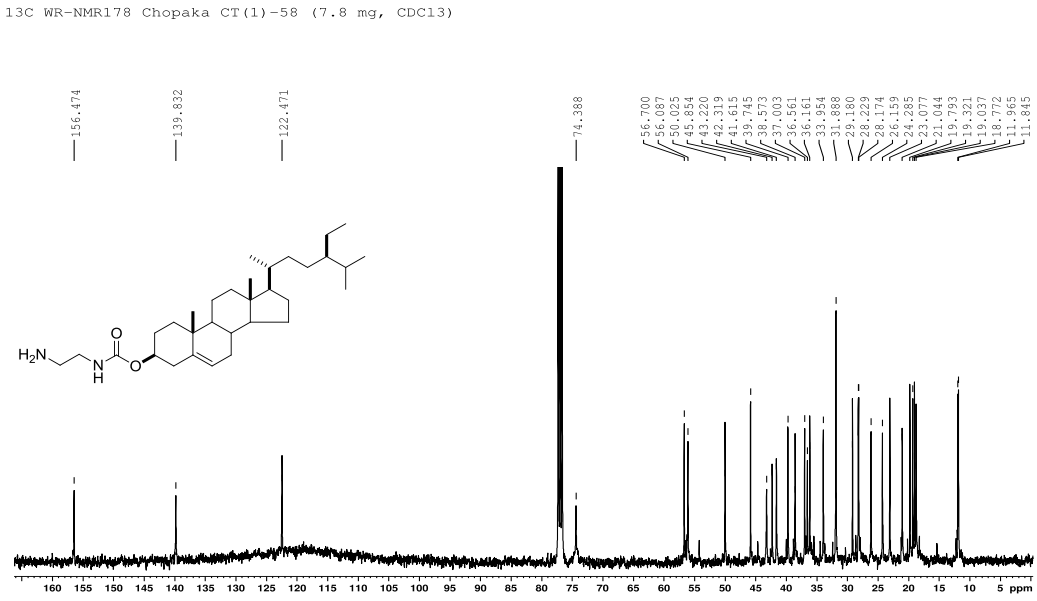

Appendix Figure 54 Expansion of ^{13}C NMR Spectrum (100 MHz, $CDCl_3$) of Lipid 3β-[*N*-(2-Aminoethyl)carbamoyl]β-sitosterol (**L1b**)

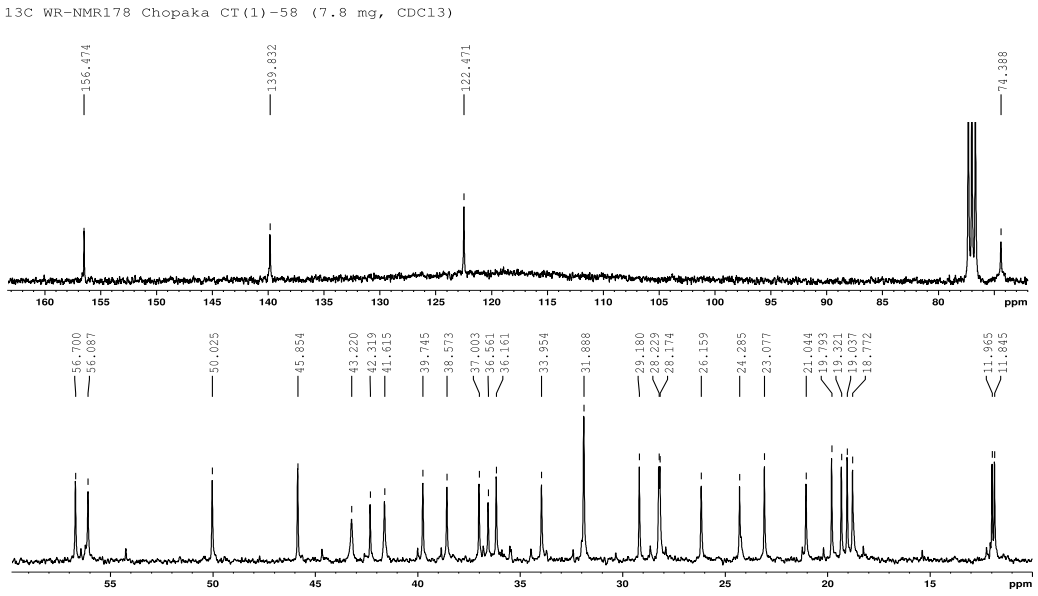

Appendix Figure 55 Expansion of ^{13}C NMR Spectrum (100 MHz, $CDCl_3$) of Lipid 3β-[*N*-(2-Aminoethyl)carbamoyl]β-sitosterol (**L1b**)

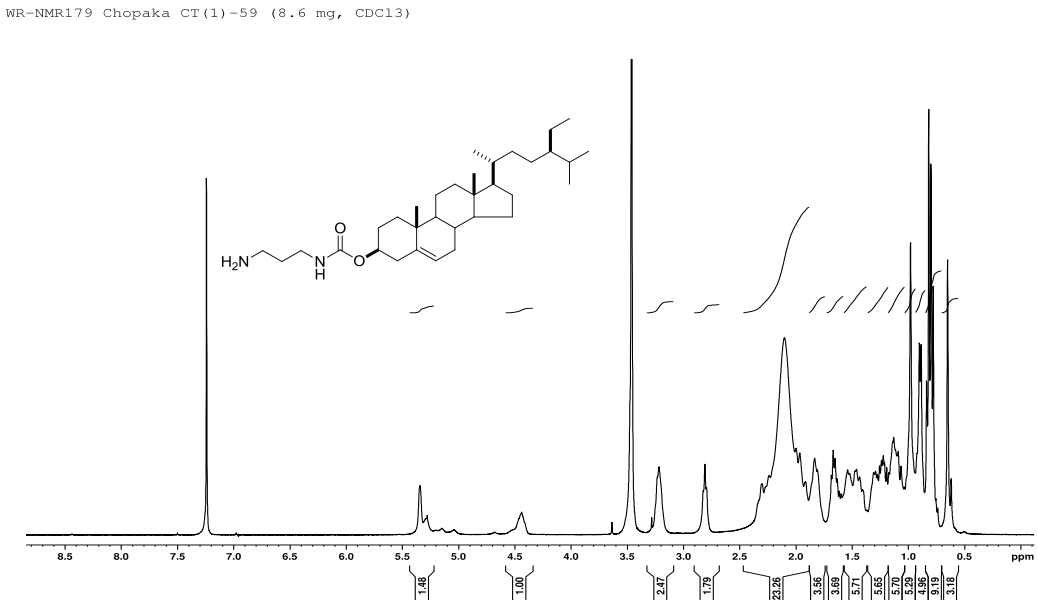

Appendix Figure 56 ^{1}H NMR Spectrum (400 MHz, $CDCl_3$) of Lipid 3β-[*N*-(3-Aminopropyl)carbamoyl]β-sitosterol (**L5b**)

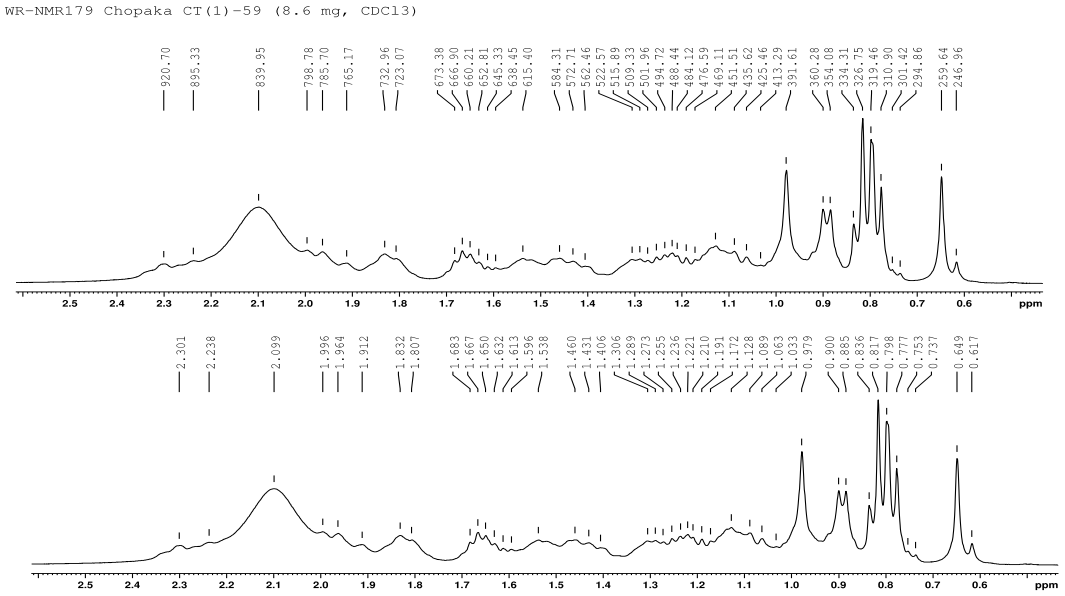

Appendix Figure 57 Expansion of ^{1}H NMR Spectrum (400 MHz, $CDCl_3$) of Lipid 3β-[*N*-(3-Aminopropyl)carbamoyl]β-sitosterol (**L5b**)

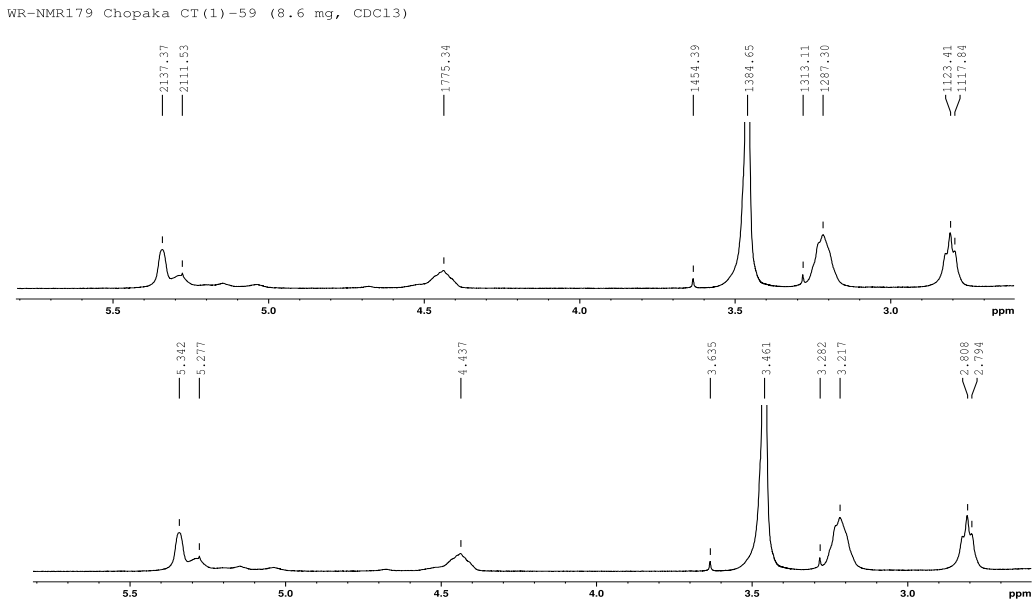

Appendix Figure 58 Expansion (cont.) of ^{1}H NMR Spectrum (400 MHz, $CDCl_3$) of Lipid 3β-[*N*-(3-Aminopropyl)carbamoyl]β-sitosterol (**L5b**)

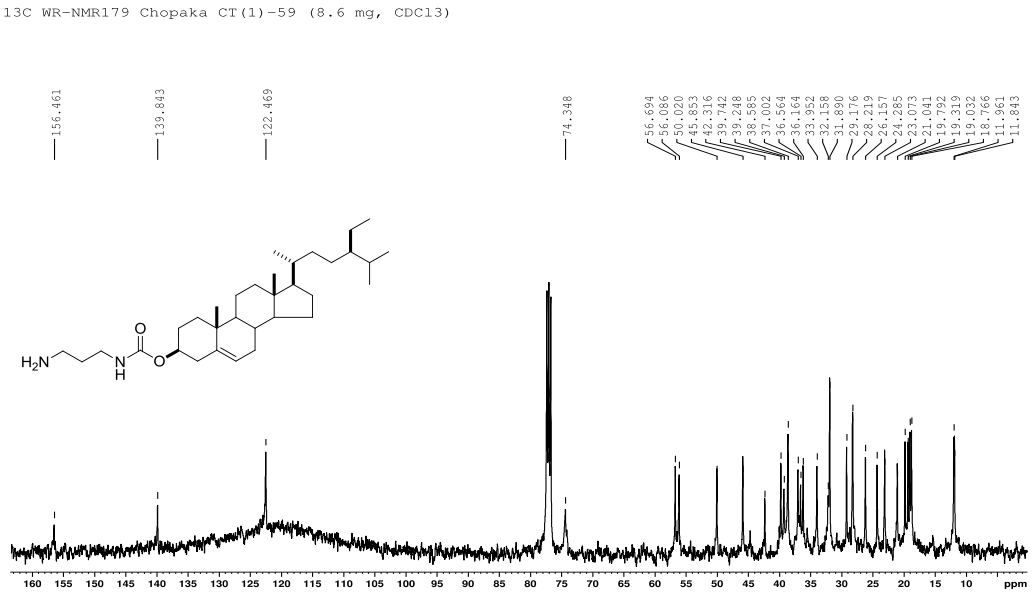

Appendix Figure 59 ^{13}C NMR Spectrum (100 MHz, $CDCl_3$) of Lipid 3β-[*N*-(3-Aminopropyl)carbamoyl]β-sitosterol (**L5b**)

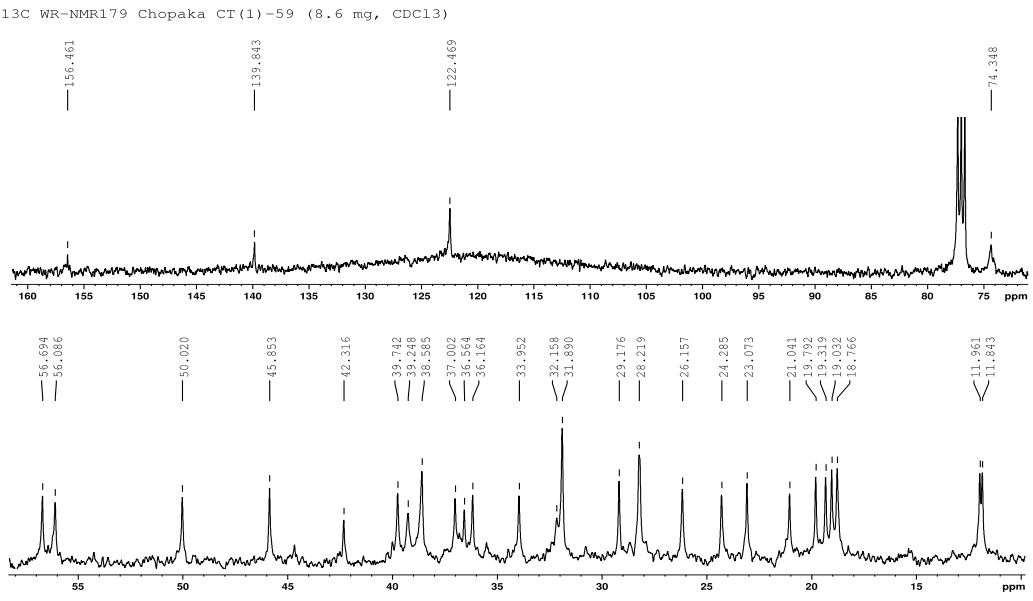

Appendix Figure 60 Expansion of ^{13}C NMR Spectrum (100 MHz, $CDCl_3$) of Lipid 3β-[*N*-(3-Aminopropyl)carbamoyl]β-sitosterol (**L5b**)

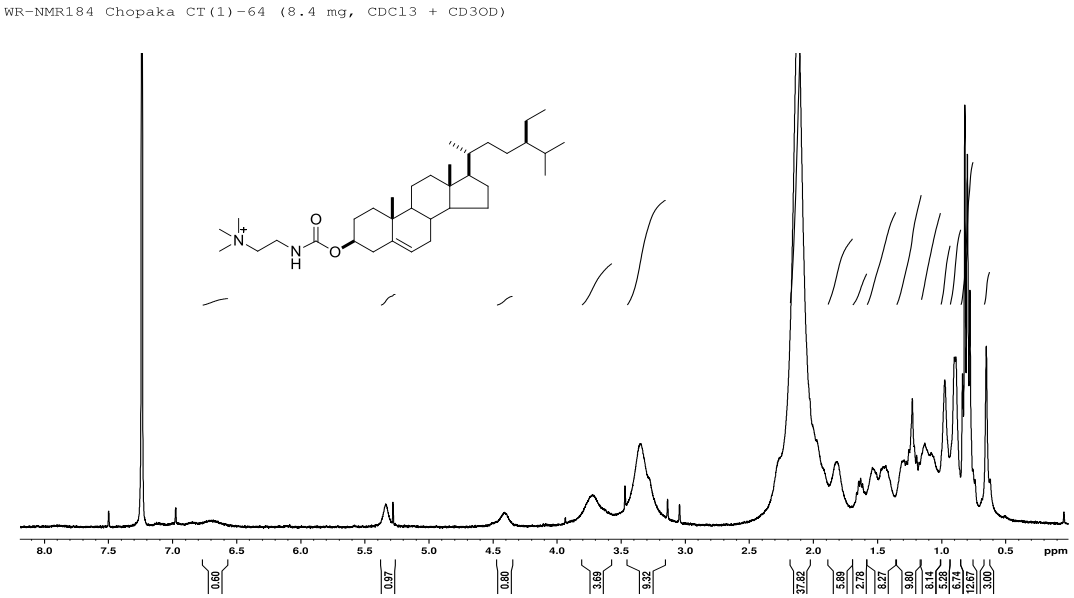

Appendix Figure 61 ^{1}H NMR Spectrum (400 MHz, $CDCl_3$ + CD_3OD) of Lipid 3β-[*N*-(2-(*N′,N′,N′*-Trimethyl)aminoethyl)carbamoyl]β-sitosterol (**L2b**)

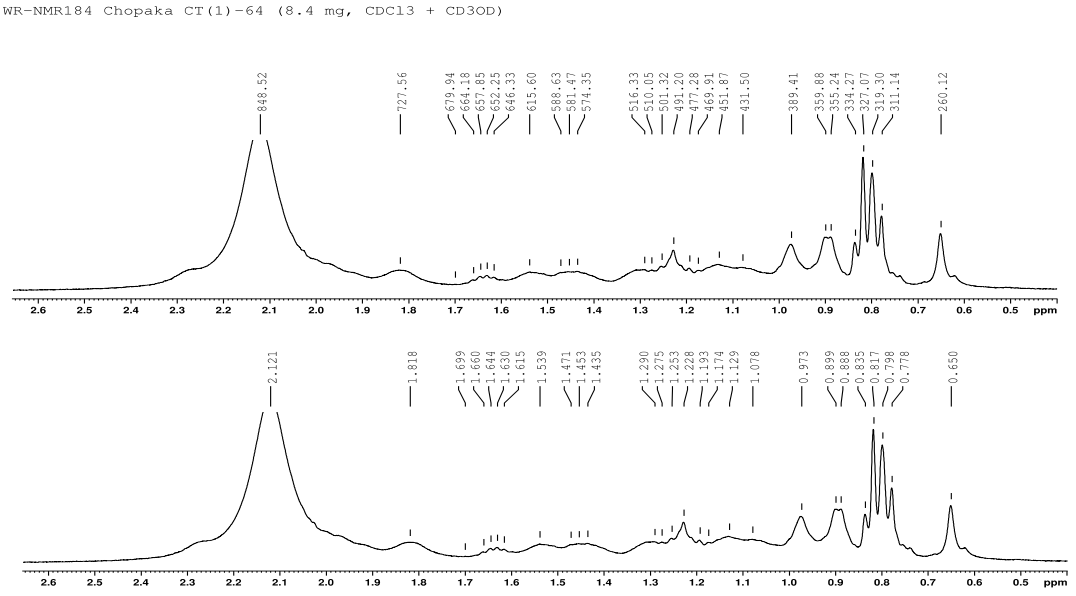

Appendix Figure 62 Expansion of ^{1}H NMR Spectrum (400 MHz, $CDCl_3$ + CD_3OD) of Lipid 3β-[N-(2-(*N′,N′,N′*-Trimethyl)aminoethyl)carbamoyl]β-sitosterol (**L2b**)

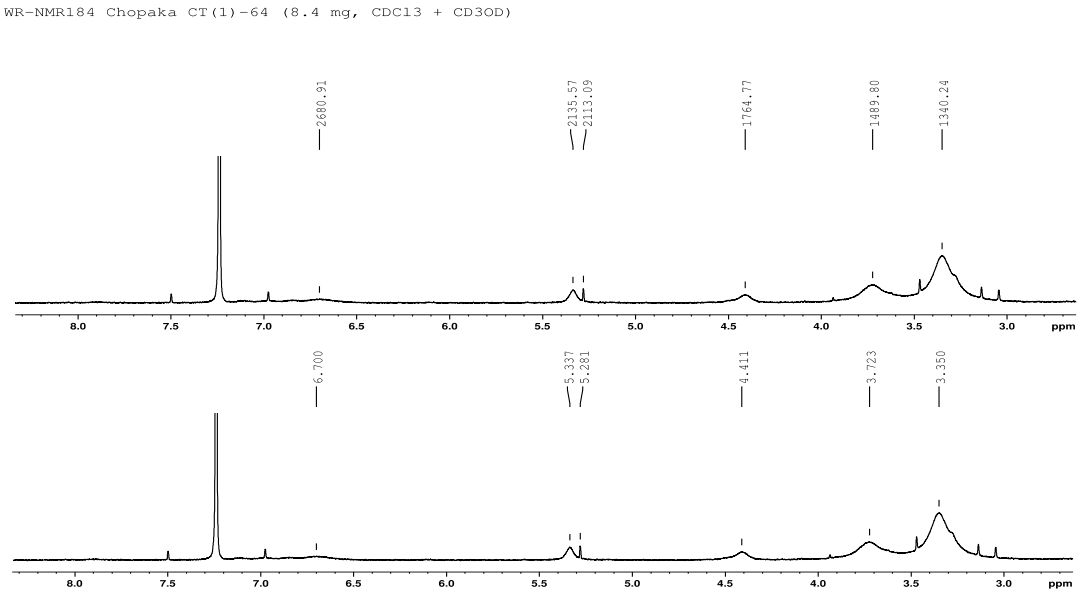

Appendix Figure 63 Expansion (cont.) of ^{1}H NMR Spectrum (400 MHz, $CDCl_3$ + CD_3OD) of Lipid 3β-[N-(2-(*N′,N′,N′*-Trimethyl)aminoethyl) carbamoyl]β-sitosterol (**L2b**)

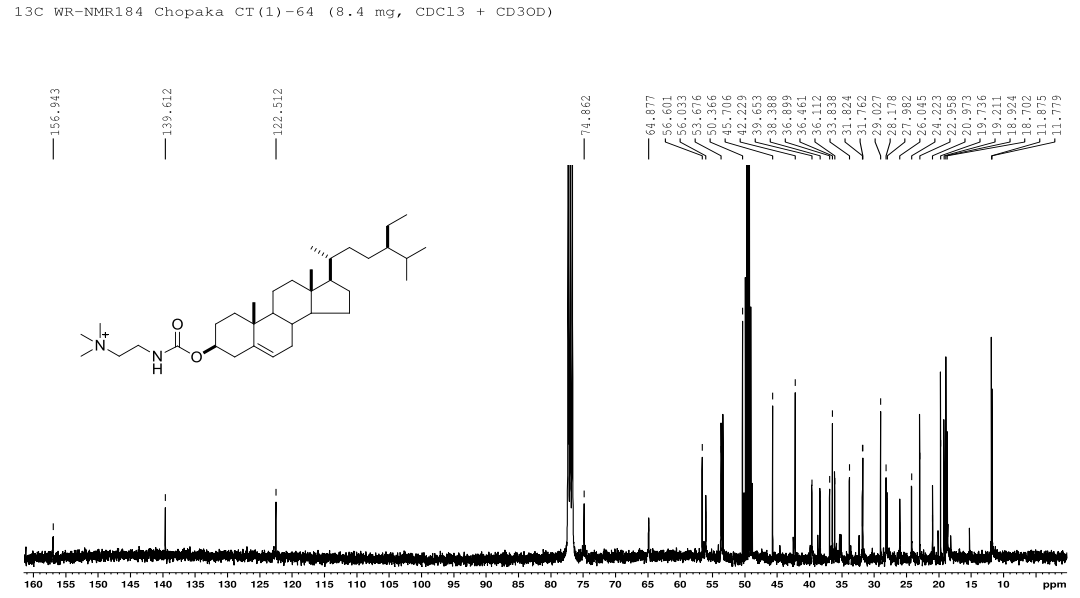

Appendix Figure 64 ^{13}C NMR Spectrum (100 MHz, $CDCl_3$ + CD_3OD) of Lipid 3β-[N-(2-(*N′,N′,N′*-Trimethyl)aminoethyl)carbamoyl]β-sitosterol (**L2b**)

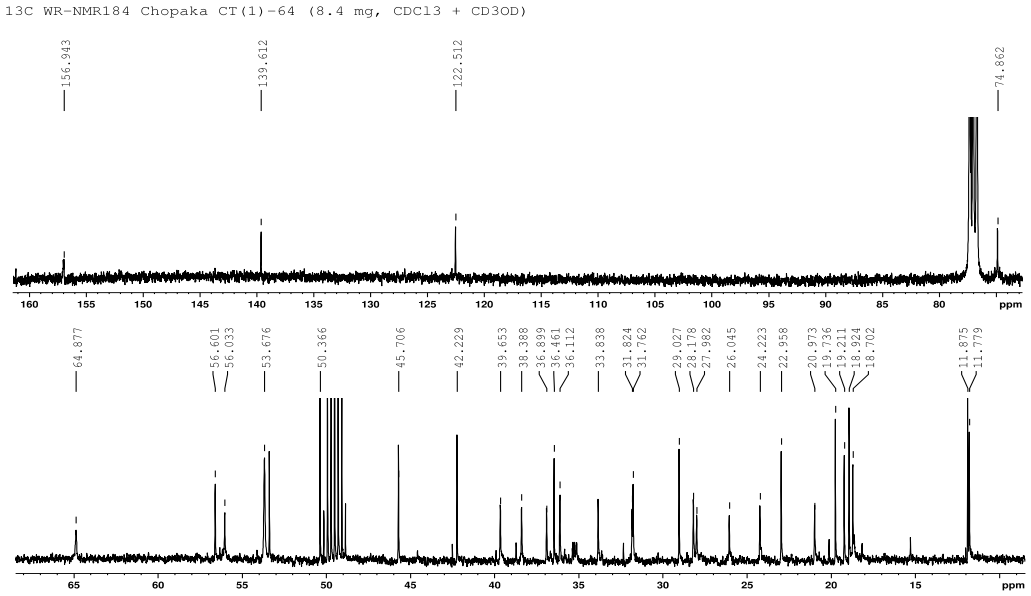

Appendix Figure 65 Expansion of ^{13}C NMR Spectrum (100 MHz, $CDCl_3$ + CD_3OD) of Lipid 3β-[N-(2-(*N′,N′,N′*-Trimethyl)aminoethyl)carbamoyl]β-sitosterol (**L2b**)

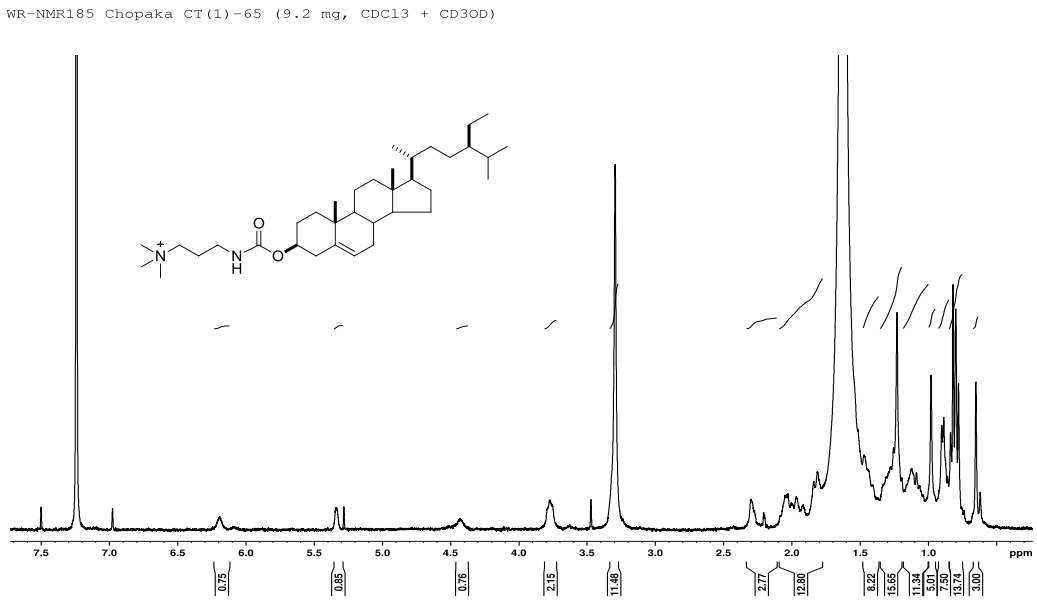

Appendix Figure 66 ^{1}H NMR Spectrum (400 MHz, $CDCl_3$) of Lipid 3β-[*N*-(3-(*N′,N′,N′*-Trimethyl)aminopropyl)carbamoyl]β-sitosterol (**L6b**)

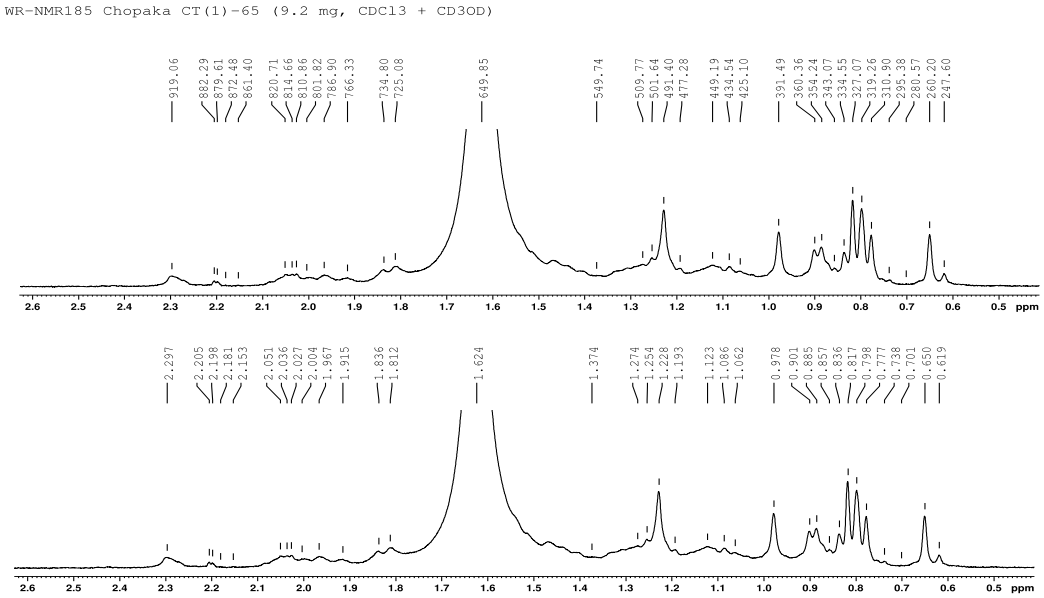

Appendix Figure 67 Expansion of ^{1}H NMR Spectrum (400 MHz, $CDCl_3$) of Lipid 3β-[*N*-(3-(*N*′,*N*′,*N*′-Trimethyl)aminopropyl)carbamoyl]β-sitosterol (**L6b**)

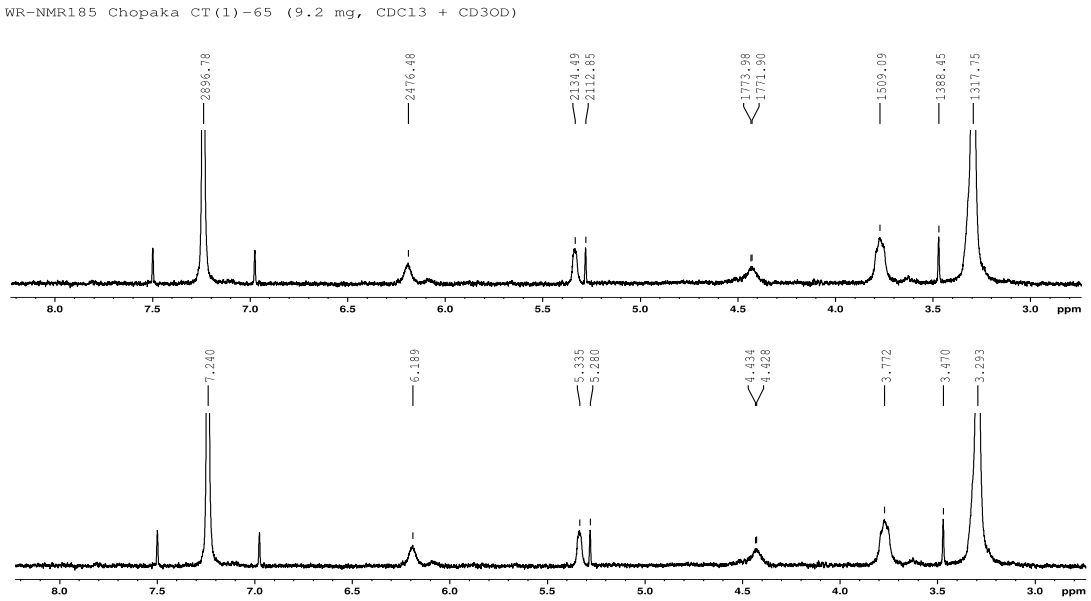

Appendix Figure 68 Expansion (cont.) of ^{1}H NMR Spectrum (400 MHz, $CDCl_3$) of Lipid 3β-[*N*-(3-(*N*′,*N*′,*N*′-Trimethyl)aminopropyl)carbamoyl]β-sitosterol (**L6b**)

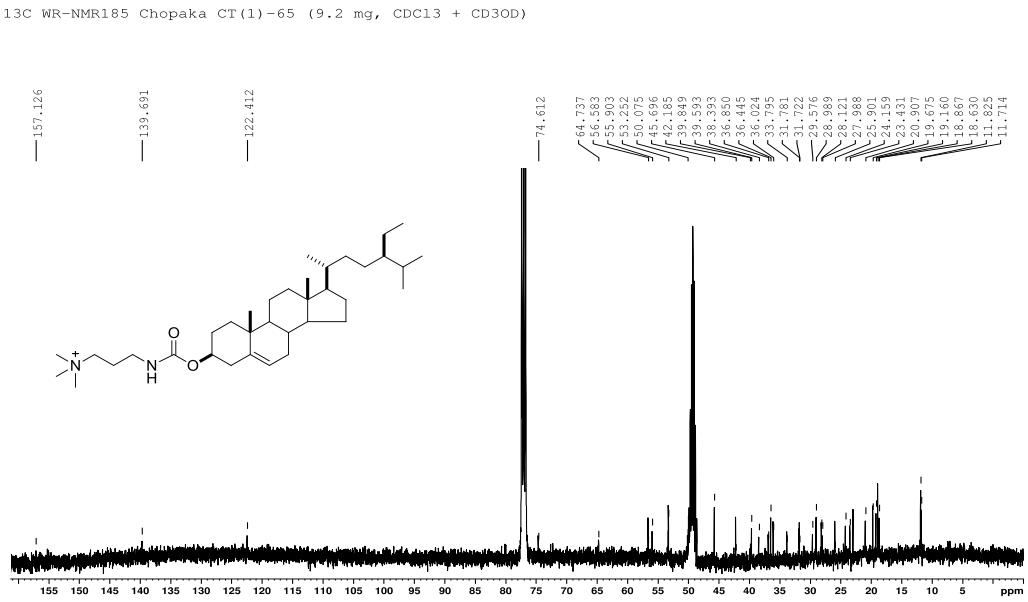

Appendix Figure 69 ^{13}C NMR Spectrum (100 MHz, $CDCl_3$) of Lipid 3β-[*N*-(3-(*N*′,*N*′,*N*′-Trimethyl)aminopropyl)carbamoyl]β-sitosterol (**L6b**)

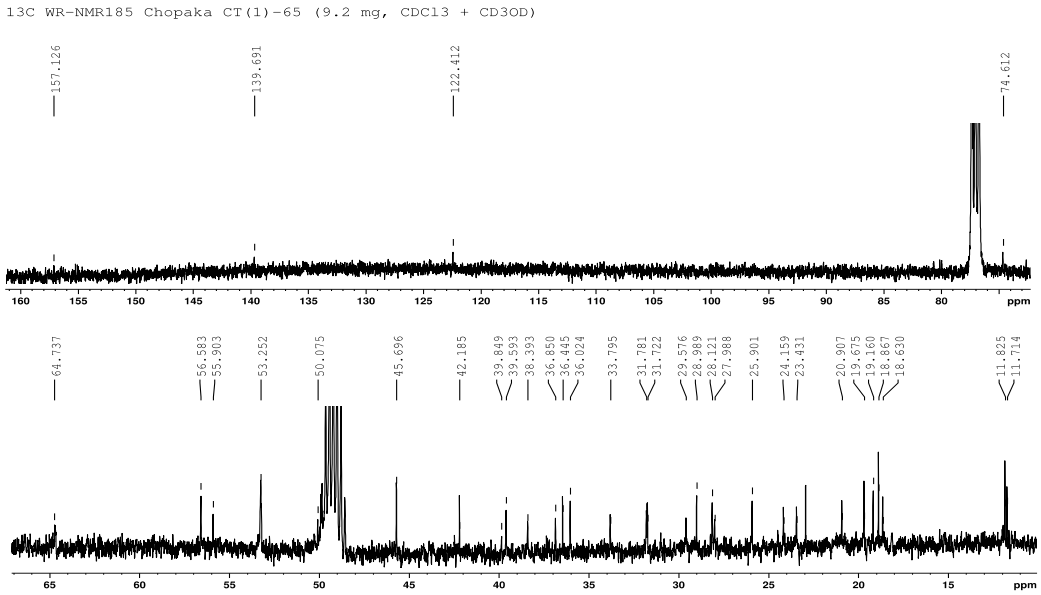

Appendix Figure 70 Expansion of ^{13}C NMR Spectrum (100 MHz, $CDCl_3$) of Lipid 3β-[*N*-(3-(*N*′,*N*′,*N*′-Trimethyl)aminopropyl)carbamoyl] β-sitosterol (**L6b**)

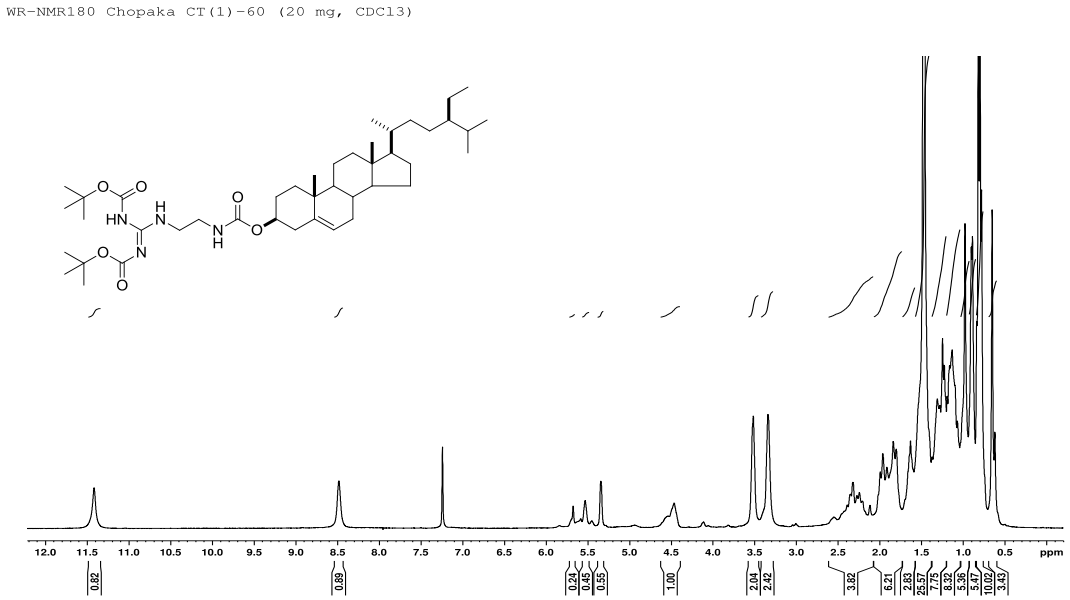

Appendix Figure 71 ^{1}H NMR Spectrum (400 MHz, $CDCl_3$) of 3β-[(2-((*N*′,*N*″-Di(*tert*-butoxycarbonyl)guanidinyl)ethyl)carbamoly]β-sitosterol (**C4b**)

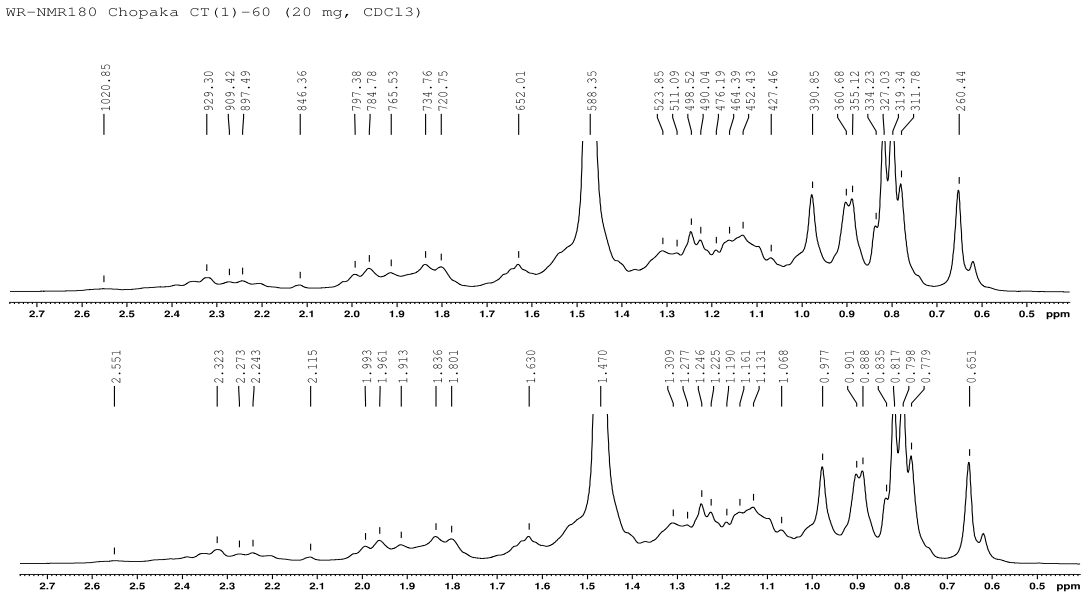

Appendix Figure 72 Expansion of ^{1}H NMR Spectrum (400 MHz, $CDCl_3$) of 3β-[(2-((*N*′,*N*″-Di(*tert*-butoxycarbonyl)guanidinyl)ethyl)carbamoly] β-sitosterol (**C4b**)

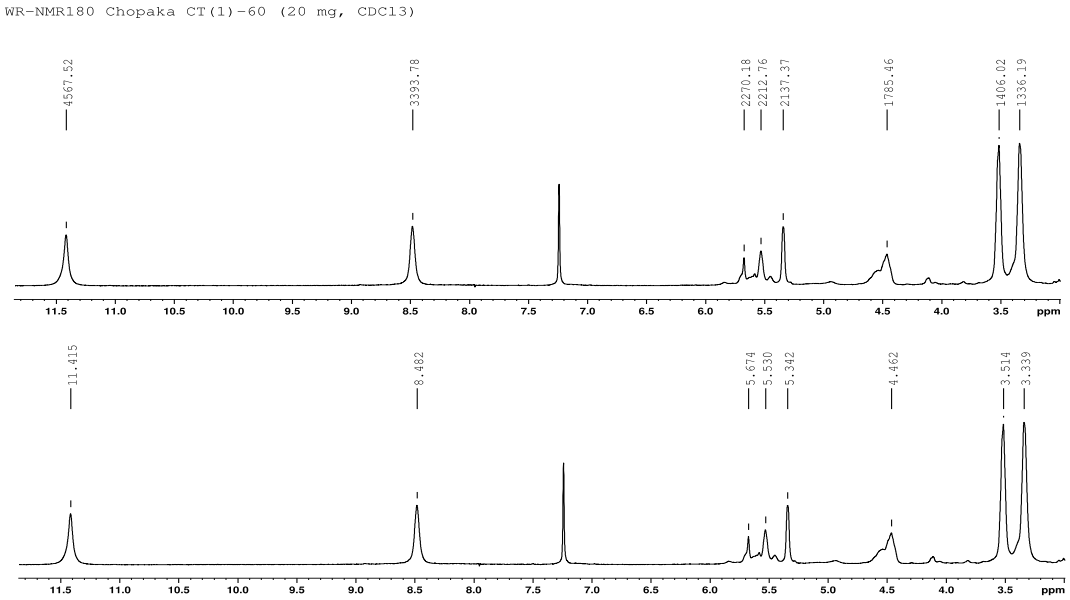

Appendix Figure 73 Expansion (cont.) of ^{1}H NMR Spectrum (400 MHz, $CDCl_3$) of 3β-[(2-((*N*′,*N*′′-Di(*tert*-butoxycarbonyl)guanidinyl)ethyl) carbamoly]β-sitosterol (**C4b**)

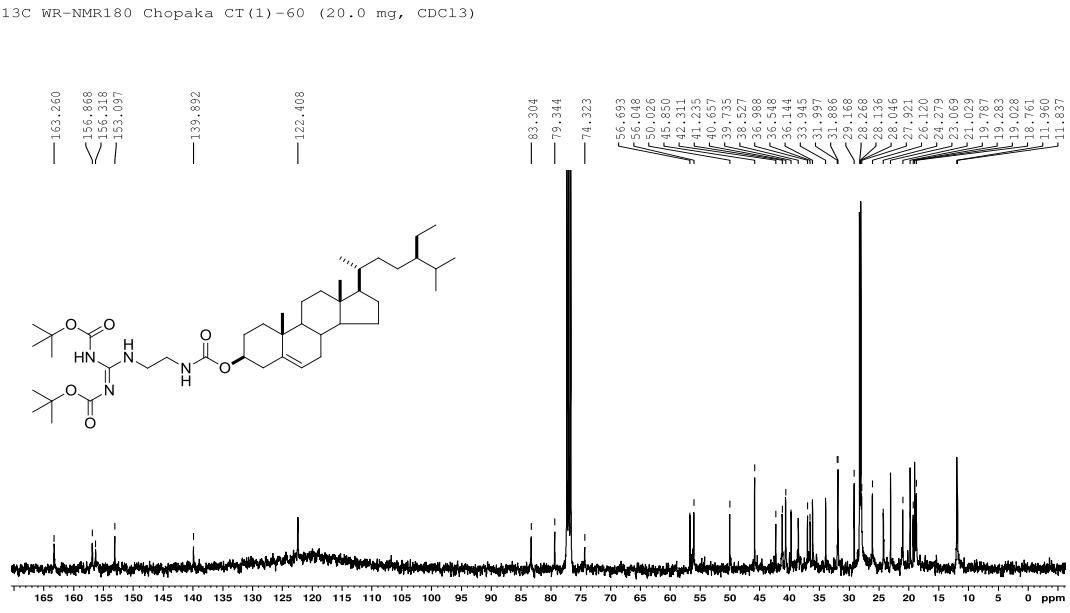

Appendix Figure 74 ^{13}C NMR Spectrum (100 MHz, $CDCl_3$) of 3β-[(2-((*N*′,*N*′′-Di(*tert*-butoxycarbonyl)guanidinyl)ethyl)carbamoly]β-sitosterol (**C4b**)

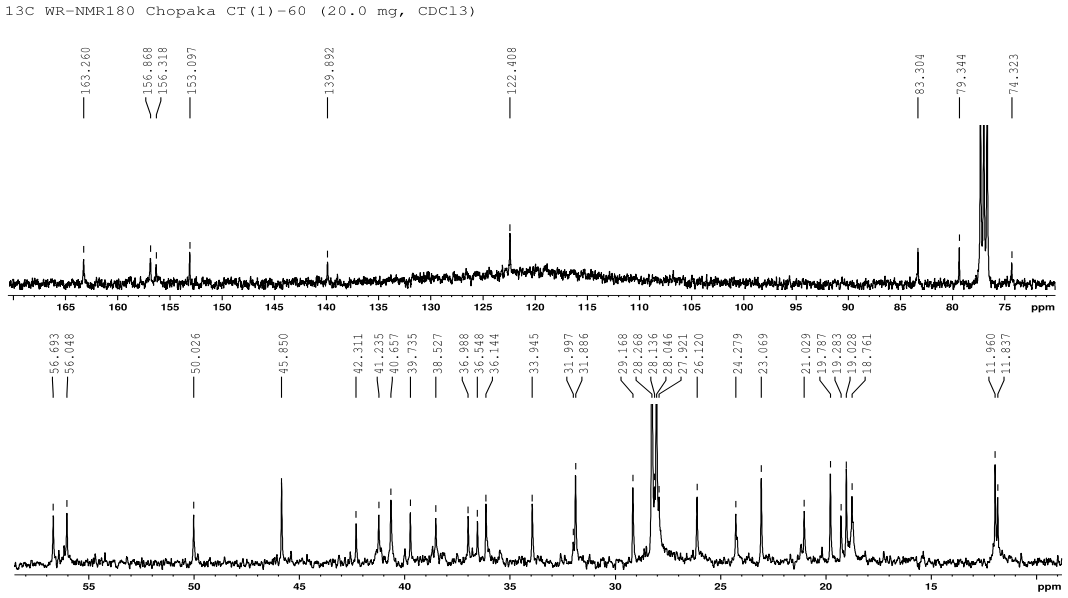

Appendix Figure 75 Expansion of ^{13}C NMR Spectrum (100 MHz, $CDCl_3$) of 3β-[(2-((*N′*,*N″*-Di(*tert*-butoxycarbonyl)guanidinyl)ethyl)carbamoly] β-sitosterol (**C4b**)

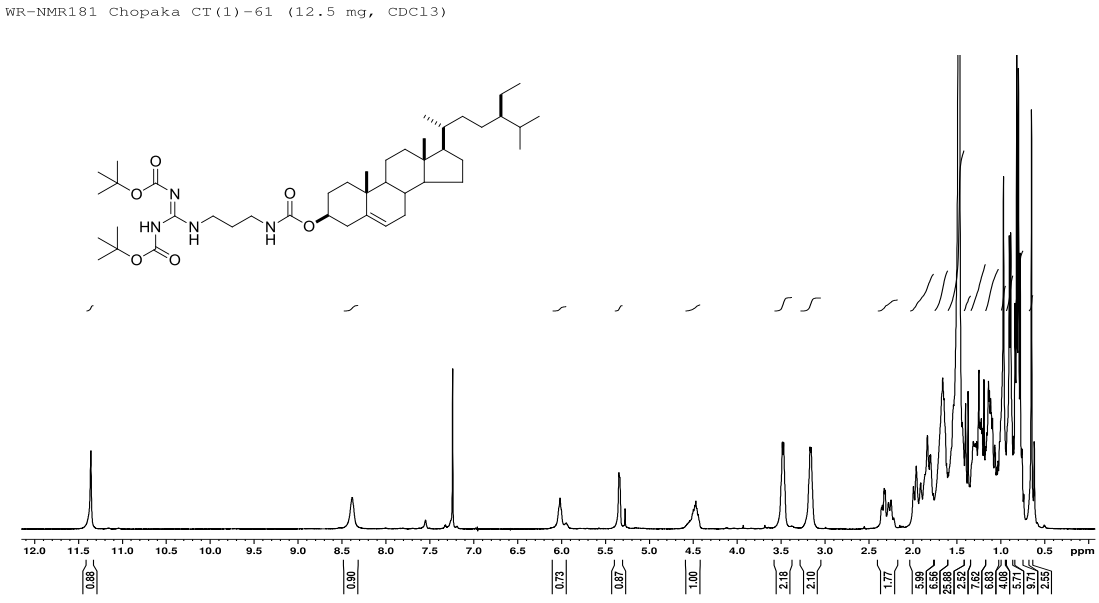

Appendix Figure 76 ^{1}H NMR Spectrum (400 MHz, $CDCl_3$) of 3β-[(3-((*N′*,*N″*-Di(*tert*-butoxycarbonyl))guanidinyl)propyl)carbamoyl] β-sitosterol (**C5b**)

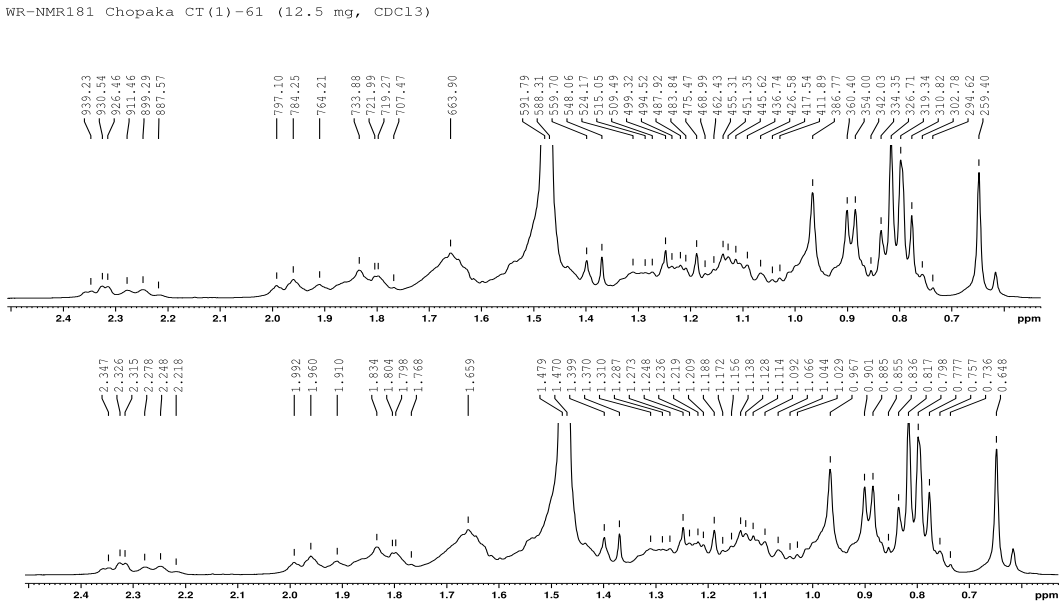

Appendix Figure 77 Expansion of ^{1}H NMR Spectrum (400 MHz, $CDCl_3$) of 3β-[(3-((*N′*,*N″*-Di(*tert*-butoxycarbonyl))guanidinyl)propyl)carbamoyl] β-sitosterol (**C5b**)

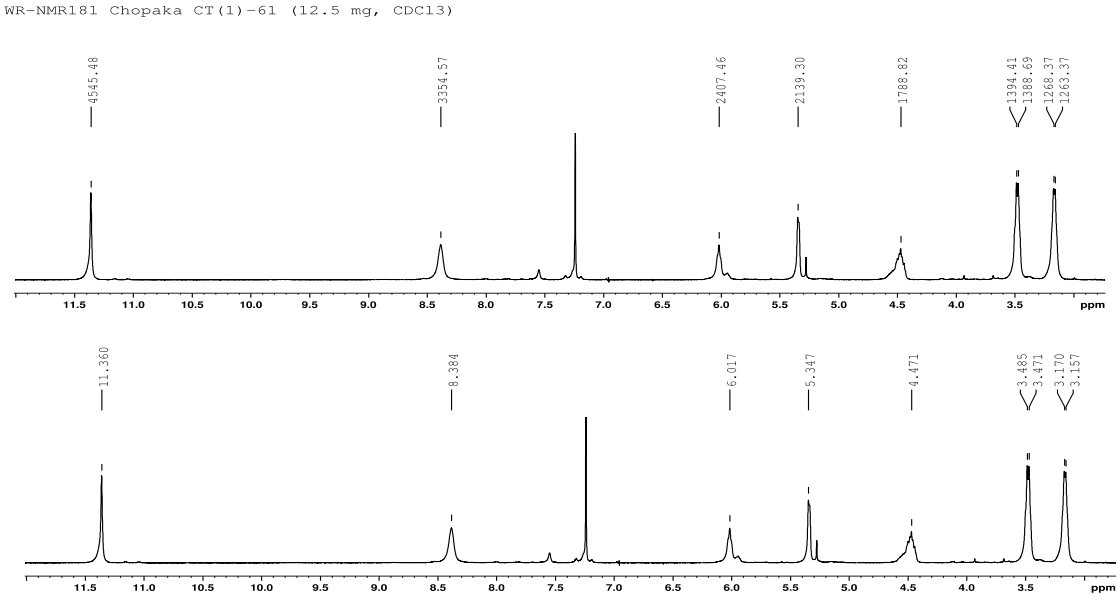

Appendix Figure 78 Expansion (cont.) of ^{1}H NMR Spectrum (400 MHz, $CDCl_3$) of 3β-[(3-((*N′*,*N″*-Di(*tert*-butoxycarbonyl))guanidinyl)propyl) carbamoyl]β-sitosterol (**C5b**)

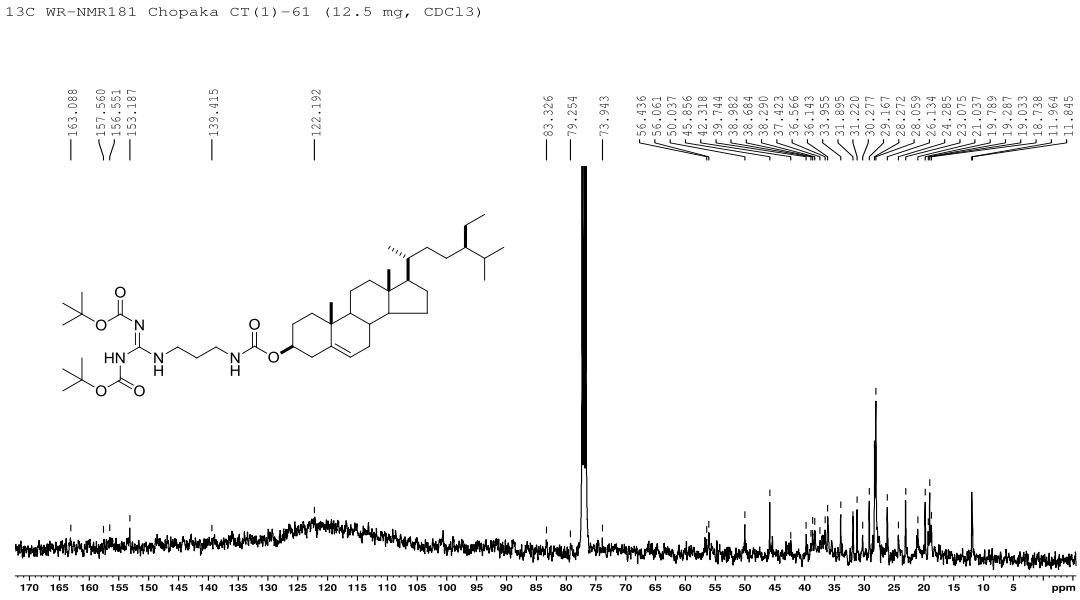

Appendix Figure 79 ^{13}C NMR Spectrum (100 MHz, $CDCl_3$) of 3β-[(3-((*N*′,*N*″-Di(*tert*-butoxycarbonyl))guanidinyl)propyl)carbamoyl] β-sitosterol (**C5b**)

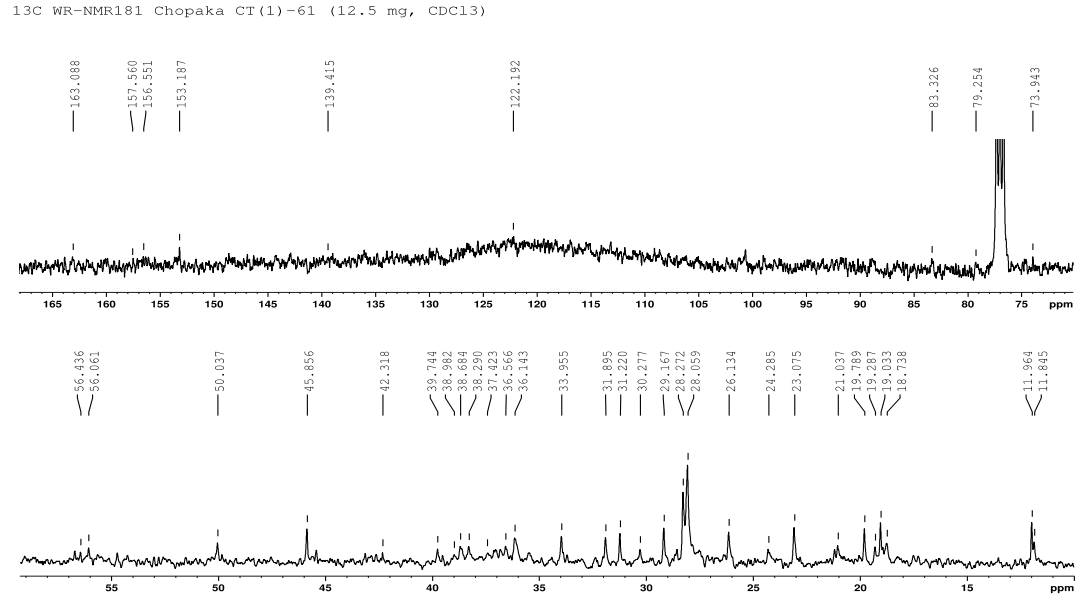

Appendix Figure 80 Expansion of ^{13}C NMR Spectrum (100 MHz, $CDCl_3$) of 3β-[(3-((*N*′,*N*″-Di(*tert*-butoxycarbonyl))guanidinyl)propyl)carbamoyl] β-sitosterol (**C5b**)

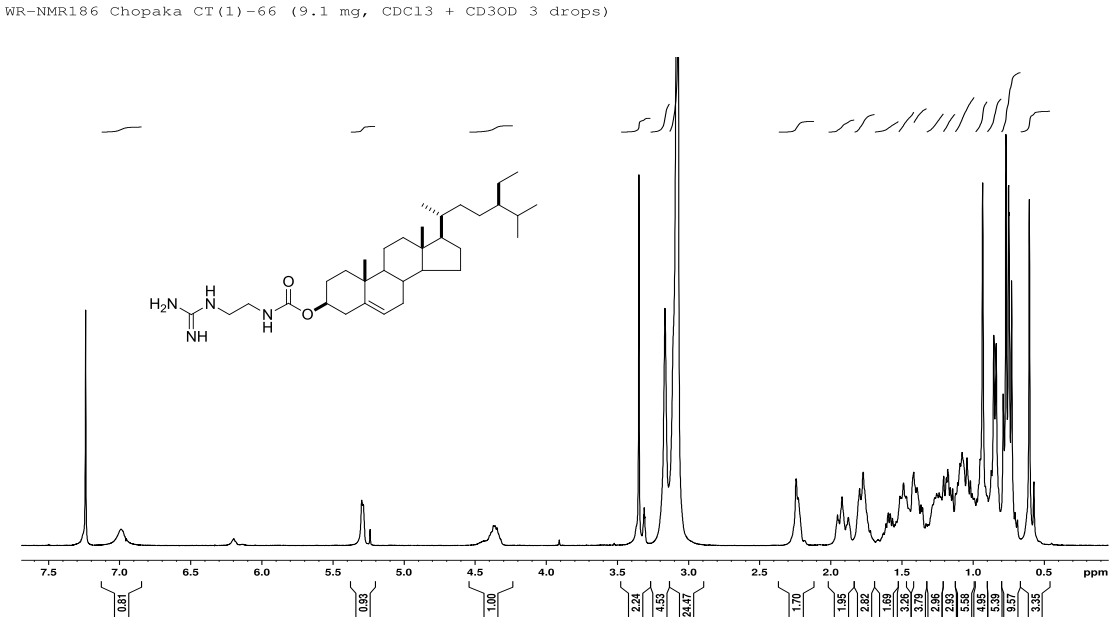

Appendix Figure 81 ^{1}H NMR Spectrum (400 MHz, $CDCl_3$ + CD_3OD) of Lipid 3β-[(2-(Guanidinyl)ethyl)carbamoyl]β-sitosterol (**L3b**)

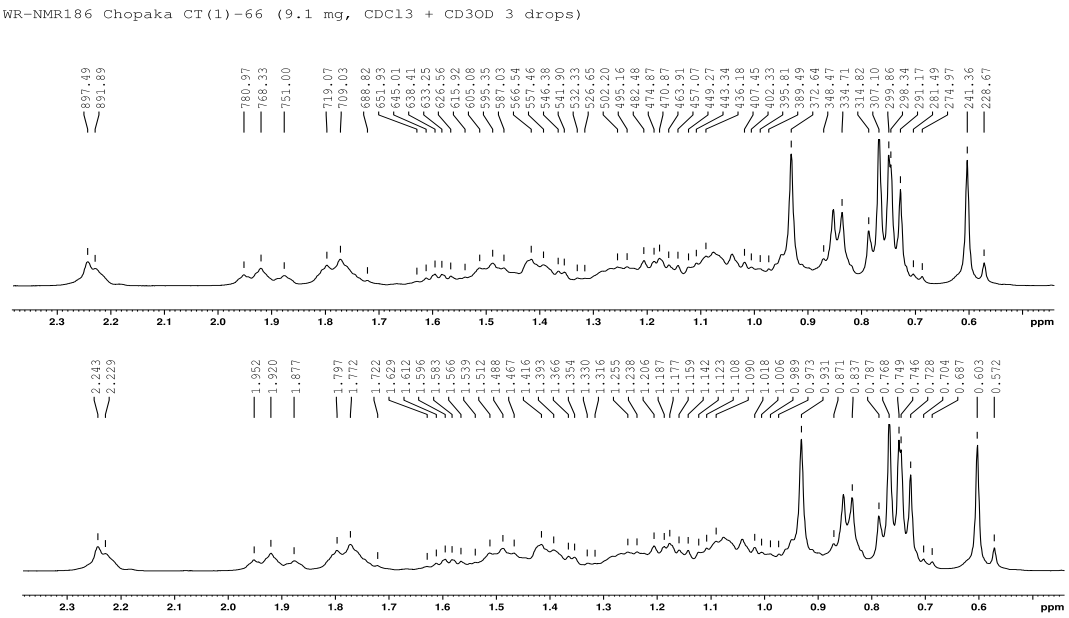

Appendix Figure 82 Expansion of ^{1}H NMR Spectrum (400 MHz, $CDCl_3$ + CD_3OD) of Lipid 3β-[(2-(Guanidinyl)ethyl)carbamoyl]β-sitosterol (**L3b**)

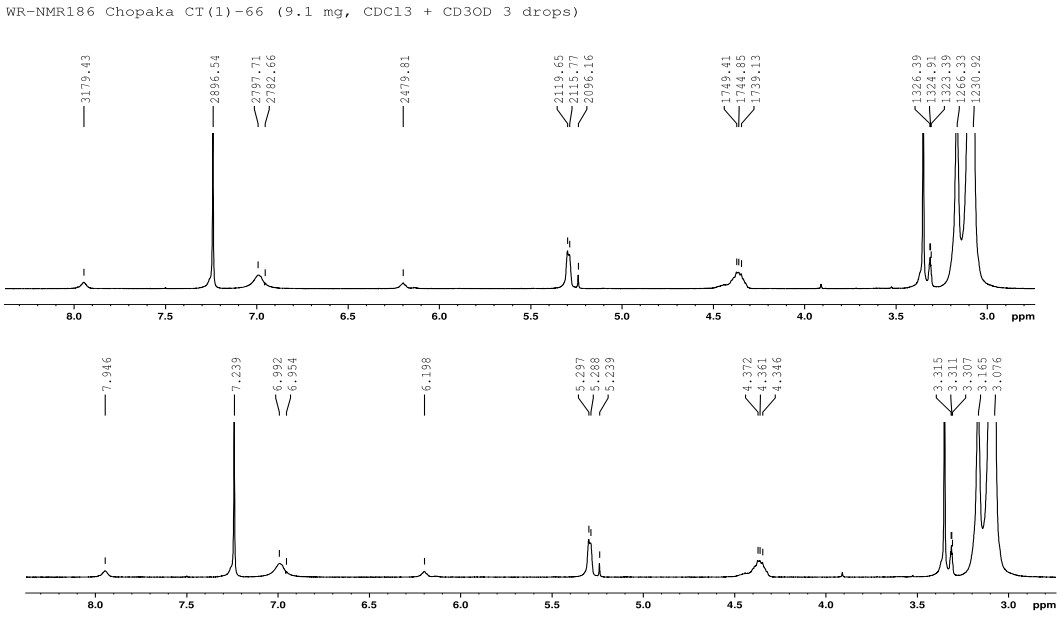

Appendix Figure 83 Expansion (cont.) of ^{1}H NMR Spectrum (400 MHz, $CDCl_3$ + CD_3OD) of Lipid 3β-[(2-(Guanidinyl)ethyl)carbamoyl]β-sitosterol (**L3b**)

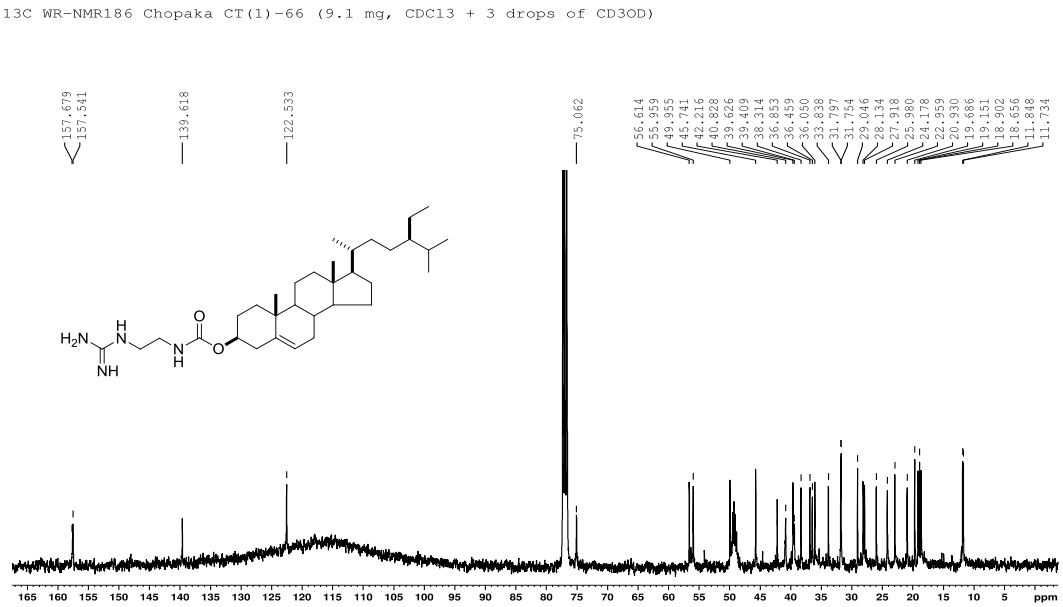

Appendix Figure 84 ^{13}C NMR Spectrum (100 MHz, $CDCl_3$ + CD_3OD) of Lipid 3β-[(2-(Guanidinyl)ethyl)carbamoyl]β-sitosterol (**L3b**)

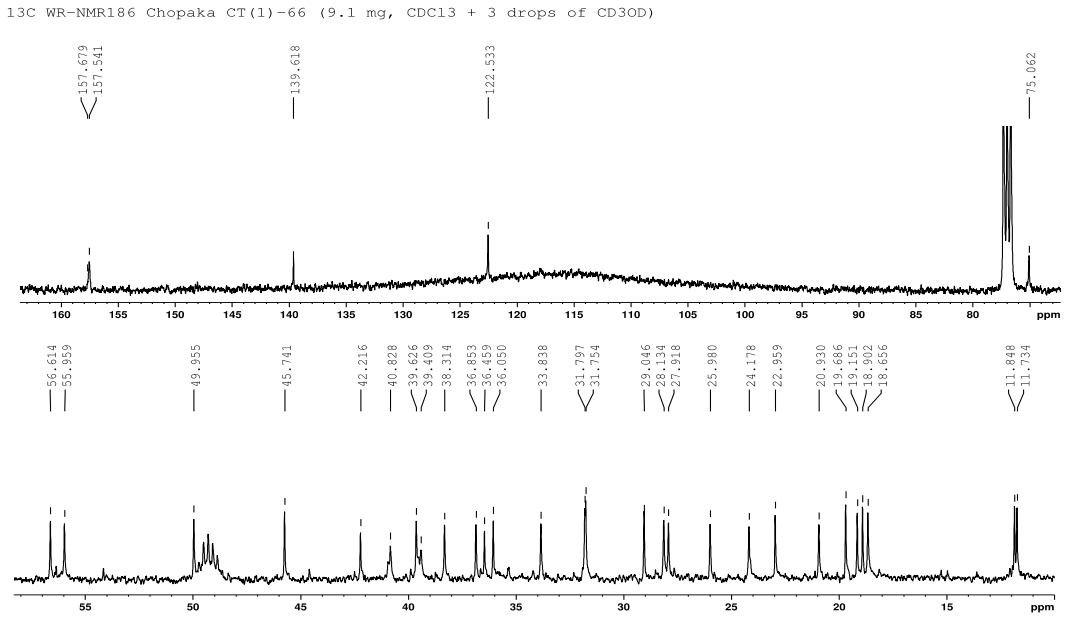

Appendix Figure 85 Expansion of ^{13}C NMR Spectrum (100 MHz, $CDCl_3$ + CD_3OD) of Lipid 3β-[(2-(Guanidinyl)ethyl)carbamoyl]β-sitosterol (**L3b**)

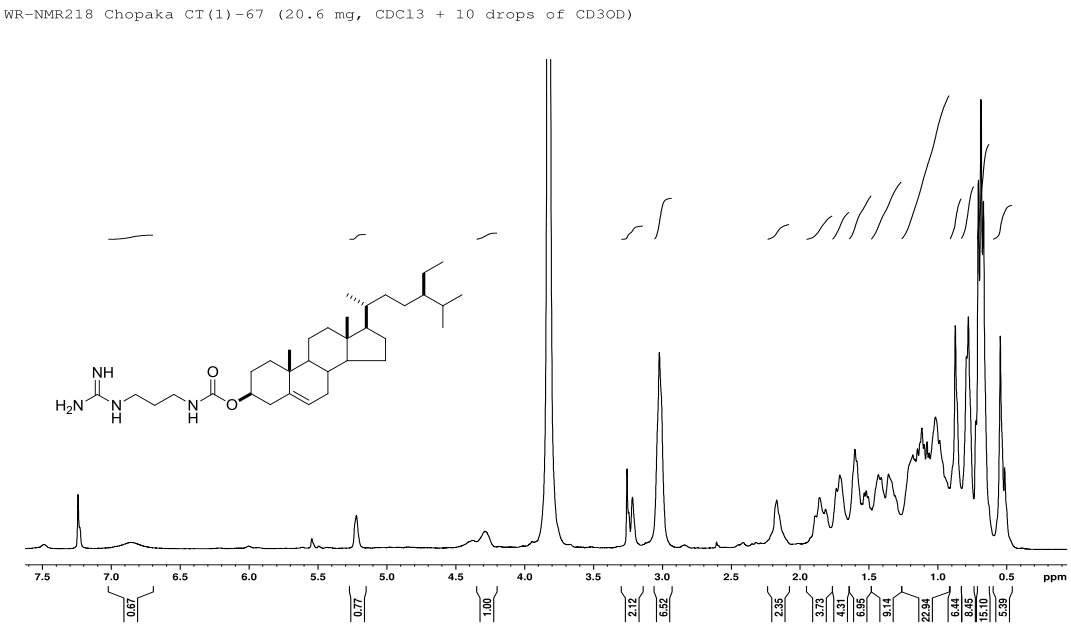

Appendix Figure 86 ^{1}H NMR Spectrum (400 MHz, $CDCl_3$ + CD_3OD) of Lipid 3β-[(3-(Guanidinyl)propyl)carbamoyl]β-sitosterol (**L7b**)

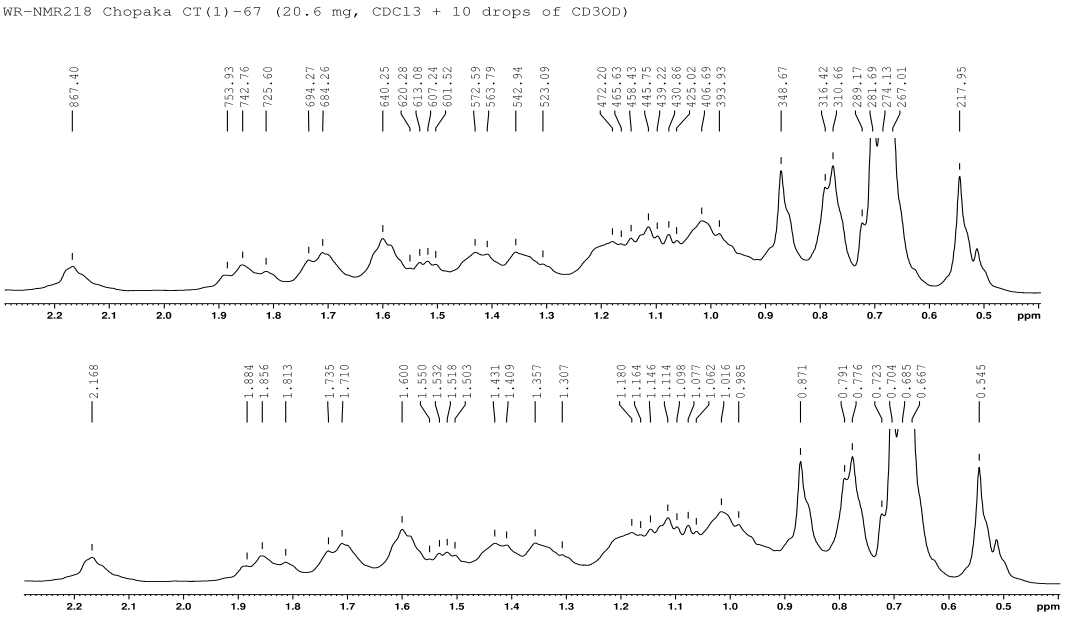

Appendix Figure 87 Expansion of ^{1}H NMR Spectrum (400 MHz, $CDCl_3$ + CD_3OD) of Lipid 3β-[(3-(Guanidinyl)propyl)carbamoyl]β-sitosterol (**L7b**)

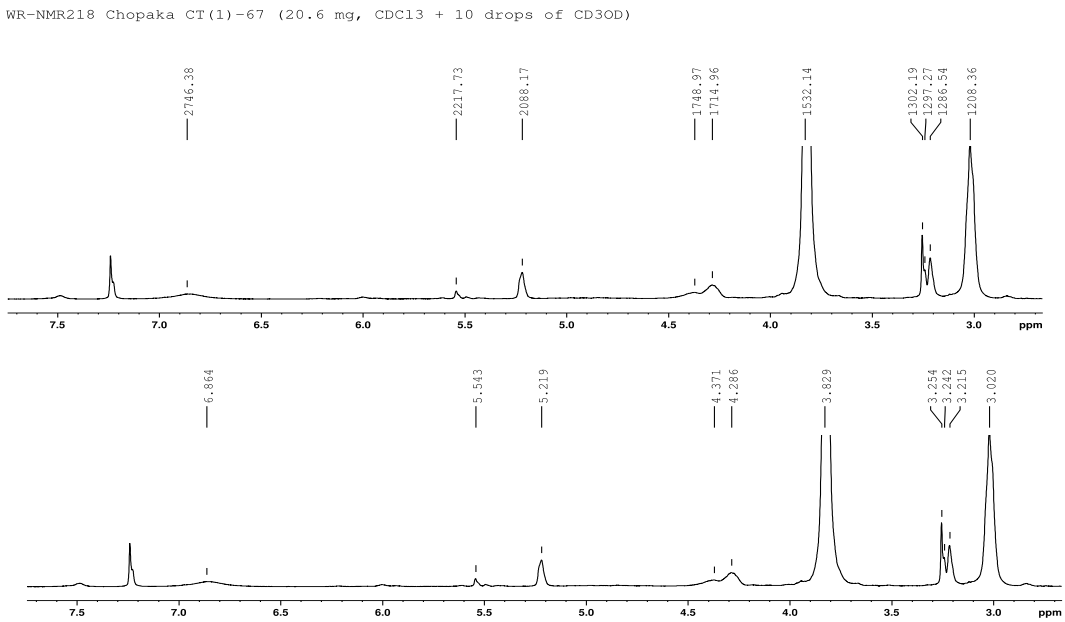

Appendix Figure 88 Expansion (cont.) of ^{1}H NMR Spectrum (400 MHz, $CDCl_3$ + CD_3OD) of Lipid 3β-[(3-(Guanidinyl)propyl)carbamoyl] β-sitosterol (**L7b**)

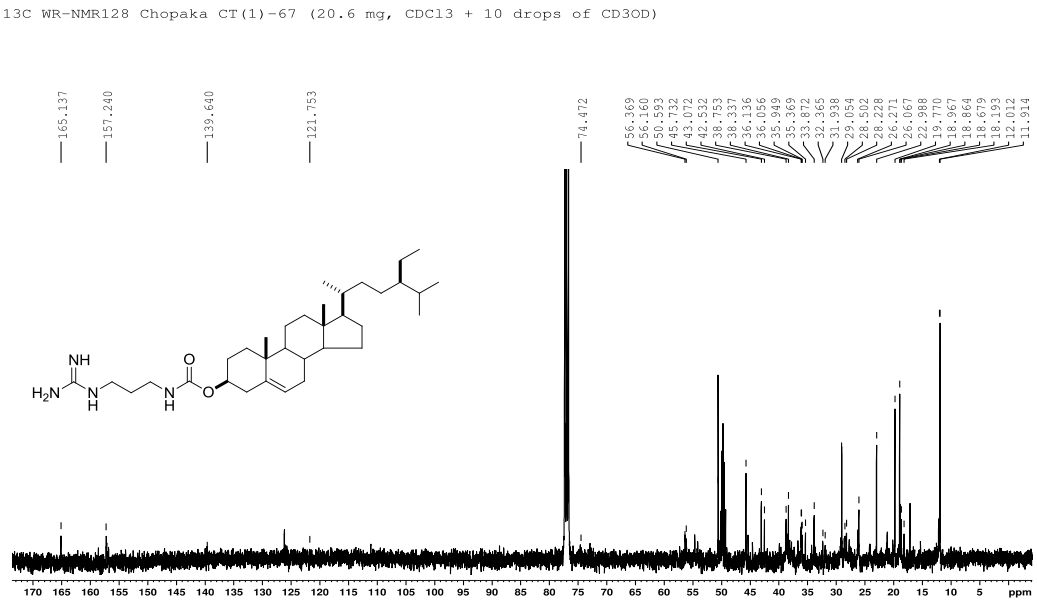

Appendix Figure 89 ^{13}C NMR Spectrum (100 MHz, $CDCl_3$ + CD_3OD) of Lipid 3β-[(3-(Guanidinyl)propyl)carbamoyl]β-sitosterol (**L7b**)

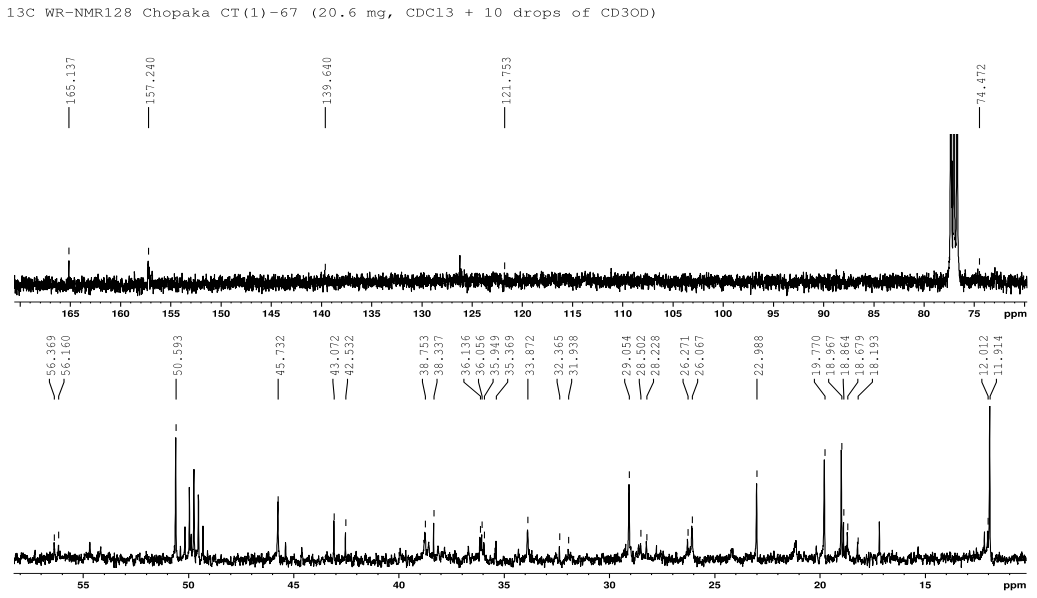

Appendix Figure 90 Expansion of ^{13}C NMR Spectrum (100 MHz, $CDCl_3$ + CD_3OD) of Lipid 3β-[(3-(Guanidinyl)propyl)carbamoyl]β-sitosterol (**L7b**)

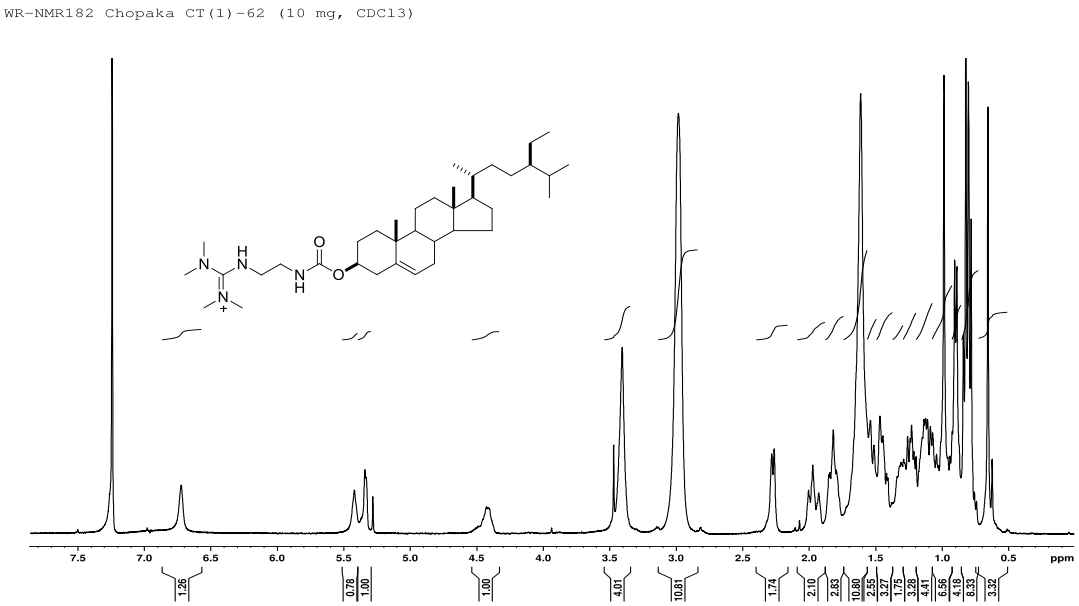

Appendix Figure 91 ^{1}H NMR Spectrum (400 MHz, $CDCl_3$) of Lipid 3β-[(2-((*N*′,*N*′,*N*″,*N*″-Tetramethyl)guanidinyl)ethyl)carbamoyl] β-sitosterol (**L4b**)

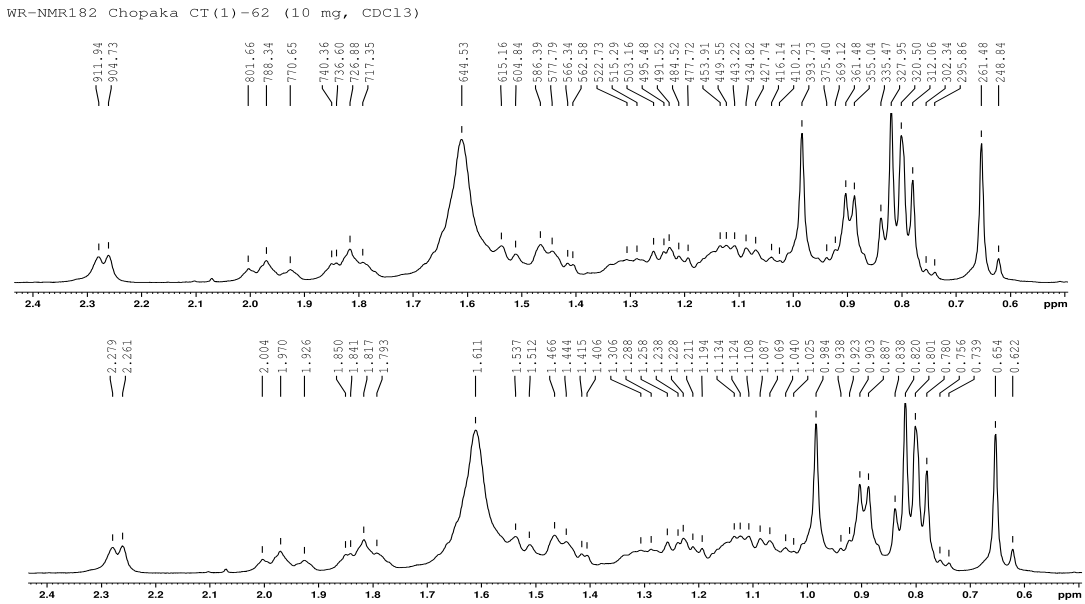

Appendix Figure 92 Expansion of ^{1}H NMR Spectrum (400 MHz, $CDCl_3$) of Lipid 3β-[(2-((*N*′,*N*′,*N*″,*N*″-Tetramethyl)guanidinyl)ethyl) carbamoyl]β-sitosterol (**L4b**)

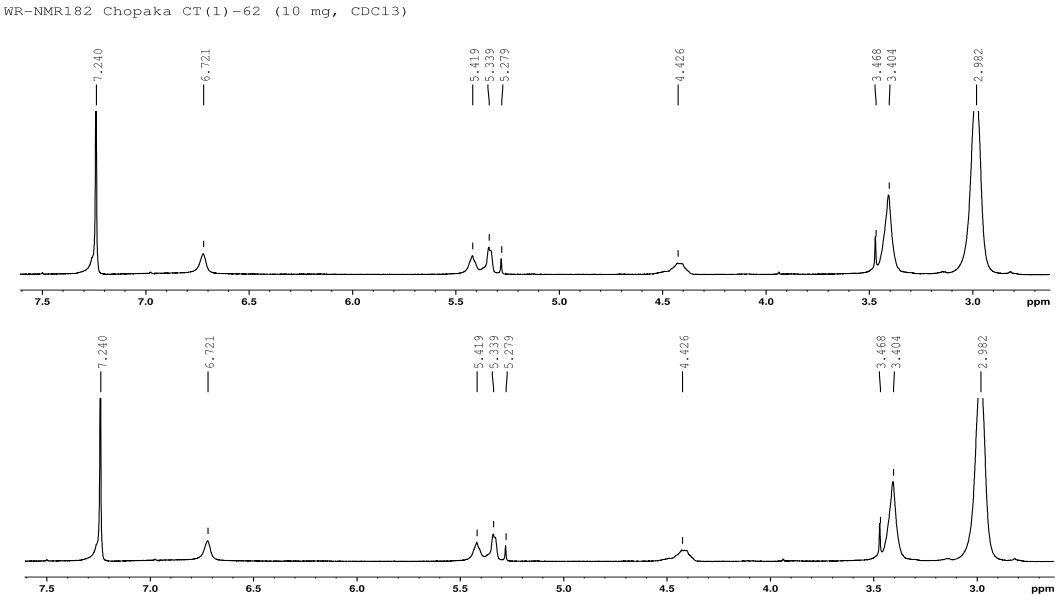

Appendix Figure 93 Expansion (cont.) of ^{1}H NMR Spectrum (400 MHz, $CDCl_3$) of Lipid 3β-[(2-((*N*′,*N*′,*N*″,*N*″-Tetramethyl)guanidinyl)ethyl) carbamoyl]β-sitosterol (**L4b**)

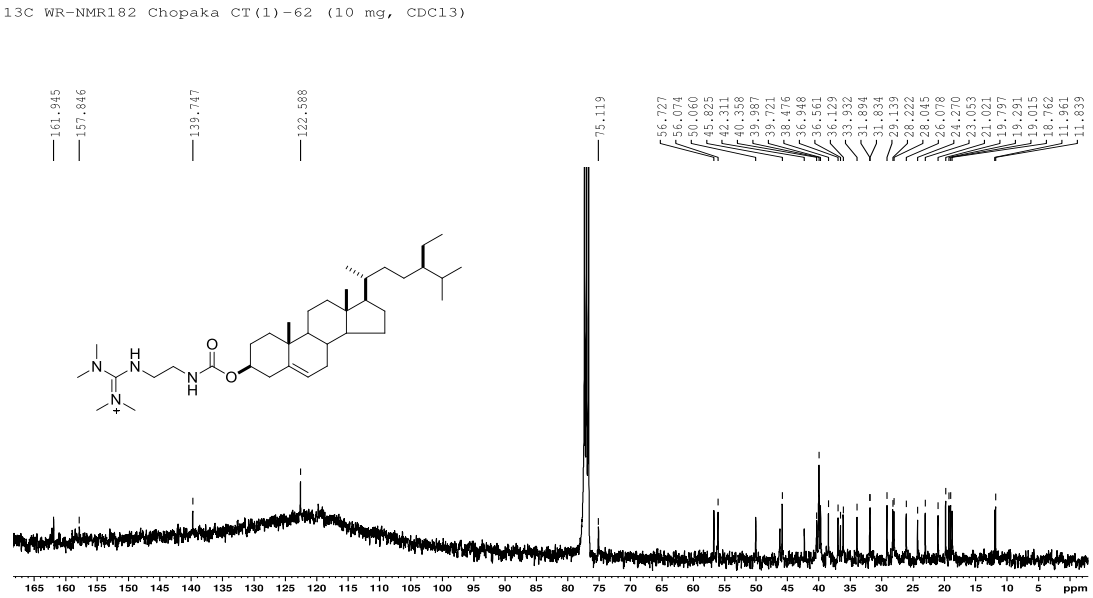

Appendix Figure 94 ^{13}C NMR Spectrum (100 MHz, $CDCl_3$) of Lipid 3β-[(2-((*N*′,*N*′,*N*″,*N*″-Tetramethyl)guanidinyl)ethyl)carbamoyl] β-sitosterol (**L4b**)

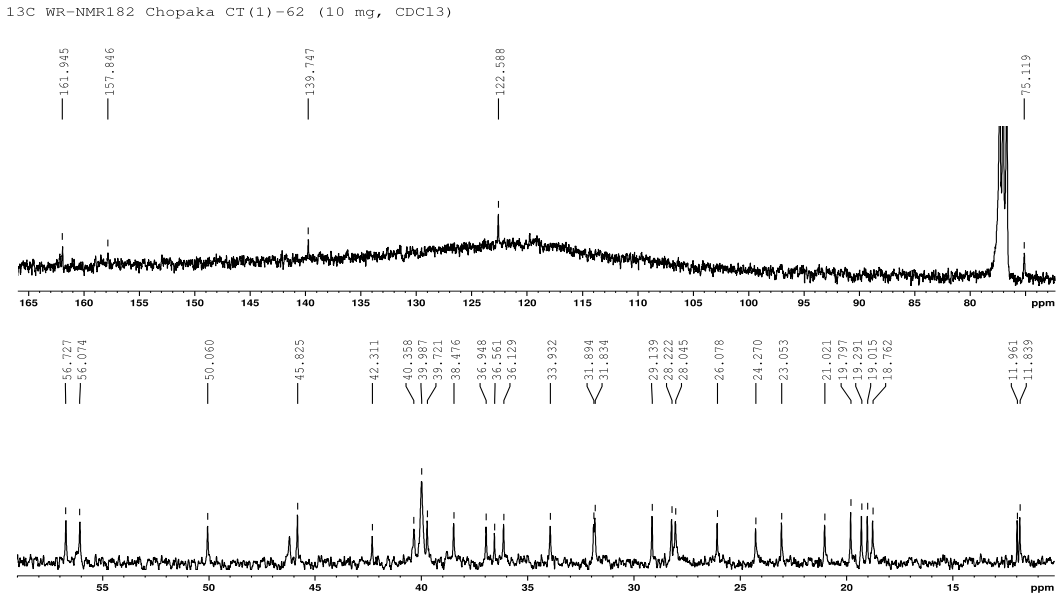

Appendix Figure 95 Expansion of ^{13}C NMR Spectrum (100 MHz, $CDCl_3$) of Lipid 3β-[(2-((*N*′,*N*′,*N*″,*N*″-Tetramethyl)guanidinyl)ethyl) carbamoyl]β-sitosterol (**L4b**)

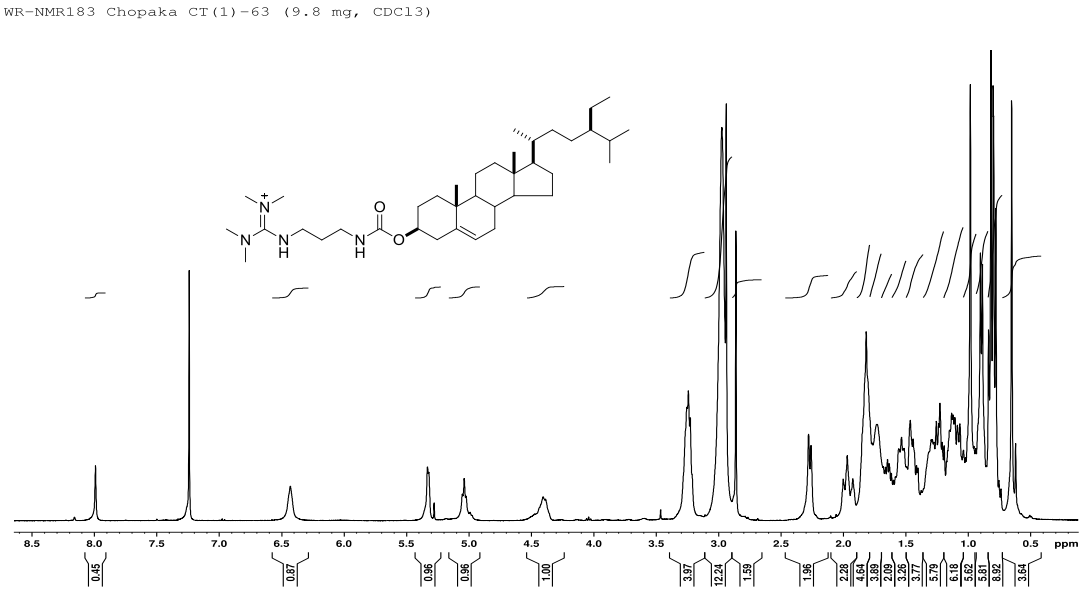

Appendix Figure 96 ^{1}H NMR Spectrum (400 MHz, $CDCl_3$) of Lipid 3β-[(3-((*N*′,*N*′,*N*″,*N*″-Tetramethyl)guanidinyl)propyl)carbamoyl] β-sitosterol (**L8b**)

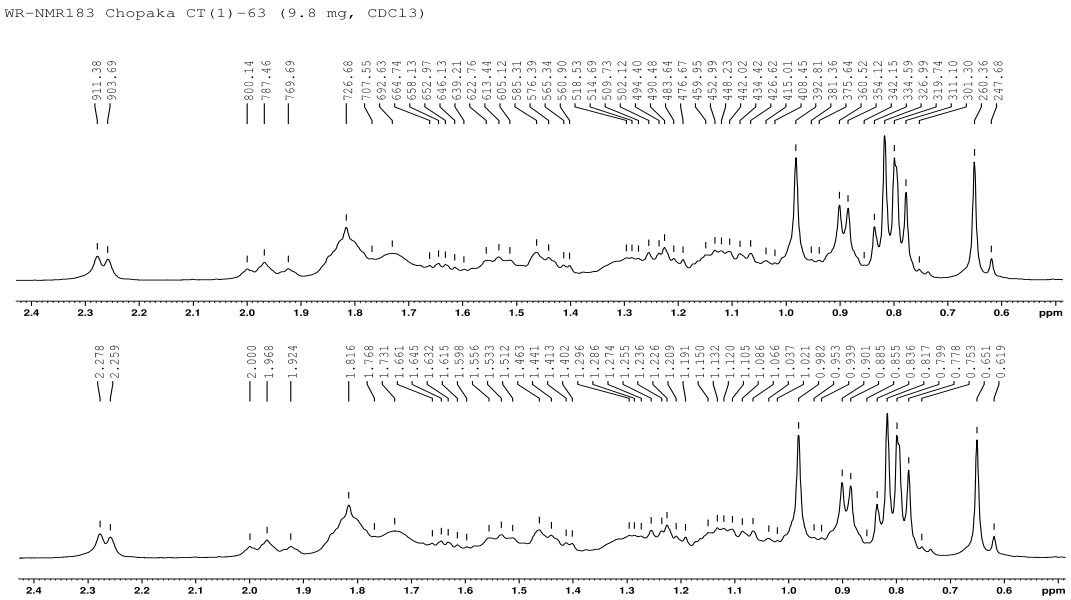

Appendix Figure 97 Expansion of ^{1}H NMR Spectrum (400 MHz, $CDCl_3$) of Lipid 3β-[(3-((*N*′,*N*′,*N*″,*N*″-Tetramethyl)guanidinyl)propyl) carbamoyl]β-sitosterol (**L8b**)

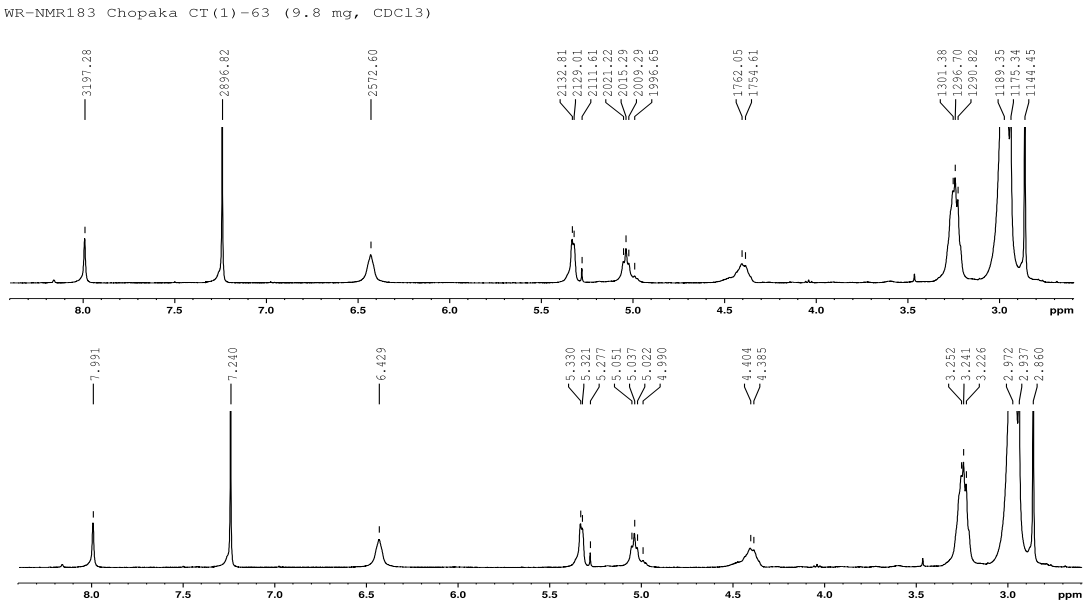

Appendix Figure 98 Expansion (cont.) of ^{1}H NMR Spectrum (400 MHz, $CDCl_3$) of Lipid 3β-[(3-((*N*′,*N*′,*N*″,*N*″-Tetramethyl)guanidinyl)propyl) carbamoyl]β-sitosterol (**L8b**)

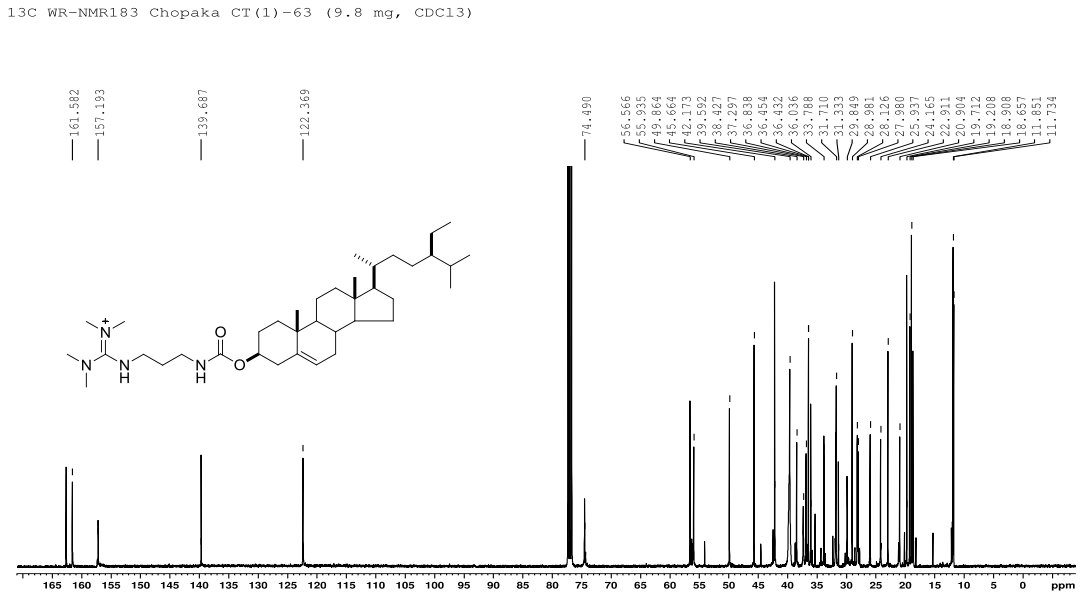

Appendix Figure 99 ^{13}C NMR Spectrum (100 MHz, $CDCl_3$) of Lipid 3β-[(3-((*N*′,*N*′,*N*″,*N*″-Tetramethyl)guanidinyl)propyl)carbamoyl] β-sitosterol (**L8b**)

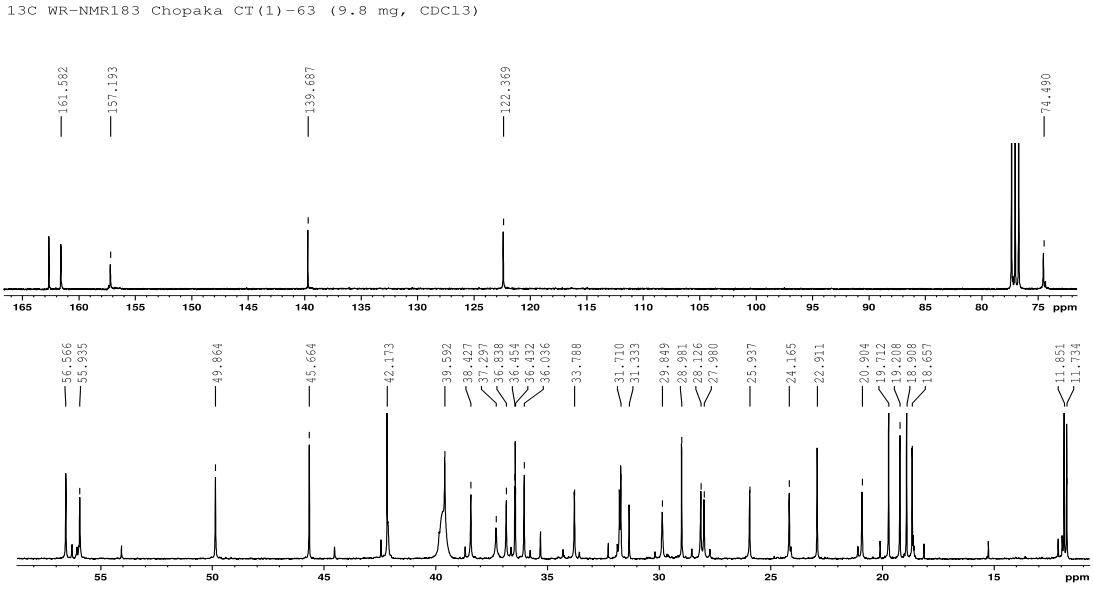

Appendix Figure 100 Expansion of ^{13}C NMR Spectrum (100 MHz, $CDCl_3$) of Lipid 3β-[(3-((*N*′,*N*′,*N*″,*N*″-Tetramethyl)guanidinyl)propyl) carbamoyl]β-sitosterol (**L8b**)

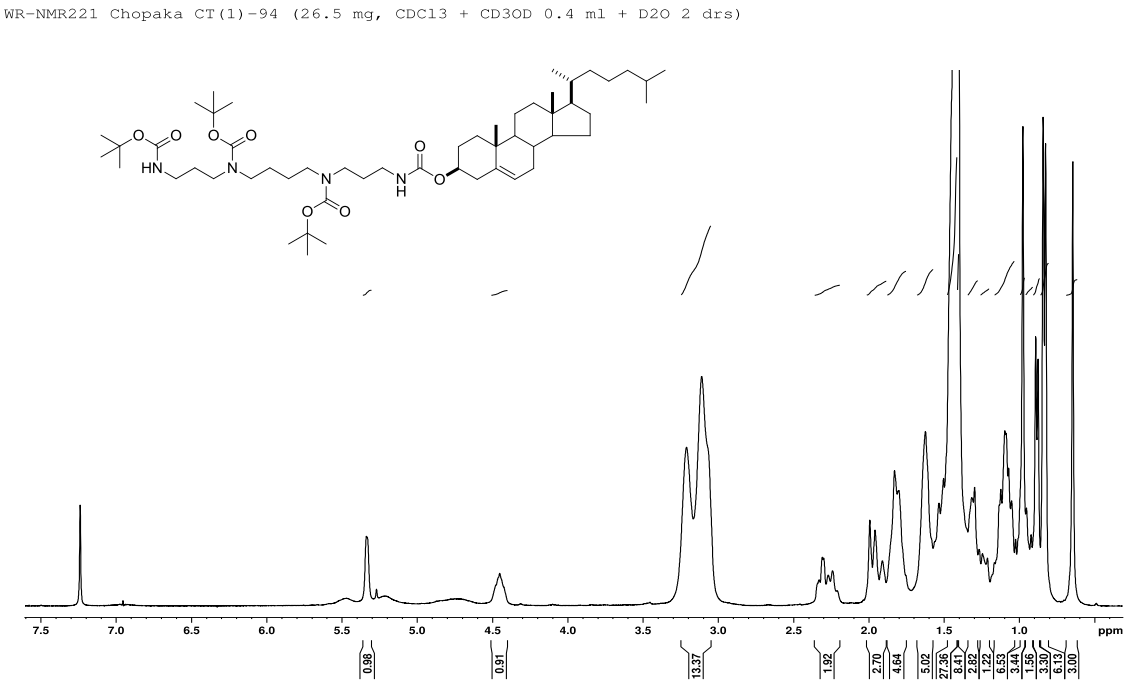

Appendix Figure 101 ^{1}H NMR Spectrum (400 MHz, $CDCl_3$) of **C6**.

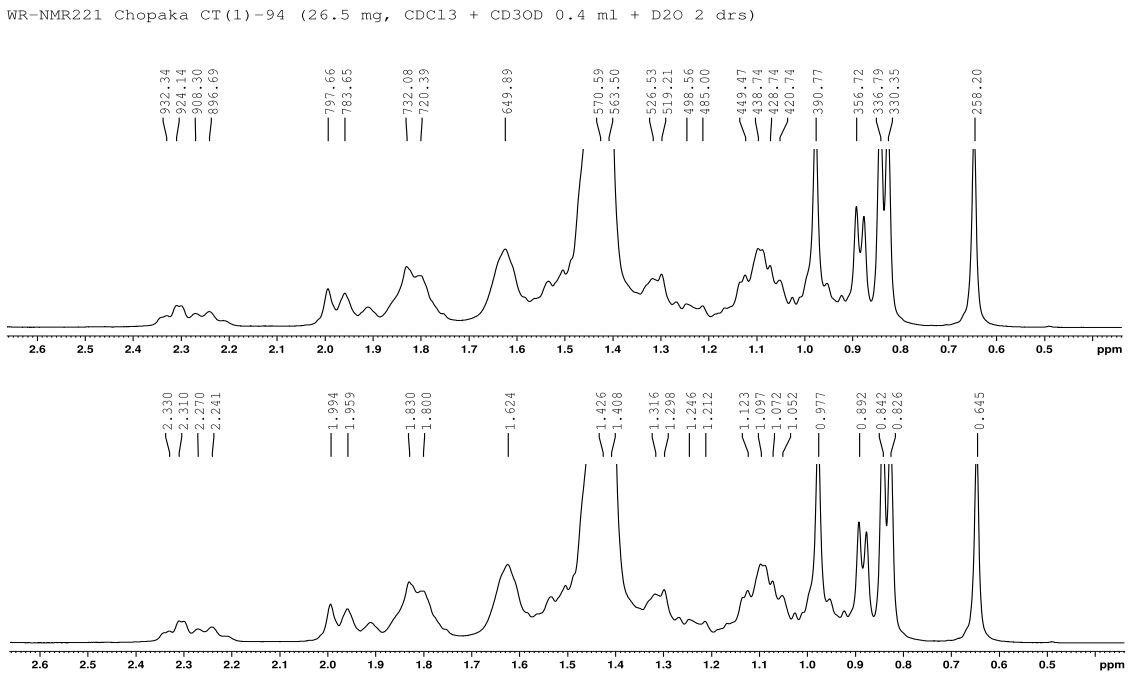

Appendix Figure 102 Expansion of ^{1}H NMR Spectrum (400 MHz, $CDCl_3$) of **C6**.

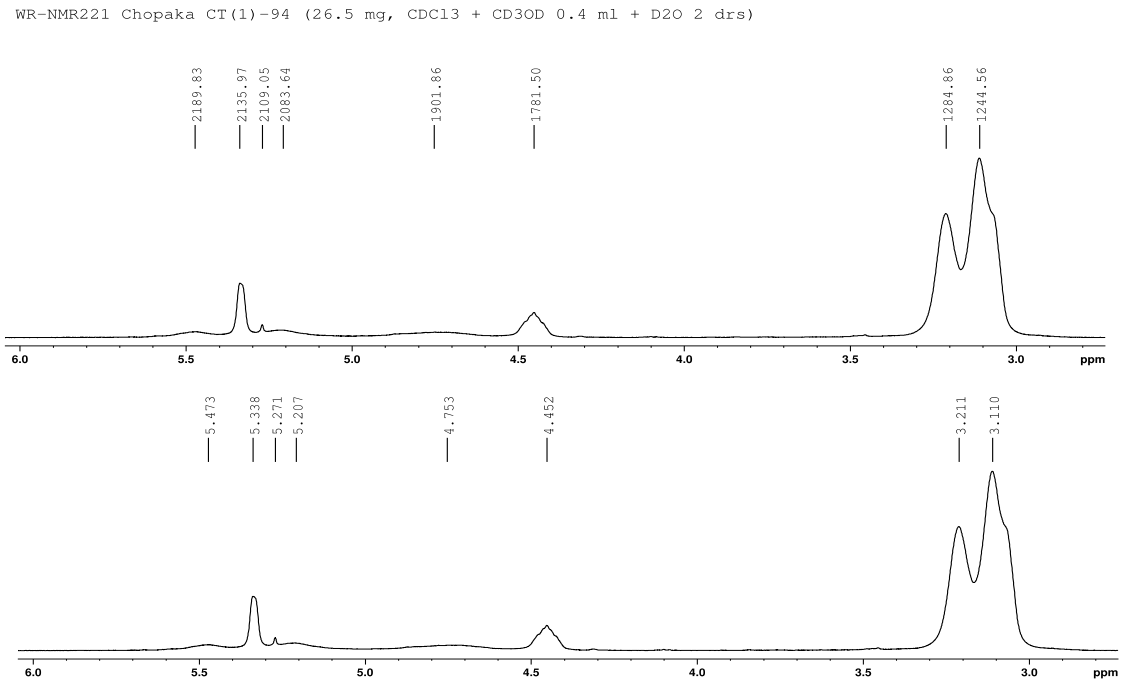

Appendix Figure 103 Expansion (cont.) of ^{1}H NMR Spectrum (400 MHz, $CDCl_3$) of **C6**.

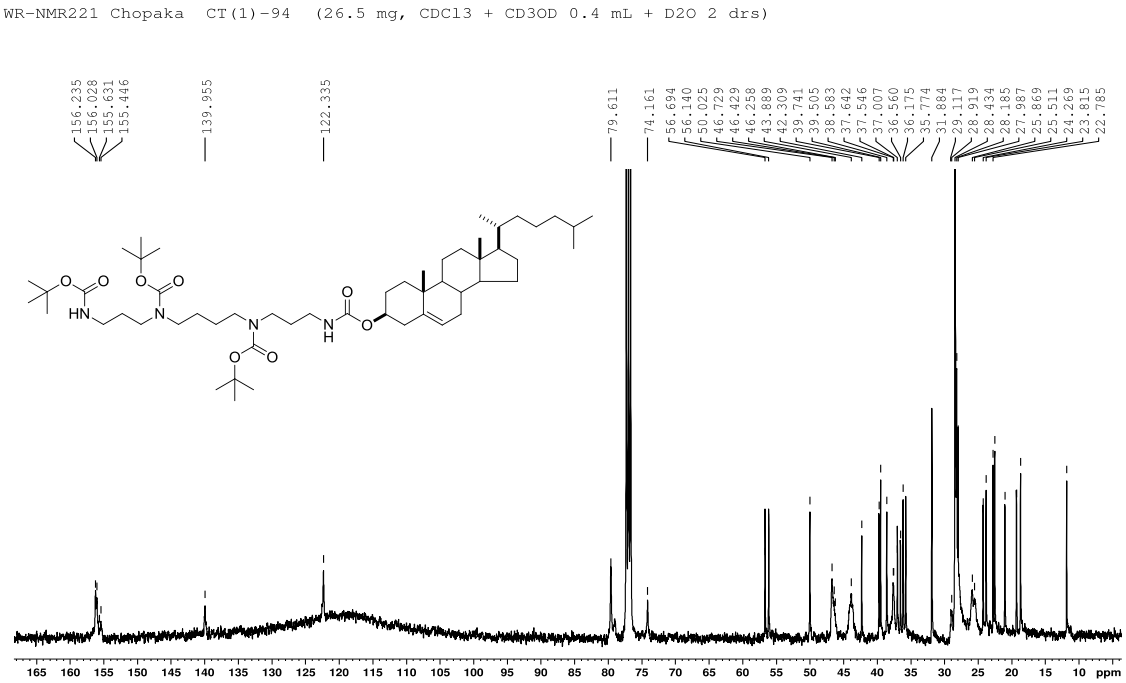

Appendix Figure 104 ^{13}C NMR Spectrum (100 MHz, $CDCl_3$) of **C6**.

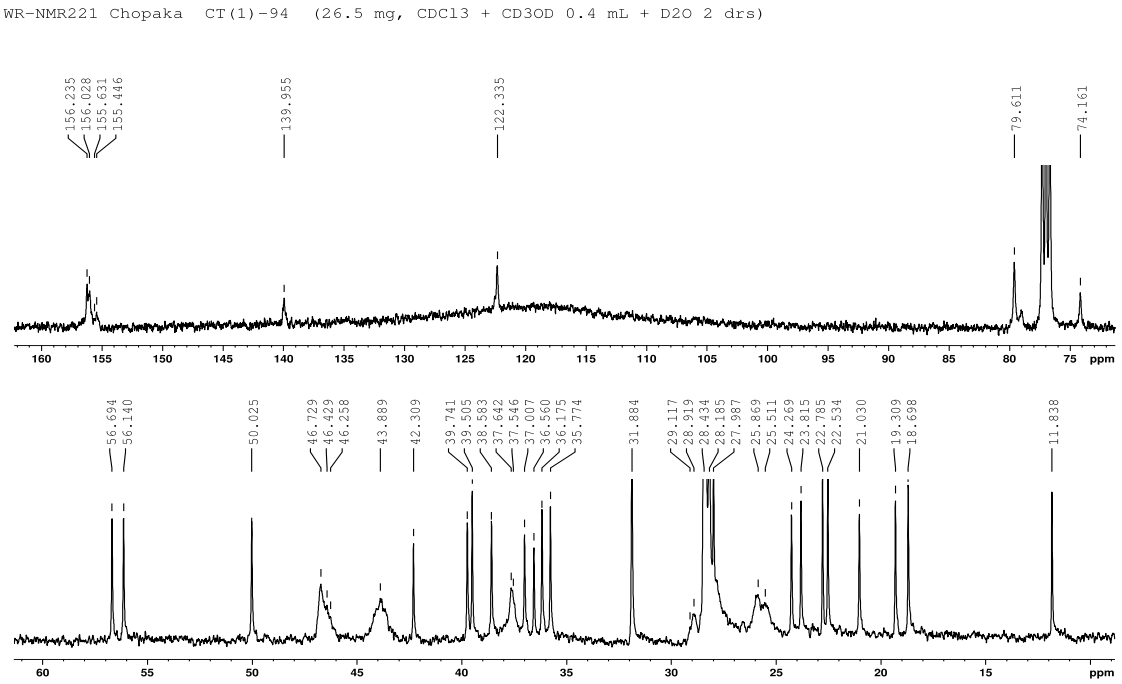

Appendix Figure 105 Expansion of ^{13}C NMR Spectrum (100 MHz, $CDCl_3$) of **C6**.

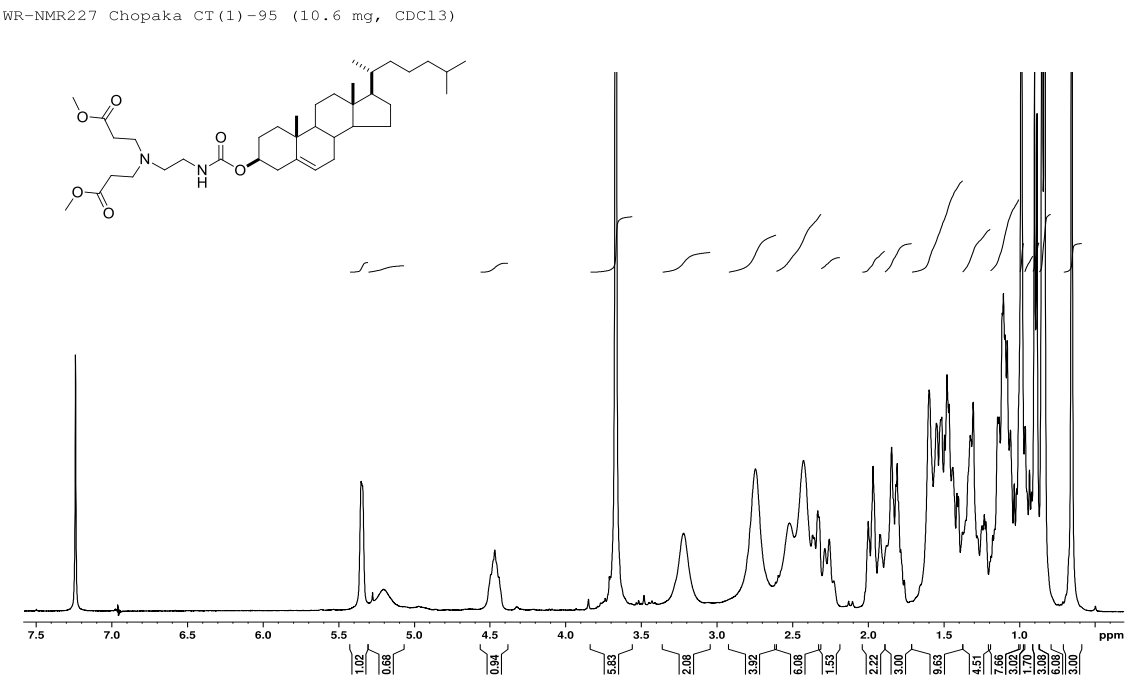

Appendix Figure 106 ^{1}H NMR Spectrum (400 MHz, $CDCl_3$) of **C7**.

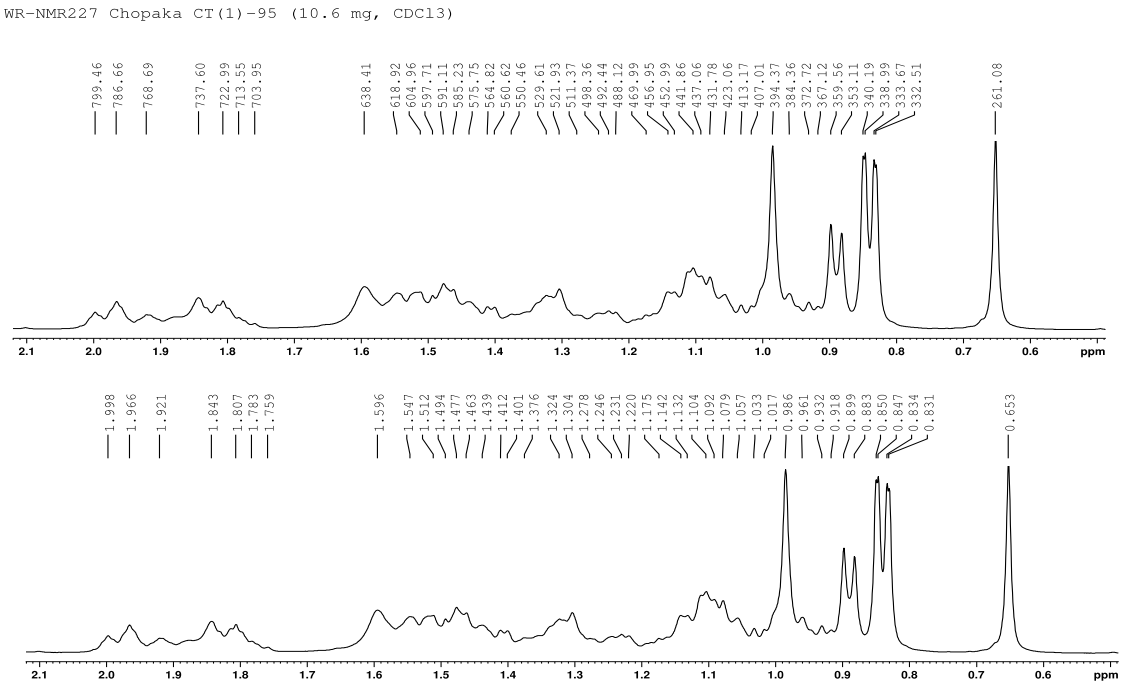

Appendix Figure 107 Expansion of ^{1}H NMR Spectrum (400 MHz, $CDCl_3$) of **C7**.

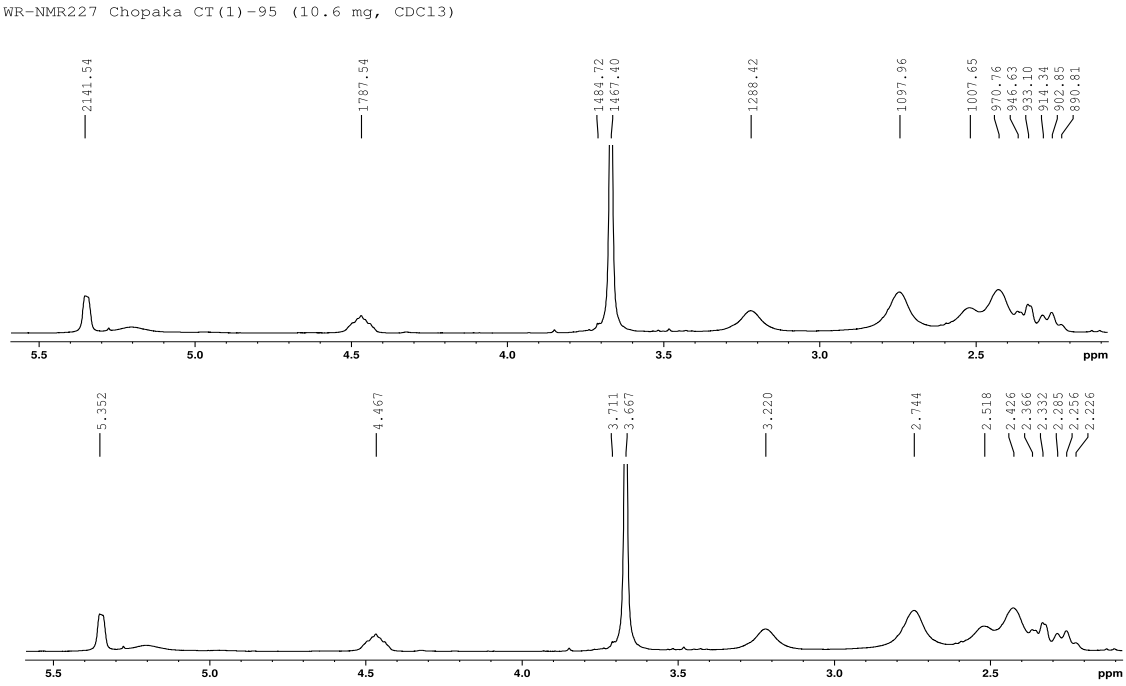

Appendix Figure 108 Expansion (cont.) of ^{1}H NMR Spectrum (400 MHz, $CDCl_3$) of **C7**.

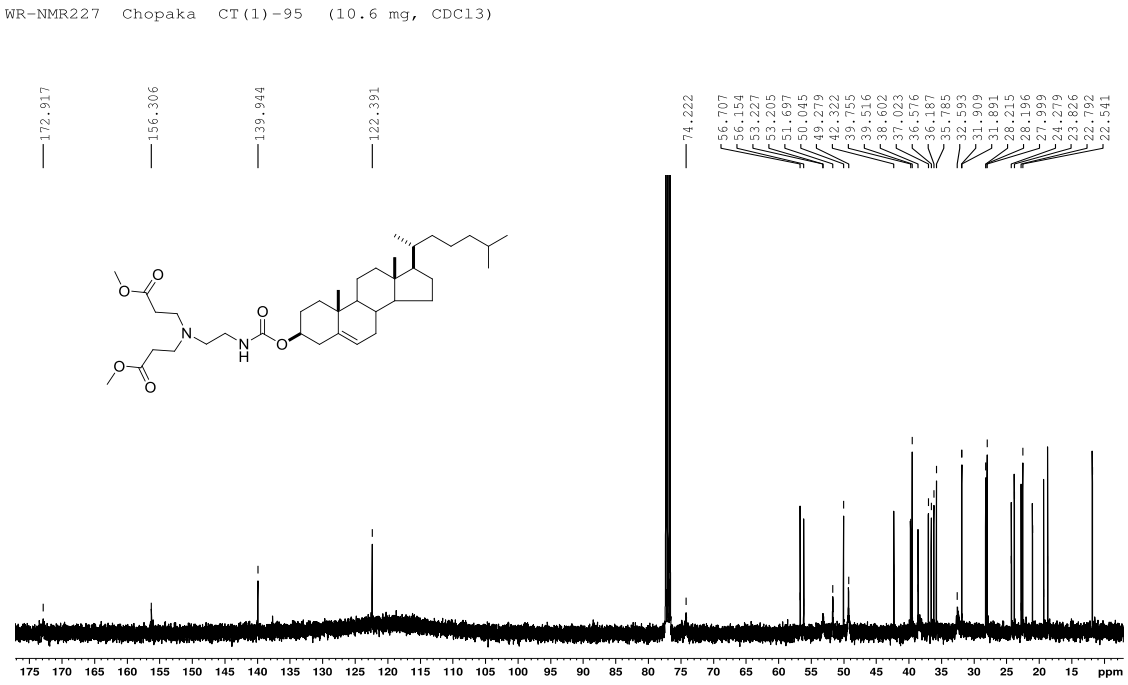

Appendix Figure 109 ^{13}C NMR Spectrum (100 MHz, $CDCl_3$) of **C7**.

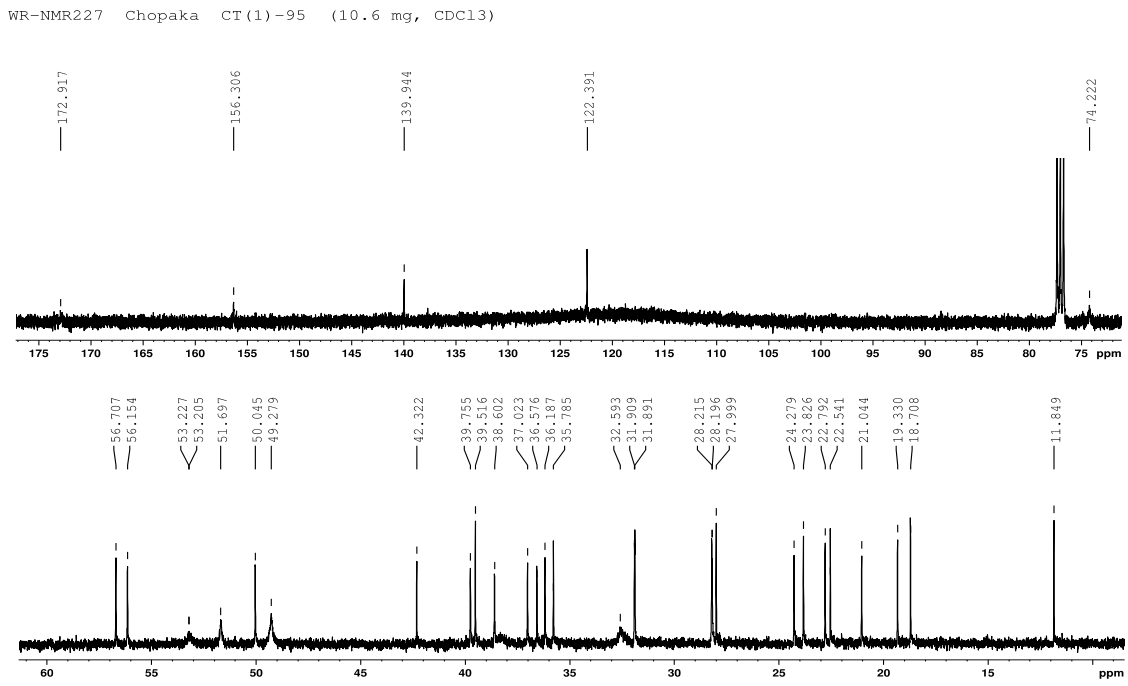

Appendix Figure 110 Expansion of ^{13}C NMR Spectrum (100 MHz, $CDCl_3$) of **C7**.

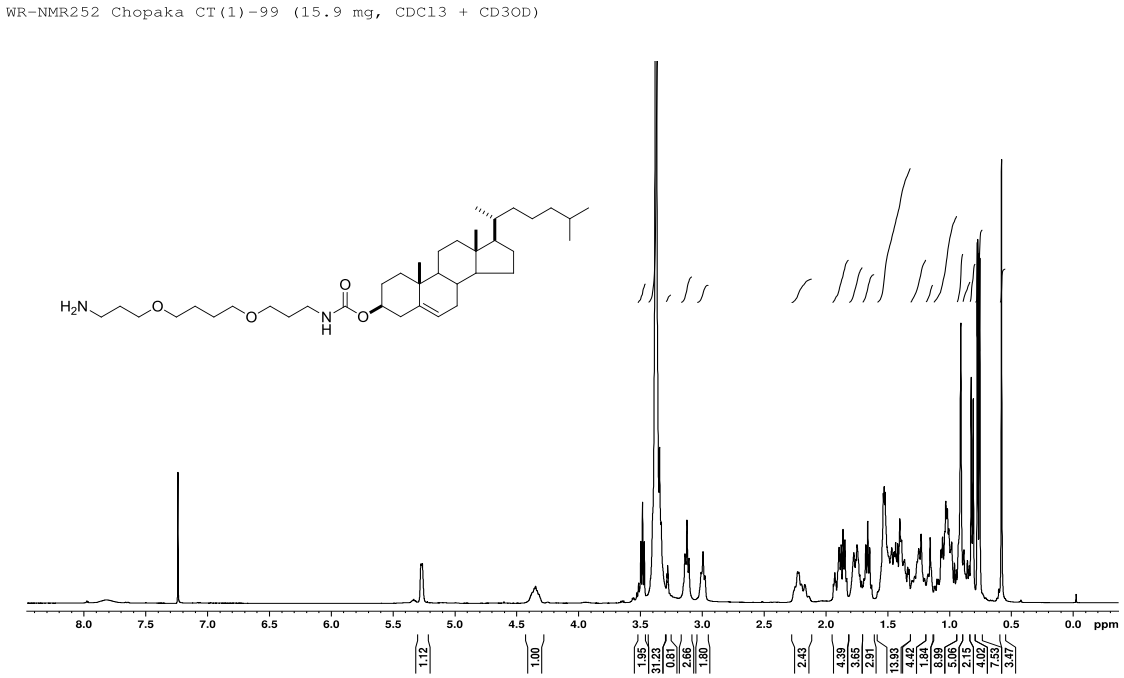

Appendix Figure 111 ^{1}H NMR Spectrum (400 MHz, $CDCl_3$) of Lipid **L9**.

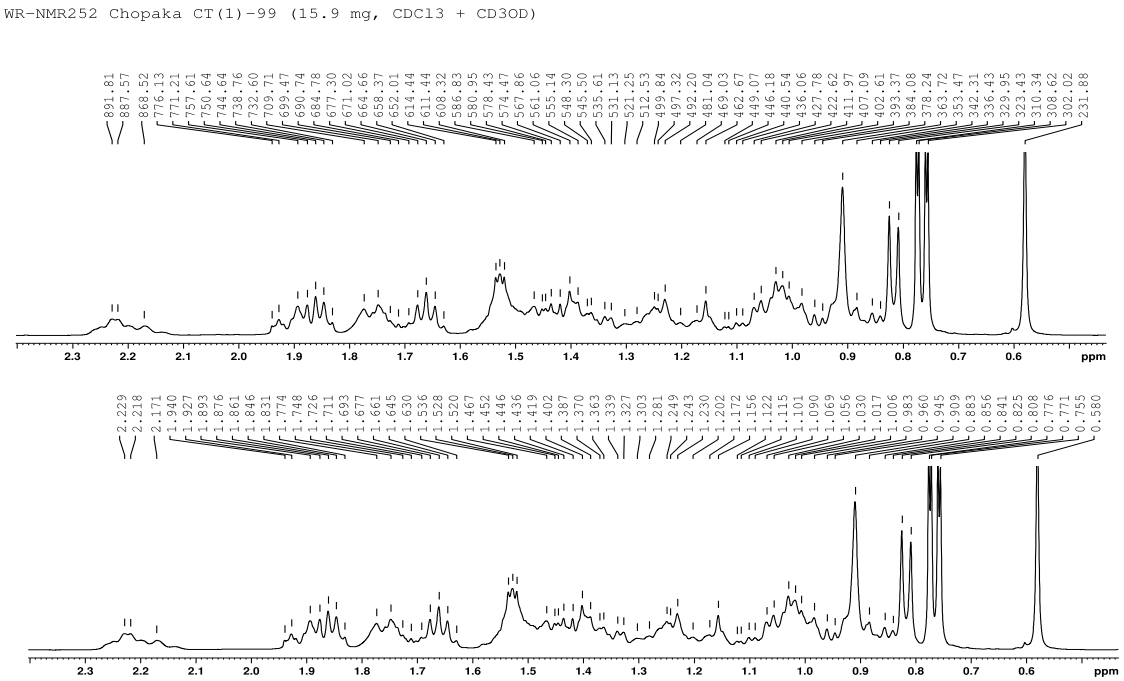

Appendix Figure 112 Expansion of ^{1}H NMR Spectrum (400 MHz, $CDCl_3$) of Lipid **L9**.

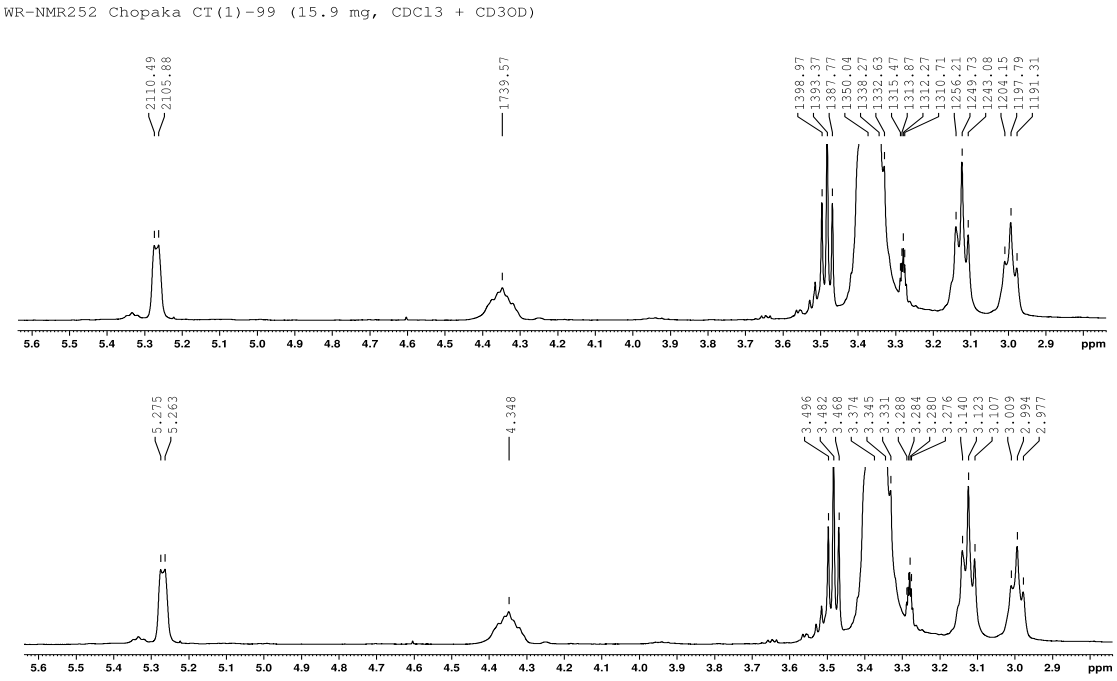

Appendix Figure 113 Expansion (cont.) of ^{1}H NMR Spectrum (400 MHz, $CDCl_3$) of Lipid **L9**.

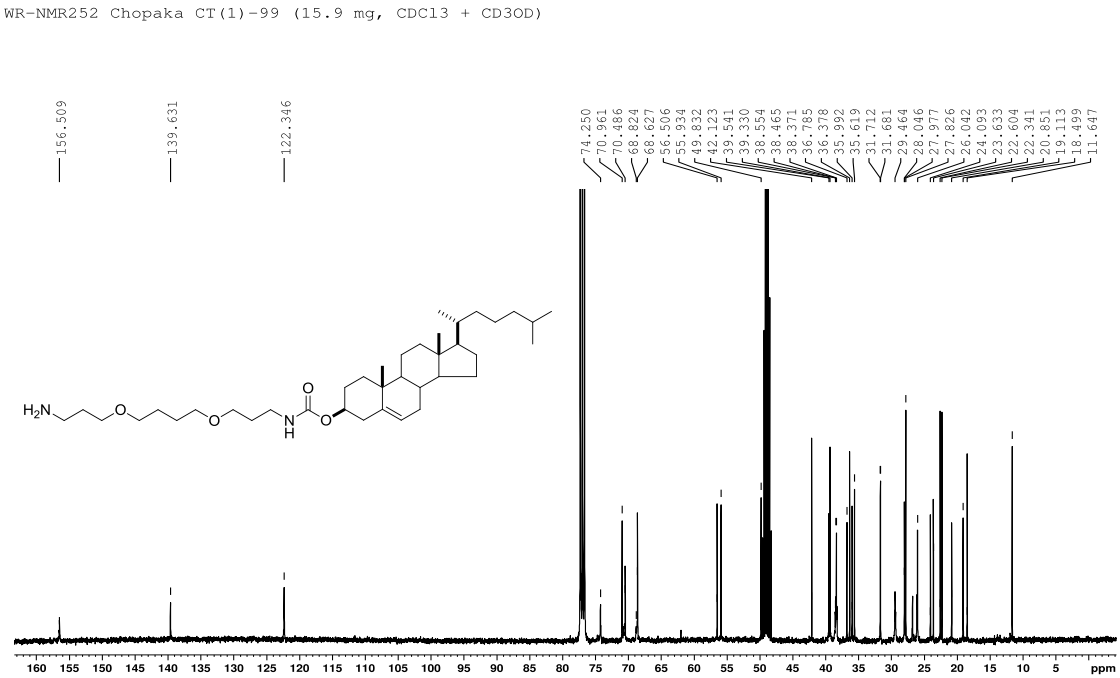

Appendix Figure 114 ^{13}C NMR Spectrum (100 MHz, $CDCl_3$) of Lipid **L9**.

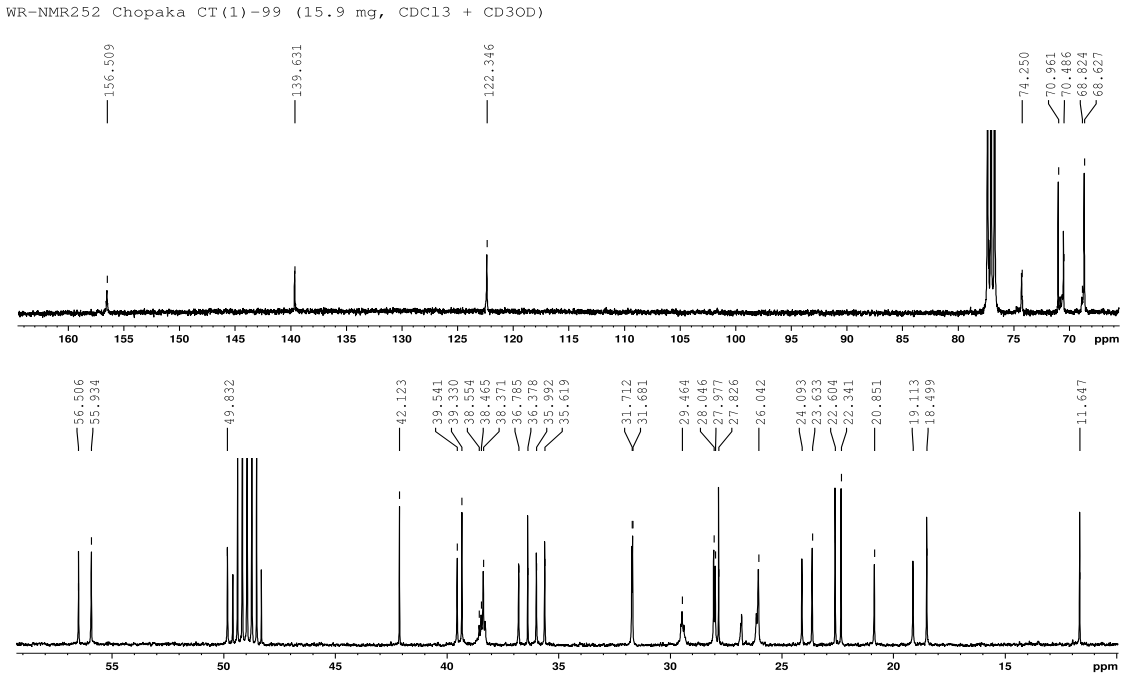

Appendix Figure 115 Expansion of ^{13}C NMR Spectrum (100 MHz, $CDCl_3$) of Lipid **L9**.

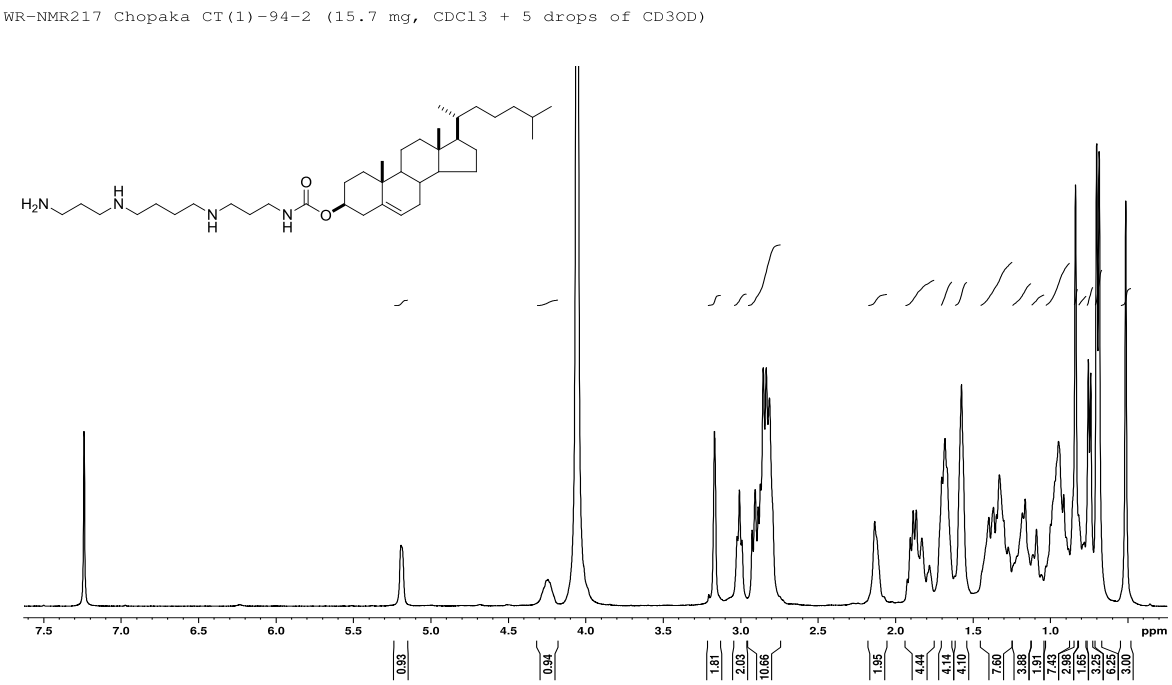

Appendix Figure 116 ^{1}H NMR Spectrum (400 MHz, $CDCl_3$) of Lipid **L10**.

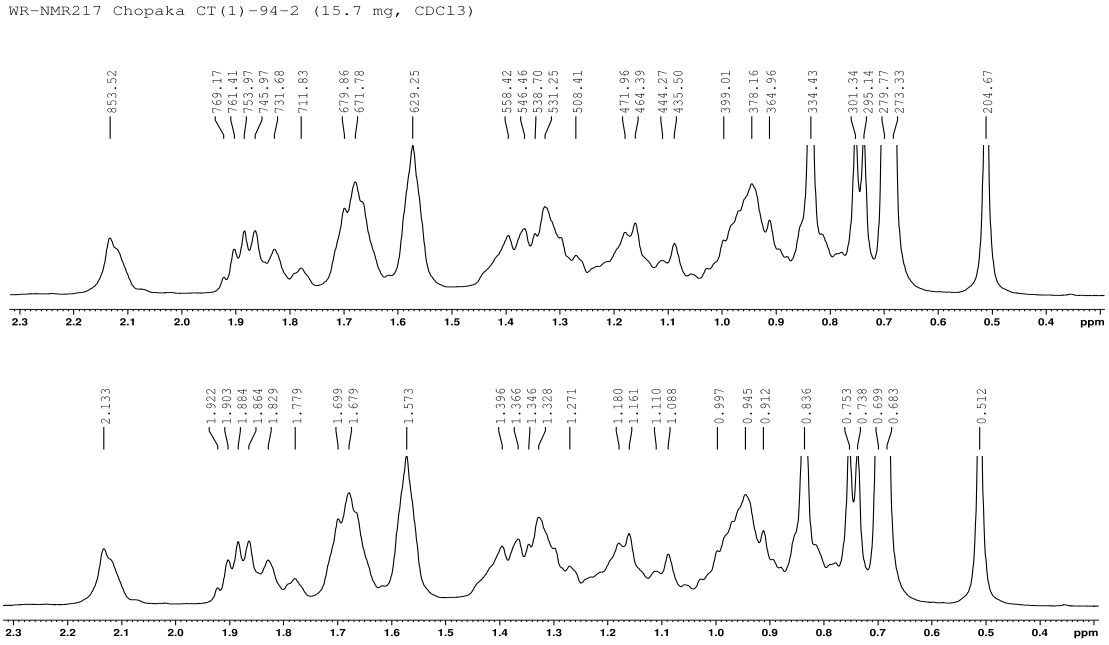

Appendix Figure 117 Expansion of ^{1}H NMR Spectrum (400 MHz, $CDCl_3$) of Lipid **L10**.

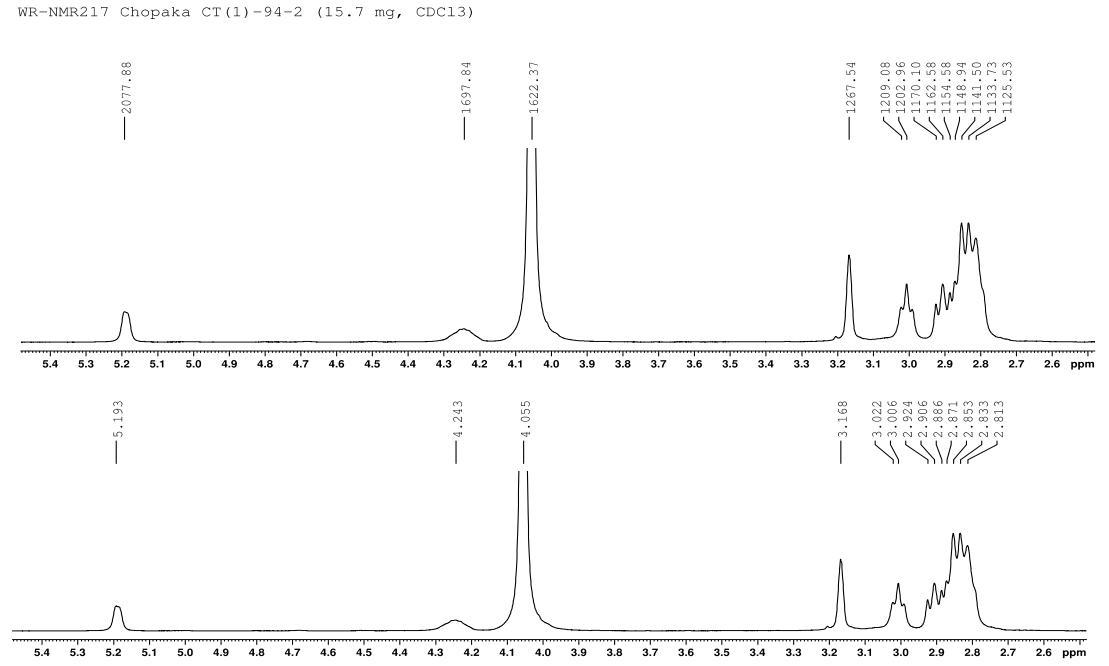

Appendix Figure 118 Expansion (cont.) of ^{1}H NMR Spectrum (400 MHz, $CDCl_3$) of Lipid **L10**.

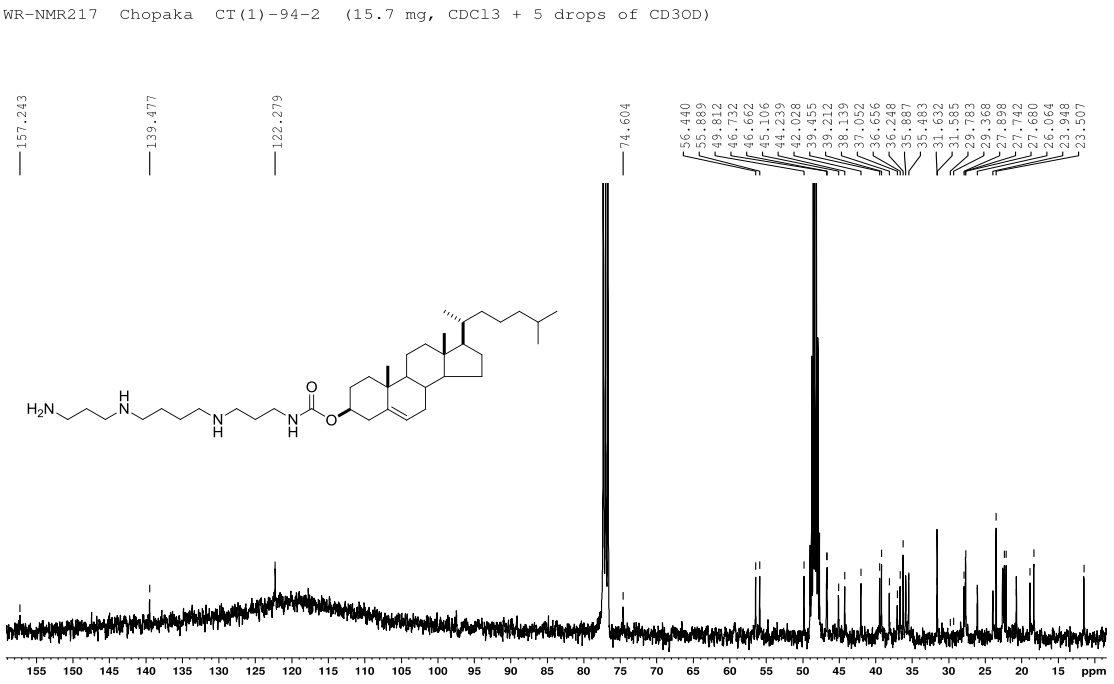

Appendix Figure 119 ^{13}C NMR Spectrum (100 MHz, $CDCl_3$) of Lipid **L10**.

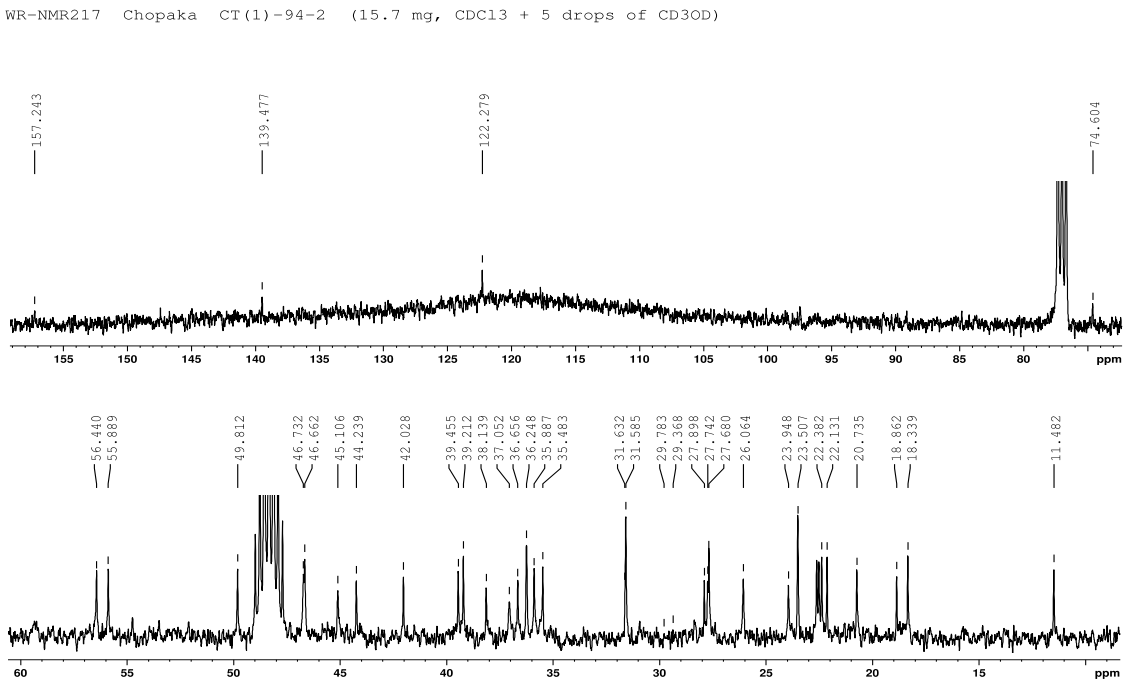

Appendix Figure 120 Expansion of ^{13}C NMR Spectrum (100 MHz, $CDCl_3$) of Lipid **L10**.

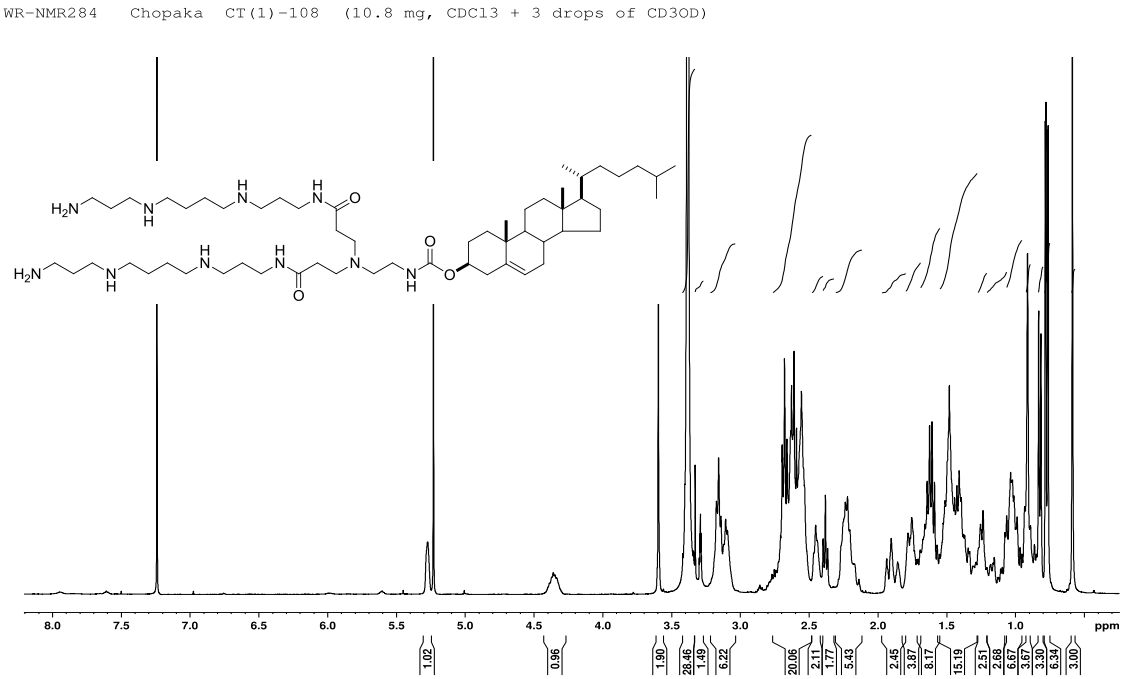

Appendix Figure 121 ^{1}H NMR Spectrum (400 MHz, $CDCl_3$) of Lipid **L11**.

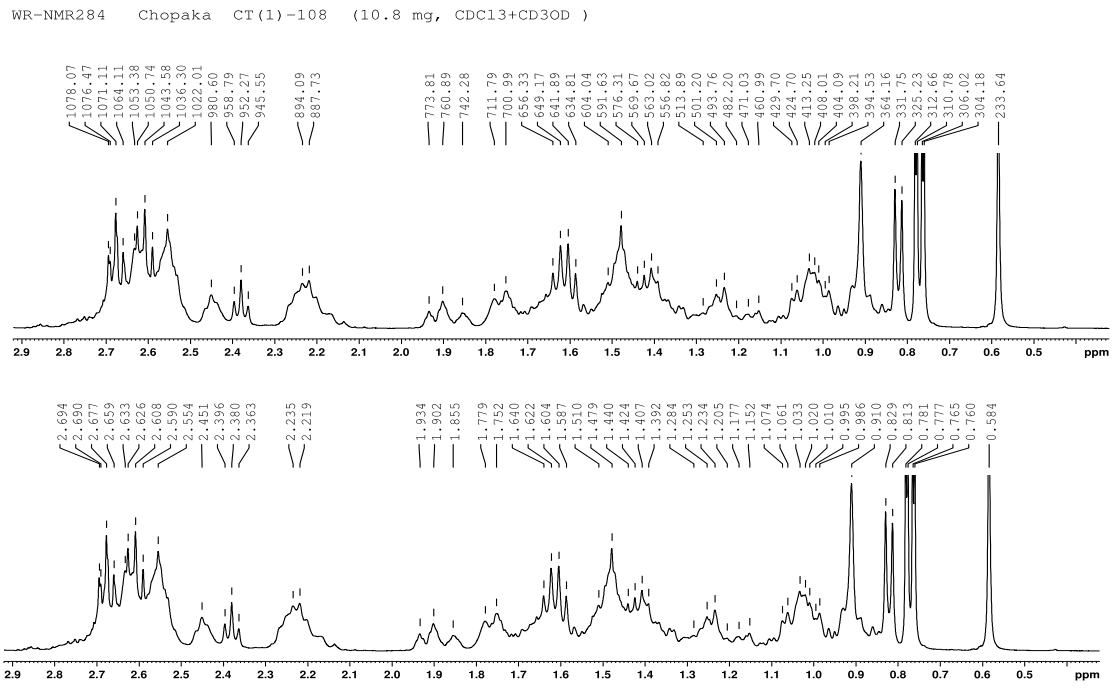

Appendix Figure 122 Expansion of ^{1}H NMR Spectrum (400 MHz, $CDCl_3$) of Lipid **L11**.

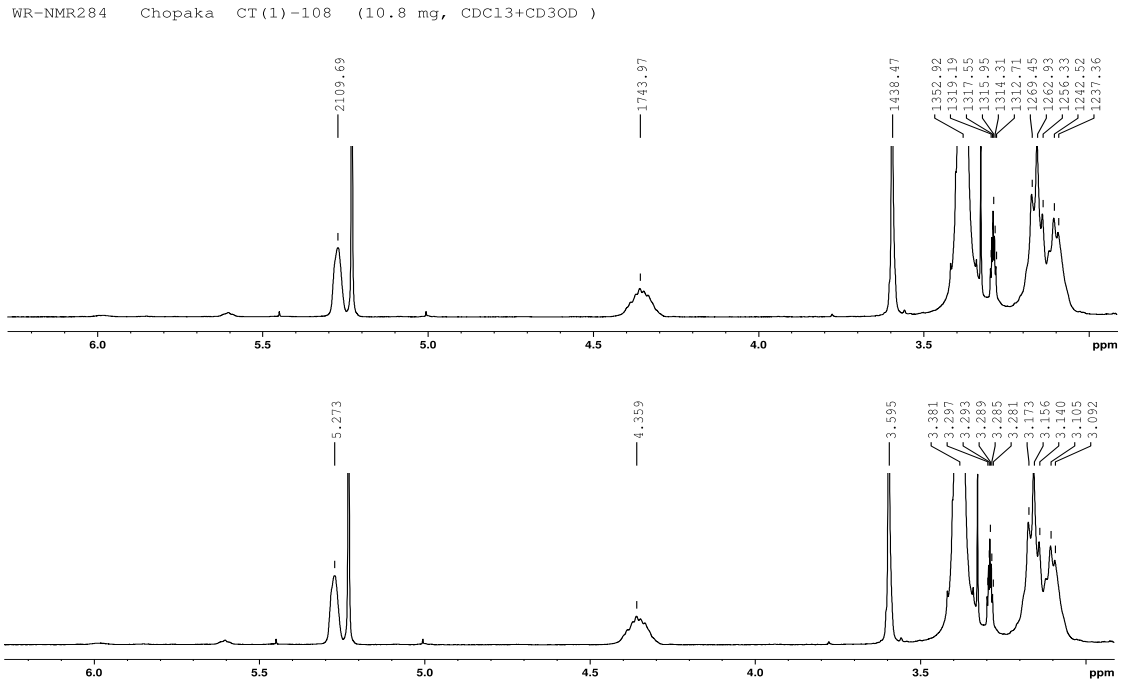

Appendix Figure 123 Expansion (cont.) of ^{1}H NMR Spectrum (400 MHz, $CDCl_3$) of Lipid **L11**.

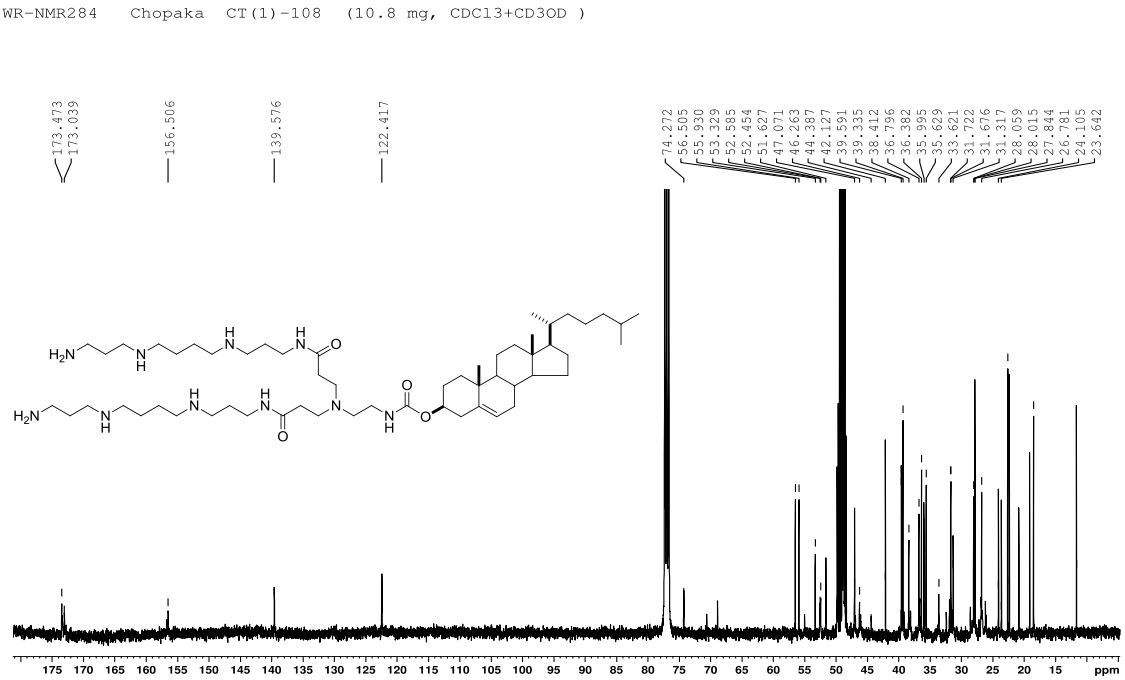

Appendix Figure 124 ^{13}C NMR Spectrum (100 MHz, $CDCl_3$) of Lipid **L11**.

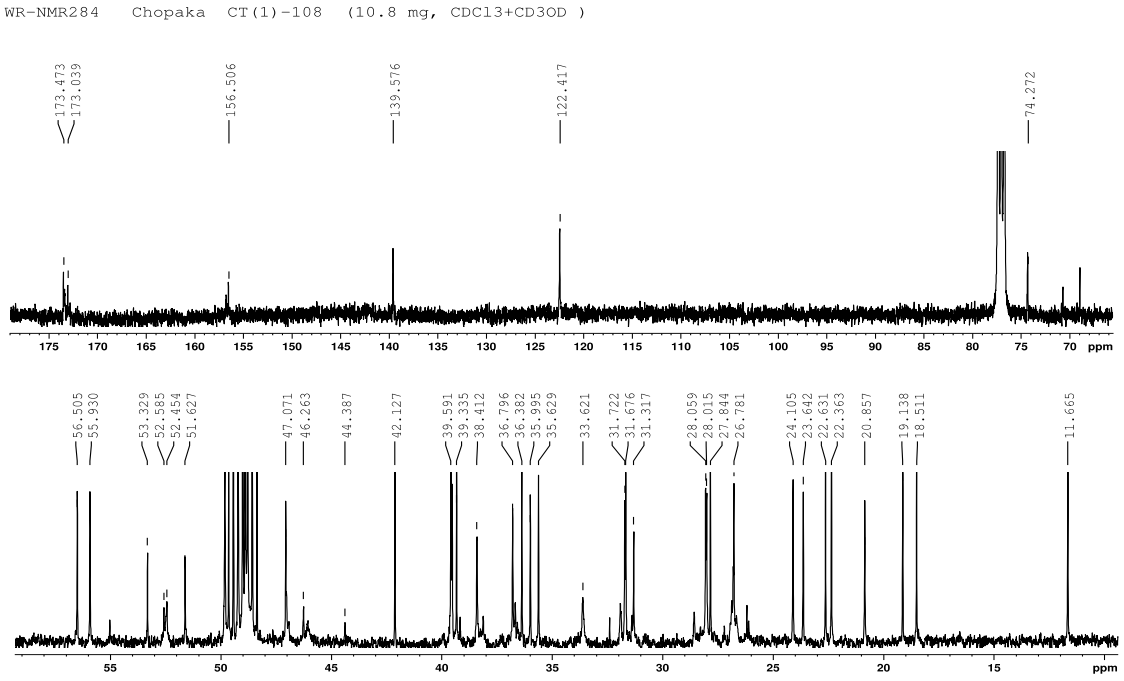

Appendix Figure 125 Expansion of ^{13}C NMR Spectrum (100 MHz, $CDCl_3$) of Lipid **L11**.

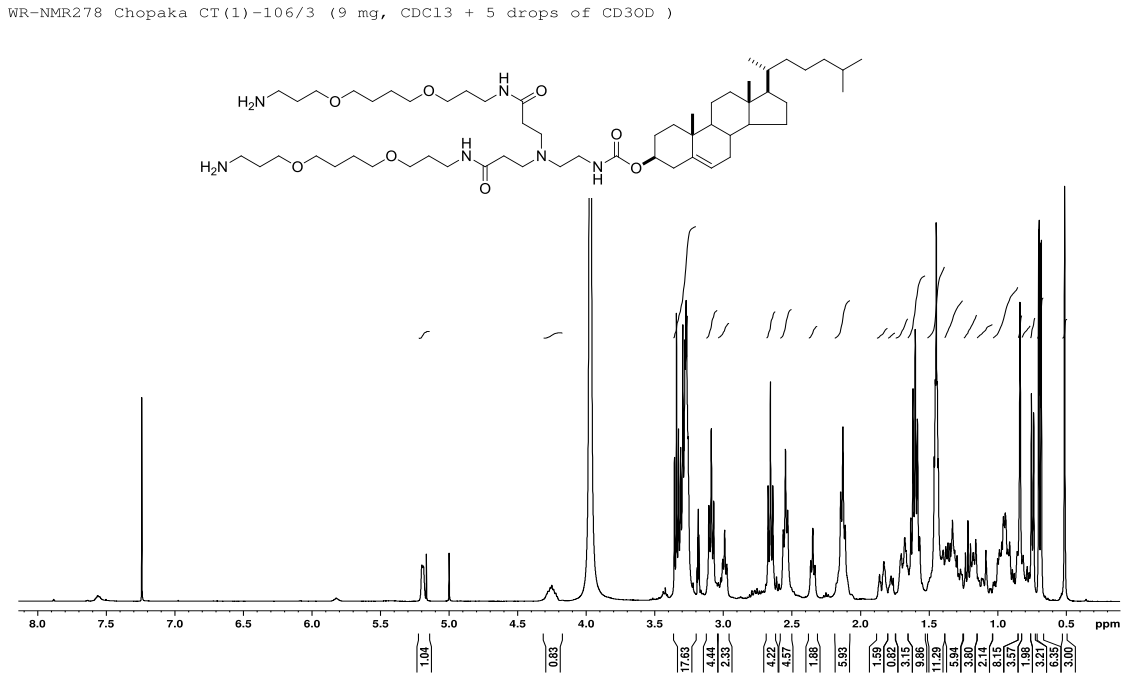

Appendix Figure 126 ^{1}H NMR Spectrum (400 MHz, $CDCl_3$) of Lipid **L12**.

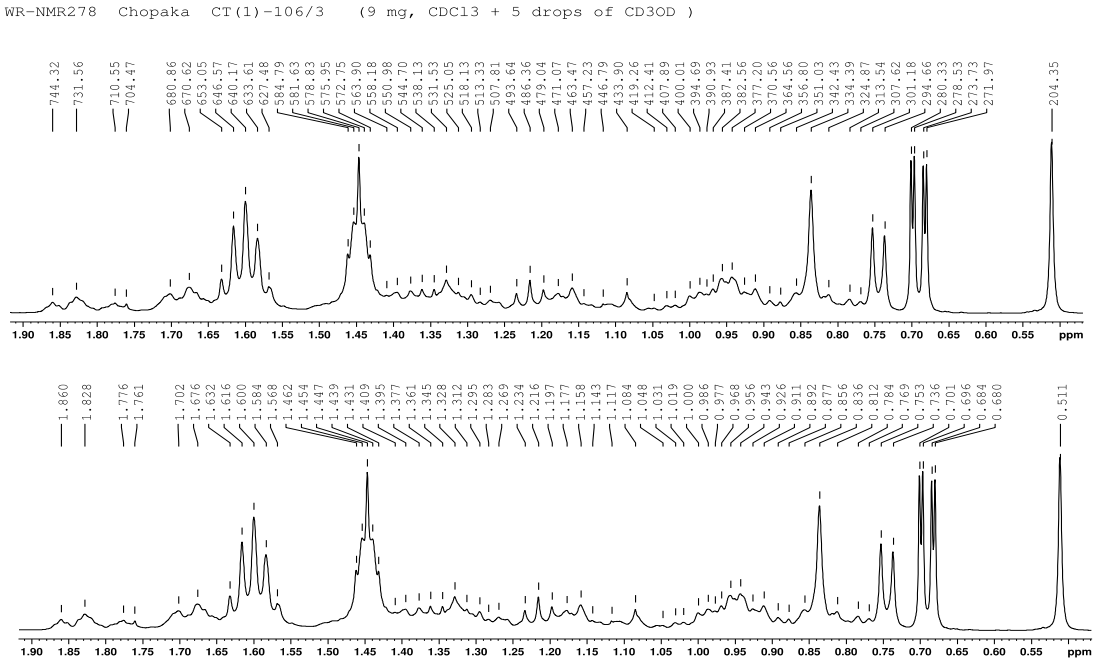

Appendix Figure 127 Expansion of ^{1}H NMR Spectrum (400 MHz, $CDCl_3$) of Lipid **L12**.

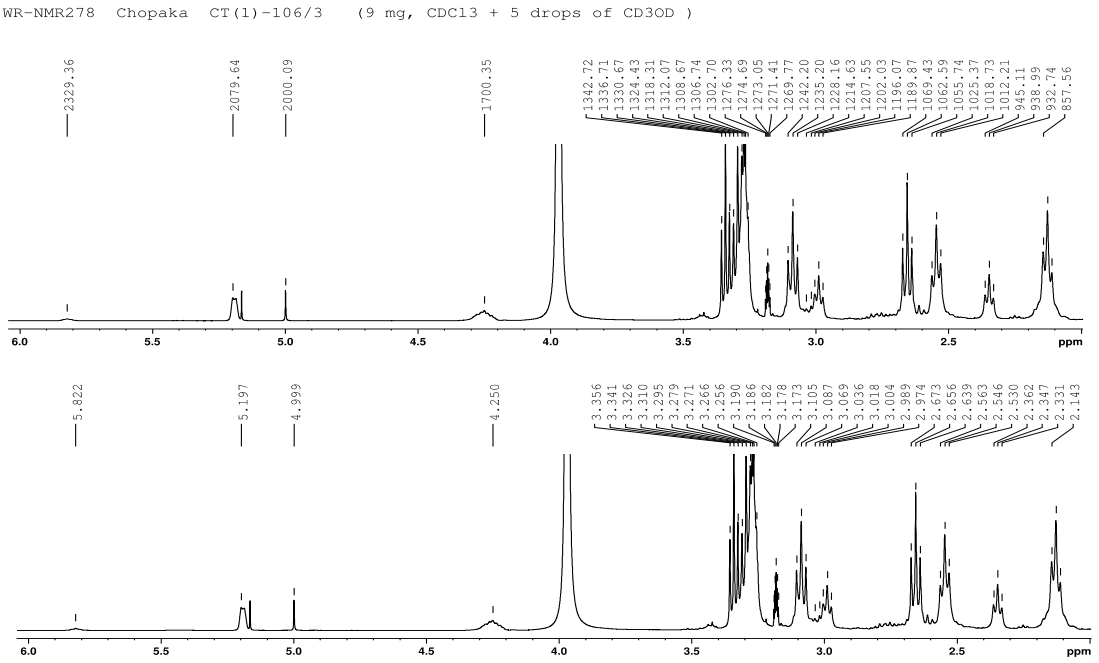

Appendix Figure 128 Expansion (cont.) of ^{1}H NMR Spectrum (400 MHz, $CDCl_3$) of Lipid **L12**.

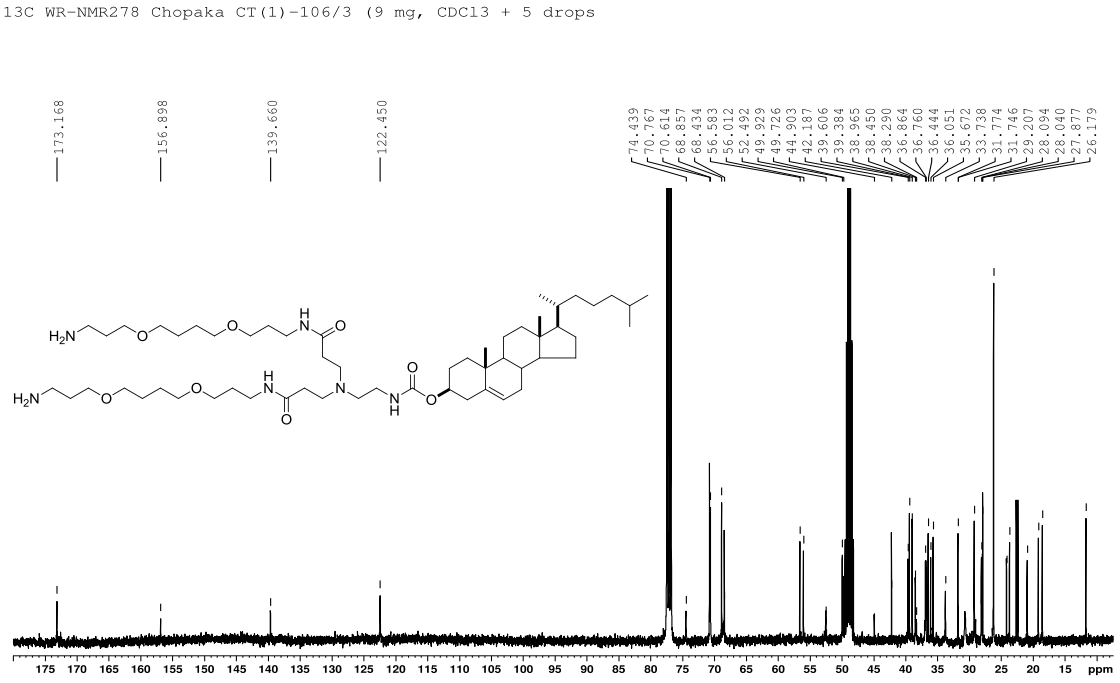

Appendix Figure 129 ^{13}C NMR Spectrum (100 MHz, $CDCl_3$) of Lipid **L12**.

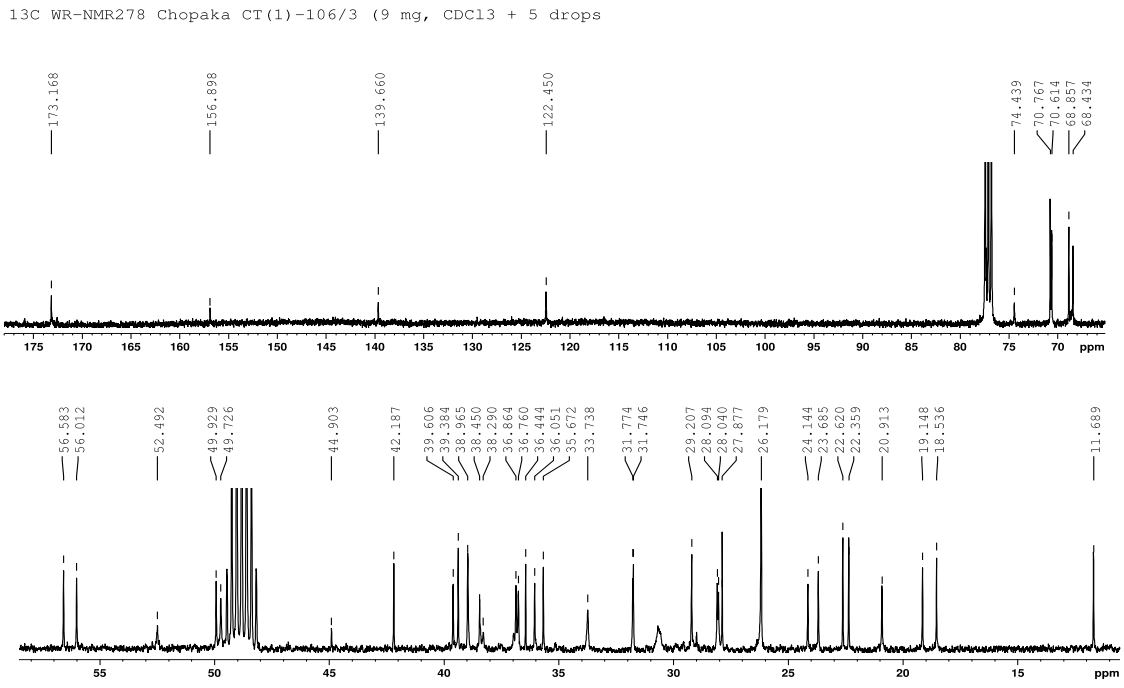

Appendix Figure 130 Expansion of ^{13}C NMR Spectrum (100 MHz, $CDCl_3$) of Lipid **L12**.

BIOGRAPHY

BIOGRAPHY

Name	Miss Chopaka Thongbamrer
Date of brith	October 9, 1992
Place of birth	Kalasin, Thailand
Institution attended	2015 B.Sc. (Chemistry) Mahasarakham University
Contact address	74 Village No. 5, Kham Muat Kaeo Sub-district, Huai Mek District, Kalasin Province, Thailand 46170
Scholarship	Science Achievement Scholarship of Thailand (SAST)